JOURNAL OF THE

Electrochemical Society

Vol. 109, No. 8 August 1962

Boston Meeting Program Issue

THE GLC PROGRAM OF PROGRESS

Technical teamwork with our chlor-alkali customers provides a base for continuing improvements in GLC anode performance.

Our program of progress gives GLC anode customers better results now than ever before —seeks still better results in the years ahead.

will lower cell operating costs

Share the rewards of this program by putting custom made GLC anodes to work now in your electrolytic cells.

We can then help you develop the technical information and specifications needed to improve cell efficiency and lower your operating costs.

PRODUCTS ELECTRODE GLC DIVISION YOU CAN TRUST ®

GREAT LAKES CARBON CORPORATION

18 EAST 48TH STREET, NEW YORK 17, N.Y. OFFICES IN PRINCIPAL CITIES

Manuscripts submitted to the Journal should be sent, in triplicate, to the Editorial Office at 30 East 42 St., New York 17, N. Y. They should conform to the revised Instructions to Authors published on pp. 131C-132C of the May issue. Manuscripts so submitted become the property of The Electrochemical Society and may not be published elsewhere, in whole or in part, unless permission is requested of and granted by the Editor.

The Electrochemical Society does not maintain a supply of reprints of papers appearing in its Journal. A photoprint copy of any particular paper, however, may be obtained by corresponding direct with the Engineering Societies Library, 345 E. 47 St., New York, N. Y.

Inquiries re positive microfilm copies of volumes should be addressed to University Microfilms, Inc., 313 N. First St., Ann Arbor, Mich.

Walter J. Johnson, Inc., 111 Fifth Ave, New York 3, N. Y., have reprint rights to out-of print volumes of the Journal, and also have available for sale back volumes and single issues, with the exception of the current calendar year. Anyone interested in securing back copies should correspond direct with them.

Journal of the Electrochemical Society

AUGUST 1962 **VOL. 109 • NO. 8**

CONTENTS

Published monthly by The Electrochemical Society, Inc., from Manchester, N.H.; **Executive Offices, Editorial Office** and **Circulation Dept.,** and **Advertising Office** at 30 East 42 St., New York 17, N. Y., combining the JOURNAL and TRANSACTIONS OF THE ELECTROCHEMICAL SOCIETY. Statements and opinions given in articles and papers in the JOURNAL OF THE ELECTROCHEMICAL SOCIETY are those of the contributors, and The Electrochemical Society assumes no responsibility for them. Subscription to members as part of membership service; subscription to nonmembers $24.00 plus $1.50 for postage outside U.S. and Canada. Single copies $1.70 to members, $2.25 to nonmembers.

Entered as second-class matter at the Post Office at Manchester, N. H., under the act of August 24, 1912.

Editorial

Engineering Research Needs

THE Engineers Joint Council, whose members represent the major U.S. Engineering Societies, set up a Research Committee to study the role of the professional engineer in the future development of American industry, education, and economy. Last May, the Committee published a report entitled "The Nation's Engineering Research Needs 1965-1985," which surveys the various fields in which engineering research and planning is needed, and makes some specific recommendations for cooperation with government, industry, and education. The fields range from obvious ones, such as urban-suburban problems, technology in the newer nations, methods of energy conversion, to novel and bold proposals such as the application of engineering methods to improvement of hospital and medical services and to the mechanics of the educational process itself.

Some 40,000 professional engineers are graduated annually, and it is estimated that twice this number will soon be needed; but the number of students registered in engineering courses has decreased sharply even in the past five years. This is attributed to greater emphasis on "theoretical science" and the profession's "poor public relations." Suggested remedies are to get more information to high school students, and to make up for lack of numbers by employing available engineers more effectively and by substituting trained technicians wherever possible. Some 11,000 technicians are trained annually and it is suggested that efforts be made to increase this number to 30,000. A real challenge is presented to the community colleges and the technical institutes, as well as to the full-scale engineering schools.

The report calls for an examination of the inroads made on our scientific and engineering capabilities by government programs, particularly in the field of military-atomic-space technology. A "crash" program of space exploration is fascinating but also truly fantastic in cost and effort, and may in addition be wasteful and disappointing because of premature launching. Major developments in science and technology are accumulative rather than simultaneous, to paraphrase Warren Weaver of the Sloan Foundation; a modern jet airplane could not have been built in 1900 even if the entire scientific and engineering effort of the world had been applied to that goal.

As for the shortage of engineers and engineering students, the EJC viewpoint may be too pessimistic. Without half trying, one can find a similar shortage of electrochemists, of physicists and physicians, and of other professional people. More people are engaged in some type of scientific, technological, or engineering work now than ever before, no matter what formal degrees they may have. This kind of talent is being spread over immensely wider fields than even existed in the past and, if there is an apparent shortage in one area, we hope it is because the men who might have qualified in that area are doing equally important work in another.

Nevertheless, we trust that the study and recommendations of the Engineers Joint Council will not go unheeded. They represent a most serious effort by leaders in the profession.

—CVK

any way you measure

ANODE PERFORMANCE

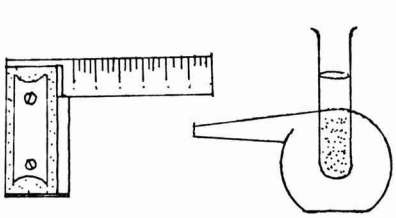

Structural and Dimensional Uniformity?

Chemical Stability of Treatments?

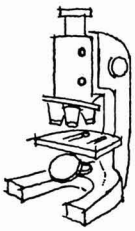

Uniform Texture?

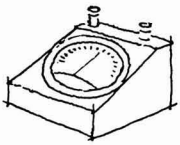

Cell Voltage?

Pounds Consumed per ton of Chlorine Produced?

STACKPOLE

GraphAnode® ANODES

prove second to none for

Economical Chlorine Production

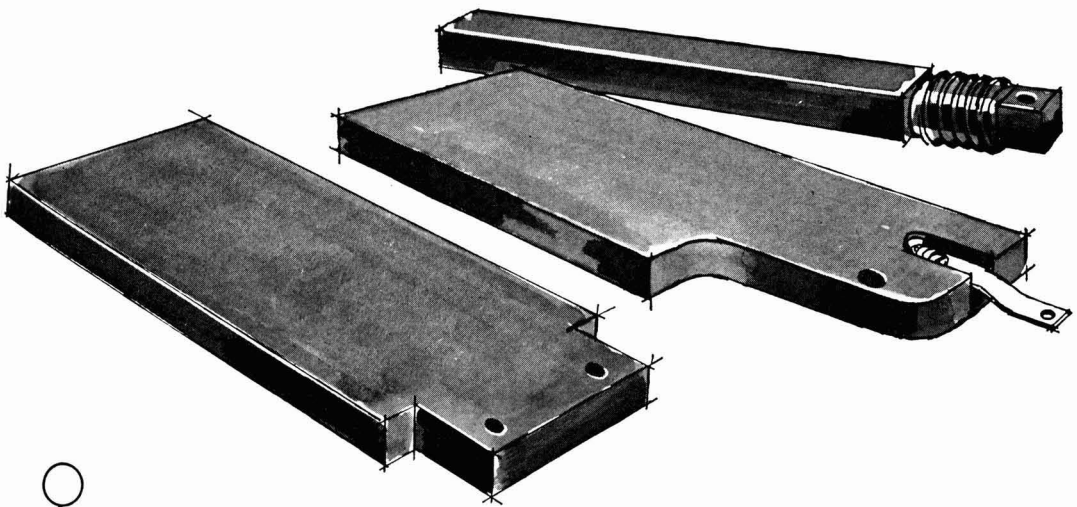

STACKPOLE CARBON COMPANY,
St. Marys, Pa.

CATHODIC PROTECTION ANODES • FLUXING & DE-GASSING TUBES • SALT BATH RECTIFICATION RODS • ROCKET NOZZLES • RISER RODS • GRAPHITE BEARINGS & SEAL RINGS • ELECTRODES & HEATING ELEMENTS • WELDING CARBONS • VOLTAGE REGULATOR DISCS • **"CERAMAGNET"®** CERAMIC MAGNETS • ELECTRICAL CONTACTS • BRUSHES FOR ALL ROTATING ELECTRICAL EQUIPMENT • AND MANY OTHER CARBON, GRAPHITE AND ELECTRONIC COMPONENTS.

POTENTIOSTATS

For:

General electrochemistry laboratory

Corrosion

Protection

Materials compatibility

S. I. T. developed:

MOD. V2 reversible potentiostat for voltage up to ± 12 V, current ± 5 A.

MOD. V3 reversible potentiostat for voltage up to ± 30 V, current ± 1 A.

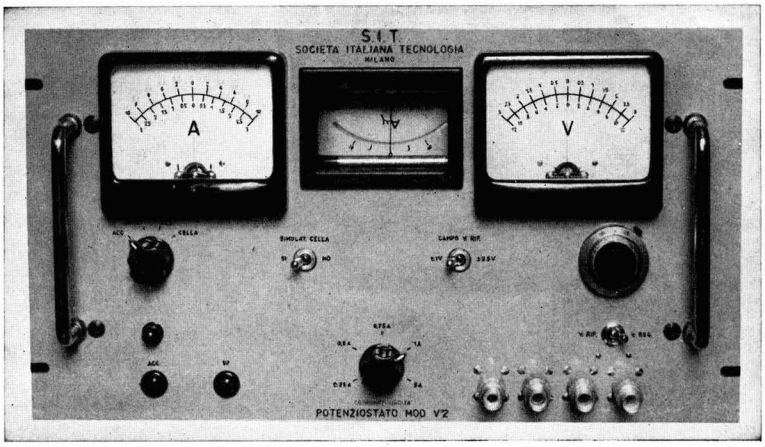

Features:

Reference voltage: 0-± 1 V, 0 ± 2,5 V fine regulation long range stability;

Reversibility: two regulating circuits for positive and negative output;

Response: potentiostas have all transistor circuits; time response is about 10^{-4} sec. and not dependent from load;

Internal load for preliminary control;

External modulation (optional) can drive the output to modulate the load;

Amperometer, Voltmeter, Galvanometer for outputs and zero readings;

Mains: 110-125-160-220 V ± 10%, 50 Hz.

Optional accessories:

Rotating electrode 1.000-30.000 turns/min. ± 1% compact realization for working in small thermostats.

Operational amplifier for recording the logarithm of outputs.

S. I. T.

Società Italiana di Tecnologia

Via Fratelli Gabba 8—Milano

ITALY

By SAM PUCKETTE
District Manager
Non-Linear Systems, Inc.
Del Mar, California
and
HENRY W. LAUB
Project Engineer, Cell Development
Diamond Alkali Company
Deer Park, Texas

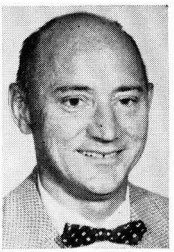

Optimizing Electrolysis Efficiency Yields up to $8,000 Annual Saving

Highly accurate method to detect small changes in voltage drop enables Diamond Alkali to check power loss in electrolytic production of chlorine from sodium chloride brines.

PHOTO COURTESY-DIAMOND ALKALI COMPANY

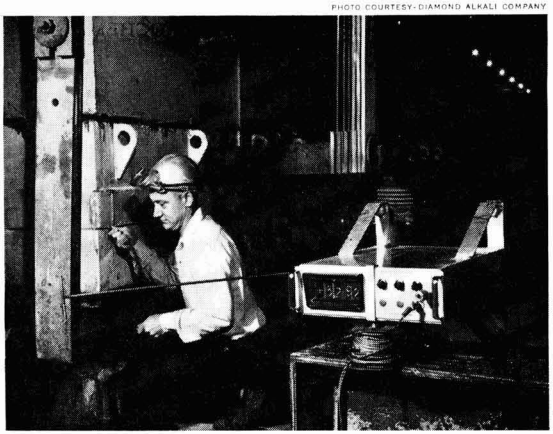

Digital Voltmeter is used to detect small voltage drops.

The method used by Diamond Alkali Company to optimize its chlorine production holds considerable interest for any firm engaged in electrolytic processing.

Heart of the problem was finding a way to quickly and accurately measure small changes in voltage and voltage drop.

Personnel at the Diamond Alkali diaphragm plant in Deer Park, Texas, had believed that optimum placement of internal cell components would provide more efficient use of power in producing chlorine from sodium chloride brines by electrolysis. Also, voltage drops in bus bar connections had to be minimized to reduce power loss. In fact, a voltage drop of 0.01 volt at 30,000 amps would result in a loss of $8,000 a year. But because the voltage changes involved were only several hundredths of a per cent, it was difficult to recognize them with existing equipment.

The answer was a bit of ingenuity and an automatic digital voltmeter made by Non-Linear Systems, Inc., originator and world's leading manufacturer of DVMs. By allowing one or two men to make the measurements and observe instantly and accurately changes as small as one millivolt in 5 volts, the NLS 4-digit voltmeter (now $1,460) aided in producing power savings of up to $8,000 annually in this one area. Of significance was the fact that personnel making measurements could observe the digital readings from as far as 30 feet away. A long cable permits the operator to place the input probes anywhere along the long line of chlorine cells.

This means that the operator need only connect the digital voltmeter input probes and immediately note any changes displayed by the large digital readout of the DVM.

For information on how digital voltmeters and other digital measuring instruments and systems might be of assistance to you, please contact one of the 19 NLS factory offices or write Non-Linear Systems, Inc., Del Mar, California.

NLS non-linear systems, inc.

Papers Solicited for

ELECTROCHEMICAL TECHNOLOGY

As announced in the February issue of the JOURNAL (page 37C), The Electrochemical Society will publish a new magazine to be named ELECTROCHEMICAL TECHNOLOGY. The first issue will be published in January-February 1963. Initially, the new publication will be issued bimonthly. It will become a monthly publication as soon as enough papers are received to justify such a step.

ELECTROCHEMICAL TECHNOLOGY will cover electroprocesses in areas of technology, engineering, design, devices, economics, and appropriate reviews. The same review procedures which apply to the present JOURNAL will also obtain with regard to the new magazine.

A. C. Loonam, Editor, is now soliciting papers for publication in ELECTROCHEMICAL TECHNOLOGY. All members and others concerned, who are engaged in the applied areas of electroprocesses, who can submit papers on timely subjects are urged to do so as soon as possible.

Triplicate copies of each manuscript, prepared in accordance with the Instructions to Authors of Papers published on pp. 131C-132C of the May JOURNAL, should be submitted to:

The Editor
ELECTROCHEMICAL TECHNOLOGY
The Electrochemical Society
30 East 42 Street, Rm. 1806
New York 17, N. Y.

Act now and enjoy the unique distinction of becoming one of the first-volume authors.

Manuscripts so submitted become the property of The Electrochemical Society and may not be published elsewhere, in whole or in part, unless permission is requested of and granted by the Editor.

The Sodium|Tin Liquid-Metal Cell

Robert D. Weaver, Stanley W. Smith, and Norman L. Willmann

Delco-Remy Division, General Motors Corporation, Anderson, Indiana

ABSTRACT

Preliminary studies of the liquid-metal cell have shown it to possess promising characteristics for application to the conversion of thermal energy. Polarization effects commonly associated with electrochemical cells are essentially absent; charge-discharge curves are straight lines passing through the open-circuit intercept. The conductivity of the fused electrolyte, 2.3 mhos, provides for low internal losses. Nongalvanic losses occur causing an apparent loss of reactants to the extent of 0.018 amp/cm^2. It is shown that a cell constructed of the materials and electrolyte employed in the study should allow operation at 0.7 amp/cm^2 at maximum power and that the coulombic efficiency would be 95% when continuously operated at this current density during balanced charge and discharge periods.

The thermally regenerative liquid-metal cell, which has elsewhere been conceived and described (1-3), effects the transformation of thermal power to electrical power by the thermal decomposition of the products of electrochemical reaction. The reactants are liquid metals which combine to form alloys and to produce electrical energy. It is this liquid alloy which is then thermally decomposed, at a higher temperature, to the original liquid-metal reactants. The transducing system is, therefore, limited to Carnot efficiencies.

The liquid-metal cell, employing Na and Sn as examples of reactants, may be represented as Na|Na^+ electrolyte|Na·Sn, in which oxidation occurs at the Na electrode. The potential of this cell is greater than that of a simple concentration cell due to the decrease in Na activity at the Sn cathode due to the formation of compounds represented by $Na_x \cdot Sn_y$. Since high potentials are desirable, the concentration of Na in the cathode will be maintained at levels usually less than 10 weight per cent (w/o). The electrochemical reaction involves the transfer of Na^+ formed at the anode, through the electrolyte, to the cathode. Thus, it is desirable to employ electrolytes which are chemically stable to Na metal and in which the only cation present is that of Na. Such electrolytes are provided by fused Na salts. The use of a fused-salt electrolyte will further provide high electrical conductivity.

The use of electrochemical cells to acquire thermodynamic data of liquid-metal alloys is well established (4, 5). Solid electrolytes have usually been employed in such cells, and none have been capable of producing power at high current densities. One other electrochemical transducer has been described which involves thermal decomposition of the electrochemical product, in this case LiH, (6-8).

This paper presents a study of the electrochemical cell associated with the liquid-metal system. Because of the novelty of this cell system and the problems attendant to the use of reactive liquid metals in a cell which is operated at high temperatures, this paper is devoted to a description of the experimental techniques involved, the materials employed, and the preliminary results obtained.

Experimental Procedures

The use of Na at high temperatures in a cell requires that a containing material be employed which is an electrical insulator, is inert to Na, is nonporous (*i.e.*, impervious), and is capable of withstanding high temperatures. Aluminum oxide has been found to be such a material. To study cell behavior, cells were constructed, as shown in Fig. 1, consisting of an alumina crucible[1] whose composition is given as 99 + % Al_2O_3. It has been found that low silica-content alumina is necessary for this work. The cell must be sealed in order to prevent long-time loss of Na through vaporization, and this has been accomplished by use of a ground tapered joint between the cell and a solid alumina cap. The angle of the joint is 5°, and the grinding is accomplished by use of diamond grinding techniques.

[1] Norton Company, Crucible No. MD 70319 B.

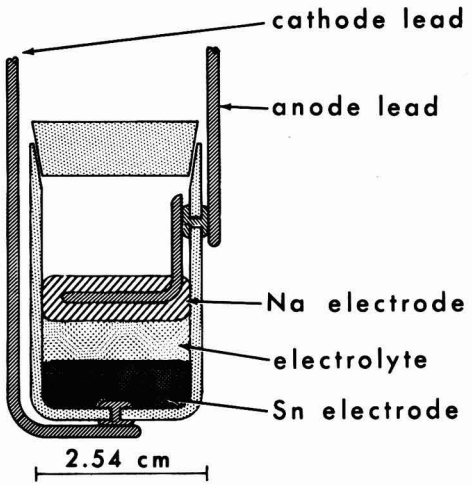

Fig. 1. Static Na|Sn cell

Electrical leads are necessary through the cell walls and necessitate a metal-to-alumina seal which is vapor tight. Such seals are made by grinding a 0.03 cm oversize hole in the cell wall and inserting a steel rivet. The rivet is seated by use of a spot welder which allows the rivet to be heated to a cherry-red heat and which supplies pressure to flatten the rivet end. Electrode wires may then be spot-welded to either end of the rivet as necessary. Such seals are quite satisfactory, but require some experience to effect a tight seal which will not crack the alumina as the rivet contracts.

The densities of the metals and the electrolytes are such that the layers are stable as shown in Fig. 1. The projected area of the metal electrodes is 3.87 cm^2. A cell such as this allows the static performance (*i.e.*, the liquid metals are not flowing) of the system to be evaluated. The cell must be operated in an inert atmosphere of N_2 or A as a safety precaution, for cracks and leaks may occur. This is accomplished by placing the entire cell in a bottomed glass tube, wires and inert gas being introduced through a rubber stopper. The lower half of the tube, containing the cell, is then placed in a vertical tube furnace.

Both cell resistance and cell voltage are functions of temperature, and it is therefore necessary to provide for a constant temperature environment for the cell. During short duration runs it is possible to control furnace temperature by means of manually operated adjustable autotransformers. Line voltage variations overnight were found to cause temperature excursions of as much as 50°C. To achieve satisfactory temperature regulation, an inexpensive thermocouple-controlled galvanometer relay[2] was employed to control furnace temperature.

The galvanometer relay was set up to short-circuit a resistor in series with the furnace heater. Temperature level was established by means of an autotransformer, and the value of the series resistor was chosen to accommodate the effects of daily line-voltage variations. The temperature of the cell was controlled for a one-month interval with variations of less than 2°C by this technique.

The use of aluminum oxide in this work is, as stated, necessary, but entails some difficulties. Thus, a cell of more than simple geometry is difficult to fabricate from a single solid block while, on the other hand, further seals are required if the cell is fabricated from parts. It has been found possible to effect a liquid-metal tight seal between pieces of alumina tubing by use of the tapered joint already described, and by use of a tapered joint which has been sealed by formation of a spinel of MgO-Al_2O_3 between the alumina surfaces.[3] It is also possible to effect a seal between flat surfaces of alumina and steel by use of a pressure seal. The surfaces of such a seal must be ground flat and polished to a near gauge-block finish. Electrical leads may be incorporated by use of the rivets as described, or if in a metal surface, successful performance has been achieved by use of brazed nickel-to-alumina feedthrough terminals[4] which may then be welded to the metal surface. The machining of solid alumina in intricate shapes has been found to be readily performed employing high-frequency abrasive cutting techniques.

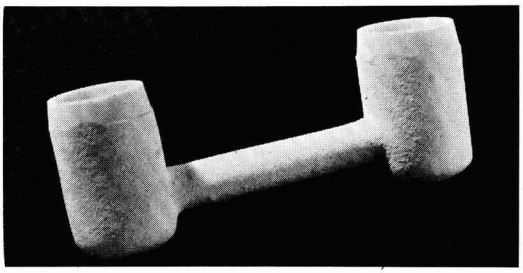

Fig. 2. Flame-sprayed alumina "H" cell

In the search for methods by which sufficient cell complexity might be achieved to allow half-cell voltage measurements to be taken,[5] an approach to a cell fabrication was made employing flame-spraying techniques. The "H" cell of Fig. 2 was prepared by flame-spraying[6] a wood mandrel, shaped to the desired inside dimensions of the "H" cell with Al_2O_3. The thickness of the flame-sprayed layer was about 3 mm. The wood mandrel was then removed by charring in a furnace at temperatures increasing from room temperature to 260°C over an 8-hr period. The charred wood residue was then removed, and the hollow cell leached with dilute HCl, dilute HNO_3, and H_2O and finally fired to 1090°C. The porous flame-sprayed cell was then reduced to near zero porosity by high-temperature firing.[7] This procedure resulted in a liquid-tight cell. Further attempts at this technique are expected to provide vacuum-tight apparatus of sufficient strength and of proper design to allow half-cell measurements to be performed.

For cells which are to be operated in an environment of vibration or with the liquid metal electrodes in a vertical position, it is necessary to separate the two liquid metals to prevent internal short circuits. Attempts to effect such separations are being made by use of an electrolyte-impregnated matrix of a porous, nonconducting substance. Various forms and compositions of alumina and MgO have been tested, the 99+% Al_2O_3 matrix having thus far been found to be best for this application. A commercially available filter disk[8] of 99% Al_2O_3, a nominal porosity of 36%, and a permeability of 20-30% has most frequently been employed as a matrix in these studies.

A liquid-metal cell, operated as a fuel cell, will be operated with a closed-ended anode, *i.e.*, the Na stream will terminate in the cell. At the cathode,

[2] Simplytrol P. R. Controller, Assembly Products, Inc., Chesterland, Ohio.

[3] Further particulars of this technique may be obtained from the Technical Development Department, Refractories Division, Norton Company, Worcester, Mass.

[4] Alite Terminals, 99% Al_2O_3 (Special) Alite Division, The U. S. Stoneware Co., Orrville, Ohio.

[5] An excellent reference source to the study of electrochemistry in fused salts has recently been published: "Reference Electrodes," David V. G. Ives and George J. Janz, Academic Press, N. Y. (1961) especially ch. 12.

[6] Cincinnati Metal-Blast Company, Cincinnati, Ohio.

[7] See Footnote 6 for further particulars, also ref. (9).

[8] Norton Alundum Lab Ware Filter Disk, Mixture RA 139, Norton Company, Worcester, Mass.

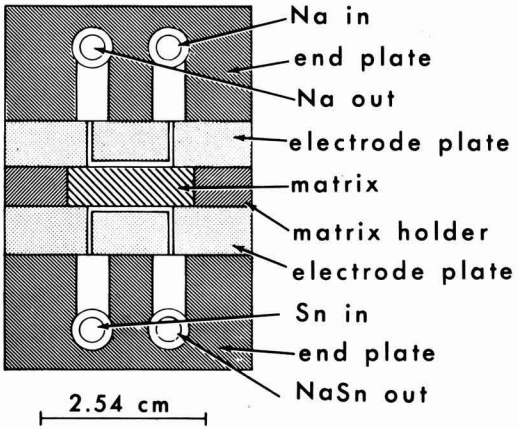

Fig. 3. Flowing-metal cell diagram

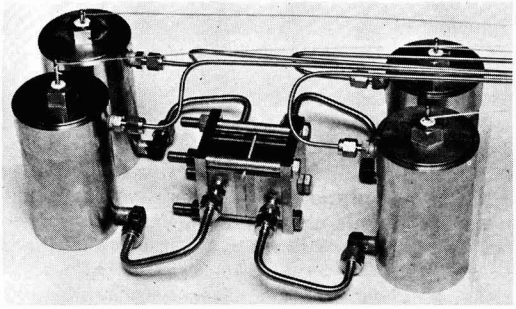

Fig. 4. Flowing-metal cell assembly

the Sn stream, low in Na content, will enter the cell, pass by the electrolyte, and exit from the cell enriched in Na content. The fact that the Sn cathode is moving past the electrolyte will tend to reduce any concentration polarization in the Sn cathode. To allow a determination of the influence of Sn velocity upon concentration polarization, the cell of Fig. 3 and 4 was constructed. Each cell-half consisted of an end plate, through which fittings allowed the reactant to be introduced and removed, and an electrode plate which allowed the liquid metal to assume a known geometry. The channel for the liquid metals in the electrode plate was a rectangle of 2.540 cm length, 1.270 cm width, and a depth of 0.0508 cm. The flow streams are therefore believed to be of uniform velocity past the electrolyte and of a known area. The assembled cell was made leak tight by use of the pressure seals already mentioned and with pressure supplied by the vice shown. The bolts employed were 5/16-18 and were tightened to a torque of 1.4 to 2 kg-m. The porous matrix was contained with a zero-clearance fit in a frame of impervious alumina.

All potential measurements were made employing potentiometers or strip-chart potentiometric recorders. Reagent grade chemicals were employed. The N_2 or A was passed over Cu turnings at a temperature of 450°C, and H_2O was removed with $CaSO_4$ drying towers. Temperatures were measured with

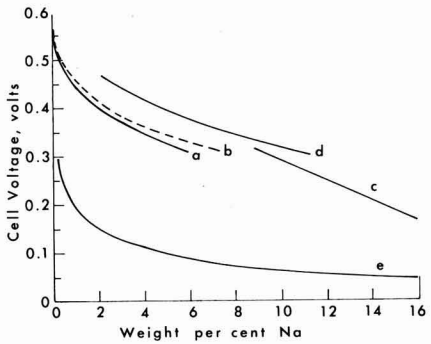

Fig. 5. Variation for Na|Sn cell voltage with Na concentration

chromel-alumel single-junction thermocouples. Electrolyte mixtures were prepared from stock reagents, in correct weight proportions, then fused to further remove traces of water.

Results

A search for a suitable electrolyte was made of the salts of Na. Anions found to be chemically compatible were: the halogens, CN^-, $CO_3^=$ and $S^=$. The electrolyte employed in these studies was an eutectic of 62.5 mole % NaI, 37.5 mole % NaCl, mp = 562°C. Cell data presented were obtained employing this electrolyte in cells which were maintained at 625°C. A low melting composition of 20.3 mole % Na_2CO_3, 47.3 mole % NaI, 32.4 mole % NaCl, mp = 520°C, has also been found. In addition a low melting mixture, mp = 512°C, for the NaI-NaCN system, of an approximate composition of 35 w/o NaCN has also been found.

Static-Cell Studies

Cell voltage *vs.* Na concentration data are presented in Fig. 5. Data for curve (a) were obtained employing the static cell loaded with Sn, the electrolyte, and Na, and raised to operating temperature. Known quantities of coulombs were then withdrawn from the cell, the open-circuit potential measured, and the weight per cent of Na in the Sn calculated. The open-circuit voltage of the cell continuously decreases during the period in which the electrolyte is molten. This nongalvanic voltage loss is presumably due to the solubility of Na in the melt or to chemical or physical decomposition of the electrolyte (I_2 coloration may be seen in the fused, evacuated melt). For this reason, the Na concentration calculated by coulomb measurement is a minimum value. Employing the results of the life-test to be described, the results presented in curve (a) have been corrected to an approximate true concentration, and these corrected data are presented in curve (b). Curve (c) was obtained from the data of ref. (4), p. 23, for a Na|Sn cell operated at 480°C and curve (d) obtained from ref. (10) for the cell operated at 500°C. Curve (e) was obtained by calculating the potential of the cell assuming behavior due to a simple concentration cell.

Charge-discharge data were obtained by employing the static cell. Such data were collected at dif-

ferent levels of Na concentration in the Sn layer. Experience with these measurements resulted in the design of the cell of Fig. 1. The data accumulated with this cell were corrected for the resistance of the leads which provided electrical contact from the top of the inert-gas enclosure to the cell rivets. The precise and repeatable measurement of the resistance of these leads, which were subject to a temperature gradient of 600°C, was found to be difficult. For this reason, the cell of Fig. 1 was modified by the addition of two rivets which served to allow the potential between the Na and Sn electrodes to be measured while passing current through the other two leads. In all cases, a plot of cell voltage against current density resulted in a straight line passing through the open-circuit intercept. The measurements were repeatedly taken to current densities of 0.775 amp/cm². From these data the conductivity of this electrolyte was calculated. The results of three identical experiments provided a value of the conductivity of 2.5 ± 0.1 mho at 625°C. Measurements of the conductivity using conventional techniques with glass conductivity cells whose constants were above 100, provided a value of 2.3 mho. This value was unaltered by the use of Ag, Pt, or 3 w/o Na in Sn electrodes. This difference in conductivity value is attributable to the assumption that the liquid-metal electrodes were flat, *i.e.*, meniscus free, which is not the case. The value of 2.3 mhos is believed to be valid.

Life-Test Studies

Most of the experiments performed with the static cell were run for not more than five days, and during these times most data were manually collected. In order to study the long-time behavior of the cell, an automated life test was established. By means of a relay which was driven by a synchronous motor, a cyclic sequence of cell operations was established, and the information obtained during each phase of the cycle was recorded with a single potentiometer strip-chart recorder. The sequence of events and the fraction of the cycle devoted to each phase were: open-circuit voltage, 10%; charging current, 40%; open-circuit voltage, 5%; cell temperature, 5%; discharge current, 40%. Each cycle was of 20-min duration, and the length of time devoted to either charging or discharging the cell was thus 8 min. Since the cell was on open-circuit during the measurement of cell temperature, the total time per cycle that the cell was on open-circuit was 4 min.

The results of this life test are presented in Fig. 6. The charge and discharge currents were adjusted during the early part of the run in an attempt to keep the voltage after charge and discharge at a constant level. The degree to which these adjustments were successful is presented in Fig. 6, curve (A) showing the variation in open-circuit voltage of the cell after the charge and discharge cycles. The cell may be considered to have operated in a stable manner during most of the 31 day period. The ratio of equivalents of Na consumed during a discharge cycle to those recharged during the charge cycle are presented in Fig. 6C. The coulombic efficiencies of the cell approached a maximum of 70% during the

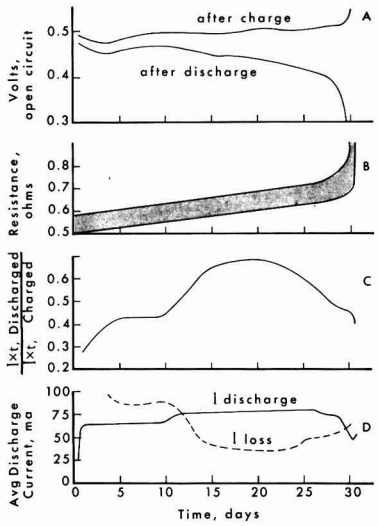

Fig. 6. Na|Sn cell life-test results

run. The average coulombic efficiency was 50.6% and 1.97 equivalents of Na were discharged during the run. Since the cell contained 0.116 equivalents at the start of the run, the quantity of electricity withdrawn from the cell was 16 times that represented by the original quantity of Na placed in the cell. The discharge current during the run is shown in Fig. 6D. The average discharge current for the entire cycle was 71.0 ma corresponding to 18.3 ma/cm². This value corresponds to an average discharge current of 45.9 ma/cm² during the 40% portion of the cycle. The difference between charge and discharge current averaged over the complete cycle, I_{loss}, is plotted as the dashed line of Fig. 6, curve (D). Measurements of cell resistance during charge and discharge were taken periodically during the run. These values were obtained by measuring the change in cell voltage due to a known current flow, both charging and discharging. The results were variable and are presented as the range of resistance shown in Fig. 6B. Based on the average coulombic efficiency and the average discharge current, the loss in current due to nongalvanic processes in calculated to be 17.9 ma/cm². This value has been applied as a correction to the data of Fig. 5, curve (b).

Inspection of the cell after the conclusion of the life test showed that cell failure was caused by loss of Na from the cell due to an imperfect seating between the cell and the cell cap. The alumina and the rivets showed no sign of attack, other than a surface blackening of the alumina, presumably due to the reduction of traces of SiO_2. The porous matrix employed showed no major attack, but after washing with water, the disk exhibited a loss of mechanical strength.

The studies performed with the static cells demonstrated that the concentration polarization was not of a magnitude to observe with the techniques employed. It was difficult to decide between concentration polarization and pen-lag effects even though the cell voltage during the life test was re-

corded employing the 12.5 mv span of a recorder whose pen-response speed was 1 sec for full-scale deflection of 25 cm. Such a low extent of concentration polarization is not significant to the operation of cells in which the greatest voltage loss is due to resistivity, and it was thus unnecessary to study this polarization further. Nevertheless, the cell of Fig. 4 was assembled and run to study the behavior of the seals and the matrix. It was found that the pressure sealing techniques were quite satisfactory and were capable of preventing liquid-metal leaks at absolute pressures as high as 2.3 atm. It was discovered, however, that the matrix employed allowed the pores to be flooded with Na metal, causing almost immediate cell failure. This short-circuiting was presumably due to the use of too large a pore size.

The high conductivity of the electrolyte, the excellence of kinetic behavior as indicated by the linear charge-discharge curves, and the low extent of nongalvanic processes have thus been demonstrated. On the basis of these results, a cell constructed of a 3 mm thick, 40% permeable matrix of the type used in these studies, employing the NaI-NaCl eutectic, should allow operation at 0.767 amp/cm^2 at 0.25v, the maximum power capability of a cell of 0.5v open-circuit potential. Such a cell would exhibit 95% coulombic efficiency when continuously operated at this current density during balanced charge and discharge periods.

Acknowledgments

The authors wish to express their gratitude to the management and personnel of development laboratories of the Norton, Alite, and Cincinnati Metal-Blast Companies. The assistance provided by these groups made possible the construction of the experimental apparatus necessary to this study.

Manuscript received Nov. 10, 1961; revised manuscript received March 15, 1962. This paper was prepared for delivery before the Detroit Meeting, Oct. 1-5, 1961.

Any discussion of this paper will appear in a Discussion Section to be published in the June 1963 JOURNAL.

REFERENCES

1. B. Agruss, Paper presented at the Detroit Meeting of The Electrochemical Society, October, 1961.
2. E. L. Shriver, "Design of a Liquid Metal Regenerative Electrochemical Cell System," Allison Division, G. M. C., 1960, Internal publication.
3. S. W. Smith and R. D. Weaver, "A Comparison of the System Weight of the Na|Sn Liquid-Metal Cell for Various Applications," Electrochemical Research Dept., Report No. 4337-E, Delco-Remy Div., G. M. C., Internal publication.
4. O. Kubaschewski and V. A. Catterall, "Thermochemical Data of Alloys," Pergamon Press, New York (1956).
5. Max. Hansen, "Constitution of Binary Alloys," McGraw-Hill Book Co., New York (1958).
6. R. E. Shearer, J. W. Mausteller, J. A. Ciarlariello, and R. C. Werner, *Proc. 14th Annual Power Sources Conference*, p. 76-7 (1960). Published by PSC Publications Committee, P. O. Box 891, Red Bank, N. J.
7. C. B. Jackson, *Proc. 12th Annual Battery Research and Development Conference*, p. 107 (1958). Published by the Battery Conference Committee, Power Sources Division, U.S.A.R.D.L., Fort Monmouth, N. J.
8. R. C. Werner, R. E. Shearer, and J. A. Ciarlariello, *Proc. 13th Annual Power Sources Conference*, p. 122-4 (1959). Published by the Power Sources Conference Committee, Power Sources Division, U.S.A.S.R.D.L., Fort Monmouth, N. J.
9. Niel N. Ault and L. H. Milligan, *Am. Ceramic Soc. Bull.*, **38** [11], 661 (1959).
10. "Selected Values for the Thermodynamic Properties of Metals and Alloys," Minerals Research Laboratory, Institute of Engineering Research, University of California, Berkeley, Calif., Sept. 1959, Na, Sn Section, p. 3-4.

Formation of Porous Metal Plates by Electrolytic Reduction

I. Electrolytic Reduction of Metal Compounds under Controlled Physical Pressure

C. M. Shepherd and H. C. Langelan

United States Naval Research Laboratory, Washington, D. C.

ABSTRACT

Porous metal plates having high surface areas and considerable mechanical strength were produced by the reduction of pasted metal compounds under controlled physical pressures in an electrolytic cell. The porosity of the metal plate is a function of the pressure applied during electrolysis and the metal content of the compound being reduced. Successful reduction depends upon using the proper combination of metal compound and electrolyte. Porous metals formed successfully by this technique included Ag, Fe, Bi, Sn, Sb, Zn, Cu, Cd, Pb, and the following mixtures, Sn-Pb, Zn-Hg, Cd-Zn, Ag-Cu, and Cu-Zn. Porosities as low as 42% and as high as 89% were obtained. A small variation in the porosity of such a metal electrode may have a serious effect on its capacity as a battery anode.

A large number of metal compounds can be mixed with a suitable liquid, pasted on a metal screen, and reduced to the corresponding metal when made the cathode in an electrolytic cell. If such an electrode is suspended openly in the electrolyte, the pasted compound may be shed from the screen before it has a chance to be reduced. If a metal deposit is obtained in this manner, it is apt to be

crumbly, slightly adherent, and have little strength. Zinc oxide gives such a deposit in a potassium hydroxide electrolyte. However, when a cell assembly consisting of pasted zinc oxide cathodes, silver anodes, and separators is packed into a tight fitting cell case and charged in a potassium hydroxide electrolyte, the zinc oxide is reduced to a compact, adherent, porous zinc plate which has considerable physical strength. It seemed probable that the tight packing of this cell assembly placed a pressure on the pasted zinc oxide which was responsible for the reduced zinc being in a compact form. Special equipment was designed for reducing pasted electrodes in an electrolytic cell under controlled physical pressure.

Metal plates formed in this manner are highly porous, resistant to crumbling in most cases, and have a large surface area that is readily contacted by liquids upon immersion. They are particularly excellent for use as battery anodes that are to be discharged at high rates.

The purpose of this study was to determine some of the factors that are involved in the formation of porous metal plates by the electrolytic reduction of pasted metal compounds under pressure.

Experimental

A paste of the proper composition was made from the particular compound and electrolyte, and it was applied evenly to both sides of a 3.8 cm^2 fine-mesh, wire screen. Enough material was used to give metal plates approximately 0.2 cm thick. The pasted screen was pressed in a die to remove any slight excess of liquid present, to remove air bubbles, to give better adherence to the wire screen grid, to distribute the paste evenly over the grid, and to give the flat, parallel surfaces that were necessary in the subsequent cell assembly. The paste extended well above the surface of the wire screen in which respect it was different from the average commercial battery plate where the paste is inside the pockets of the grid. The problems involved in pasting are so serious that they have been made the subject of a separate study (1).

The order of assembly of the charging equipment is shown in Fig. 1. The pressed electrode was placed between two flat-sheet, inert anodes, generally nickel, each of which was wrapped in a single layer of unsealed cellophane. The electrode assembly was then put in a cell case which consisted of a snug-fitting, flexible bag made of 3-mil polyethylene. The cell assembly was put in a rigidly secured container and placed solidly against one end. A thick polystyrene pressure plate was placed against the other side of the cell assembly. The rounded tip of the lever arm was placed in the rounded indentation in the center of the pressure plate. The upper extension of the lever arm was kept level as weights were added to the hook to give the desired pressure on the pasted electrode. The applied pressure is a linear function of the weight used and was determined theoretically and checked by calibration. After the pressure was applied to the cell assembly, the current was turned on and sufficient electrolyte was added to cover the electrodes. The cells were charged at a rate that gave complete reduction in about 18-24 hr. In general, the charging conditions did not appear to be critical.

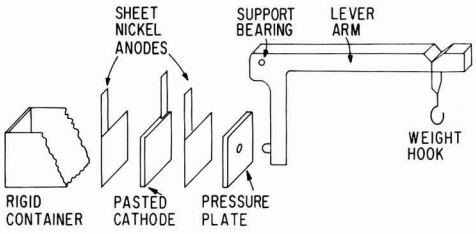

Fig. 1. Apparatus for reducing pasted electrodes under controlled pressure.

At the end of the charge, the porous metal electrode was removed from the cell, thoroughly washed, dried in a vacuum and stored in an inert atmosphere. The porosity, P, which is defined as that fraction of the total volume of the plate that is occupied by pores or void spaces, was determined by liquid absorption. The results were reproducible to ± 0.0007.

Results

Sixty grids were pasted with a mixture of 5.0g ZnO and electrolyte and then reduced in 32.6% KOH to form porous zinc plates approximately 2 mm thick and containing 4.0g of zinc. The average porosity obtained at various pressures is plotted in Fig. 2 and was found to decrease from 0.81 to 0.71 as the pressure was increased. The rate of decrease was fastest at the lowest pressure where the porosity was highest and the physical structure was weakest. When the initial pressure on the cell assembly was greater than 0.2 kg/cm^2, the paste generally flowed to a certain extent and formed a bulge around the edge of the electrode which reduced to give a crumbly metal. This undesirable condition was avoided by holding the pressure during the first 20 min or so of charging at 0.2 kg/cm^2. The paste was then stiffened by the presence of reduced metal, and the pressure could be increased to as much as 0.8 kg/cm^2. At the end of approximately another 20 min the pressure could be increased to as much as 1.6

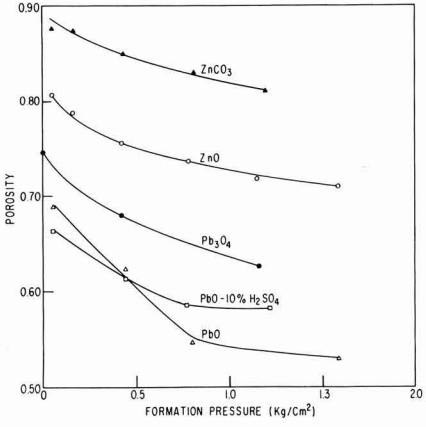

Fig. 2. Effect of formation pressure on porosity

kg/cm². An increase in the length of these initial forming periods at low pressures was accompanied by an increase in the porosity. The optimum length of the initial low-pressure formation periods varied somewhat with the material being reduced and the conditions of reduction.

Porous zinc electrodes were also produced by the reduction of $ZnCO_3$ in 32.6% KOH. Results are shown in Fig. 2.

A number of these zinc electrodes were discharged individually in an alkaline cell between two AgO cathodes at 20°C and 10 amp using 10 cc of 40% KOH electrolyte. Under these conditions, the zinc electrode was the limiting factor on cell capacity. In Fig. 3, the capacity in minutes is plotted against per cent porosity. A peak is reached at a porosity of 82%. At higher porosities, the physical structure is weakened and the zinc crumbles during discharge, and at lower porosities the electrode is stronger physically, but the total surface area is less; therefore, the current density is higher and the capacity is lower. The curves in Fig. 2 and 3 show that the capacity was seriously affected by the porosity and consequently was also affected by the pressure used during the electrolytic reduction. The maximum capacity was obtained only under a fairly narrow range of porosities. Careful control of these conditions is essential if one is interested in specialized characteristics such as high current density discharge rates or minimization of battery weight.

The porosity-pressure curves for lead plates formed by the reduction of Pb_3O_4 and PbO are shown in Fig. 2. Pb_3O_4 can be reduced at zero pressure to give a solid physical structure. Many materials that reduce satisfactorily in an electrolytic cell under pressure, either fail to reduce at all if no pressure is applied or reduce incompletely or reduce to give a nonadherent, spongy metal deposit. All of the reductions discussed here were made with a 32.6% KOH electrolyte unless otherwise indicated on the porosity-pressure curves. PbO was reduced in a 32.6% KOH and also in a 10% H_2SO_4 solution. The difference between the two pressure-porosity curves for PbO is not nearly as large as the difference between the PbO and Pb_3O_4 curves. In the case of a particular metal, changing the compound to be reduced probably has more effect on the porosity than changing the electrolyte that is being used with a given compound.

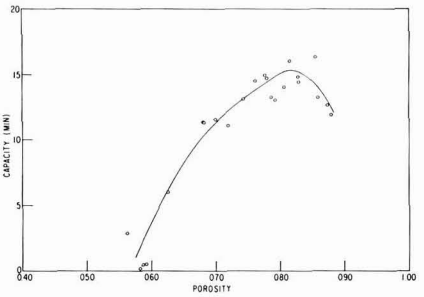

Fig. 3. Effect of porosity on cell capacity

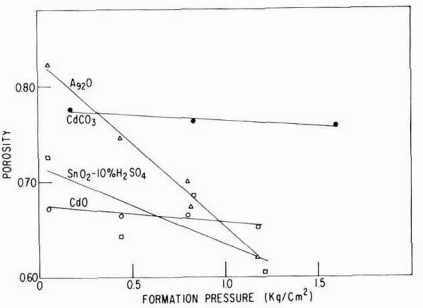

Fig. 4. Effect of formation pressure on porosity

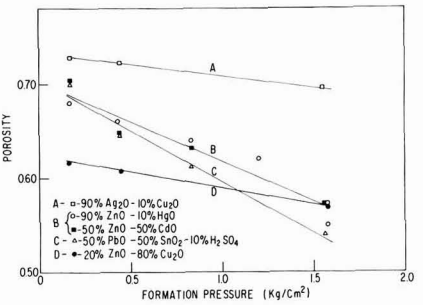

Fig. 5. Effect of formation pressure on porosity

Porosity-pressure curves for the formation of porous plates of cadmium, tin, and silver are shown in Fig. 4. Results obtained from the reduction of various mixtures are shown in Fig. 5. Satisfactory porous plates were not obtained whenever a mixture of compounds was tried that contained an appreciable amount of a compound that would not reduce by itself. Porosity curves for copper and antimony are given in Fig. 6. By using three different compounds, it was possible to prepare copper plates covering most of the range between 0.40 and 0.90 porosity.

In addition to the compounds shown in Fig. 2, 4, 5, and 6 successful reductions to satisfactory porous metal plates were also obtained using FeS, AgO, $Bi_2O_2CO_3$, and PbO_2 in KOH electrolyte. The reduc-

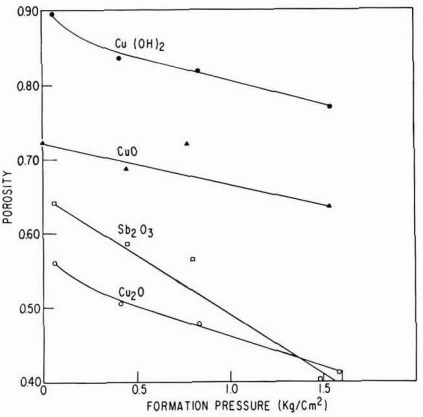

Fig. 6. Effect of formation pressure on porosity

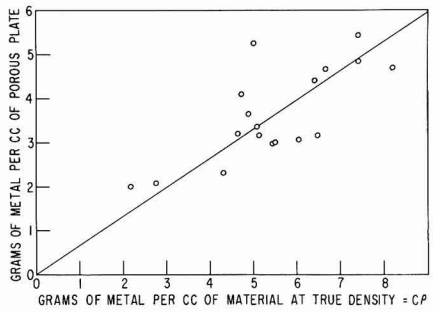

Fig. 7. Estimation of porosity from the amount of metal in the original material. Pressure = 1.5 kg/cm².

tion of HIO_3 in a saturated solution of KIO_3 gave a porous plate of iodine that was adherent and had some physical strength. This was the only porous plate of a nonmetallic substance that was formed by electrolytic reduction.

A wide range of porosities was obtained from the various compounds that were successfully reduced. In the case of a particular metal such as zinc, lead, cadmium, or copper, the compound that contained the lowest percentage of that metal gave a porous plate having the highest porosity when reduction was made at constant pressure. This is illustrated in Fig. 2, 4, and 6. In Fig. 7 the grams of metal per cubic centimeter of porous plate have been plotted against the grams of metal per cubic centimeter of compound at its true density for a formation pressure of 1.5 kg/cm². Similar curves were obtained at other formation pressures, and in all cases a straight line through the origin gave a reasonable fit and was statistically significant.

An approximate prediction of the porosity may be made from the empirical equation

$$P = 1 - (0.472 + 0.127p)C\frac{\rho}{\rho_m} \qquad [1]$$

where P is the porosity expressed as a fraction, ρ_m is the density of the metal, p is the formation pressure, C is the per cent of metal in the compound being reduced, and ρ is the true density of the compound. Porosities were calculated by means of Eq. [1] on all available data and found to have an average deviation of 0.056 from the measured values.

The shape and slope of the porosity curve may be a function of the particular metal involved. In Fig. 2, it can be seen that the $ZnCO_3$ porosity-pressure curve is roughly equidistant from the ZnO curve, and the curve for Pb_3O_4 is roughly equidistant from the two PbO curves. In Fig. 4 the straight lines for $CdCO_3$ and CdO are nearly equidistant and the same is true for the CuO, Cu_2O, and Cu $(OH)_2$ porosity-pressure curves in Fig. 6. Although these data are too limited to be conclusive, they do indicate that the porosity-pressure curves for various compounds of a given metal may be approximately equidistant.

Discussion

Not all metals can be formed into porous plates by electrolytic reduction using the techniques described here. All but one of the metals that were reduced in this manner were observed to have 18 electrons in their penultimate electron shell.

On the basis of their behavior in electrode systems and various other properties, Piontelli (2) divided metals into three classes, namely normal, inert, and intermediate. Lyons (3) has discussed Piontelli's classification of metals on the basis of their electrodeposition from aqueous solutions. These divisions are shown in Table I which omits some of the metals that cannot be electrodeposited readily. All but one of the metals that formed porous plates by reduction was in the normal group. One success was obtained in the inert group.

The normal metals have considerable variation in their properties, particularly in regard to their electrodeposition from aqueous solutions. A study of these anomalies shows that they can be reconciled by dividing the normal metals into two sub groups, the normal-electropositive, which contains the normal metals having a low electronegativity and the normal-electronegative which contains the normal metals having a high electronegativity. The normal-electronegative metals can be electrodeposited readily from aqueous solutions, and most of them are plated commercially at efficiencies of approximately 100%. The amount of ionic character in a bond involving a metal of this group is considerably less than for the corresponding compound involving a metal of the normal electropositive group.

All of the porous metals that were formed by the technique described here belong to this normal-electronegative group with the exception of iron and of antimony which is on the border line and possibly should be reclassified. No failures were obtained within this group. However, no experiments

Table I. Electrolytic classification of metals

Normal (normal-electropositive)			Inert							Normal (normal-electronegative)					Intermediate
Li															
Na															
K	Ca	Sc	Ti	V	Cr	Mn	Fe	Co	Ni	Cu	Zn	Ga	Ge	As	
Rb	Sr	Y	Zr	Nb	Mo	Tc	Ru	Rh	Pd	Ag	Cd	In	Sn	Sb	Te
Cs	Ba	La*	Hf	Ta	W	Re	Os	Ir	Pt	Au	Hg	Tl	Pb	Bi	Po
Fr	Ra	Ac**													

* Lanthanides.

** Actinides.

were conducted using gold, gallium, indium, and thallium. Attempts to reduce porous plates from arsenic, selenium, and tellurium compounds were unsuccessful, even though some reduction could be obtained. Most of the 15 inert metals lying to the right of vanadium in Fig. 1 can be electrodeposited successfully from the proper aqueous solution with current efficiencies that vary from quite low on up to 100% in a few cases. However, all attempts to produce pure porous plates of these metals were failures. A considerable number of unsuccessful attempts were made using various electrolytes and a good many different compounds of nickel, cobalt, iron, manganese, chromium, molybdenum, and tungsten. All attempts were unsuccessful that used mixtures of these compounds and other compounds that reduced readily such as HgO. However, FeS containing 20% graphite reduced readily in a 15% KOH solution. When success is obtained with any of these metals, it probably will be under conditions that are much more restricted than those observed in the normal-electronegative group.

Given a metal that can be formed by reduction using these techniques, it is necessary to find the proper combination of metal compound and electrolyte that will make this reduction possible. Whenever a compound of a metal in the normal-electronegative group that was slightly soluble in the electrolyte was tried, successful reduction to a porous metal plate was always achieved. A slight solubility is not a necessary condition and probably not a sufficient one. If the compound was highly soluble in the electrolyte, failure resulted due to the paste dissolving off the grid. In the case of moderately soluble compounds, the reduction is generally more apt to be successful if the electrolyte is saturated with the compound to be reduced. The solubility of the material indicated that electrodeposition from the metal ion could be the major factor in the reduction mechanism.

A number of compounds were found that could be reduced to a porous metal plate even though they were very insoluble in the electrolyte. Most of these could be checked in the literature and were found to be relatively good conductors of electricity. This suggests the possibility that the compound is reduced to metal in the solid state without first going into solution.

Some compounds might be reduced by atomic hydrogen evolved at the cathode. Sancelme (4) has proposed this mechanism for the reduction of certain oxides. His compounds were placed loosely on top of a platinum cathode, and consequently their reduction might also be explained on the basis of other mechanisms.

Manuscript received Oct. 20, 1961; revised manuscript received April 11, 1962. This paper was prepared for delivery before the Houston Meeting, Oct. 9-13, 1960.

Any discussion of this paper will appear in a Discussion Section to be published in the June 1963 JOURNAL.

REFERENCES

1. C. M. Shepherd and H. C. Langelan, *This Journal*, **109**, 661 (1962).
2. R. Piontelli, *J. Chim. Phys.*, **45**, 115 (1948).
3. E. H. Lyons, *This Journal*, **101**, 363 (1954).
4. A. Sancelme, *J. Chim. Phys.*, **49**, C117 (1952).

Formation of Porous Metal Plates by Electrolytic Reduction

II. Electrode Pasting

C. M. Shepherd and H. C. Langelan

United States Naval Research Laboratory, Washington, D. C.

ABSTRACT

The successful formation of a porous metal plate from a pasted electrode under pressure in an electrolytic cell depends on the use of an ideal paste wherein the individual particles of the pasted material are compacted closely together. Just enough liquid is present to fill the interstices between the particles and to take care of what is adsorbed on the surface and in the pores of the particles.

Ideal pastes were prepared from 29 water-insoluble, inorganic metal compounds, and it was found that the ease of pasting and the quality of the paste improves markedly with decrease in particle size of the material being pasted. The best pasting conditions are obtained with materials whose particle size distribution has a geometric mean diameter of less than 0.7μ. The best estimate of pasting quality can be obtained from R, the ratio of the true density of a material to its tap density. When R is greater than 3.8 for a material, it has good pasting qualities.

In using the techniques of Shepherd and Langelan (1) to prepare a porous metal plate by electrolytic reduction of a pasted compound under controlled pressure, successful results depend on several essential factors, one of which is the pasting properties of the compound or mixture that is being used. There is an optimum range of pasting conditions which must be maintained in order to obtain a good porous metal plate. For some materials, this range is very narrow and difficult to maintain. For other materials the range is somewhat wider; satisfactory pasting is comparatively easier to achieve, and the quality of the reduced metal plate is better. The problem is aggravated by the fact that the com-

pound is spread as a stiff paste on top of a wire screen which has a minimum of support to hold it in place and then is immersed in an electrolyte which may tend to cause shedding. A much simpler problem exists in the pasting of commercial battery plates, where the paste is held in pockets and can vary in consistency from very stiff to soft and mushy.

A brief study was made here of each of a large number of compounds in an attempt to find some of the general principles involved in pasting. Although the substances surveyed were limited to metal compounds that were insoluble in water, it is highly probable that the results of this study will apply to many other types of materials. The metal compounds tested included many that could not be reduced to porous metal plates.

Experimental

Five to ten grams of powdered material plus a suitable amount of liquid were made into a paste and applied evenly to both sides of a 3.8 cm^2 wire screen. The pasted screen was wrapped in a single layer of facial tissue to prevent sticking, then put between two Teflon sheets, placed in a close fitting metal die the size of the screen, and pressed in a Carver press at enough pressure to give a final, flat, smooth homogeneous pasted electrode. The plunger was made slightly smaller than the cavity of the die, thus avoiding a waterproof seal and making it possible to press excess liquid out of the pasted plate. An ideal paste was completely retained under these conditions. When the first increment of the pressure was applied to a properly prepared paste, the paste flowed some and was accompanied by a flow of liquid out of the paste. Consequently, the pressure dropped. Further increments of pressure were applied fairly rapidly until a pressure was reached that held steady for several seconds before it started to drop. This pressure was called the minimum pasting pressure. At this point the pasted grid was finished and ready to remove from the die. Large variations of the pasting pressure had no detectable effect on the porosity of the final metal plate as long as the minimum pasting pressure was achieved.

If the compound was to be reduced to metal, the plate was removed from the die and placed quickly without drying or curing into a special cell where it was reduced electrolytically under a controlled physical pressure.

Experimental Results and Discussion

It was found that a porous metal plate having optimum properties in regard to such characteristics as strength and resistance to crumbling could be produced whenever the individual particles in the pressed paste were compacted closely together and had just enough liquid present to fill the interstices. Pastes of this type, prepared from various compounds, were found to have a number of physical properties in common and are defined here as ideal pastes. The ideal paste has a dry appearance, is slightly flexible, and yet is not crumbly. The percentage of liquid present in a particular powder-liquid combination is fixed within fairly narrow limits. An excess of liquid tends to separate from the ideal paste, particularly when it is subjected to pressure. A deficiency of liquid causes the paste to be dry and crumbly. In this condition it readily absorbs liquid. This description of an ideal paste is not limited to pastes that can be reduced electrolytically to a porous metal plate. This study was made using a large number of various water-insoluble, reducible, and irreducible metal compounds pasted with water or aqueous electrolytes and undoubtedly can be extended to pastes made from many other types of compounds and liquids. If the compound was to be reduced electrochemically to the metal, the liquid medium used to prepare the paste was some of the electrolyte in which the reduction was to take place. If the material being pasted was slightly soluble, then a saturated solution of the material in the electrolyte was used in most cases as the pasting liquid. All of the numerical data presented here were obtained from pastes made with a liquid binder of pure water.

The amount of liquid used is the main factor that has to be controlled in making a satisfactory paste. The best results are obtained by using a very slight excess of liquid in forming the paste. This excess is pressed out and can be detected when the pasted grid is removed from the die. Under ideal conditions the excess liquid is accompanied by no more than a very slight trace of the material being pasted. The reading of the minimum pasting pressure is clear on a paste containing the proper amount of liquid. If the paste is too dry, it does not flow well under pressure and forms low spots in the electrode where the amount of paste is less than average. A dry paste does not wet the grid properly and will not be adherent. It is grainy, crumbly, and tends to shed, particularly on edges and corners, whenever it is handled and when the electrolyte is added. When this dry paste is charged, reduction may be incomplete in the low spots, and any metal formed there may be crumbly and nonadherent. The pressure present in the electrolytic cell is light and is applied mainly to the high spots where the paste is thickest and these areas reduce satisfactorily.

If the paste is too wet, it is sticky and tends to pull off the screen when removed from the die. If the paste is excessively wet it flows off the screen like water when pressure is applied in the die.

There is a considerable variation in the pasting properties of various compounds. It was possible to divide all of the compounds tested into five arbitrary groups depending on their ease of pasting and quality of the paste. These groups were labeled "very poor," "poor," "fair," "good," and "very good." Since these divisions were based on the judgment of the operator, they were not sharp and there was a certain amount of overlapping. It was very difficult to maintain proper pasting conditions with compounds in the very poor group. The poor group was somewhat better. Compounds in the good group pasted satisfactorily by using a little care. Compounds in the very good group were pasted successfully over a fairly wide range of conditions, and the pasted grids were subjected to considerable handling and other abuse without showing any appreciable deteriora-

tion. The liquid content in the paste had a wider range of acceptable limits for a very good material than it had for a very poor material. Compounds in the good and very good groups were the only ones that came close to forming "ideal" pastes. The fair to very poor groups deviated to some extent from the above description. Thus, the ideal paste can be looked on as a limit that is approached as one moves from a very poor to the very good material. Very poor compounds when pasted and reduced electrolytically under pressure generally gave porous metal plates that were grainy and crumbly whereas the good and very good compounds gave porous metal plates that had good physical properties and were not crumbly. The fair and poor compounds also produced good porous metal plates, if they were properly pasted.

At this point the concept of an ideal paste and the outline of pasting conditions as given here are qualitative descriptions based on the qualitative observations and personal opinion and evaluation of the authors. A more scientific evaluation of pasting is needed. It is desirable to have some quick reproducible test or measurement that will predict the pasting properties of a powdered material, thus simplifying industrial control and also making it possible to evaluate the relationship of pasting properties to other variables. The liquid content and minimum pasting pressure give a fairly good estimate of the paste group, but can be determined only after the material has been successfully pasted and consequently the pasting properties are already known.

It was found that good predictions of pasting properties could be made from the quantity R_1, which is defined as the ratio of the true density to the apparent density. The apparent density is defined as the grams per cubic centimeter of unpacked material, which is free from pockets or unfilled cavities. In this condition, adjacent particles are as close together as they will get without being subjected to some compacting, mechanical force such as tapping. In Fig. 1 the pasting properties of the various materials under study are plotted against values of the dimensionless quantity R_1. The compounds and mixtures are listed from top to bottom in the order of their ease of pasting. The paste groups are also indicated. These materials cover a wide range of water-insoluble metal compounds. There are a few materials of this type that would not fit into this analysis such as MoS_2 which does not wet and $CaSO_4$, which hardens.

The data in this report are subject to considerable variation because the relationships are not exact and because the assignment of paste groups is an arbitrary factor. By the use of statistical procedures all of the relationships presented in this paper were shown to be highly significant. The Spearman rank coefficient of correlation, r_s, for the data in Fig. 1 is 0.914. Values of r_s for other relationships are given in Table I.

An excellent prediction of the paste groups can be made from

$$R = \frac{\rho}{\gamma}$$

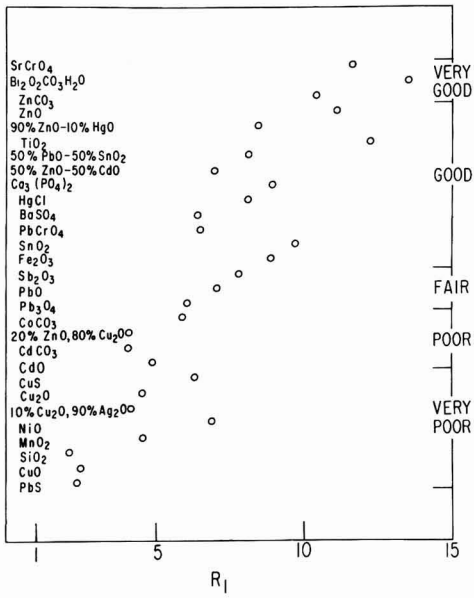

Fig. 1. Relationship between the ease of pasting and R_1, the ratio of the true density to the apparent density.

where ρ is the true density of the material and γ is its tap density. The tap density which has also been called packed density, bulkiness, and bulk density is the density in grams per cubic centimeter obtained by placing the powder in a cylinder and tapping to a constant volume. There are a large number of factors in the determination of the tap density that may cause variations as high as 7% in the results (2-5). All of the measurements used here were made with a glass cylinder which weighed 22g and had an internal diameter of 1.15 cm. The height of powder at the end of the tapping was approximately 6 cm and the tapping rate was 30 times per minute. The cylinder was inclined 10° from the vertical and dropped in a free fall of 2 in. on a hardwood base. If a loose layer formed on the top of the powder, it was either poured off or compacted by rapid vibration. Tapping was continued until no change in volume was observed for eighty taps. Under these fixed conditions the results were reproducible in most cases to within 2% if ordinary care were taken.

Average values of R for the various paste groups are shown in Table I. R can be determined in a few

Table I. Properties of the paste groups

Paste group	Average value of $R = \frac{\rho}{\gamma}$	Average value of particle size, d_μ μ	Average value of the minimum pasting pressure kg/cm²	Average H_2O content vol-%
Very good	5.48	0.303	4.16	59.7
Good	4.61	0.536	59.7	54.2
Fair	3.22	0.780	156	42.8
Poor	2.53	0.971	194	36.5
Very poor	2.12	1.240	245	32.1
Spearman rank coefficient of correlation, r_s	0.918	0.794	0.834	0.821

minutes and gives an excellent estimate of the pasting properties. All of the materials in the good and very good paste groups had values of R greater than 3.8. All of the materials that were more difficult to paste were in the very poor, poor, and fair paste groups and had values of R less than 3.8.

Roller (2) and Shapiro and Kolthoff (6) have shown that the bulkiness of various powders increases rapidly as the particle size decreases below a critical value. As a consequence, R should increase with decrease in particle size, and the particle size should decrease in going from the very poor to the very good paste group. The particle size distribution was determined microscopically on the materials listed in Fig. 1. The geometric mean diameter, d_g, was chosen as the typical particle size. It is defined by the formula

$$\ln d_g = \sum f \left(\frac{\ln d}{n} \right)$$

where n is the number of particles and f is the frequency of occurrence for particles having a particular measured diameter, d. The average values of d_g for each of the paste groups are shown in Table I. From a practical viewpoint most materials that had a value of d_g less than 0.7 microns fell in the good or very good paste groups and could be pasted easily. This was not a particularly sharp division and did not give as good a separation of the paste groups as R. Moreover, it was much more difficult to determine. However, it seems likely that the particle size distribution is the most important factor in determining the paste group of a given material. Consequently, a poor pasting material can be converted in most cases into a good pasting material by preparing it in a finer size.

The average values of the minimum pasting pressures for each of the paste groups are shown in Table I. The very poor paste group had an average minimum pasting pressure that was more than 50 times as large as the average for the very good group.

The average water content of the different paste groups is shown in Table I. Humidity changes affect the pasting of a very poor compound since the volume of liquid used is quite small and must be held within very narow limits. For a very good material the volume of pasting liquid can be varied over much wider limits and still give satisfactory pasting conditions over a moderate range of humidities. If a satisfactorily pasted screen is allowed to dry, it cracks and becomes crumbly. The time of storage in open air before this deterioration occurs depends on the humidity and was about 2 min for a very poor paste and about 20 min for a very good paste. Longer storage periods can be achieved by the use of controlled humidity chambers.

The pasting properties of a particular compound depend to a certain extent on the liquid used in making the paste. A better, more homogeneous paste is obtained in most cases if the compound is slightly soluble in the liquid or reacts chemically with it to a limited extent. An excessive reaction or a high solubility is generally undesirable. Water is a comparatively poor liquid for pasting water insoluble compounds. Ten per cent H_2SO_4 is much better. The best liquid tested was 32.6% KOH, and this was used for pasting most of the compounds that were reduced electrolytically. Tests on a number of compounds using these three liquids show that, if the compounds are labeled by rank according to ease of pasting with a particular liquid, there is a good correlation with the results obtained by using another pasting liquid. Thus, the compounds that paste best with water paste best with 32.6% KOH and the ones that paste poorest with water are poorest with KOH even though water gives poorer over-all results. The difference in the pasting properties of liquids showed up mainly in the fair, poor, and very poor groups. All of the numerical data presented in this report were obtained by using pure water as the liquid medium.

In preparing a porous metal electrode of controlled porosity by electrolytic reduction of a pasted metal compound a number of difficulties are encountered due to the fact that the paste rests on top of the grid and is subjected to physical pressure. These difficulties are minimized by preparing an ideal paste of controlled composition and physical properties from a material having a fine particle size distribution.

Manuscript received Oct. 20, 1961; revised manuscript received April 11, 1962. This paper was prepared for delivery before the Houston Meeting, Oct. 9-13, 1960.

Any discussion of this paper will appear in a Discussion Section to be published in the June 1963 JOURNAL.

REFERENCES

1. C. M. Shepherd and H. C. Langelan, *This Journal*, **109**, 657 (1962).
2. P. S. Roller, *Ind. Eng. Chem.*, **22**, 1206 (1930).
3. D. M. Peppard, *Anal. Chem.*, **24**, 1869 (1952).
4. T. T. Cocking, *Pharm. J.*, **107**, 226 (1921).
5. J. C. Macrae, P. D. Finlayson, and W. A. Gray, *Nature*, **179**, 1365 (1957).
6. I. Shapiro and I. M. Kolthoff, *J. Physical and Colloid Chem.*, **52**, 1020 (1948).

Multiple Rate Transitions in the Aqueous Corrosion of Zircaloy

B. Griggs, H. P. Maffei, and D. W. Shannon

Hanford Atomic Products Operation, General Electric Company, Richland, Washington

ABSTRACT

The weight gain of Zircaloy-2, -3, and low nickel Zircaloy-2 during water and steam corrosion is shown to go through two or more repetitive cycles. The evidence indicates these weight gain curves truly represnt the corrosion kinetics. Several corrosion mechanisms are considered in the light of these kinetics. While no definite mechanism can be established, a supposition that stresses in the film periodically cause it to crack at or near the oxide-metal interface appears consistent with the data. Preliminary micrographic evidence supporting the existence of a cyclic corrosion process also is shown.

The rate of corrosion of Zircaloy-2 in high-temperature water has usually been represented (1, 2) as an initial cubic relation of weight gain to time, followed by a linear relation. The "transition point" between these two modes of corrosion is sometimes accompanied by a change in the appearance of the oxide film (2, 3) from black to gray or white. Most of the previous data have indicated only one transition point in the corrosion process. More recently, there has appeared (4, 5) some evidence that the cubic portion of the curve is followed by two linear curves, the first a short steep curve and the second a flatter curve for the balance of the test.

The "weight gain *vs.* time" data for several Zircaloys presented were obtained over several years at the Hanford Atomic Products Operation. These weight gain curves demonstrate a cyclic corrosion process with several rate transitions. The two-step transition (4, 5) would be interpreted as the second cycle of this repetitive process.

Experimental Details

Zircaloy coupons were exposed in refreshed autoclaves at 360° and 400°C. Deionized water (4 ppm O_2 from air) was pumped through the preheater, through the AISI 316 stainless steel autoclave, and out through a cooler and relief valve. The 5-gal, 360°C autoclave was operated at a flow of about 8 l/hr. The 1-liter, 400°C autoclave was operated at a flow of 0.4 l/hr. The coupons were suspended on AISI 347 stainless steel wire racks.

The coupons were rolled sheet material of Zircaloy-2, -3, and low nickel Zircaloy-2 (Table I), prepared by chemical etching 2 mils of each surface in 33 w/o HNO_3-1.85 w/o HF, and thorough rinsing. The etched coupons were weighed, autoclaved, dried at 110°C for 1 hr, reweighed, and returned to the autoclave for further exposure.

Coupons were weighed to ±0.02 mg and measured to ±0.002 dm^2. The samples in Fig. 4, however, were weighed to only ±0.2 mg and measured to

Table I. Alloys used in studies

Alloy No.	Alloy	Description
1021	Zircaloy-2	Rolled sheet (30 mils) produced from ingot 5Y-HO-9. Analysis below.
ZH	Zircaloy-2	Rolled sheet (62 mils) produced from ingot SA-11857. Analysis below.
L or H	Low nickel Zircaloy-2	Rolled sheet (25 mils) produced from ingot 28260-4-6V. Analysis below.
KE-46	Low nickel Zircaloy-2	Rolled sheet (30 mils) produced from ingot KE-46. Analysis below.

Analyses

	Per cent					ppm					
Alloy	Sn	Cr	Fe	Ni	N_2	O_2	Al	Cd	B	Cu	Pb
1021	1.34	0.16	0.13	0.05	0.004	—	40	<0.5	<0.5	16	60
ZH	1.31	0.14	0.18	0.05	0.003	1083	32	<0.5	0.4	23	33
L	1.50	0.097	0.14	<0.003	0.003	—	<30	<0.5	<0.5	<20	<15
KE-46	1.39	0.09	0.14	<0.002	0.005	—	26	<0.5	0.4	<20	<20

	ppm								
Alloy	Mg	Mn	Si	Ti	V	Mo	Co	Zn	C
1021	<20	<10	30	10	<10	<10	<5	—	42
ZH	13	57	27	25	<20	<10	<5	<50	—
L	<15	<10	43	20	<20	<20	<5	<10	176
KE-46	<20	<20	49	<20	<20	<20	<20	—	<100

± 0.002 dm^2. Coupons were about 7 to 13 cm^2 of surface area. Corrections for edges and holes were included in the areas. Weight gains were not corrected for hydrogen pickup. Errors in weight of ± 0.02 mg could give rise to a maximum deviation of ± 0.3 mg/cm^2 and ± 0.2 mg/cm^2 for samples of 7 cm^2 or 13 cm^2, respectively.

Discussion

The corrosion of Zircaloy-2 in high-temperature water and steam produces adherent layers of zirconium oxide on the surface of the metal. Inert marker experiments indicate that the corrosion takes place by the diffusion of oxygen ions through the oxide film to form new film near the metal surface (1, 2). This oxide is quite inert and has not been removed quantitatively without damage to the metal. Therefore, corrosion measurements on Zircaloy are determined by weight gain until it becomes apparent the oxide is sloughing. Using weight gain as a true measure of corrosion involves several assumptions. These assumptions are:

1. The ZrO_2 corrosion product is not lost from the sample. During the period prior to the first transition, the black oxide adheres tightly and there is no evidence of spalling. After the first transition, some alloys spall severely and thereby make weight gain measurements useless. However, Zircaloy-2 is noted for its adherent oxide and even after extensive corrosion, weight gains are thought to indicate the corrosion process, although some errors result. Zirconium oxide is very insoluble in water and losses from this source are insignificant.

2. Substances other than oxygen are not picked up from the system. Since all the corrosion experiments were done with high-quality demineralized water, there is no possibility for salt deposition nor were any foreign deposits observed. The weight gains of samples in different stages of the corrosion process, all of which were exposed in the same autoclave at the same time, differ considerably. Presumably any deposition would be more or less uniform on all samples. Thus there is no apparent deposition on the samples. From 5-50% of the corrosion hydrogen is absorbed by the metal. However, even at 100% absorption, the hydrogen weight gain cannot exceed 13% of the oxygen weight gain. Usually, the hydrogen analysis is destructive, and thus hydrogen cannot be corrected for until testing is complete. For normal Zircaloy-2, the hydrogen weight is negligible except for very long exposures.

3. The composition of the corrosion product is known and constant. X-ray analysis of the film before and after transition shows the film to be ZrO_2 and indicates no gross change in its composition. The oxide is said to absorb some water (6), but no hydrates are known, and the film is assumed to have constant water content after drying at 110°C.

These assumptions have been considered correct in most previous studies of zirconium corrosion. If so, the weight gain and the corrosion process go through a series of repetitive patterns, finally approaching a linear relation with time. This repetitive pattern was common to all alloys tested.

The weight gain data and the corrosion rates of Zircaloy coupons is seriously affected by minor surface or metal impurities (1, 11). Graphs of different runs using different coupon stock, different autoclaves, different surface preparation, and different autoclaving conditions show the generality of this repetitive process (12). Figures 1 and 2 are characteristic of good Zircaloy in 360°C water or 400°C steam, respectively. Figure 3 shows the corrosion curve for a poor alloy.

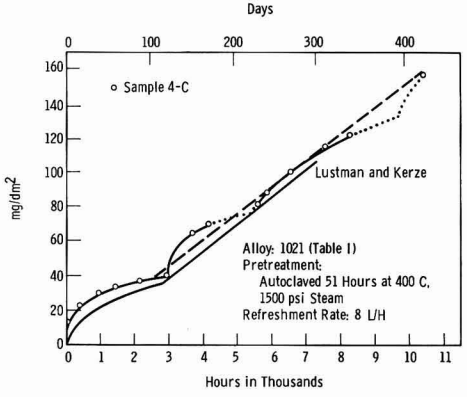

Fig. 1. Corrosion of Zircaloy-2 in 360°C, 3200 psi water

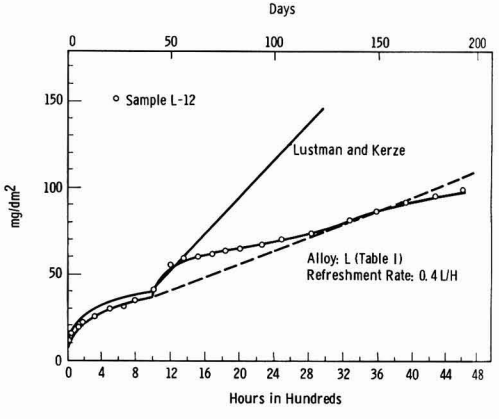

Fig. 2. Corrosion of low nickel Zircaloy-2 in 400°C, 1500 psi steam.

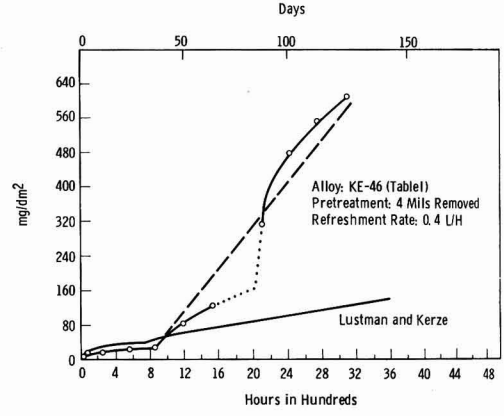

Fig. 3. Corrosion of low nickel Zircaloy-2 in 400°C, 1500 psi steam.

The weight gain of a sample *vs.* time appears in the form of at least two, and as many as four, more or less repetitive curves which resemble the initial cubic curve. Since the weight gain is more accurate than the deviations from linearity, the cycles cannot be explained by experimental error. The successive cycles of the weight gain curve are similar, but not identical. In general, the weight increase during the second cycle is somewhat lower than during the first cycle. The slope at the end of the cycle increases slightly with each cycle, finally approaching a straight line drawn from the transition point. The repetitive effect can also be observed in data from other laboratories (4, 5, 7).

Although all cycles on all coupons have nearly the same period, there is enough difference in their periods to make the use of average weight gains for several coupons misleading. There is also a difference in corrosion from one grain to the next (8), making the weight gain of a single coupon an average for many grains. Therefore, as the number of cycles increases, the coincidence of their periods could decrease and the resultant curves appear as a linear relation with time. The average corrosion of a large number of samples should cause the corrosion curve to appear as a linear function much sooner than would that of the individual samples. An example of this is shown by Fig. 4. These data show an almost linear relation with time. However, this curve was not constructed from repetitive measurements on the same sample, but from samples removed from test for each point. The cyclic behavior is lost due to variation from sample to sample.

It is not possible to define the corrosion mechanism with the available data. However, a mechanism based on mechanical stresses in the film which periodically causes the film to break away from the metal appears consistent with the data. In this model, the ZrO_2 film grows until the stresses, continually set up in the oxide, are relieved by a series of microcracks parallel to the corroding surface. This crack layer is connected to the surface by a network of larger transverse cracks, illustrated in Fig. 6, thus making the bulk of the oxide porous and not protective. After these cracks form, the diffusion path to the metal through any remaining adherent oxide is much shorter; hence, the corrosion rate increases and initiates a second cycle. This alternating process of growth and cracking continues until differences in cycle period from grain to grain become sufficiently out-of-phase to make the average weight gain of the sample appear linear with time.

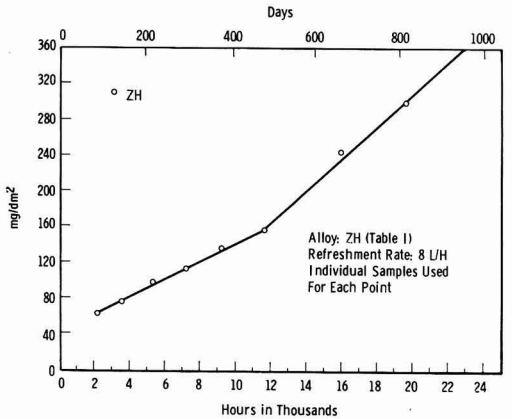

Fig. 4. Corrosion of Zircaloy-2 in 360°C, 3200 psi water

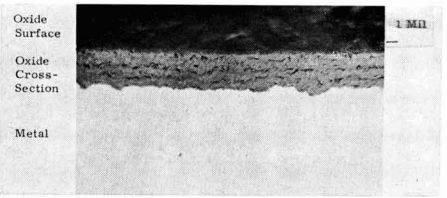

Fig. 5. Cross section of oxide on Zircaloy-2 coupon exposed 10,414 hr in 360°C water. Polishing angle: approximately 20° to oxide surface; etch: vacuum cathodic etch; magnification, 250X, bright field.

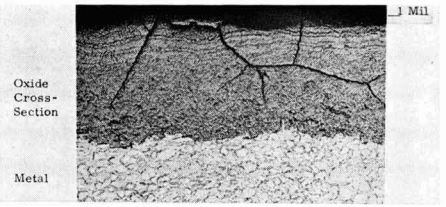

Fig. 6. Cross section of oxide on low nickel Zircaloy-2 coupon exposed 3100 hr in 400°C, 1500 psi steam. Polishing angle: approximately 20° to oxide surface; etch: vacuum cathodic etch; magnification, 75X, bright field.

Several mechanisms of Zircaloy corrosion after the "transition point" have been proposed, but none have gained universal acceptance (1, 2). These include phase transformation of the oxide film at the transition point (1) and cracking of the film at a critical thickness (1, 9). A mechanism similar to the above cracking has been described for titanium in oxygen (10).

A metallurgical section of a Zircaloy-2 coupon exposed to 360°C water for 10,414 hr is shown in Fig. 5. (The corrosion curve is in Fig. 1.) A low nickel Zircaloy-2 exposed in 400°C steam for 3100 hr is shown in Fig. 6. (The corrosion curve is in Fig. 3.) These coupons show a layered structure with the number of layers corresponding to the number of apparent cycles on the weight gain curve. This agreement tends to confirm the conclusion that the corrosion process is cyclic.

The corrosion rate curves presented by Lustman and Kerze in their Fig. 11.38 (1) are plotted to show agreement or disagreement of our data with theirs. The 360°C data agree fairly well. The 400°C data do not agree (Fig. 2 and 3). The KE-46 low nickel Zircaloy-2 is higher than the Lustman and Kerze curve. For reasons not as yet known, the other alloys corrode at a rate lower than the Lustman and Kerze data. Superior corrosion resistance in more recent lots of material may be part of the answer.

It is not possible to tell whether the Lustman and Kerze data show the cyclic process. First, their data do not cover a sufficient time span. Second, only the averages are probably represented and thus any

cyclic behavior is masked. On the other hand, their data are not inconsistent with a cyclic process.

In summary, the weight gain data of several zirconium alloys of various pretreatments all show periodic changes in corrosion rate. Layers observed in the corrosion product oxide further substantiate the cyclic character of the corrosion past the transition point.

Acknowledgments

The assistance of R. A. Thiede, W. C. Craven, S. D. Deusser, D. B. Mackey, and G. W. Mettler in autoclaving samples and processing data is gratefully acknowledged. For the cathodic vacuum etching and the electron microscopy, the authors are indebted to R. L. Hales. All are members of Hanford Laboratories.

Manuscript received Sept. 11, 1961; revised manuscript received March 26, 1962.

Any discussion of this paper will appear in a Discussion Section to be published in the June 1963 JOURNAL.

REFERENCES

1. B. Lustman and F. Kerze, Jr., "Metallurgy of Zirconium," pp. 635-640, McGraw-Hill Book Co., New York (1955).
2. G. E. Zima, HW-60908, p. 10 (1959).
3. B. Cox, AERE-R-2931 (1959); *This Journal*, **108** (1961).
4. H. Coriou *et al.*, CEA-1387 (1959); *Mem. Sec. Rev. Met.*, **57**, 511 (1960).
5. S. H. Bush, R. S. Kemper, and D. L. Gray, HW-69681 (1961).
6. A. B. Riedinger, KAPL-2000-3, p. 57 (1958).
7. A. B. Riedinger, M. S. Thesis, Union College (1958).
8. J. P. Pemsler, NMI-1177 (1957).
9. U. R. Evans, "The Corrosion and Oxidation of Metals: Scientific Principles and Practical Applications," pp. 45-6, Edward Arnold Ltd., London (1960).
10. J. Stringer, *Acta. Met.*, **8**, 758 (1960).
11. D. W. Shannon and B. Griggs, HW-60433 (1959).
12. B. Griggs, H. P. Maffei, and D. W. Shannon, HW-67818 REV (1960).

The Growth of Electrodeposits

J. M. Keen and J. P. G. Farr

Department of Industrial Metallurgy, The University, Birmingham, England

ABSTRACT

The crystal habit of copper electroplate has recently been explained in terms of the aggregation of growth layers. Experiments are described to test the applicability of this, the concept of "bunching," to the development of other electrodeposits. Zinc has been electroplated from acid sulfate solutions on zinc polycrystalline and single crystalline cathodes and on copper single crystal surfaces. The surface features observed are explained and related to those of copper electrodeposits, in terms of the supposed atomic structure of the substrate surface, of the bulk crystal structure of the deposited metal, and of the growth process. Exploratory work on the deposition of lead, cadmium, and iron on the same metals, respectively, indicates that, although the idea of "bunching" may be of wide application, caution is required in explaining growth features where chemical or electrochemical processes may be structure determining.

Recent work by Storey and Barnes (1) has indicated that the conclusions drawn from a study of the electrolytic growth habit of single crystals of copper (2-4) can be applied to the growth of polycrystalline copper substrates. Electropolished and electroetched surfaces behaved similarly. Briefly, Pick and his colleagues found, for copper, that epitaxial growth occurred with coarse crystallographic facets developing on the surface of the electroplate, up to 50 ma/cm^2. The structure could be related to the atomic configuration of the original substrate surface and to the conditions at the interface between the metal and the electrolyte. In particular the structures were consistent with the supposition that growth occurs by a bunching mechanism (5).

In normal laboratory solutions, as in practical plating solutions where additives are absent, there is an abundance of surface active material, impurity that will compete with depositing atoms for available growth sites on the substrate. Thus, if growth occurs by the spreading of atomic layers, these will tend to coalesce because of the continuous deactivation of growth sites; the coarsening will eventually be observable under the microscope, and ultimately non-epitaxial nucleation will be required if growth is to be maintained at a given rate. "Break-away" then occurs.

While the idea of "bunching" gives a satisfactory qualitative explanation of growth and it may lead to useful experiments on both the plating process and on the metallurgy of the metal produced, it is clearly not without inadequacies. It is not quantitative, even as applied to electrodeposition under laboratory conditions, but explains the growth process as being to a large extent controlled by adsorption of adventitious substances of unknown chemical nature, specific effect, or concentration. However, the concept is a general one and should apply not only to the deposition of copper; an important test of the idea is to compare the electrolytic growth of other metals. For this reason a metallographic and crystallographic study has been made of the growth of zinc electrodeposits from acid zinc sulfate solutions under conditions which were thought to be

comparable with those under which the study of copper had been made. Zinc has been plated onto single crystalline and polycrystalline substrates and onto single crystal copper surfaces. The electrolytic growth of lead, cadmium, and iron have also been examined.

Experimental Part

Preparation of the cathodes.—(In general the anodes were of similarly prepared metal.)

Copper.—Single crystal substrates were prepared as by Pick et al. (2). After electropolishing, the mounted specimens were washed with dilute phosphoric acid (6) and with water immediately before plating.

Zinc.—Large-grained polycrystalline cathodes were prepared by the critical strain-anneal method; single crystals were grown by a modified Bridgman technique. Crystals were cut and mounted in cold-setting resin. Such specimens had a heavily deformed surface layer which had recrystallized to a depth of some 900μ. After mounting they were polished carefully metallographically, the deformed layer remaining after diamond polishing being removed by electropolishing. The best surfaces were produced in a 50% by volume orthophosphoric acid-ethyl alcohol solution using a stainless steel cathode with the anode held horizontally. Optimum polishing conditions were found to exist between 1.6 and 2.0v with the solution at room temperature. All traces of deformation were removed by polishing for 4 to 6 hr.

Immediately before plating the specimens were given a further electropolish for 5 min, washed with methanol, aqueous sodium hydroxide and briefly (2-3 sec) with concentrated nitric acid. They were then washed thoroughly with water and transferred to the plating bath.

In experiments on cleavage surfaces, these were produced by cleaving a suitable crystal at liquid nitrogen temperature. A number of such faces were plated without further preparation, the remainder were mounted and etched as has been described.

Cadmium.—This metal is exceptionally soft so mechanical polishing was avoided in the later stages of electrode preparation. Coarse-grained 99.995% cadmium cathodes were prepared by the strain-anneal method. Immediately before plating they were electropolished in an aqueous phosphoric acid bath, etched lightly in dilute nitric acid, and washed with water.

Lead.—Large-grained cathodes were obtained by annealing at 150°C in vacuum. These were masked, electropolished in perchloric acid-aqueous ethanol and immediately before plating lightly etched in dilute nitric acid followed by washing with water.

Iron.—Large-grained electrodes were prepared from 99.985% N.P.L. iron by the strain-anneal method. Before plating they were electropolished in perchloric acid-acetic acid, lightly etched in dilute nitric acid, and washed.

Where "stopping-off" was required, "Lacomit" (supplied by W. Canning & Company Limited, Great Hampton Street, Birmingham) was used.

The plating solution.—Zinc.—"Analar" zinc sulfate, "M.A.R." sulfuric acid, and double-distilled water were used. The following solutions were examined: 0.5M zinc sulfate containing 0.5M, 0.1M, 0.05M, 0.025M, and 0.005M sulfuric acid, respectively. As hydrogen was evolved at the cathode, the efficiency of plating was not 100%, but the evolution was not sufficient to necessitate an increase in concentration of the zinc ions in order to maintain the comparison with copper.

Cadmium.—The electrolyte was a solution of 180 g/l "Analar" cadmium sulfate and 27.1 m/l "M.A.R." sulfuric acid in double distilled water.

Lead.—The electrolyte was prepared by saturating a dilute aqueous solution of perchloric acid containing 118.2 ml of "Analar" grade perchloric acid (S. G. 1.70), with "Analar" lead monoxide and filtering. To this was added a further 118.2 ml of "Analar" perchloric acid and the volume made up to two liters with double distilled water, giving 0.5M lead perchlorate in 0.5M perchloric acid.

Iron.—"Analar" grade ferrous sulfate and "M.A.R." sulfuric acid were used. The following three electrolytes were tried: (i) 0.5M ferrous sulfate, 0.5M sulfuric acid; (ii) 0.5M ferrous sulfate, 0.025M sulfuric acid; (iii) 0.5M ferrous sulfate, 0.025M sulfuric acid, 0.01M hydrazine sulfate.

The plating cell.—The electrolyte was contained in a 2 liter beaker suspended in a constant temperature bath normally maintained at 25°C ± ¼°. The relative positions of anode and cathode were fixed by means of a perspex jig, out of contact with the electrolyte. The current used was supplied from a 12v battery through variable series resistances.

The plating technique.—This was so designed that the cathode could be transferred to the cell and brought up to full current density with the least possible delay. After plating the current was switched off, the specimen removed from the cell and immersed in water. It was washed with methanol and stored in a vacuum dessicator over phosphorous pentoxide.

Examination of the deposits.—The cathodes were examined before and after plating by a selection of the following techniques.

Optical microscopy.—The structures were examined using direct and oblique illumination and line profile techniques. A number of plated specimens were sectioned to reveal surface contour and the metallurgical nature of the deposit.

Optical goniometry.—The Miller indices of the growth facets on deposits grown on single crystal substrates were deduced from their inclination to the cathode surface as was determined using a two-circle goniometer.

X-ray diffraction.—The complete orientation of single-crystal cathodes was determined before and after plating by the back reflection Laue method. Strain or distortion in the surface or deposit could also be detected. The interpretation of the diffraction pattern, as is fully described by Greninger (7) and by Barrett (8), was simplified by the low symmetry of zinc. It was found that, using white copper radiation produced at 18 ma and 40 kv with an ex-

posure time of 25 min, zinc deposits were penetrated to a depth of 35.8μ by the x-rays. This is a thickness twice that corresponding to the passage of 36 coulombs in a standard deposition experiment. However, although complications arose occasionally, in general the reflection from the base through the deposit was weak compared with reflection from the deposit, and any misorientation between the two was immediately obvious.

Reproducibility.—It is probably true that all workers who have investigated the surface topography of electrodeposits have found difficulty in obtaining reproducibility. The experiments described did not prove exceptional, and it was regarded as essential to apply a criterion to test that solutions gave reproducible structures in the deposition of zinc. During work by Pick *et al.* (2) on copper a satisfactory criterion was developed which fulfilled the requirements of structure sensitivity and convenience. This was based on the sensitivity of the structures obtained on a copper (100) surface to solution impurity. The structure accepted as typical of a satisfactory solution is shown in Fig. 9; all the structures described by Pick and his co-workers were obtained from solutions tested to give this structure on a copper (100) substrate. It was decided to use a similar criterion for zinc; a zinc single crystal surface, with an (0001) orientation, was plated at 10 ma/cm^2 for 60 min in a solution of 0.5M zinc sulfate, 0.5M H_2SO_4 maintained at 25°C. Figure 1a shows the deposit structure considered typical from such a solution. From solutions of different acidity the structures were not identical and secondary standards were necessary. These are also illustrated in Fig. 1.

Results

As far as possible the results of this investigation are given pictorially and in comparison with the growth of copper deposits.

The first point of note is that, in general, zinc deposits give less variety of structure than do copper. Figure 2 shows the variations in crystal habit produced in plating zinc onto zinc cathodes of orientations shown in Fig. 3; these structures may be compared with those observed in copper deposition (4). The crystallographic indices of facets developing as determined by goniometry are given in Table I.

The second point is that, unlike in copper deposition, hydrogen is evolved and also zinc is an amphoteric metal. It may be thought that the effect of hydrogen evolution is trivial; however, the volume of gas evolved is sufficient to lead to a marked disturbance of the layers of electrolyte in the immediate vicinity of the cathode. Figure 4 gives some indication of the relative effects of acid concentration and current density. There are more inclusions at low acidity and low current density; under these conditions it is thought that the pH may rise locally allowing basic salts to form (9).

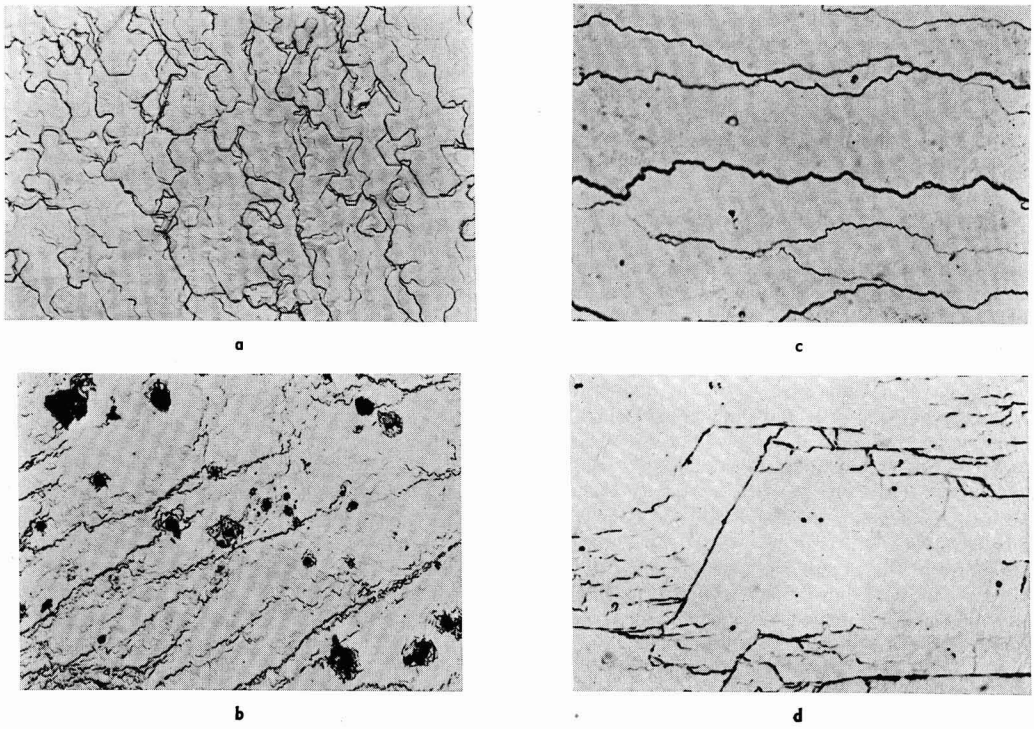

Fig. 1a. Reproducibility test, standard structure; deposit produced at 10 ma/cm^2 for 60 min at 25°C in 0.5M $ZnSO_4$, 0.5M H_2SO_4 electrolyte on a (0001) electropolished face; magnification 900X. Fig. 1b 270X; Fig. 1c 270X; Fig. 1d 86X. (Fig. 1b, c, d. Secondary standards; reproducible structures.) Fig. 1b 30 ma/cm^2, 20 min, 25°C, 0.5M $ZnSO_4$, 0.1M H_2SO_4 electrolyte; Fig. 1c 30 ma/cm^2, 20 min, 25°C, 0.5M $ZnSO_4$, 0.5M H_2SO_4 electrolyte; Fig. 1d 30 ma/cm^2, 20 min, 25°C, 0.5M $ZnSO_4$, 0.005M H_2SO_4 electrolyte. Deposits on (0001) faces.

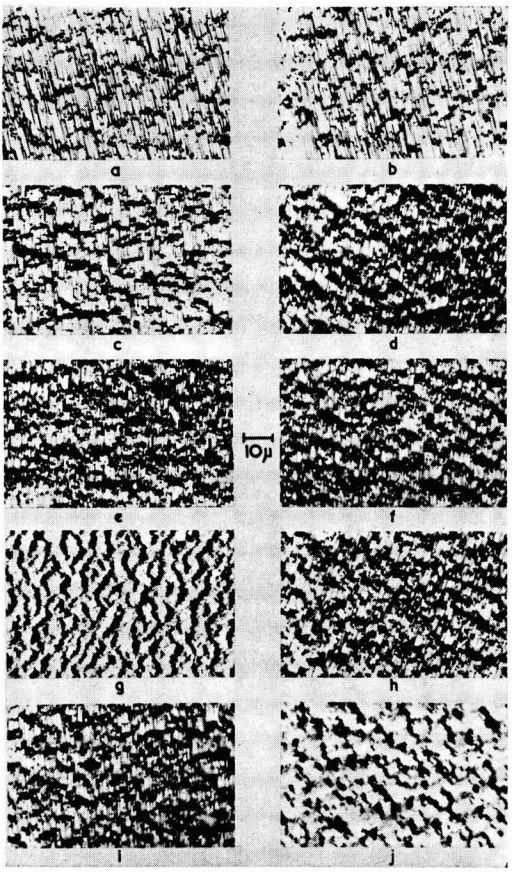

Fig. 2. Structure of deposits formed on single crystal substrates of orientation given in Fig. 3.

The third notable feature is that deposit structures developed with time in a way directly comparable with the growth of copper; see, for example, Fig. 5. Some analysis of the coarsening exhibited was possible.

The effect of temperature was complex; it is shown in Fig. 6, but no explanation for the variation in structure is offered at this stage.

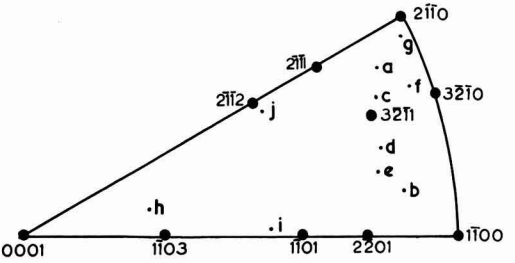

Fig. 3. Orientations produced in plating zinc on zinc cathodes

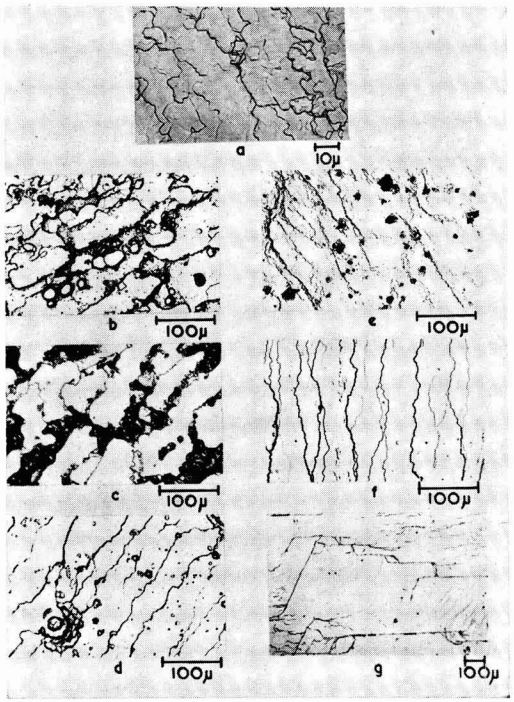

Fig. 4. Effect of acid concentration and current density on the structure of deposits formed on single crystal bases with an orientation within 4° of (0001). (a) 5 ma/cm² 0.5M H_2SO_4; (b) 5 ma/cm² 0.1M H_2SO_4; (c) 5 ma/cm² 0.05M H_2SO_4; (d) 5 ma/cm² 0.005M H_2SO_4; (e) 30 ma/cm² 0.1M H_2SO_4; (f) 30 ma/cm² 0.05M H_2SO_4; (g) 30 ma/cm² 0.005M H_2SO_4. Deposition was for 36 coulombs/cm² and the concentration of zinc sulfate was 0.5M in each case.

Table I. Indices of reflecting facets from deposits on single crystal bases with orientations as shown in Fig. 3

Specimen	Indices of reflecting facets									
a	(0001) vs	{1$\bar{1}$01} s	{10$\bar{1}$1} m	{01$\bar{1}$1} w						
b	(0001) vs	{1$\bar{1}$01} s	{10$\bar{1}$1} w	{01$\bar{1}$1} vw	(2$\bar{1}\bar{1}$0) w			(1$\bar{2}$12) w	(2$\bar{1}\bar{1}$4) vw	
c	(0001) vs	{10$\bar{1}$1} s	{1$\bar{1}$01} s	{01$\bar{1}$1} w	(2$\bar{1}\bar{1}$4) vw					
d	(0001) vs	{1$\bar{1}$01} s	{10$\bar{1}$1} m	{01$\bar{1}$1} w						
e	(0001) vs	{1$\bar{1}$01} s	{10$\bar{1}$1} m	{01$\bar{1}$1} mw						
f	(0001) vs	{1$\bar{1}$01} s	{10$\bar{1}$1} s	{01$\bar{1}$1} vw	(2$\bar{1}\bar{1}$2) w			(3$\bar{2}$10) vw		
g	(0001) vs	{1$\bar{1}$01} s	{10$\bar{1}$1} s	{01$\bar{1}$1} vw	(2$\bar{1}\bar{1}$2) vw					
h	(0001) vs	{1$\bar{1}$01} s	{10$\bar{1}$1} m	{01$\bar{1}$1} vw						
i	(0001) vs	{1$\bar{1}$01} s	{10$\bar{1}$1} m	{01$\bar{1}$1} w						
j	(0001) vs	{1$\bar{1}$01} s	{10$\bar{1}$1} s	{01$\bar{1}$1} w	(2$\bar{1}\bar{1}$2) w	(2$\bar{1}\bar{1}$1) w		(2$\bar{1}\bar{1}$0) vw	(2$\bar{1}\bar{1}$4) vw	

vs, very strong; s, strong; m, medium; mw medium weak; w, weak; vw, very weak (just detectable).

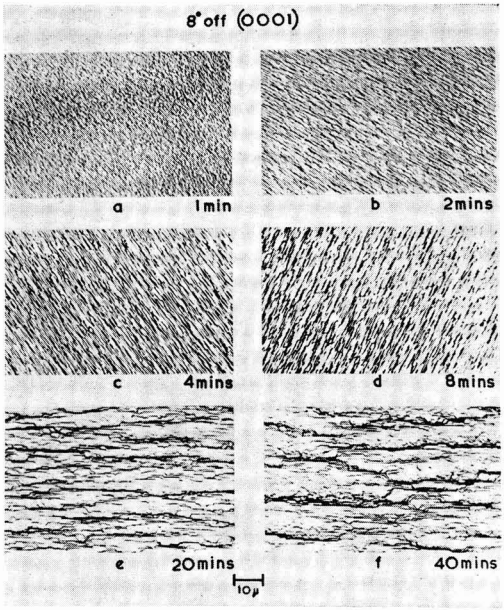

Fig. 5. Time series. The cathode was plated at 30 ma/cm^2 in an electrolyte of 0.1M H_2SO_4 and 0.5M $ZnSO_4$ at 25°C.

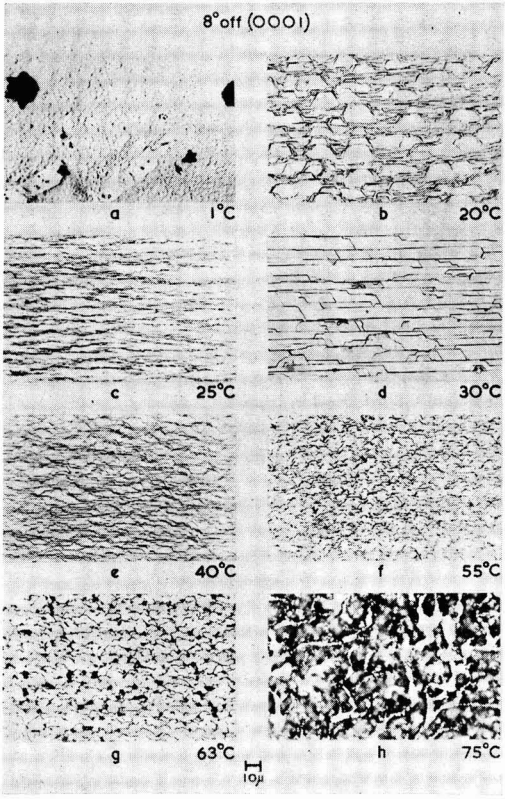

Fig. 6. Temperature series. These deposit structures were observed on a zinc single crystal cathode after deposition for 20 min at a current density of 30 ma/cm^2 in 0.5M $ZnSO_4$, 0.1M H_2SO_4 electrolyte.

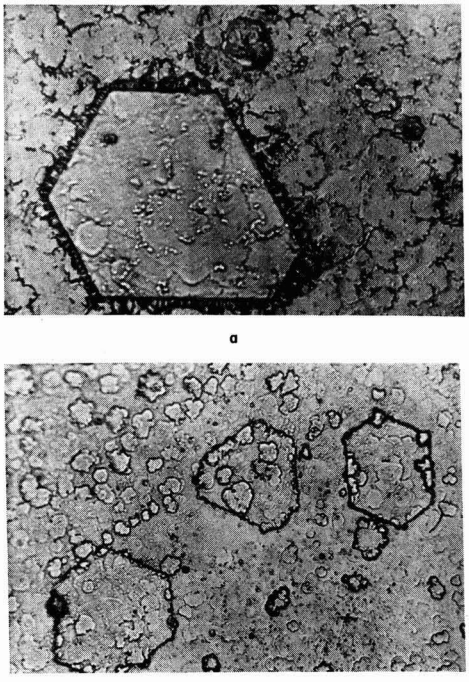

Fig. 7a and b. Epitaxial deposits on cleavage surfaces. Magnifications, a (top) 1200X, b (bottom) 900X.

Influence of the Substrate

The influence of the nominal orientation of the etched zinc single crystal cathode has been shown in Fig. 2. Deposits on unetched cleavage surfaces were very different from those shown in this figure. In general such deposits were not epitaxial and were

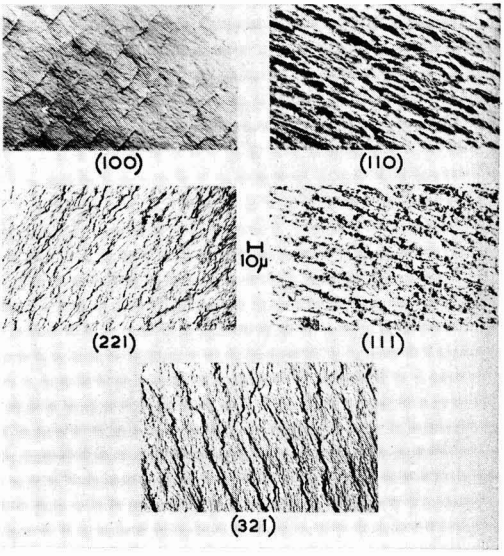

Fig. 8. Zinc deposits produced on copper single crystal bases of various orientations by plating at 10 ma/cm^2 for 60 min in a 0.5M $ZnSO_4$, 0.5M H_2SO_4 electrolyte at 25°C. Magnification 575X.

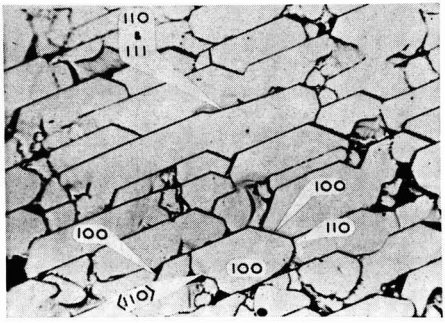

(100)

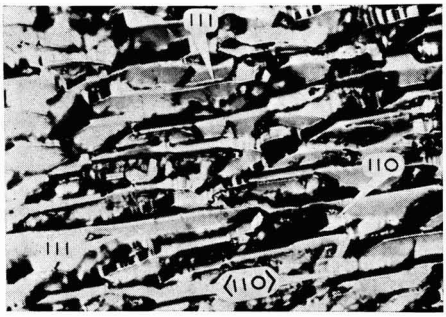

(331)
(Resembles 221)

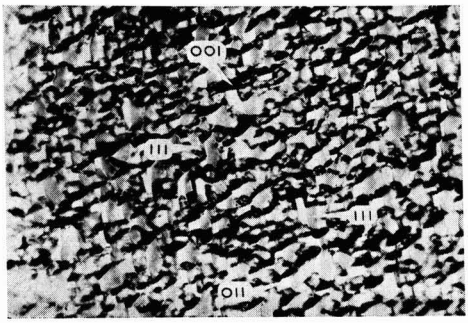

(321)

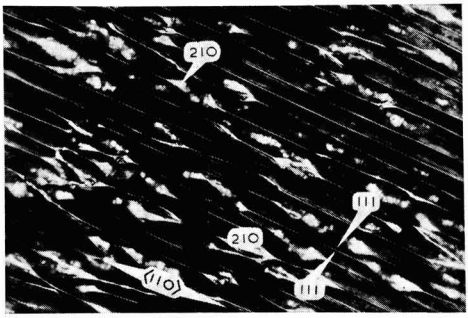

(110)

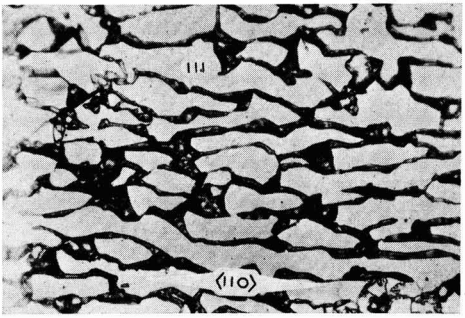

(111)

Fig. 9. Copper deposits produced on copper single crystal bases of the same orientation as in Fig. 8, by plating at 10 ma/cm² for 60 min in a 0.5M $CuSO_4$, 0.5M H_2SO_4 electrolyte at 25°C (2). Magnification 460X.

fine but nonuniform [cf. Cavallero and Bolognesi (10)]. Hexagonal growth features and spirals were sometimes visible. The deposits on etched cleavage surfaces were quite different from those obtained on electropolished surfaces near (0001); compare Fig. 7 and 4. Certain areas of the cleaved surfaces were heavily twinned; the deposit structure on the twin was typical of that on orientations away from (0001), but around the twin growth was typical of the cleavage plane. Cleavage steps only influenced the deposit locally.

More interest attaches to the deposition of zinc on prepared copper surfaces. The deposits coarsened with time, an effect that might be expected if conventional bunching occurs, but the deposits showed a marked difference from the development of copper on the same substrates; compare, *e.g.*, Fig. 8 and 9. In Table II the results of a goniometric examination are given.

Figure 10a shows the structure of a grain of a polycrystalline zinc cathode after the passage of 36 coulombs during electrodeposition. Figure 10b shows the same area after removing part of the electrodeposit by mechanical and electropolishing, and etching the surface so produced. Clearly the development of the crystal habit is continuous, and the distribution of etch pits indicates that the regions where neighboring growth features impinge are disordered and probably contaminated.

Finally, in Fig. 11 and 12, examples are shown of the growth of cadmium and lead polycrystals. The comparison of the structures observed with the habit of copper electrodeposits [*e.g.*, Fig. 9, also ref. (4)] is discussed below. No iron was deposited on iron or copper electrodes from electrolytes (i) and (ii) described above. Iron was deposited with very slight evolution of hydrogen from solutions containing hydrazine sulfate. X-ray diffraction photographs taken of the deposit on individual grains showed them to be polycrystalline. Iron deposits on copper single crystals were discontinuous. The growth of iron under our conditions clearly could not be compared with the growth of the other metals considered and will not be discussed further.

Discussion

Deposit Topography

At first sight, the considerable differences between the crystal habits of electrodeposited copper

Table II. Crystallographic relationships between the zinc deposit and the various copper bases

Base orientation (Copper)	Orientation of deposit w.r.t. base Zinc	parallel to	Copper	
(111)	(0001)		(111)	plane
	$3 \times [1\bar{1}20]$		[110]	directions
	$\{10\bar{1}1\}$		{111}	zones
(100)	(0001)		(100)	plane
	$1 \times [1\bar{1}20]$		[110]	directions
	$1 \times [\bar{1}100]$		$[\bar{1}10]$	
	$\{10\bar{1}1\}$		{111}	zones
(110)	(0001)		(111)	plane
	$3 \times [1\bar{1}20]$		[110]	direction
	$\{10\bar{1}1\}$		{111}	zones
(117)	(0001)		(113)	plane
	$1 \times [1\bar{1}20]$		[110]	direction
	{1011}		{111}	zones
(321)	(0001)	4½° off	(100)	plane
	$1 \times [11\bar{2}0]$		[110]	directions
	$1 \times [1\bar{1}00]$		$[1\bar{1}0]$	
	$\{10\bar{1}1\}$		{111}	zones
(221)	(0001)		(111)	plane
	$3 \times [11\bar{2}0]$		[110]	direction
	$1 \times \{10\bar{1}1\}$		{111}	zones

and zinc are disconcerting, but some understanding can be obtained from a consideration of the crystallography of the two metals. Pick, Storey, and Vaughan (2) have explained the structure forms on copper in terms of the arrangement of atoms in the substrate surfaces; the surface atoms of zinc substrates are arranged very differently due to the difference in crystal structures. The close-packed planes are normally present in the final form, to the exclusion of planes of higher indices, and so the number and symmetry of these has a direct bearing on the deposit topography. Copper, having a greater symmetry has many more close-packed planes than zinc and so one would expect to find different structures on zinc electrodeposits if growth occurs by a bunching mechanism. However, the arrangement of the surface atoms in the copper (111) and zinc (0001) planes are identical; correspondingly very similar deposit structures have been obtained by the deposition of (*a*) zinc onto a zinc (0001) plane; (*b*) zinc onto a copper (111) plane; (*c*) copper onto a copper (111) plane (Fig. 13).

The apparently complex structures observed on the various zinc substrates orientations shown in Fig. 2 can be interpreted in terms of one basic model. Ball models of facets of the zinc crystal show clearly that apart from the (0001) basal plane the faces of the $\{10\bar{1}1\}$ zones are far more important than the remainder, and these faces do not vary very much in importance one from the other. For any base orientation away from the (0001) plane there are no planes suitably orientated, sufficiently close packed and isolated to predominate over the remainder. Thus a simple platelet, block, or ridge

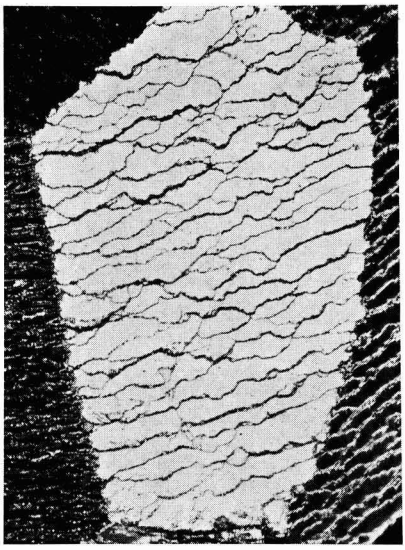

10a

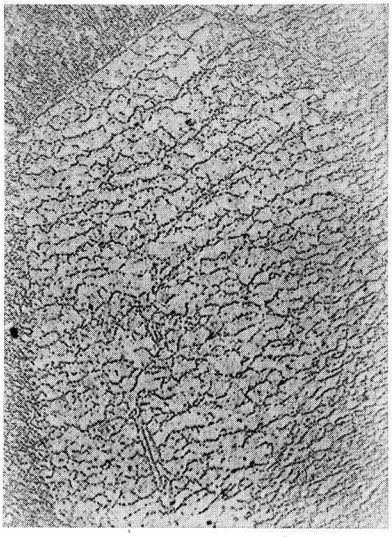

10b

Fig. 10a (top). Deposit on a single grain of a zinc polycrystalline cathode after passing 36 coulombs/cm^2; Fig. 10b (bottom) Etched horizontal section through the same deposit. Magnification 320X.

structure is not formed. One has, instead, complete zones of faces developing. This is illustrated in Fig. 14b which is an idealized structure for an orientation near a $(1\bar{1}00)$ plane. As can be seen from the stereographic projection illustrating the facets developed on this orientation in practice (Fig. 14a) there is some complication of the idealized structure by a few minor facets which develop between two adjacent $\{10\bar{1}1\}$ zones. Figure 14b shows only one step edge whereas a real surface will be covered by many such steps; the density and closeness of packing of these will be determined by the base orientation.

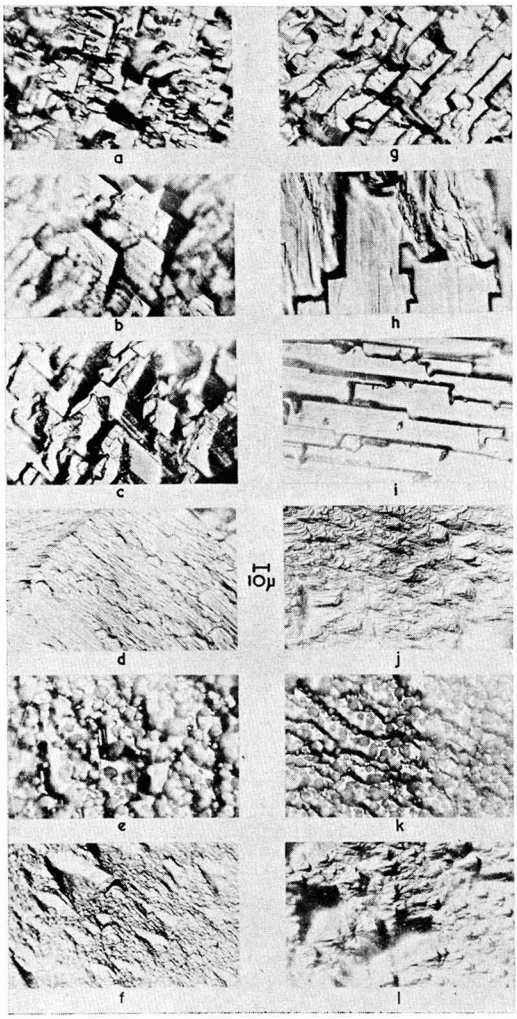

Fig. 11. Structure of cadmium deposits on cadmium polycrystals, produced by plating in 1.4*N* $CdSO_4$, *N* H_2SO_4 electrolyte at 25°C. (a) to (f) current density 10 ma/cm²; (g) to (l) current density 30 ma/cm².

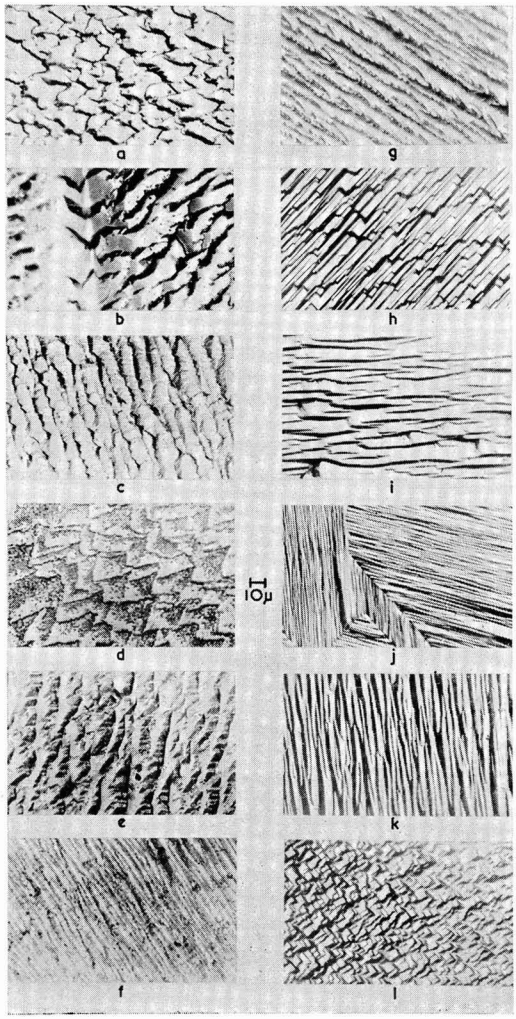

Fig. 12. Structure of lead deposits on lead polycrystals, produced by plating in 0.5M lead perchlorate, 0.5M perchloric acid electrolyte at 25°C; (a) to (f) current density 10 ma/cm²; (g) to (l) current density 20 ma/cm².

The structure on any substrate orientation is made up of "unit blocks" which can be obtained from the one in Fig. 14b by rotating that structure with respect to the plane of the paper until the desired substrate orientation is obtained. Thus for base orientations near a $\{1\bar{1}0l\}$ zone there is one zone of $(1\bar{1}0l)$ faces with their close-packed direction parallel to the surface and a second zone at approximately 60° to the surface. Hence the deposit structure consists of long lands of the former zone of planes terminated by facets of the second zone, *i.e.*, a pencil-like type of structure (Fig. 2 a, b, g).

As the substrate orientation approaches the (0001) plane the (0001) face becomes increasingly dominant, and at the same time the angles which the zones subtend at the surface decrease, the differences between these angles decrease, and so the zones became more equivalent to each other. Thus in the limiting case–the (0001) basal orientation–each of the three $\{10\bar{1}l\}$ zones are of equal importance and an hexagonal structure results (Fig. 1). Just off this orientation a platelet structure will be formed.

From Fig. 14c it can be seen that on base orientations on a $\{2\bar{1}1l\}$ zone, two zones of $(10\bar{1}l)$ faces will develop to an equal extent, and on orientations between this and a $\{10\bar{1}l\}$ zone or the (0001) plane there will be a gradual transition in structure similar to that already described. It is worth noting that at a $(2\bar{1}\bar{1}2)$ orientation the (0001) $(10\bar{1}0)$ and $(1\bar{1}00)$ planes lie symmetrically in the surface. With the development of the two $\{10\bar{1}l\}$ zones and the basal plane a pyramidal structure results as is shown in Fig. 2j. Figure 15 shows the development of this type of structure.

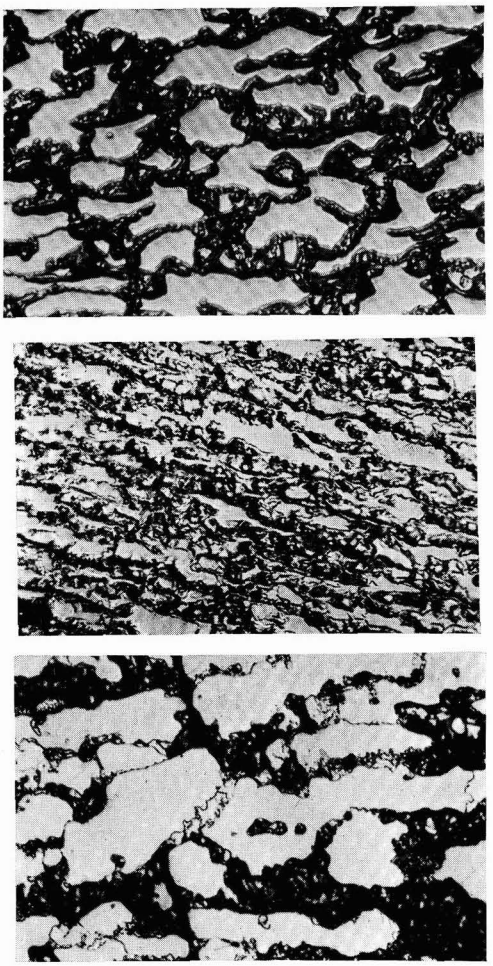

Fig. 13. Comparison between the structure obtained by Pick, Storey, and Vaughan (2) on a (111) face of a copper single crystal and structures obtained during the present investigation by plating zinc on a copper (111) face and zinc on a zinc (0001) face. (a) (top) Deposit structure on a copper single crystal orientation 3½° off (111) formed by plating at 10 ma/cm² in a 0.5M $CuSO_4$, 0.5M H_2SO_4 electrolyte (2); copper anode. Magnification 610X. (b) (center) Deposit structure on a copper single crystal orientation 3° off (111), formed by plating at 10 ma/cm² in a 0.5M $ZnSO_4$, 0.5M H_2SO_4 electrolyte; zinc anode. Magnification 610X. (c) (bottom) Deposit structure on a zinc single crystal, orientation 3½° off (0001) formed by plating at 5 ma/cm² in a 0.5M $ZnSO_4$, 0.5M H_2SO_4 electrolyte; zinc anode. Magnification 168X.

Deposits of Zinc on Copper Single Crystals

The final structure of the zinc deposits is influenced by the copper substrate in the very early stages of deposition. During this time the crystallographic orientation of the deposit will be fixed. Once the copper substrate is covered, the electrochemical conditions are those where zinc is plated on a zinc substrate; the deposits are influenced by variations in current density and electrolyte composition in exactly the same way as deposits on zinc cathodes, and for the same reasons.

The deposits obtained were epitaxial, usually with the basal plane parallel with the closest packed copper plane in the surface, and with the close-packed directions of the two lattices parallel.

The lattice parameters for the zinc and copper structures are widely different, as are the crystal symmetries. However, the spacings along the $[11\bar{2}0]$ and [110] directions (*i.e.*, the close-packed directions) are 2.644Å and 2.556Å, respectively, a misfit of only 4.22%. The degree of misfit between the deposit and the base will depend on the orientations of one with respect to the other. The orientation of the deposit will be determined by the energies involved which will be minimized by having the close-packed directions parallel and the basal plane parallel to the low index plane, thereby minimizing the misfit. Due to the high symmetry of copper, this results in a platelet structure on all orientations (Fig. 8). The angle of the platelets to the surface is determined in the first instance by the angle of the nearest (111) or (100) plane to the surface. In the case of a (110) orientation (Fig. 8) this is at 35° to the surface giving platelets a ridgelike appearance. These ridges are not identical with those obtained in copper deposits on this orientation (Fig. 9). The basal plane is not always parallel to a low index plane because a smaller degree of misfit can sometimes be obtained by having the close-packed and densely packed zones parallel.

Deposits on Cleavage Surfaces

Zinc deposits on lightly etched zinc cleavage surfaces were markedly different from structures on lightly etched electropolished faces of the same nominal orientation. Electropolished surfaces are known to be undulating, providing an abundance of growth sites and steps for growth by bunching. Zinc cleavage surfaces are not perfect [see, *e.g.*, Bassett, Menter, and Pashley (11)]; they contain cleavage steps, twins, and a certain rumpling due to basal plane bending and kinking. In the vicinity of imperfections the deposit structures were similar to those on electropolished surface. It is presumed that, on the remainder of the surface, there are insufficient step sites for the number of atoms arriving and growth proceeds by way of epitaxial nucleation. This is indicated by the circular layers on the upper surfaces of the large hexagonal growth features (Fig. 7), remote from the edges. The structure of the deposit away from the hexagons was very similar to the substructures on the hexagon, which suggests that the whole of the deposit, except possibly the initially formed hexagons, grew by a nucleation process, bunching following during the growth process. On unetched cleavage surfaces deposit structures were anomalous, possible indicating that under the present conditions the freshly prepared surface rapidly became contaminated.

Development of Zinc Deposit Structures with Plating Time

The principles of the "bunching" process have been mentioned earlier, and the results shown in Fig. 5 support the hypothesis. Howes (16), in particular, has shown that the average step height of a copper deposit increases with time, and that steps

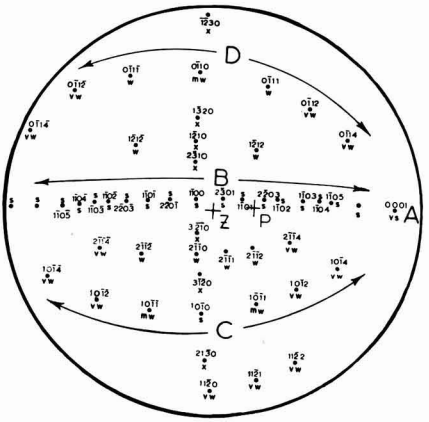

a

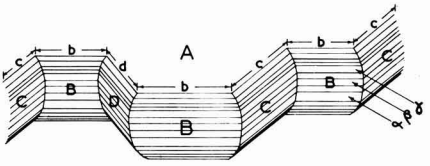

b

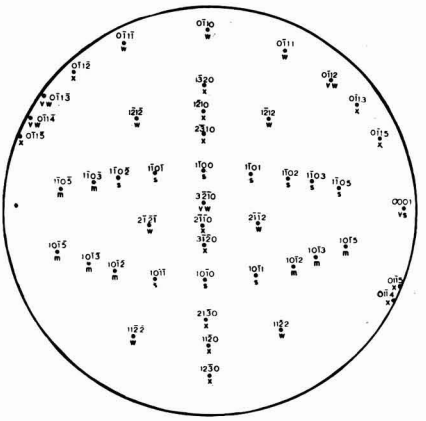

c

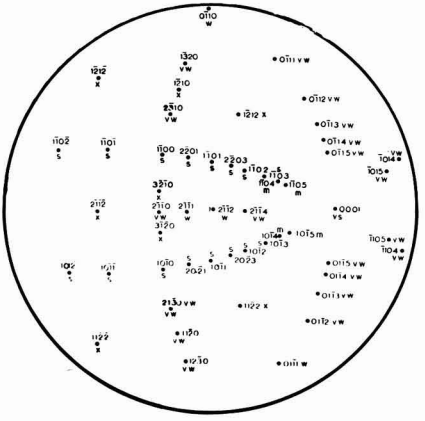

d

Fig. 14. Surface topography of zinc electrodeposits. (a) Stereographic projection of the facets developed (as indexed by optical goniometry) on a substrate of orientation Z, near $(1\bar{1}00)$ (actually orientation b, Fig. 3). The strength of reflection is indicated. Zones of planes B, C, D occurred, together with basal plane A. (b) Idealized structure corresponding to the reflections indicated in Fig. 14(a). The plane of the paper corresponds to the point P in the stereographic projection. The lettering corresponds to the zones. In reality, because the basal plane A lies at an angle to the plane of the paper in the idealized drawing, A intersects zones B, C, D so that re-entrant facets probably do not occur at the step edges. α, β, γ correspond to the $(1\bar{1}00)$ $(1\bar{1}01)$ and $(1\bar{1}02)$ faces, respectively. (c) Stereographic projection of facets developing on a substrate oriented on a $\{11\bar{2}1\}$ type zone, *i.e.*, at orientation f, Fig. 3. (d) Stereographic projection of facets developing on a substrate oriented at $(\bar{2}112)$, *i.e.*, Fig. 3j.

of small height are gradually eliminated. During the present investigation, it was found that the number of platelets per square centimeter varied exponentially with plating time. The rate of bunching corresponded roughly to a first order process.

Deposits of Lead and Cadmium
Electrochemical Effects

It should be emphasized that this discussion has concerned the accommodation of flux of atoms in the growing crystal lattice. Of course the electrochemistry of deposition cannot be ignored; Frumkin (12) recently reviewed the effect of the structure of the electrolytic double layer on the kinetics of electrode processes. It is not possible to study these effects in a conventional electroplating experiment because of the overwhelming interference of transport effects. Even the extent to which the idea of "bunching" may be applied is limited by the electrochemistry of the deposition process. Figures 11 and 12 show cadmium and lead deposits. Clearly the structures observed in these exploratory experiments indicate a growth process that may resemble that of copper and zinc. The lead deposits show ridge and platelet structures similar, but not identical, to those on copper. Lead has the same crystal structure as copper but with a larger lattice spacing (a = 4.9495Å for lead, 3.6153Å for copper), and it would appear that the crystallographic influences of the base are similar. However, the deposit structures obtained on cadmium were dissimilar to those obtained on zinc, although crystallographically the two metals are very similar. They are both close-packed hexagonal with axial ratios greater than ideal, and their equilibrium crystal forms, as calculated by Stranski (13) are identical. Work is needed on large-grained or single crystalline cathodes to clarify the relation between substrate orientation and the growth forms, but it is likely that the exchange current for cadmium is much greater than that for zinc from sulfate solutions, hydrogen is not evolved, and the conditions for the adsorption of surface active material are widely different. It would be of interest to know whether the electrodeposition of cadmium occurs predominantly directly at growth sites, or if an appreciable surface diffusion of adatoms is involved [c.f., Conway and Brockris (14)].

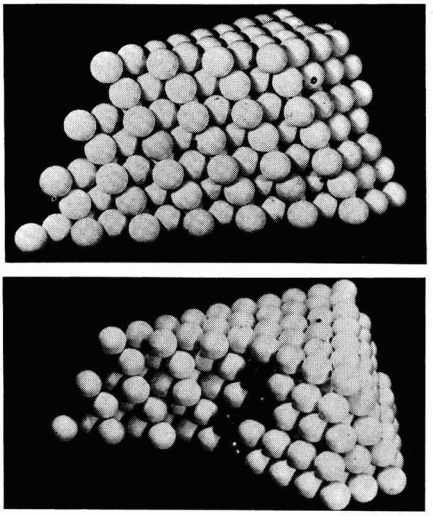

Fig. 15a. (top) Model of the (11$\bar{2}$1) plane in zinc; Fig. 15b. model showing the development of a (11$\bar{2}$1) face into a (1$\bar{1}$01) face by bunching.

Conclusions

It is concluded from this examination of zinc electrodeposited on zinc and copper substrates that the concept of "bunching" may be applicable to a range of electroplating systems.

Limitations in the application of the bunching hypothesis result from the many chemical and physical processes involved in a single electrodeposition. Most of these factors are uncontrollable except under special laboratory conditions. The idea may only apply where deposition involves a surface concentration of adatoms rather than deposition directly onto active sites.

Acknowledgments

The authors wish to thank Messrs. Joseph Lucas Ltd., Birmingham, England, for their generous financial support, and Professor E. C. Rollason for providing laboratory facilities.

Manuscript received Aug. 4, 1961; revised manuscript received March 16, 1962. This paper was prepared for delivery before the Detroit Meeting, Oct. 1-5, 1961.

Any discussion of this paper will appear in a Discussion Section to be published in the June 1963 JOURNAL.

REFERENCES

1. G. G. Storey and S. C. Barnes, *Trans. Inst. of Metal Finishing*, **37**, 11 (1960).
2. H. J. Pick, G. G. Storey, and T. B. Vaughan, *Electrochim. Acta*, **2**, 165 (1960).
3. T. B. Vaughan and H. J. Pick, *ibid.*, **2**, 179 (1960).
4. S. C. Barnes, G. G. Storey, and H. J. Pick, *ibid.*, **2**, 195 (1960).
5. F. C. Frank, "Growth and Perfection of Crystals," John Wiley & Sons, Inc., New York (1958).
6. E. C. Williams and M. A. Barrett, *This Journal*, **103**, 363 (1956).
7. A. B. Greninger, *Trans. A.I.M.E.*, **117**, 61 (1935).
8. C. S. Barrett, "Structure of Metals," 2nd, ed., McGraw Hill Book Co., p. 185 (1952).
9. R. Sato, *This Journal*, **106**, 206 (1959).
10. L. Cavallaro and G. O. Bolgnesi, *Rev. Met.*, **52**, 706 (1955).
11. G. A. Bassett, J. W. Menter, and D. W. Pashley, *Discussions Faraday Soc.*, **28**, 1 (1959).
12. A. N. Frumkin, *This Journal*, **107**, 461 (1960).
13. I. N. Stranski, *Discussions Faraday Soc.*, **5**, 13 (1949).
14. B. E. Conway and J. O'M. Bockris, *Proc. Roy. Soc.*, **A248**, 394 (1958).
15. V. A. Roitar, V. Juza, and S. Poluyan, *Acta Physicochim.*, **10**, 389 (1939).
16. V. R. Howes, *Proc. Phys. Soc.*, **74**, 616 (1959).

Decay of Cathodoluminescence and Nonradiative Processes in Manganese Activated Phosphors

G. F. J. Garlick
Physics Department, The University, Hull, Yorkshire, United Kingdom
and M. Sayer
Physics Department, University of British Columbia, Vancouver, British Columbia, Canada

ABSTRACT

Cathodoluminescence emission spectra and decay processes have been investigated as a function of primary electron energy and density for single crystals, evaporated layers, and powder layers of manganese activated calcium fluoride and zinc silicate. The emission spectra were found to be unchanged by the conditions of excitation. The value of the decay constant for powder layers was also unchanged, but that for single crystals and evaporated layers increased as the primary energy was decreased. This behavior is explained in terms of an Auger recombination leading to an interaction between the luminescence centers and the high density of electrons in the conduction band at low primary voltages. It is shown that for such an effect to occur the rate of nonradiative recombination of electrons in the conduction band of the host lattice must be small. This criterion is satisfied in the case of single crystals and evaporated layers, but not in microcrystalline powder layers.

Cathodoluminescence represents the final stage of a series of processes beginning with the absorption of an electron beam in a crystal and ending with the emission of radiation. Information regarding the intermediate stages in the process can only be inferred from the characteristics of the final emission. In many phosphors, the nature of the final radiative transition is uncertain and deductions about the pre-

ceding stages may be ambiguous. The inclusion of manganese as an activator ion in several crystal lattices is known to give rise to an emission resulting from a spin-flip transition within the 3d shell of the manganese ion itself. Under ultraviolet excitation, such a phosphor is characterized by an exponential growth and decay of emission with a time constant independent of the intensity of excitation. Such a phosphor should be of use in experiments designed to investigate the intermediate stages in the cathodoluminescence process.

Many investigations of cathodoluminescence emission spectra and growth and decay time constants have been reported in the literature. Almost without exception, the measurements have been made on phosphors in the form of microcrystalline powders. It is possible that the properties of a phosphor in this form differ from that of the same material in the form of a single crystal. In the present work, the cathodoluminescence of zinc silicate and calcium fluoride with controlled concentrations of manganese has been investigated with special reference to the effect of primary electron energy and density on the emission spectra and decay constant. The phosphors were studied in three different forms, single crystals, evaporated layers, and microcrystalline power layers.

Experimental

Single crystal specimens of calcium fluoride approximately 1 mm in thickness were obtained from large single crystals containing different amounts of manganese. These crystals were grown from the melt by the Stockbarger technique (1) at the Department of Natural Philosophy of the University of Aberdeen. The plates were either cleaved directly from the bulk or cut with a wire saw and polished, using diamond paste. The results reported in this paper were obtained for specimens cut from a crystal containing 0.9% manganese. Powder layers were formed by grinding the single crystal and settling the powder from an aqueous suspension. Evaporated layers were produced by vacuum evaporation of a calcium fluoride-2% manganese fluoride powder mixture with subsequent heat treatment of the evaporated layer (2). Evaporated and powder layers of zinc silicate were prepared in a similar manner with an activator concentration of between 1 and 2% manganese. No large single crystals of zinc silicate were available, but measurements were made on a sintered layer formed by fusing the powder at a temperature close to the melting point. After cooling, the face of the sintered layer was ground smooth with carborundum and polished using diamond paste.

The phosphors were examined in a demountable cathode-ray tube for primary electron potentials of 1-15 kv, and for a steady and uniform excitation of 1-10 $\mu a/cm^2$ over a selected phosphor area. Emission spectra were measured by means of a double monochromator and photomultiplier system, while decay measurements were obtained by measuring the fall of emission after cut-off of steady excitation using a photomultiplier and cathode-ray oscilloscope. The specimen temperature could be varied from room temperature up to a few hundred degrees centigrade. With the system used secondary electron emission characteristics could not be measured, and in order to reduce spurious effects from this source most specimens were aluminized by vacuum evaporation, the coating being connected to the final anode of the cathode-ray tube. Several measurements using unaluminized specimens were also performed to check that the results obtained were independent of the aluminum coating.

Results

Emission spectra.—No significant change in the emission band due to manganese was found as the electron potential or beam current density were varied over a wide range. Small shifts in the spectrum to longer wavelengths were found as the manganese concentration was increased in the case of calcium fluoride. The shift occurred for concentrations at which spin-spin interaction was beginning to be evident in electron resonance spectra of the same specimens. From these results it is evident that the high concentration of electrons at low primary energies has little effect in any direct way on the 3d shell energy levels.

Decay of the emission.—In contrast to spectral measurements, the measurements of decay constant showed variations with form of specimen and with primary electron energy. The results for calcium fluoride and zinc silicate are shown in Fig. 1 and 2, respectively. In all cases powder layers showed

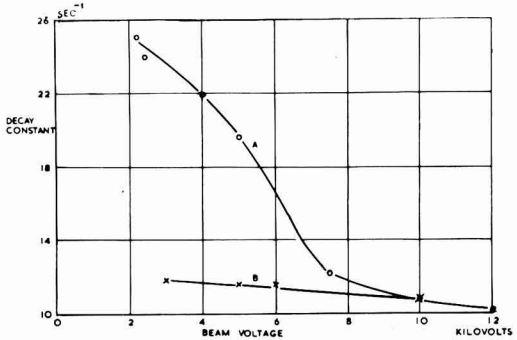

Fig. 1. Decay constant *vs.* primary electron energy for manganese activated calcium fluoride: (A) single crystal; (B) powder layer.

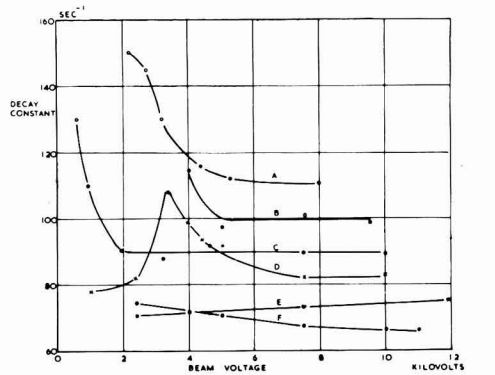

Fig. 2. Decay constant *vs.* primary energy for manganese activated zinc silicate: (A), (B), (C), evaporated layer; (D), sintered layer; (E), (F), powder layer.

little change in decay constant with electron energy, the value being identical with that measured using ultraviolet excitation, and characteristic of the Mn^{2+} center in the particular host lattice. This is in agreement with the results of other workers (3). The behavior of single crystals and evaporated layers was more complex. For single crystals, the decay constant was high at low primary energies and decreased as the electron energy was increased until the value approached that for powder layers. The variation with primary electron energy was relatively independent of whether the crystal surface facing the electron beam was polished, freshly cleaved, or coated with aluminum. This result is shown more effectively by the logarithmic plot of the change in decay constant $\delta - \delta_\infty$, where δ_∞ is the decay constant at large primary energies, *vs.* primary

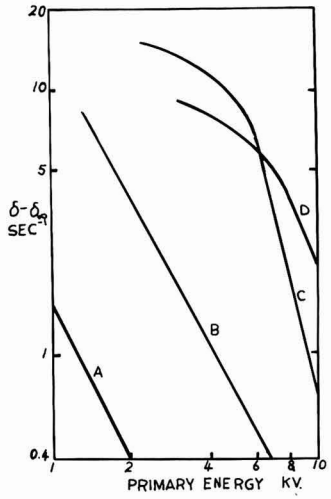

Fig. 3. Change in decay constant $\delta - \delta_\infty$ *vs.* primary energy for single crystal specimens of calcium fluoride: (A) cleaved unaluminized; (B) cleaved, aluminized; (C), (D) polished, aluminized.

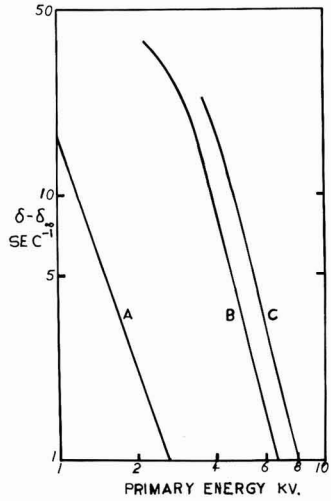

Fig. 4. Change in decay constant $\delta - \delta_\infty$ *vs.* primary energy for zinc silicate: (A) evaporated layer unaluminized; (B) evaporated layer, aluminized; (C) sintered layer, aluminized.

energy shown in Fig. 3 and 4 for calcium fluoride and zinc silicate, respectively. Except at low primary energy, these plots are linear with approximately the same slope. This suggests that the decay constant may be represented by a relation

$$\delta - \delta_\infty = CV^{-p} \qquad [1]$$

where C and p are constants. The average value of p obtained from the graphs is 3.0 ± 1.0 for calcium fluoride and 3.6 ± 0.2 for zinc silicate. The existence of an aluminum coating on the surface was not critical, the principal effect being an over-all shift of the curve to higher voltages. Further changes along the voltage axis could be tentatively attributed to the method of surface preparation, *e.g.*, the curve for a cleaved crystal appeared at a lower voltage than that for the polished specimen. A similar dependence on electron energy was observed for evaporated layers, although the over-all decay constants were usually higher than those for either powders or single crystals. This over-all increase was attributed to an increase in the transition probabilities of the luminescence centers due to perturbations introduced by the imperfect host lattice. In a few cases, the most notable being the sintered zinc silicate layer, the decay constant showed a maximum at an intermediate primary energy. This behavior is a guide to the interpretation of the results and will be discussed later.

Variation of the beam current density produced a change in the decay constant at low primary energy, but was less effective at higher primary energies. This behavior in a crystal of calcium fluoride is shown in Fig. 5.

Effect of phosphor temperature.—The change in decay constant with temperature was relatively independent of the primary beam energy and density and agrees with that for photoexcitation. This is shown in Fig. 6 for a single crystal of calcium fluoride. The effect of nonradiative transitions within the emission centers was only noticeable at temperatures between 100° and 200°. The absolute luminescence efficiency at ordinary temperatures was only a few per cent.

Discussion of Results

The important effect shown in the above experiments is the change of decay constant with primary energy for single crystals and evaporated layers

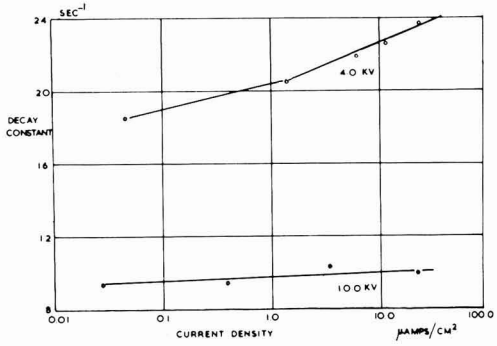

Fig. 5. Decay constant *vs.* beam current density for a single crystal of calcium fluoride: Mn: (A) 4 kv; (B) 10 kv.

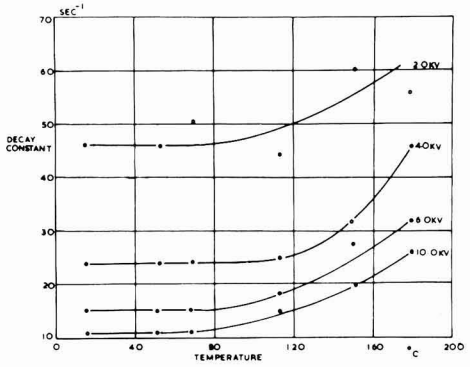

Fig. 6. Decay constant vs. temperature at different primary energies for a single crystal of calcium fluoride: Mn.

which is in contrast with the negligible effect for powder layers. The energy of the primary electrons is a measure of the penetration of the beam into the crystal, the most generally accepted relation being of the form $R = AV^n$, where R is the penetration depth, V is the primary voltage, and A and n are constants characteristic of the material (4, 5). The most obvious interpretation of the results is that the change in decay constant is due to either (a) a 'dead' surface layer or (b) thermal effects arising from the increased density of power dissipation at low primary voltages. If (a) is the case, the effect should be enhanced in powder layers in which the surface area is greatest. This disagrees with experiment. If macroscopic thermal effects are involved, a crystal temperature of the order of 200°C would be required to give the observed decay constants at low beam voltages. Calculations involving the thermal conductivity of the crystals indicate that under the given experimental conditions the crystal temperature rises by a maximum of 1°-2°C. A third possibility is in the increase of electron density within the crystal at low primary energies, due to the power-law dependence of the penetration depth on the primary energy. This may be considered in conjunction with the model for the cathodoluminescence process shown in Fig. 7.

Electron transitions may occur either in the lattice or in the luminescence centers. Due to the small number of activator ions, the bulk of the excitation is assumed to take place in the lattice, with subsequent transfer of energy to the luminescence centers. The emission spectrum is unchanged for optical and electron excitation; hence it may be assumed that the emission arises from a self-contained, monomolecular transition within a luminescence center with radiative and nonradiative transition probabilities δ and ϕ, respectively. The lattice excitation arises from the production of secondary electrons in the conduction band and positive holes in the valence band. As an approximation, if recombination is neglected, it may be assumed that the primary beam excites

$$n_1 = I = [i_0 V/\Delta E \cdot AV^n] \qquad [2]$$

secondary electrons, where ΔE is the energy required to produce a hole-electron pair, and i_0 is the beam current density. Under these conditions, bimolecular recombination kinetics are to be expected in the lattice with a nonradiative recombination probability β (this includes both band-to-band and impurity transitions) and a probability for energy transfer to a luminescence center γN, where N is the total number of centers. The detailed kinetics of such a model have been treated elsewhere (6). It is found that the maximum value of decay constant is determined by the sum of the transition probabilities for the center $(\delta + \phi)$ sec^{-1}. This would be the value obtained in a measurement using ultraviolet radiation for direct excitation of the center. If the excitation takes place via the lattice a value of $(\delta + \phi)$ sec^{-1} is obtained if recombination processes in the lattice are completed in a time short compared to the lifetime of the radiative decay. Any process which increases the rate of lattice recombination is therefore ineffective to explain decay constants greater than $(\delta + \phi)$ sec^{-1}. A marked change can occur if the lifetime of a free lattice electron is comparable with that of an excited center, but this is again ineffective since the analysis shows that the decay constant is decreased under these circumstances. This is also the case if the effect of saturation of luminescence centers is included. Thus an increase in decay constant cannot be attributed to a change in any lattice process, but can only be a property of the luminescence center itself.

If any form of interaction between the electron density in the conduction band and the luminescence centers is to be reflected in the magnitude of the decay constant, two criteria must be satisfied: (a) the electron density must be large, (b) the lifetime of electrons in the conduction band must be comparable with that of the luminescence centers. Both criteria are principally determined by the parameter β, since it can be shown that (6)

$$n_1 = I/(\beta + \gamma N)^{1/2} \qquad [3]$$

and the lattice time constant

$$b = (I/(\beta + \gamma N)^{1/2} \qquad [4]$$

In a region of heavy recombination, *e.g.*, the surface regions of a crystal, β is large, and therefore n_1 is small and also decays in a time short compared to the lifetime of an excited center. Thus interaction between the electron density and the centers occurs for a very small fraction of a center lifetime. In the relatively perfect lattice of a crystal, recombination will be reduced, β is small, n_1 is large and remains

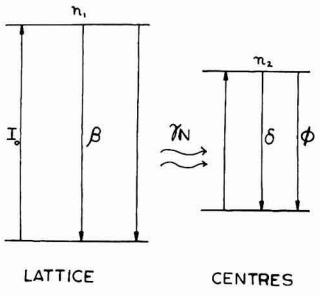

Fig. 7. Model for the luminescence process

appreciable throughout a large portion of the center lifetime. In this case a perturbation of the centers may be observed. Note that the effect of the surface will be enhanced in microcrystalline powders in that the average penetration depth is less than that for a single crystal due to the random orientation of the individual crystallites to the primary beam. A maximum in the value of decay constant is to be expected if the disordered surface region extends for a considerable depth into the crystal.

This behavior is observed in the sintered layer of zinc silicate (Fig. 2, curve D) and may also explain the nonlinearity at lower voltages of curves C and D of Fig. 3 for the polished specimens of calcium fluoride. The presence of such a region would also give rise to a shift of the curves along the voltage axis in the direction of higher voltages. Further comment may be made for the case of the evaporated layers. It has been shown that increased lattice recombination cannot increase the luminescence decay constant beyond that defined by the center transition probabilities $(\delta + \phi)$ sec^{-1}. Thus the over-all increase in decay constant in the evaporated layers must be due to an increase in the center probability $(\delta + \phi)$ sec^{-1} caused by perturbations in the imperfect crystal field surrounding the activator atoms. However, interaction with the excited lattice electron density can still occur as in the single crystal since the localized electron density is still predominantly determined by lattice recombination processes independent of the centers.

The specific nature of the interaction between the secondary electron density n_1 and the luminescence centers requires interpretation. A purely electrostatic interaction between the electron-hole plasma in the lattice and the luminescence centers is difficult to formulate. However, it has been well established in semiconductors such as germanium and silicon that at large majority carrier densities a recombination process proportional to the square of the carrier density is observed (7, 8). This is termed Auger recombination and involves three carriers—an electron and hole which recombine, transferring energy to a third electron. It is suggested that this process is observed in the present experiments. Two forms of interaction may be possible: (*a*) Auger recombination between a free hole, a free electron, and an excited luminescence center; the energy transferred to the center could raise its effective temperature for a short time with a resulting increase in nonradiative transition probability; (*b*) Auger recombination involving two free electrons and a bound hole in the vicinity of an excited center, the energy imparted to the second electron being dissipated by phonon generation in the vicinity of the center. This again results in an increase of nonradiative transition probability. Both processes may be termed a form of microscopic thermal quenching.

A quantitative estimate of the decay constant-beam voltage may be made on this basis since

$$\delta = (\delta + \phi)_\infty + Bn_1^2 \qquad [5]$$

where B is a constant.

If the approximation is made that n_1 is constant for a time comparable to the center lifetime, substituting for n_1 from [2]

$$\delta - (\delta + \phi)_\infty = B\left\{\frac{1}{\Delta E}\frac{i_e V}{A V^n}\right\}^2 = D\left\{\frac{i_e}{V^{n-1}}\right\}^2 \qquad [6]$$

Using the reported values of n (4), the decay constant should show a power law dependence on V with exponents 3.8 and 4.0 for calcium fluoride and zinc silicate, respectively. Considering the many approximations involved in the calculations, these values are compatible with the experimental values of 3.0 ± 1.0 and 3.6 ± 0.2, respectively. Note that the relation also indicates that the variation of decay constant with current density is greater at low rather than high primary voltages. This is also in agreement with experiment.

Conclusion

It has been shown that a rise in decay constant at low primary electron energies may occur in phosphors in which the rate of lattice recombination is relatively small. The suggestion that the rise is due to an interaction between the conduction electrons and the excited luminescence centers by means of Auger recombination in the lattice is borne out by the quantitative agreement between experiment and theory.

Acknowledgments

This work was submitted as part of a Ph.D. thesis to the University of Hull. One of the authors (M. S.) wishes to thank the University of Hull and the Department of Scientific and Industrial Research for Research Studentships.

Manuscript received Jan. 15, 1962. This paper was prepared for delivery before the Indianapolis Meeting, April 30-May 3, 1961.

Any discussion of this paper will appear in a Discussion Section to be published in the June 1963 JOURNAL.

REFERENCES

1. D. C. Stockbarger, *J. Opt. Soc. Amer.*, **39**, 731 (1949).
2. C. Feldman and M. O'Hara, *ibid.*, **48**, 816 (1958).
3. J. W. Strange and S. T. Henderson, *Proc. Phys. Soc.*, **58**, 368 (1946).
4. C. Feldman, *Phys. Rev.*, **117**, 455 (1960).
5. A. F. Makov, *Sov. Phys. Solid State*, **2**, 1934 (1961).
6. M. Sayer, *Proc. Phys. Soc.*, **B78**, 1017 (1961).
7. A. P. der Carvalho, *Compt Rend.*, **241**, 461 (1957).
8. J. R. Haynes and J. A. Hornbeck, *Phys. Rev.*, **100**, 606 (1955).

Transient Effects in Cadmium Sulfide-Cadmium Selenide Type Photoconductors

Ronald D. Weiss[1]

Clairex Corporation, New York, New York

ABSTRACT

Cadmium sulfide and cadmium selenide sintered polycrystalline layers have been investigated with respect to the transient effects in their photoconductive rise and decay curves. Under suitable conditions both types of layers exhibit a maximum in the rise curve and a minimum in the decay curve. The specific results are strongly dependent on the excitation history of the layer. The relationship of these effects to trapping processes is discussed, and some comparisons with earlier experimental works are made. The dependence of photosensitivity on these effects is emphasized.

A transient effect was previously found to be associated with single crystal photoconductors of both CdS (1) and CdSe (2). The experiments of Bube and others have shown that, because of their excitation history, the photoconductive response curves of CdS and CdSe single crystal photoconductors exhibit both a maximum in the rise curve and a minimum in the decay curve. The present paper will show that the effect is more strongly evidenced with CdS and CdSe polycrystalline sintered layers at room temperature.

Figure 1, curve a, is representative of most room temperature photoconductive response curves reported by others. In the same figure, curve b represents the general shape of the photoconductive response curve, which was obtained for these sintered layers under similar conditions. It is interesting to note that at the onset of the excitation the latter curve goes through a maximum before approaching its long time equilibrium or steady-state photocurrent value. The area between the long time equilibrium value and the maximum of curve b is the principal subject of this work, *i.e.*, the additional amount of photocurrent above the long time equilibrium value [overshoot (2)]. A result similar to the foregoing may be obtained by replacing the initial dark or quenching[2] history, required prior to the onset of the excitation, by a relatively high light intensity or excitation history. In this instance the photoconductive response curve must be taken from the high light intensity to the lower light intensity (the level at which the long time equilibrium value had been previously established). This second curve will be of the same shape as curve b, except for its inverted nature, *i.e.*, the photocurrent will now pass through a minimum below the long time equilibrium value before approaching this value [undershoot (2)].

[1] Present address: Applied Research Laboratory, General Instrument Corporation, Newark, New Jersey.

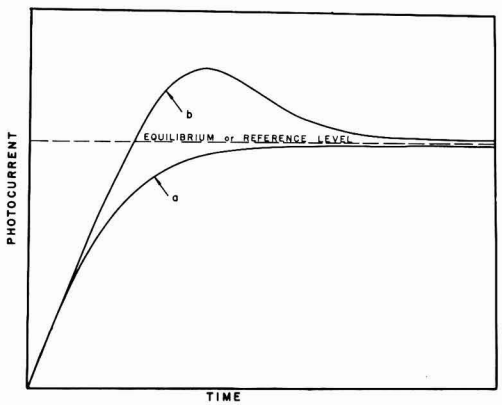

Fig. 1. Comparison of the general nature of the photoconductivity curves (until the equilibrium condition is established) of the works being discussed.

Experimental Apparatus and Procedure

Since the transient effect evidences itself in the growth of the photoconductivity a special procedure was devised to measure the true effect. The experimental procedure consists of three basic operations. The first operation is to determine the long time equilibrium value of the sintered polycrystalline layer at the reference light level of the experiment. This long time equilibrium value is defined by the steady-state photocurrent of the layer after it has been subjected to the reference light level for a considerable length of time. The time required for the steady-state photocurrent condition is primarily dependent on several factors, *i.e.*, the type of photoconductor, the intensity of the light, and the previous history of the layer. To ensure attainment of the steady-state photocurrent in all the layers of a particular group, the group was subjected to the necessary conditions for a period not less than ten days. This time had proved more than sufficient for all the layers in question. The second operation is to expose the layer to either an intense light, semidark, or dark environment for fixed amounts of time. This second operation will determine the type of transient obtained in the photoconductive response curve. The intense light environment will produce a minimum (with respect to the equilibrium value), whereas

[2] The term "quenching" is generally associated with the emptying of filled traps. In most photoconductors this quenched condition is obtained by either storage in a dark environment, heating of the photoconductor, or excitation with infrared. The net result of these methods is a de-excited photoconductor, a condition which can be reproduced.

the dark or semidark environment will produce a maximum. The third and final operation involves the measurement of these layers, at fixed intervals, at the reference light level established in the first operation.

The measuring circuit used was a series circuit consisting of a 1.34v Mallory Mercury battery (RM 42R), a Hewlett Packard ammeter (Model 412a), and the photocell. Provisions for taking these measurements requires an accurate light source which is stable and reproducible over long periods of time. This requirement is necessary in order to determine accurately photocurrent variations from the equilibrium value. It is for these reasons that the photometer used has been operated by means of the circuitry recommended by the National Bureau of Standards (3). The photometer bulbs used are of the GE No. 1763 series. They have been aged or seasoned prior to this application to avoid drift during the long periods of their use. The GE No. 1763 bulb is a secondary standard (operating color temperature 2870°K) which is checked periodically against a set of primary standards (4). In this manner, all available light levels have been maintained to within 1 or 2% over indefinite periods of time. In very low light level applications a series of Bausch and Lomb neutral density filters, which were found to be linear in the visible spectrum, were used. It should also be noted that the photoconductive layers were in the form of hermetically enclosed units. The hermetic enclosure gives some assurance that the measurements will not be affected by daily changes in atmospheric conditions. Since the results of one photoconductive layer could be misleading, measurements have been made with several layers of the same type. The statistical averages of these groups were used for all the data contained herein.

Experimental Results

Transient Maxima

Most of the data presented at this time deal specifically with transient maxima (overshoot) rather than minima (undershoot). The present data on transient maxima seem to indicate that at very high light levels there exists a saturation point at which no maximum or overshoot will be observed; however, to date this saturation point has not been determined accurately. It is quite reasonable to assume that this saturation point is related to a situation where the saturation of photocurrent (5), by means of light intensity, can occur.

Both transient maxima and minima have been shown to be functions of several factors aside from temperature (1, 2).[3] Recent experimentation has confirmed that these transients are strongly dependent on reference levels, time of exposure to the excitation, and type of photoconductive material used. This section will attempt to discuss these factors in greater detail. At this time a short explanation of the notation used throughout the paper will be helpful. The changes due to the transient effect have been designated as $\Delta I/I_o$, where ΔI is the change in photocurrent from the equilibrium value (I_o). I_m is the current value associated with the maximum height of the transient obtainable for a given set of conditions. In most curves presented 100 $\Delta I/I_o$ ($\Delta I/I_o\%$) is plotted as a function of time or time intervals. The ΔI is the maximum change in photocurrent, observed at the onset of the excitation, above the equilibrium value (I_o).

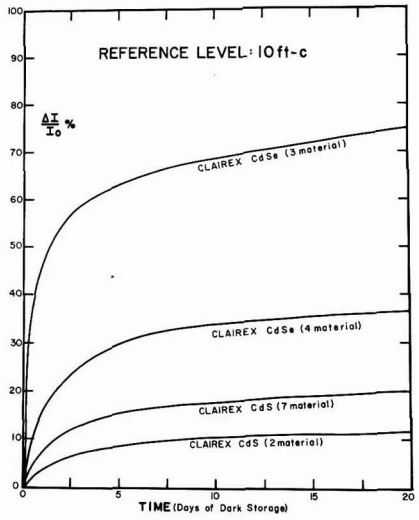

Fig. 2. Transient maxima or overshoot of several CdS and CdSe photoconductive layers obtained for a reference level of 10 ft-c.

Maxima or overshoot experiments, as described above, were performed on several polycrystalline cadmium sulfide and cadmium selenide photoconductive layers. The results of these experiments are shown for a particular reference level, in Fig. 2, for layers coming from a dark history. It can be seen from this set of curves that under the same conditions the cadmium selenide materials exhibit greater transient maxima than do the sulfides. This characteristic of cadmium selenide has been found to be true at all the reference levels thus far tested. It should also be noted that the maxima curves are all of an exponential nature, indicating that there is an upper limit for maxima ($\Delta I/I_o$), at each reference level, for a particular material. Figure 3 is a comparison of transient maxima of several commercially available photoconductors (all of the polycrystalline sintered layer type). These curves were taken at a reference level of 2 ft-c. Although the RCA prepared photoconductive layers show more of a transient maxima effect than the Clairex ones, it does illustrate that the effect is inherent in sintered polycrystalline materials at room temperature. As previously indicated experimentally it would normally be expected that CdSe layers would exhibit greater transient maxima than would CdS layers, but our data indicate that the RCA prepared CdS layers exhibit greater transient maxima than even the Clairex CdSe layers. This anomaly as well as other evidence suggested that this transient effect may be either a function of the layer thickness and/or the activation of the layer. These two possibilities were investi-

[3] It is known that heating effects will often cause similar overshoots. However the circuit used in the experimental set up is so designed that any joule heating (I^2R) within the layer is negligible.

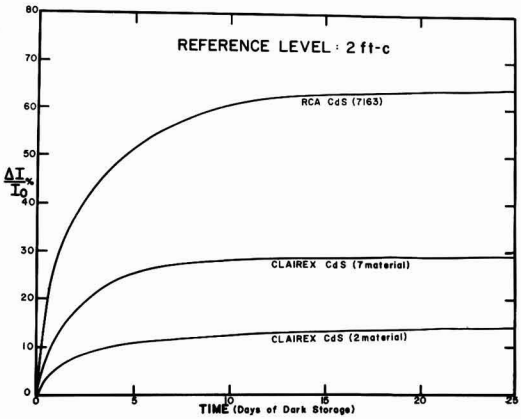

Fig. 3. Transient maxima or overshoot of several commercially available CdS photoconductive layers obtained for a reference level of 2 ft-c.

gated and yielded the results shown in Fig. 4 and Fig. 5. The data in Fig. 4 represent transient maxima, obtained at one reference level, for a particular CdS material which was varied in layer thickness. The thickness of layer (b) was 2-3μ, 4-6μ for (a), and 8-10μ for (c). It is evident from this phase of the data that the transient effect is not a function of the layer thickness. The second part of this investigation, however, yielded more interesting results. In this instance, variation of the copper activator concentration was made for a particular group of CdS layers, all having the same thickness. Thus, for a reference level of 10 ft-c we obtained the data in Fig. 5. These data illustrate that the transient effect, among other parameters, is directly dependent on the concentration of activator within the photoconductive layer. This experiment was repeated using several of the known photoconductor activators, and similar results were obtained as those already reported here for copper. Figure 5 shows the increase in the transient effect as a function of activator concentration. In addition these data show that the transient effect as a function of activator concentration also reaches an ultimate value.

In order to verify some of the room temperature transient data previously reported for single crystals of CdSe (2) and to gain additional information on room temperature transient data in CdS, if any, some

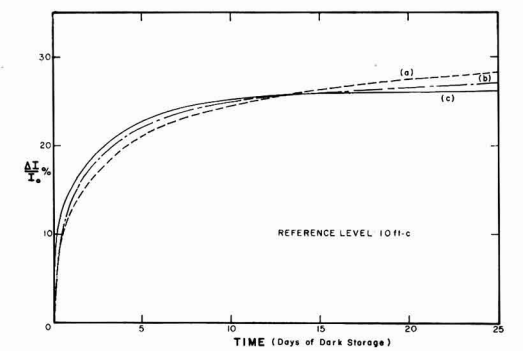

Fig. 4. Comparing transient maxima or overshoot of the same type CdS layers for which the layer thickness is the variable.

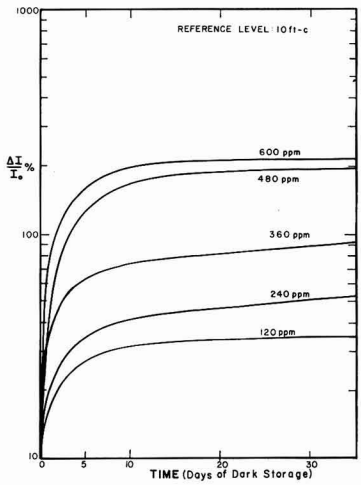

Fig. 5. Comparing transient maxima or overshoot of the same type CdS layers for which the activator concentration is the variable.

single crystals of these types were mounted and hermetically sealed in glass enclosures. They underwent the previously described experimental procedures, and transient maxima were observed in both types of crystals at room temperature. We believe that this is the first time that transient maxima have been reported for CdS single crystals at room temperature. It should be noted that single crystal transient maxima obtained for similar conditions were not as uniform, from crystal to crystal, as are the polycrystalline layers from layer to layer. This nonuniform result had been anticipated with single crystals because of the individuality of these crystals. This individuality is not as predominant with polycrystalline layers because of the statistical distribution that one gets with the many small fused single crystals. Because of this individuality of single crystals no direct comparison with the available data can be made at this time.

The reference level for which the long time equilibrium values are established is an extremely important factor in relation to the transient effect. Figure 6 is a comparison of transient maxima curves

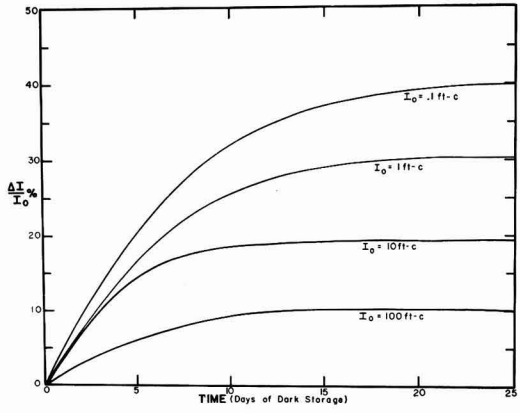

Fig. 6. Comparison of transient maxima or overshoot of the same type CdS photoconductive layers for which the reference level is the variable.

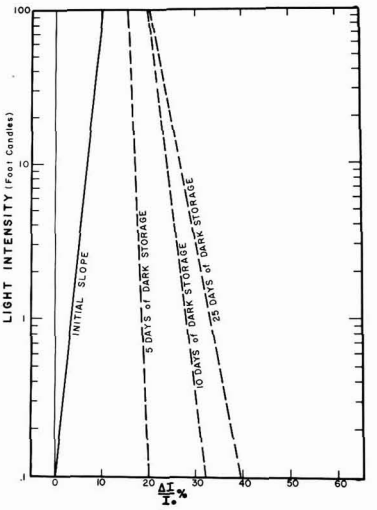

Fig. 7. The "initial slope" is based on some arbitrary photocurrent at 0.1 and 100 ft-c after the equilibrium condition has been established. The change of slope with time of dark storage is due to the fact that transient maxima or overshoots at high light levels are considerably smaller than those associated with the low light levels.

for the same CdS layer at several different reference levels (ranging from 0.1 to 100 ft-c in various steps). These data establish the fact that the transient maxima effect is more pronounced at low reference levels than at high reference levels. When considering this aspect it is easy to conceive that the slope of the photocurrent *vs.* light intensity curve will be strongly dependent on the excitation history of the layer prior to the taking of measurements. Figure 7 is a plot of the slopes for a group of CdS layers corresponding to various days of dark storage. These slopes are based on the data presented in Fig. 6. It is from these data that one may also envisage that at some high light level no transient maximum will be observed.

Decay of the Transients

The transient effect, as its name implies, is not a permanent effect, and photoconductors evidencing this effect have the ability, with light irradiation and time, to return to their long time equilibrium condition. The experimental results obtained for the recovery of sintered polycrystalline photoconductive layers to such an equilibrium condition, is presented herein.

A large group of these sintered layer photoconductors was subjected to an absolute dark environment for several months. The photoconductors were individually taken out of the dark and subjected to various light intensities for approximately 20 hr of continuous exposure. The initial photocurrent readings (I_m) of transient maxima from the dark were taken for the purpose of this experiment as the 100% value. The percentage decrease in photocurrent with time of light exposure is represented by $\Delta I/I_m\%$; this will be the expression used for this decaying effect. The data for the curves of Fig. 8 were taken with a Multi-Ranger Rustrak recorder (Model No. 111-A) which directly recorded the current readings of the

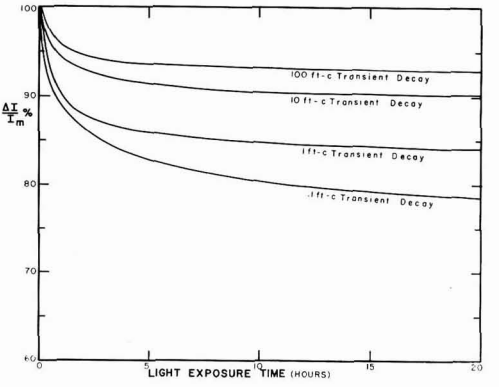

Fig. 8. Transient maxima or overshoot decay for a period of 20 hr for CdS type layers at various constant light intensity levels.

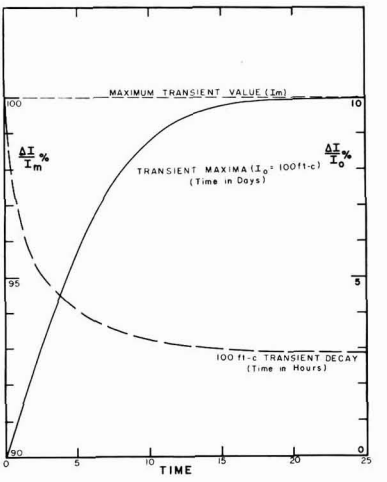

Fig. 9. Comparison of the growth of the transient maximum with the decay of that maximum for a reference level of 100 ft-c.

Hewlett Packard ammeter in the series circuit previously described. It should be noted, percentagewise, that there is less decay, with exposure time, from maxima at high light levels than from maxima at low light levels. This is apparent since there is correspondingly less overshoot associated with the higher light levels than the lower ones. Again attention should be called to the exponential nature of these transient decay curves.

In Fig. 9 the transient decay curve of Fig. 8 (for the 100 ft-c reference) has been superimposed upon the maximum curve of Fig. 4 (also for the 100 ft-c reference). We have equated the 100 ft-c maximum with I_m at 100 ft-c (the 100% level of the decay experiment). The superimposed curves show that in 20 hr of light exposure, at least for the case of the 100 ft-c reference, most of the transient maximum associated with this reference level has been erased or disposed of. These data also suggest that at low light levels the existence of these transient maxima will be of long time duration.

Rise Times

These experiments, as well as previously reported data (6-8), have evidenced the fact that photocon-

ductors coming from long time dark histories had much longer rise times than the same photoconductors which had a long time light history. The difference between these two conditions is approximately 37% for the case of the CdS layer under discussion, with a 10 ft-c reference. Specifically, those photoconductive layers taken from the dark had an average rise time of 31.5 msec, whereas the same layer with a long time 10 ft-c light history had an average rise time of 19.8 msec. Here again the excitation history of the layer plays a decisive role in their respective rise and decay times.

Discussion

When considering the data already presented in this paper, it is plausible to associate the transient effect with some trapping mechanism. It is at this time that a comparison of these data with some related data (2, 6, 9) and corresponding photoconductivity models is made.

The major difference between most previously reported works and this work is the manner in which the respective samples reach their true equilibrium condition. In Fig. 1 this difference has been shown by superimposing the general shapes of photoconductivity curves obtained from the aforementioned works with those obtained here (curve a is that curve which was reported by others (7-9) and curve b for the work reported herein). The general assumption of the band model necessitates an attempt to explain the transient effect in terms of what has already been recognized. Bube (2) has taken this first step by analyzing the transient effect as follows. He has asserted, in terms of the dual trap theory (8, 10), that the slow rise of the photocurrent from a quenched state is due to both the simultaneous increase of the concentration of holes in recombination or type I centers (*i.e.*, centers which have a greater probability for recombination than for thermal freeing) and a decrease in the concentration of holes in compensated acceptor or type II centers (*i.e.*, centers which have larger capture cross sections for holes than electrons). This theory implies that most holes are located in class II centers initially. Considering this aspect and the conditions set forth for transient minima (undershoot) it may be postulated that for transient maxima (overshoot) the density of free plus shallow trapped electrons must be greater than the density of holes in the Class II centers. Now, on excitation, the rate of ejection is greater than the rate of recombination, and simultaneously during this process both the free and shallow trapped electrons are being drained off rapidly. Thus the free electron density will eventually decrease until equilibrium is reached. A set of equations similar to those presented for undershoot (2) can be presented for overshoot by considering the rate of change of the density of free electrons (dn/dt) in the presence of excitation. By equating this term to zero, n_{max} can also be calculated, whence for the case of overshoot n_{max} must be greater than n_{equil}.

It has been stated that the prerequisite condition of this theory is that most holes must initially be located in centers of type II in order for the transient effect to be observed. For the case of CdS, elevated temperatures (above 100°C) were believed necessary to reproduce this situation (2). Nevertheless the existence of this transient effect at room temperature has been found for all CdS photoconductors reported here. In light of these results there now appears to be some correlation between the transient effect at high temperature with lightly activated materials and that at room temperature with highly activated materials. More specifically the degree of activation will strongly effect the temperature at which CdS will exhibit these transients.

The decreasing amount of overshoot observed with higher light intensities is obviously related to the previously obtained results on undershoot. Bube has reported (2) that if sudden changes in light intensity are made, whereby the lower light intensity of the change lies above the supralinear range,[4] no undershoot can be observed. Thus, it can now be said that above the supralinear range no undershoot nor overshoot can be observed in CdS or CdSe-type photoconductors.

If one assumes the transient effect is common to all photoconductive type materials, some clarification of conflicting rise time data can be made. Earlier papers (6-8) on CdS-type photoconductors convey the idea that the equilibrium value can be immediately reached by the first excitation of a quenched photoconductor (Fig. 1, curve a). Although the photoconductors prepared for this study follow curve b of Fig. 1 , it is still possible, under certain conditions, to reproduce most experimental variations in rise times that have been previously associated with photoconductors that follow curve a. The earlier papers have shown that previously quenched photoconductors will exhibit a decrease in their response times (to the equilibrium value) when subjected to a short quenching history and re-excited a second time. This decrease in response time, under similar conditions, has also been observed (see section on Rise Times) with photoconductors characteristic of curve b, Fig. 1. However there exists one major difference, *i.e.*, the decrease is observed only if the response time is taken with respect to the transient maximum and not the equilibrium value. In another work (11) the authors have shown that previously excited photoconductors exhibit an increase in their response time (to the equilibrium values) when also subjected to a short quenching history and re-excited again. Duplication of this result can be obtained only if the photoconductors under discussion have also had an initial excitation history. However, in both these cases the response time is obviously taken with respect to the true equilibrium value and not the transient maximum. The experimental data show that one can observe entirely different results by mistaking the equilibrium value for the transient maximum. The importance of recognizing this difference for the proper evaluation of photoconductive rise times is also emphasized.

[4] It is known that the photocurrent *vs.* light intensity curve is usually divided into three distinct ranges, *i.e.*, at low light intensities, a range where the photocurrent varies as the square root of light intensity; at intermediate light intensities, a range where the photocurrent is proportional to the light intensity; and at high light intensities, a range where the photocurrent rises supralinearly with the light intensity.

Acknowledgment

The author wishes to extend his gratitude to the members of the Clairex Corporation for making this paper possible. It is also his pleasure to acknowledge the many helpful discussions with Dr. Bernard Kramer of New York University.

Manuscript received Dec. 27, 1961; revised manuscript received March 20, 1962.

Any discussion of this paper will appear in a Discussion Section to be published in the June 1963 JOURNAL.

REFERENCES

1. K. W. Boer, *Physica*, **20**, 1103 (1954).
2. R. H. Bube, *J. Phys. Chem. Solids*, **1**, 234 (1957).
3. "Instructions for Using the Radiation Standards, (revised Dec. 27, 1951)." A reprint furnished by the National Bureau of Standard with their Standard Lamps.
4. National Bureau of Standards Report of Calibration for Color Temperature and Luminous Intensity of two 100 watt Inside frosted Lamps. NBS 5632, 5633. Test #2.1/163319.
5. R. H. Bube, *J. Appl. Phys.*, **31**, 1301 (1960).
6. H. Kallmann and B. Kramer, *Phys. Rev.*, **87**, 91 (1952)
7. R. H. Bube, "Photoconductivity of Solids," p. 290, John Wiley & Sons, Inc., New York (1960).
8. A. Rose, "Performance of Photoconductors," in Photoconductivity Conference, p. 3, John Wiley & Sons Inc., New York (1956).
9. H. Kallmann and P. Mark, *Phys. Rev.*, **105**, 1445 (1957).
10. R. H. Bube, article in Photoconductivity Conference, *op. cit.* p. 575.

The Dember Effect in ZnS-Type Materials

F. F. Morehead and A. B. Fowler

Thomas J. Watson Research Center, International Business Machines Corporation, Yorktown Heights, New York

ABSTRACT

A convenient system is described for measuring the diffusion current pulse produced by the sudden incidence of strongly absorbed radiation (Dember effect) on powder materials of the ZnS type. A model adequately representing the physics of the effect is given. It is shown that it is desirable to eliminate d-c contact effects in order to obtain reliable and reproducible results. The sign of the Dember current pulse indicates the sign of the more mobile carrier when the incident radiation is in the strongly absorbed, fundamental region. Reversals in the sign of the pulse are often encountered for weakly absorbed, longer wavelengths and are attributed to the effect of fast surface states. The excitation spectra for the Dember effect, photoluminescence, and electrophotoluminescence in a ZnS phosphor are given and correlated.

The relaxation processes involved in the Dember effect have kinetics determined by many factors: the variable dark times between light pulses, temperature, irradiation with long wavelength light during "dark" times, etc. These effects are described. It is found, for example, that the spectral dependence of the relaxation effected by long wavelength radiation correlates with the photoluminescence quenching spectrum of phosphor materials. Some of the potentialities of the Dember effect in studying these materials are pointed out.

One of the many photoeffects discovered before 1935 is the Dember effect, a diffusion dependent photovoltage. Strongly absorbed radiation incident on only one face of a crystal produces a diffusion current of the more mobile carrier away from the illuminated surface. The sign of the current is determined by the sign of the mobile carrier. The effect was first reported by Dember in Cu_2O (1) but except for a few papers by Russian workers, notably Zhuze and Ryvkin (2), and Bukke (3), and recent reports on AgCl (4) and GaAs (11), little use of the Dember effect has been reported in the evaluation of photoconductors and phosphors.

The technique employed in the present work and described in detail in a later section is essentially the transient condenser method (2) in which the possibility of spurious effects from illuminated contacts between the electrodes and the phosphor is eliminated. Several approximate quantitative treatments of the basic equations governing the effect are in the literature (5, 6), but even for the simplest, steady-state cases the results are too complex to be of much value in interpreting experimental results. A simple, phenomenological treatment, based on experiments, will be pursued in describing the physics involved in the measurements.

The purpose of this paper is simply to show that the Dember effect is an easily made measurement which gives information concerning the sign of the more mobile, or majority, carrier in materials for which Hall effect or thermoelectric power measurements are extremely difficult. Dember measurements can detect the approximate position of the absorption edge, its shift with temperature, the existence of significant impurity absorption and of fast surface states. The results of these measurements usually show useful correlation with the photoconductive, photoluminescent, electroluminescent, and electrophotoluminescent properties of these ZnS-type materials.

Experimental Technique

The experimental arrangement for observing this effect in polycrystalline material is shown in Fig. 1. A suitable mixture of the powder and an insulating

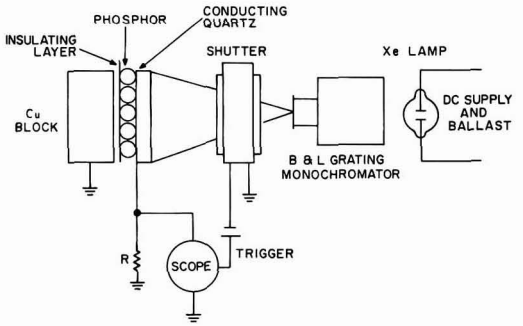

Fig. 1. Schematic arrangement of Dember pulse apparatus

binder (which is sometimes omitted) is compressed between the two plates of what is essentially an electroluminescent cell. One or more layers of ¼ mil Mylar are usually included to eliminate the possibility of electrode effects. None of the latter has ever been observed, however, with the Mylar omitted, and so in most measurements the layer between the powder and the silica disk which bears a conducting coat of SnO_2 is omitted. This latter arrangement permits transmission of intense u.v. down to below 300 mμ. When strongly absorbed light is flashed onto the transparent electrode, a current pulse is observed in the external circuit, a typical oscillogram of which is shown in Fig. 2a. The diffusion of the more mobile carrier away from the illuminated electrode leaves this electrode charged oppositely to that of the diffusing carrier, so that the positive current pulse shown in Fig. 2a identifies these carriers as electrons. A return pulse of lower peak value and opposite sign results when the shutter is closed, as shown in Fig. 2b.

A high pressure Xenon lamp is used as a source. The 250 mm Bausch and Lomb grating monochromator emits equal photon intensities (about 4×10^{14} photons/cm²/sec) for appropriate slit width settings determined at each wavelength with a thermocouple. The Graflex 1000 shutter flashes the full intensity onto the cell in less than a millisecond. For studies of the temperature dependence of the effect, both the insulating layer and the binder are omitted. The latter omission causes considerable loss in signal, but it is important to eliminate effects which might be caused by the temperature dependence of the dielectric constant of the binder. The cell chamber can be evacuated to a pressure below 1μ Hg and the Cu block electrode cooled to liquid nitrogen temperature or heated to above 200°C.

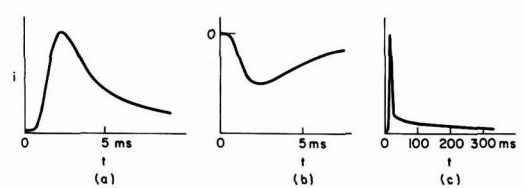

Fig. 2. (a) Typical electron diffusion current pulse; (b) return pulse (electrons); (c) contact current tail of (a).

Experimental Results and Discussion

The physics of the effect.—A brief description of the phenomenological physics of the "condenser method" for measuring the Dember effect in powdered materials may prove helpful in the subsequent examination of results. It will be shown that in addition to the fast displacement current there exists a slow interparticle contact current. This latter current can be observed either as a steady-state short circuit d-c current in the absence of an insulating layer or as the long tail on the displacement current pulse when the insulator is present. It will also be shown that the fast, displacement current is the more reliable and reproducible indication of the type and quantity of the more mobile carrier and that the effects of the contact current should be minimized. The rise time of the Dember current pulse (cf. Fig. 2a) is the same order as the shutter opening time t_s (about 1 msec) and is never significantly slower. The fall time from the current maximum can be related roughly to an exponential decay time, RC. The peak current i_m is given by

$$i_m = (i_m)_0 \frac{RC}{t_s}(1 - e^{-t_s/RC})^1 \qquad [1]$$

where $(i_m)_0$ is the maximum peak current that would occur for t_s/RC equal to zero. This equation relates only the effect of shutter speed for a given material in a given set of experimental conditions. This relationship has been found to hold experimentally by varying the shutter speed. A fast shutter is therefore advantageous.

A long tail with a much slower time constant (cf. Fig. 2c) is considered to be due to the direct flow of current between particles, although the detailed mechanism is unknown. This latter current flow must depend on the effect of internally scattered radiation in changing the contact emf between particles and evidently requires a much longer time to establish than the photodiffusion emf responsible for the fast displacement current pulse. Since the contact photovoltages must involve accumulation or depletion of space charge, it is reasonable that they should require a longer time to reach a peak value. This slow current will be discussed further later.

The fast current pulse is due to the charge which moves in the external circuit corresponding to the diffusion of the more mobile carriers away from the

[1] A "curtain" shutter, moving with velocity v, exposes fresh areas of the cell with maximum current I_m amp/cm² at the instant of exposure which subsequently decays exponentially with a time constant RC. For a square cell of width w and length l, along which latter the shutter moves, the shutter opening time $t_s = v$. For $t \leq t_s$, the measured current at time t from the start of the shutter movement

$$i(t) = I_m w \int_0^x e^{-\frac{x}{vRC}} dx$$

$$= (I_m wl) \frac{RC}{t_s}[1 - e^{-t/RC}]$$

where $x = vt$. For $t \geq t_s$

$$i(t) = i_m w \int_0^t e^{-\frac{t-x/v}{RC}} dx$$

$$= (I_m wl) \frac{RC}{t_s}[e^{t_s/RC} - 1]\, e^{-t/RC}$$

The maximum value of $i(t)$ occurs at $t = t_s$

$$i_m = (I_m wl) \frac{RC}{t_s}(1 - e^{-t_s/RC})$$

which, for $(i_m)_0 = I_m wl$ is Eq. [1].

illuminated surface of the top layer of particles. It is independent of interparticle contacts and the more reliable and reproducible indication of the quantity and type of mobile carriers in the material. One therefore should choose those experimental parameters (intensity of incident light, cell thickness, volume fraction of material in the phosphor-liquid dielectric mixture, etc.) which enhance the fast pulse and minimize the slow interparticle current.

The RC decay time of the fast displacement current pulse arises from a capacitance C which is experimentally equal to the cell capacitance and an R which apparently arises from isolated photoconducting areas on the particle surfaces parallel to the direction of the measured current. Incident light (which is not absorbed by the imbedding medium) can be scattered into the interior of the cell and illuminate these parallel particle surfaces. Hence the equivalent circuit can be characterized as a series resistance R and capacitance C. R can be estimated from the reduction in current pulse height caused by the insertion of a large resistor in series with the cell. R varies directly with cell thickness in the range of 50-500μ; it decreases with increasing light intensity as shown in Fig. 3. C can be estimated from the value of R and the exponential decay time of the pulse. This value of C agrees well with the capacitance of the cell computed from the current produced by applying a high frequency a-c field. C is very nearly independent of light intensity (cf. Fig. 3). As long as the oscilloscope input resistance used to measure the Dember current is small compared to R, the decay time of the current (the fast part) is independent of the cell thickness, since R varies directly and C inversely with thickness.

The charge Q moves a diffusion length d from the surface of the top layer of particles. The fraction of this charge which contributes to the pulse current observed in the external circuit is d/l, where l is the thickness of the cell. Since the exponential decay time RC is independent of l, the peak external current

$$i_m = \frac{Q(d/l)}{RC} \qquad [2]$$

varies inversely with the cell thickness l. Typically $(i_m)_0$ varies with the intensity of the incident light as shown in Fig. 3 for a ZnS:Cu, Cl phosphor for 320 mμ excitation.

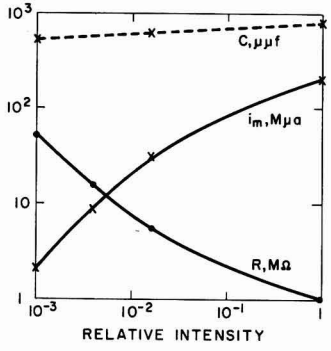

Fig. 3. Variation with incident intensity of 320 mμ light of: i_m, the peak pulse current; R, the effective resistance; and C, the capacitance. See text.

One can estimate a lower limit for the diffusion distance d from the peak current, $(i_m)_0$, produced by a known photon flux $W_{h\nu}$ falling on a cell of known thickness l. Because of the insulated contact each photon striking the surface of the cell can produce at most one mobile carrier to diffuse away from that surface an average distance d and contribute to $(i_m)_0$ in the ratio d/l. Since

$$(i_m)_0/e < W_{h\nu}\frac{d}{l} \qquad [3]$$

we have

$$d > l[(i_m)_0/e\, W_{h\nu}] \qquad [4]$$

The maximum estimate of the lower limit of d is obtained at that incident intensity for which the current is varying most strongly with intensity. Experimentally this variation is at most linear and occurs in Fig. 3 for a value of the intensity 2×10^{-3} times the maximum photon flux used, which is 2×10^{16} photons/sec. For this case $W_{h\nu}$ is 4×10^{12} photons/sec, l is 55μ, and i_m is 5×10^{-9} amp. Substitution of these values in Eq. [4] shows that d must be at least 0.4μ. This distance represents an appreciable penetration into the particle bulk and at least indicates that more than the surface is involved in these measurements.

The effect of variation of the volume fraction of the active material in the imbedding medium on $(i_m)_0$ can be summarized as follows: For thin cells (less than 100 microns) $(i_m)_0$ increases first linearly with increasing volume fraction of the phosphor, but appears to saturate above 40%. For thicker cells the saturation occurs at lower values of the volume concentration. The value of the volume concentration of the active material used in most measurements was 30%.

In the absence of an insulating layer a direct photocurrent is produced by the incident, strongly absorbed radiation. It is probably due to the photovoltaic effects at the interparticle contacts. One can measure an open-circuit voltage and a short-circuit current with an electrometer and from these values compute an effective d-c resistance, assuming ohmic character. With the insulating Mylar present, this interparticle current and the fast displacement current build up a charge on the Mylar which is measurable as an open-circuit voltage on the electrometer. This voltage increases with cell thickness, indicating that most of the charge accumulating on the insulating layer is carried by the interparticle contact current since the fast displacement current pulse decreases linearly with increasing cell thickness, as described above. The open-circuit voltage of a cell without the Mylar layer increases with increasing cell thickness. This result is as one might expect since the photovoltages of a larger number of contacts add to give a larger value for a thick cell than for a thin cell.

The decay of the slow, interparticle contact current, which forms the tail of the Dember pulse as shown in Fig. 2c, can also be characterized as the exponential decay of a series RC circuit. The capacitance is that of the ¼ mil Mylar layer and the

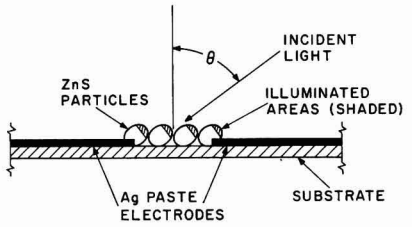

Fig. 4. Experimental arrangement used to measure the angular dependence of a d-c Dember voltage. See text.

resistance is the effective d-c photoresistance of the cell without the insulating layer, calculated from the open-circuit voltage and the short-circuit current of the latter cell. This agreement of the decay time of the Dember pulse tail with the product of the capacitance of the Mylar and the computed resistance of the d-c cell substantially identifies the two effects. That is, the direct photocurrent and the slow Dember pulse tail have the same origin, probably interparticle contact photovoltages.

This interparticle contact current depends on a gradient in the incident flux, as the following experiment demonstrates. A mixture of ZnS and binder was laid on two silver paste electrodes as shown in Fig. 4. A measurable open-circuit direct photovoltage (or a short-circuit current) is produced which is a function of the angle θ between the direction of the field between the two electrodes and the direction of the incident light. For θ different from zero there will be a component of the incident light in the same direction as that of the electrodes; this parallel component is proportional to $\sin\theta$. Since the measured photovoltage varies as the ¼ power of the intensity over two orders of magnitude in intensity, while the intensity of the light incident on the sample varies as $\cos\theta$, the expected variation in the open-circuit photovoltage is

$$V_{oc} = (\overline{V_{oc}})_m \cos^{1/4}\theta \sin\theta \qquad [5]$$

Equation [5] fits the experimental values of V_{oc} quite well for $(\overline{V_{oc}})_m = 1.8$v, correctly predicting a maximum of 1.3v at $\theta = 63° 25'$.

Experimentally it has been found that the value of the peak pulse displacement current is far more reproducible than the d-c contact photovoltage, both for measurements made at different times on the same sample and for different samples prepared in the same way from the same starting material. The uncertainty concerning the exact mechanism of the d-c effect makes it a less reliable indication of the sign of the more mobile carrier than the displacement current pulse. However, for fundamental radiation, the two effects do have the same sign for all samples examined thus far.

In summary the experimental conditions that have been found to favor the displacement pulse and to minimize the interparticle contact current tail are the following: (i) high intensity of incident light, (ii) as thin a cell as feasible, (iii) not too high a volume concentration, to minimize interparticle contacts, and (iv) the fastest available shutter speed.

Effects observed in ZnS *phosphors–general remarks.*—A large difference in depth between the electron trapping states and hole trapping states is the usual situation in ZnS. This fact, plus the higher microscopic mobility of electrons, leads to the possibility that not only completely compensated but also a significant range of p-type samples will yield electronic Dember currents. (An experimental technique for distinguishing the two types when both give electronic Dember currents will be described later.) At room temperature the absorption of fundamental radiation by compensated or n-type ZnS results in a concentration gradient in both holes and electrons. The holes are quickly trapped at the compensated and hence ionized acceptor levels which usually lie around 1 e. v. up from the valence band edge. The electrons are not strongly trapped at the shallow (~ 0.25 e. v.) ionized donor levels (in both compensated and n-type material) and therefore readily diffuse in the concentration gradient established by the strongly absorbed incident light. An electronic Dember current results.

Despite the rather large energy difference between acceptor levels and the valence band in ZnS, which allows almost no dark conductivity for even strongly p-type materials at room temperature, a p-type Dember current from fundamental radiation has been observed in such samples. Band gap radiation at the surface produces, as always, both electrons and holes in a strong gradient. In strongly p-type material, electrons will first be captured in the uncompensated and therefore unionized acceptors before the diffusion current of the holes is impeded by the resulting ionized acceptors, which are hole traps. More holes than electrons can move in the concentration gradient and a net hole current is observed. It should also be remarked that a given number of uncompensated acceptors per unit volume can produce a hole current only if the number of compensated acceptors (hole traps) is small. If this latter number is large, an electron Dember current results.

Excitation spectrum of the Dember effect, photoluminescence, and electrophotoluminescence.—Figure 5 shows the spectral distribution of the size and

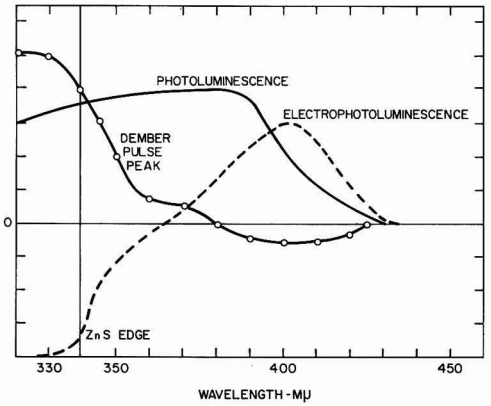

Fig. 5. Excitation spectra of photoluminescence, Dember pulse, and electrophotoluminescence for a ZnS:Cu,Cl phosphor. See text.

sign of the peak Dember pulse current for a ZnS phosphor containing 4 x 10^{-3} (mole fraction) Cu and 3 x 10^{-3} Cl. Significant absorption by impurities is shown by the finite positive current (indicating electron diffusion) extending up to 380 mμ. Unactivated ZnS yields a significant Dember pulse below 350 mμ at room temperature, indicating an absorption edge at around 340 mμ. The weaker absorption of wavelengths above 380 mμ by the Cu, Cl activated phosphor results in a reversal of the direction of the Dember pulse. This reversal is ascribed to the effect of fast surface states whose rapid capture of electrons produces a net flow of these carriers toward the illuminated surface and hence a negative pulse [cf. ref. (4)]. The weakly absorbed long wavelength light produces too moderate a concentration gradient in the mobile carriers to overcome their rapid depletion by the surface states. An attempt to change the occupation and hence the effect of the surface states with various ambient gases was unsuccessful. The close-packed and necessarily enclosed structure of the cell may have been responsible for this failure.

The excitation spectrum of the green photoluminescence of this ZnS:Cu, Cl phosphor is also shown in Fig. 5. No luminescence is excited by wavelengths greater than the Dember pulse cut-off around 450 mμ.

The electrophotoluminescence excitation spectrum in Fig. 5 shows the effect of a pulsed electric field applied to the cell on the luminescence excited at each wavelength. In the long wavelength region the usual Godden-Pohl (7) effect appears. A pulsed enhancement of the photoluminescence occurs for both the application and the reversal of the electric field. This behavior is depicted in Fig. 6a for 400 mμ. The field (of either polarity) served to empty filled traps, either by direct field ionization or by the impact of field-accelerated electrons, and a temporary increase in emission results. It is interesting to note that the applied fields required to produce this effect are only of the order 5 x 10^3 v/cm for electroluminescent ZnS:Cu, Cl phosphors, but over 5 x 10^4 v/cm are necessary for nonelectroluminescent ZnS:Cu, Cl phosphors. This observation corroborates the postulated existence of regions of much higher than average fields in the electroluminescent material (8).

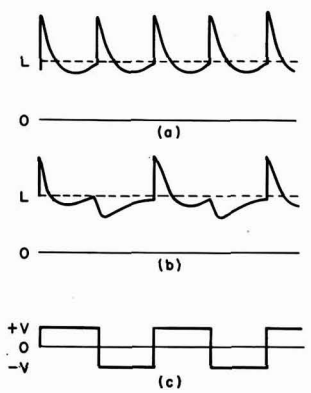

Fig. 6. Field modulation of photoluminescence in a ZnS:Cu,Cl phosphor (electrophotoluminescence): The effect of pulsed electric field (c) on the luminescence excited by 400 mμ (a) and 320 mμ (b). The dashed line is the unmodulated photoluminescence.

For short wavelengths a different type of modulation of the luminescence by the field occurs, which has been described by Halsted (9). Here the field apparently moves the mobile carriers into or out of the narrow excitation region determined by the absorption constant of the material for the incident light. If electrons are the more mobile carriers and if the radiative recombination is that of a free electron and a trapped hole, then making the illuminated surface positive will increase the luminescence by pulling more electrons into the excitation region. Application of a negative voltage to the surface produces a temporary diminution in the emission. This type of electrophotoluminescence is illustrated in Fig. 6b for which the exciting wavelength is 330 mμ. The electrophotoluminescence excitation spectrum in Fig. 5 shows the peak relative change (arbitrary units) in the photoluminescence produced by applying a negative field of 3 x 10^4 v/cm. At 365mμ there is a change in sign of this electrophotoluminescence, denoting a transition from one effect to another. Above 365 mμ the field has the effect of emptying electron traps while below this point the field moves the free carriers in and out of the excitation region. For the field of opposite polarity (positive) the sign of the electrophotoluminescence is opposite to that shown in Fig. 5 below 365 mμ and the same as shown above that wavelength. The results of the electrophotoluminescence and Dember measurements are consistent with mobile electrons and the radiative recombination of free electrons and trapped holes.

Relaxation and temperature effects.—In most instances the size and in some cases the direction and shape of the Dember pulse is a sensitive function of the time the cell has remained in the dark since last exposed to the exciting light. When the wavelength of the incident radiation is in the fundamental region, longer dark relaxation times give larger peak Dember currents. The more time that is available for the relaxation of the polarization field produced by a previous exposure to the strongly absorbed radiation, the greater the diffusion current which can flow when the excitation is again applied to the sample. In many cases the maximum current flows following a definite dark time. Both longer and shorter dark times can result in a smaller pulse peak. There are at least two possible explanations for the occurrence of this maximum. One possibility is the increase in the effective mobility of the carriers caused by filling some of the traps in the excitation region. The degree to which these traps are filled is greatest for short dark intervals.

One other possible explanation invokes the undoubted heterogeneity of the powder samples. A distribution of p-type and n-type (or compensated) particles is assumed. The electronic displacement in the n-type particles relaxes after only small dark intervals; the polarization of the p-type particles relaxes much more slowly since the holes are

trapped in much deeper levels than are the electrons (~1.0 e. v. for holes, ~0.25 e. v. for electrons). At the dark time for which the maximum electron Dember current is produced nearly all of the electrons in the n-type particles and only a few of the holes in the p-type particles have returned to the region from which they were excited near the surface. Longer dark times allow the return of an appreciable number of holes, so that the net electron Dember current pulse is reduced.

In some instances the sign of the Dember current pulse for sufficiently long periods of dark relaxation is opposite (p-type) in sign to that measured for short periods in the dark (n-type). A relatively short exposure (1 min) to intense long wavelength radiation (over 600 mμ) produces the same reversal (or reduction in value) in the Dember pulse (at 320 mμ) as the extended dark period (overnight). The effect of the long wavelength light will be discussed in more detail in the section on optical relaxation effects.

One can conclude from the above model that a Dember signal that monotonically increases with increasing dark time characterizes n-type or completely compensated material. A maximum pulse at a particular dark time indicates an appreciable amount of p-type material. A more convenient experimental criterion is the following: the Dember pulse is measured after 1 min in the dark (Pulse A) and after 1 min exposure to intense IR (Pulse B). Figure 7 schematically illustrates the four experimental possibilities and lists the nature of the material deduced from the experiment. If Pulse B is equal to or greater than a positive Pulse A, then there is no detectable p-type material. For Pulse A positive and greater than Pulse B (positive or negative), the absolute value of B − A is taken as a measure of the degree of p-type uncompensation in the sample. If Pulse A as well as Pulse B is negative, the value of Pulse B alone measures the degree of p-typeness, since there is apparently no measurable electron current. The deduced Pulse C is, in each instance, a measure of the p-typeness of the material.

Since the interparticle contact photocurrent does not, in general, reverse its direction at the same wavelength as the Dember pulse (cf. Fig. 5), quite complicated pulse shapes are possible in this re-

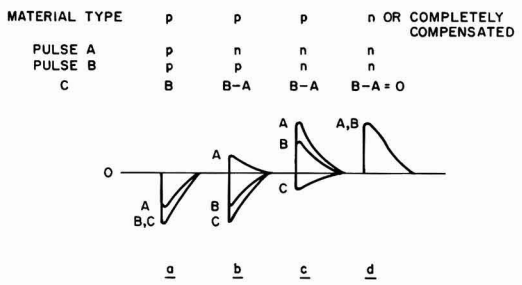

Fig. 7. Four possible Dember pulse combinations obtained from ZnS materials: Pulse A, after 1 min dark relaxation; Pulse B, after 1 min infrared exposure; Pulse C, deduced p-type current in Pulse B. See text.

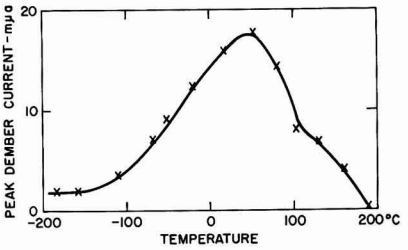

Fig. 8. Temperature dependence of the Dember pulse peak (30 sec dark interval) for a ZnS:Cu,Cl phosphor.

versal region. At least two extrema are observed when the reversal is present. The relative size and position of these extrema depend on the dark relaxation time, the wavelength, and the intensity of the exciting light. Some materials have given as many as four extrema in this reversal region.

A typical dependence of the height of the Dember pulse on temperature is shown in Fig. 8, for a ZnS:Cu, Cl 4 x 10^{-3} phosphor. The exciting wavelength was 320 mμ and a dark interval of 30 sec was used at each point. The Dember pulse is smaller at high temperatures for n-type or compensated specimens for either of two reasons. One is that both electrons and holes can diffuse in the concentration gradient, yielding a lower net electron current; the other is that the electron mobility could decrease at high temperatures. At low temperatures the electrons are frozen at shallow (~ 0.25 e. v.) traps. In the region of maximum response only the holes are immobilized at deep (~ 1 e. v.) hole traps, resulting in a large electron diffusion current. Shorter (< 30 sec) dark times tend to shift the temperature of maximum response to higher temperatures.

For a specimen of unactivated ZnS fired at 1200°C in a sealed vacuum and presumed (because of the higher volatility of S_2 compared to Zn) to contain excess Zn and therefore some uncompensated donors (sulfur vacancies) an interesting behavior was observed. At room temperature only a small peak Dember current (<10^{-8} amp) appeared for reasonable dark times of the order of minutes. This current could be increased to around 1.0 x 10^{-7} amp by very long periods of relaxation in the dark or by heating to above 150°C and returning to room temperature before flashing with the 320 mμ. After cooling the sample to nitrogen temperature from room temperature and subsequent exposure to the 320 mμ light, the measured current was 1.5 x 10^{-7} amp. If the sample was first heated to 150°C before cooling to −180°C, a peak Dember pulse of 2 x 10^{-7} amp was measured. The second pulse at −180°C is in every case negligibly small, less than 10^{-9} amp. The high value of the first pulse at this temperature may be due to the freezing of the dark electrons on the uncompensated donors, with a consequent decrease in the scattering due to charged, ionized donors present at room temperature. Thus a higher Dember current pulse results than for even the completely relaxed sample at room temperature (2 x 10^{-7} *vs.* 1 x 10^{-7} amp). ZnS materials expected to be completely compensated do not exhibit this behavior.

Optical relaxation effects.—The continuous exposure of the test cell to a beam of radiation other than that which is flashed onto it to produce a pulse of diffusion current usually results in lower peak value. This reduction of the pulse height is most prominent when the two beams of radiation are the same wavelength. An exception to this behavior is the case in which the continuous exposure is to wavelengths in the fundamental and the pulsed beam is in the reversed region at longer wavelengths. (cf. Fig. 5). The extrinsic carriers ionized by the weakly absorbed long wavelength radiation move in the polarization field maintained by the strongly absorbed fundamental radiation. The result is an increase in the reversed pulse normally observed in this wavelength region. In fact, to obtain this increase, simultaneous exposure is not necessary in some cases, so that a previous exposure to fundamental radiation suffices to enhance the reversed current in the long wavelength region. Hence, in order to obtain unambiguous results from long wavelength excitation, one should proceed from long to short wavelengths in measuring the spectral dependence of the Dember effect, using a sample kept in the dark for a prolonged period.

In some cases ZnS materials which yield positive (electron current) Dember pulses for short dark time intervals not only give reduced positive signals for long relaxation periods, but for sufficiently long dark times produce a negative (hole current) Dember pulse. This reversal in sign (for fundamental excitation) can also be effected by exposure to long wavelength radiation. Figure 9a shows the size of the Dember pulse peak obtained at 320 mμ for a ZnS sample after relaxing for 30 sec while exposed to the radiation whose wavelength is indicated on the abscissa. The unactivated ZnS was fired for 24 hr at 900°C in a sealed quartz tube in a sulfur pressure of

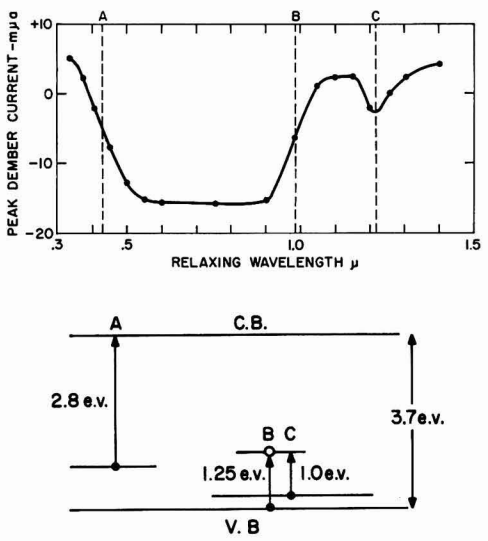

Fig. 9a. (top) The Dember pulse peak measured at 320 mμ after 1 min exposure to the plotted wavelengths for an undoped p-type ZnS sample. Fig. 9b (bottom) The energy levels deduced from (a). The transitions A, B, and C are described in the text.

6 atm. There is no luminescence. Figure 9b shows an energy level scheme consistent with the data of Fig. 9a. Wavelengths between 450 mμ (A) and 1.0μ (B) raise electrons from the valence band to the ground state of an unionized acceptor, freeing a hole in the valence band to return to the excitation region and relaxing the sample (transition B). Radiation of 1.2μ (C) lifts an electron from an excited hole state of the unionized acceptor (which is in thermal contact with the valence band) to the ground state of the unionized acceptor (transition C). The hole, which is now situated at the excited hole state of the acceptor, can now be thermally released into the valence band. Wavelengths below 450 mμ (A) are more effective in ionizing electrons from a filled center (transition A) than holes from an empty center, increasing the probability of a positive (electron current) Dember pulse. The proposed energy level structure of the acceptor is remarkably close to that deduced by Apple and Prener (10) from the infrared fluorescence and diffuse reflectance of ZnS into which Cu had been fired under sulfur pressure to produce uncompensated acceptors. Whether the acceptor in the present material is due to impurities such as Cu which were present in the "pure" (RCA luminescent grade) unactivated material or simply arise from a singly ionized zinc vacancy is uncertain.

A ZnS: 1.5 x 10^{-3} Cu, 1.0 x 10^{-3} Cl blue-green emitting phosphor also exhibited this reversal of a positive (electron current) pulse at 320 mμ after relaxing with long wavelength radiation. A relaxation spectrum similar to Fig. 9a was obtained. The Dember pulse in the 350 to 420 mμ region, which is negative for short dark times, becomes positive after long wavelength relaxation. The complete Dember current spectrum (cf. Fig. 5) is reversed in this instance in going from short dark times to long wavelength relaxation between pulses. One possible explanation of the positive (electron current) pulses obtained in p-type samples such as those described above for short dark times is that of holes going toward the surface, from which they could escape (depolarize) more readily than from the bulk where they might be trapped more deeply. Since going to longer exciting wavelengths could hardly reverse this process, as it does in the present instance, this explanation must be discounted.

For the above phosphor (ZnS: 1.5 x 10^{-3} Cu, 1.0 x 10^{-3} Cl) the blue-green photoluminescence produced by 365 mμ ultraviolet is strongly quenched when infrared radiation is also shone on the sample. The spectral dependence of the quenching effect is in close agreement with the relaxation spectrum. This result confirms the hypothesis that the release of holes into the valence band from the empty activator level (transitions B and C in Fig. 9b) is the first step in both the quenching of luminescence and the optical relaxation of the Dember polarization.

Measurements on other materials.—Some measurements have been performed on other compounds than ZnS in powder form, including CdSe, ZnSe, ZnTe, and mixed crystals of ZnS and ZnSe. The results are of the same form as for ZnS, yielding information on the type of carrier which is either more mobile or a true majority carrier. The shift in band

edge of ZnS, ZnSe alloys as a function of composition, as well as its shift with temperature, is easily measured, for example. Shifts in stoichiometry produced by various thermal treatments have been followed in at least a semiquantitative sense with CdSe as well as ZnS.

Similar measurements are possible with thin films deposited on a conducting substrate. A piece of conducting quartz separated from the film by a quarter mil Mylar layer forms the second electrode of the Dember cell. Films of p-type CdTe and both p- and n-type CdSe have been prepared (by G. Somorjai) and measured in this manner.

Summary and Conclusions

The pulsed Dember effect measured as described above is a useful tool for indicating the type of mobile carrier and to a degree the extent of activation of powder and thin film materials of the ZnS type. The displacement current pulse is probably a more reliable and certainly a more reproducible measurement than a direct current measurement relying on interparticle contacts. Careful control of such experimental parameters as cell thickness, volume concentration of the material, and radiation intensity are necessary for good reproducibility.

The change in size and direction of the Dember pulse can be used to follow shifts in stoichiometry and impurity content resulting from various treatments. For example, unactivated ZnS fired in sealed quartz tubes under various sulfur pressures shows a shift from n- to p-type pulses with increasing sulfur pressure. The algebraic value of the peak current is linear with $\sqrt{p_{S_2}}$. Uncontrolled impurities in the starting material have lead to ambiguous results in many cases, however. Experiments of this type are still being pursued.

In luminescent materials, measurements of the Dember effect and of the electrophotoluminescent response can unambiguously determine the nature of the radiative recombination under certain conditions. Often a relaxation spectrum such as that shown in Fig. 9a can be obtained. Information on the existence and nature of such levels as shown in Fig. 9b can thus be obtained and correlated with, for example, the photoluminescence excitation and quenching spectrum of the same material. Such levels can even be demonstrated to exist in materials that are otherwise uncommunicative, that is nonluminescent.

Acknowledgments

The writers wish to thank Drs. S. P. Keller, R. S. Title, F. Jona, G. Mandel, L. Suchow, and G. Somorjai for much helpful discussion and many suggestions. The services of Mr. J. A. Kucza for many preparations and Mr. W. N. Hammer for assistance in making many of the measurements is gratefully acknowledged.

Manuscript received Jan. 15, 1962.

Any discussion of this paper will appear in a Discussion Section to be published in the June 1963 JOURNAL.

REFERENCES

1. H. Dember, *Physik. Z.*, **32**, 554, 856 (1931); **33**, 207 (1932).
2. V. P. Zhuze and S. M. Ryvkin, *Doklady Akad. Nauk. SSSR*, **62**, 55 (1948).
3. E. E. Bukke, *Optika I. Spektroskopiya*, **3**, 334 (1957).
4. A. M. Goodman and G. Warfield, *Phys. Rev.*, **120**, 1142 (1960).
5. R. H. Bube, "Photoconductivity of Solids," p. 384, John Wiley & Sons, New York (1960).
6. J. S. Moss, L. Pincherle, and A. M. Woodward, *Proc. Phys. Soc.*, **66B**, 743 (1953).
7. B. Gudden and R. Pohl, *Z. Physik.*, **2**, 192 (1920).
8. W. W. Piper and F. E. Williams, "Solid State Physics," Vol. 6, Academic Press, New York (1958).
9. R. E. Halsted, *Phys. Rev.*, **99**, 1897 (1955).
10. E. F. Apple and J. S. Prener, *J. Phys. Chem. Solids*, **13**, 81 (1959).
11. C. M. Hurd, *Proc. Phys. Soc. London*, **79**, 42 (1962).

The Effect of the Phosphor-Embedding Medium on the Performance of Electroluminescent Cells

Gabriel P. Katona[1]

Corning Glass Works, Corning, New York

ABSTRACT

The higher the dielectric constant of the phosphor-embedding medium, the higher is the field on the embedded phosphor. When working with ZnS-type phosphors, not much is to be gained from embedding media having dielectric constants higher than 50. In the case of embedding media having a low dielectric constant the emission can be increased by making the embedding medium of greater loss materials. This move will not necessarily lower the efficiency, but at points it will even improve it. It is shown that maximum efficiency can be obtained when the dielectric constant of the embedding medium and the phosphor are identical.

The primary goals of research for better electroluminescent lamps and devices are to develop materials and structures that will result in higher brightness and better luminous efficiency. Much has been reported in the literature of the work to achieve these aims through improved phosphors. In this paper the effect of the dielectrics on the brightness and efficiency of electroluminescent cells is discussed.

[1] Present address: Nolte and Nolte, New York, N. Y.

Dielectrics perform two basic roles in electroluminescent structures: (*a*) they act as embedding media, (*b*) they are used as breakdown protecting layers. The second function will be discussed in a later article.

The properties of the embedding medium have a multifold effect on the performance of an electroluminescent lamp. Such effects can be due to dielectric properties of the materials, physicochemical interaction between the phosphor and dielectric, viscosity of the dielectric allowing movement of the embedded phosphor, moisture penetrability of the dielectric affecting maintenance, etc. This paper investigates the effect of the dielectric properties.

The availability of embedding materials embracing a wide range of dielectric properties is rather limited. Therefore, the considerations to be presented may aid in the selection of the materials that are most suitable for a required purpose.

The same green emitting ZnS:Cu, Cl electroluminescent phosphor was used throughout the investigation; thus the considerations presented can be assumed to be valid in case of other phosphors only when the voltage response of the other phosphor is similar to that of the phosphor used here. Definitions of the symbols used are listed at the end of the paper.

Effect of the Dielectric Constant

Roberts (1) and Kerner (2) have shown that the internal field, directly acting on the embedded phosphor, is related to the applied field by

$$E_o = E_2 \frac{3K_1}{2K_1 + K_2 - N(K_2 - K_1)} \qquad [1]$$

The value of $K_2 = 10$ was used for the dielectric constant of the phosphor in the subsequent calculations. This is an approximate average of the various values reported in the literature for ZnS-type electroluminescent phosphors.

The internal field was calculated as a function of the dielectric constant of the embedding medium, by means of Eq. [1]. The results are shown in Fig. 1. The arbitrary value of 23% by volume of phosphor was used. The applied field was 100 v/cm.

As Fig. 1 and Eq. [1] indicate, by choosing embedding media having a dielectric constant higher than the dielectric constant of the phosphor, the internal field acting on the phosphor becomes greater than the field applied across the cell proper.

Using the above example of 23% by volume phosphor and 100v applied across a thickness of 1 cm, it is possible to obtain internal field values which are higher than the applied electric field. When the dielectric constant (permittivity) of the embedding medium is infinite, it allows unimpeded passage of the applied field, which then appears across a continuous phosphor layer that is in effect 0.23 cm thick. The resultant field across the phosphor then is 100/0.23 = 435 v/cm.

The results obtained by using Eq. [1] were used to plot the effect of the dielectric constant of the embedding medium on the emission intensity. A cell was prepared by embedding a commercial EL phosphor in glass[2] and the brightness values, measured as a function of voltage on this cell, were used for the calculations. The phosphor concentration was 23% by volume, and the frequency was 1000 cps. The dielectric constant of the embedding glass was about 5.

[2] Corning Code 1970, a glass specially developed for electroluminescent phosphor-embedding purposes.

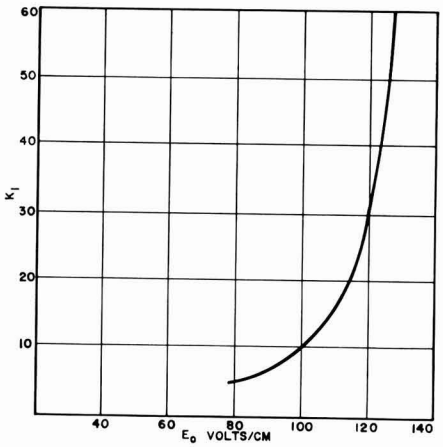

Fig. 1. Effect of the dielectric constant of the phosphor embedding medium on the internal field.

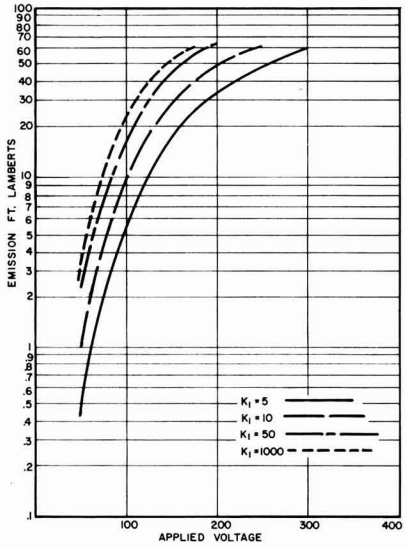

Fig. 2. Effect of the dielectric constant of the phosphor embedding medium on the emission intensity.

As Fig. 2 shows, by raising the dielectric constant of the embedding material from 5 to 10, a brightness gain of about 100% can be predicted. By further raising the dielectric constant from 10 to 50 a further brightness gain of nearly 100% can be predicted. By raising the dielectric constant from 50 to 1000, a brightness gain of only about 30% could be realized theoretically within the validity of Eq. [1]. These data indicate that, when striving to raise the dielectric constant of the presently available embedding media by intensified materials development efforts, a practical limit of 50 would be adequate.

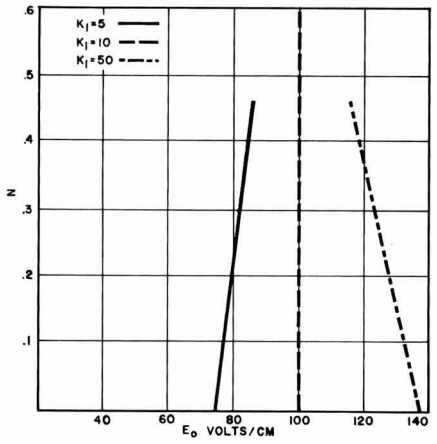

Fig. 3. Effect of the phosphor volume ratio on the internal field

Effect of Phosphor Concentration

Equation [1] can also be used to calculate the effect of phosphor concentration on the field distribution within the electroluminescent layer. Figure 3 shows the internal field as a function of the volume fraction of the embedded phosphor. As above, the dielectric constant of the phosphor was assumed to be 10, and the applied field, 100 v/cm.

Effect of the Loss Tangent

The complex dielectric constant of the form

$$K^* = K' - jK'' \qquad [2]$$

was substituted into Eq. [1] for the dielectric constants of the embedding medium (K_1) and the phosphor (K_2). Thus one obtains

$$E_o = E_2 \frac{3(K'_1 - jK''_1)}{(K'_1 - jK''_1)(2+N) + (K'_2 - jK''_2)(1-N)} \qquad [3]$$

By using the loss characteristics of the phosphor that was used throughout this work (3) it was found that the phosphor can be represented only by its dielectric constant and that neglecting the phosphor loss has only a very small effect on E_o in case of phosphor concentrations in the 20% by volume range.[3] Consequently Eq. 3 was modified to read:

$$E_o = E_2 \frac{3(K'_1 - jK''_1)}{(K'_1 - jK''_1)(2+N) + K_2(1-N)} \qquad [4]$$

By substituting $K''_1 = K'_1 \tan\delta$ one obtains for the absolute value of the internal field:

$$E_o = 3E_2 \sqrt{\left\{\frac{K'_1K_2(1-N) + K'^2_1(2+N)(1+\tan^2\delta)}{[K_2(1-N) + K'_1(2+N)]^2 + [(2+N)(K'_1\tan\delta)]^2}\right\}^2 + \left\{\frac{(1-N)(K'_1K_2\tan\delta)}{[K_2(1-N) + K'_1(2+N)]^2 + [(2+N)(K'_1\tan\delta)]^2}\right\}^2} \qquad [5]$$

The values of E_o *vs.* tan δ are shown in Fig. 4 for different values of K'_1. The phosphor concentration was chosen to be 20% by volume and the applied field was 27.39 kv/cm (69.57 v/mil). The calculations were executed by a Royal McBee LGP-30 digital computer. The corresponding tan δ *vs.* emission curves are plotted in Fig. 5 and were obtained by utilizing the E_o *vs.* emission values of the same phosphor. This curve was calculated from an experimental E_2 *vs.* emission curve, using Eq. [1].

The curves indicate that, in the case of embedding media having a relatively low dielectric constant, the emission can be considerably enhanced by choosing a lossy material. Only small effects can be achieved by progressing from a low loss value to about tan δ = 0.5. There is no reason to believe that Eq. [5] should not be valid for higher values of tan δ, because (except for the assumption of spherical phosphor particles) the equation was derived by rigorous mathematical treatment from Eq. [1].

By using the values plotted in Fig. 5, one can observe that, when an embedding medium with a dielectric constant of 2.5 (approximately the permittivity of polystyrene) is used, the emission of the electroluminescent cell theoretically can be increased by a factor of 6, by theoretically increasing the loss tangent to 1 (45°). When an embedding medium having a dielectric constant of 5 (approximately Corning Code 1970) is used, the emission theoretically can be doubled by increasing the loss tangent from a low value to 1.

It is evident that it would be more advantageous to select embedding media with a high dielectric constant, if one wishes to increase the output of the lamp. If such a material is not available, the same effect can be obtained by using a higher loss material, although possibly at the cost of lower efficiency and heating of the lamp.

An attempt was made to check Eq. [5] and Fig. 5 experimentally. The dielectric constants and loss tangents of various liquids were measured on a General Radio 650A impedance bridge at 1 kc, using a GE three terminal, liquid sample holder (G. E. Co., Cat.

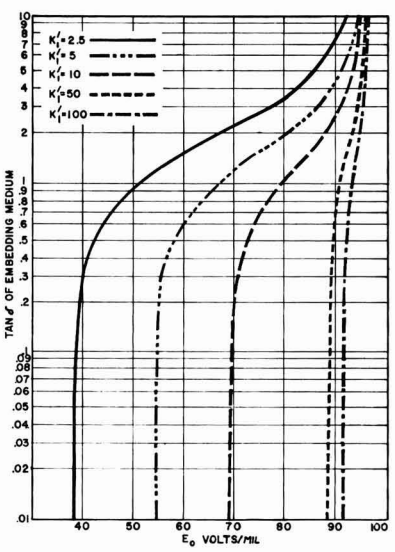

Fig. 4. Internal field as a function of the loss tangent of the phosphor embedding medium.

[3] This is not necessarily applicable to all electroluminescent phosphors and phosphor-embedding medium combinations. For detailed discussion on the subject see: A. N. Ince and C. W. Oatley, *Phil. Mag.*, 46, 1081 (1955); W. Lehmann, *This Journal*, 103, 24 (1956).

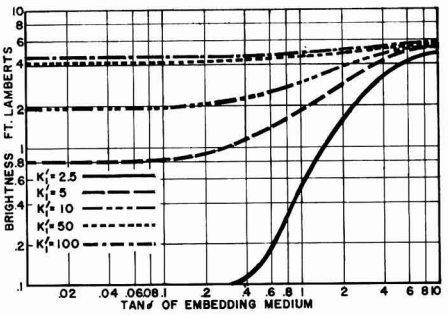

Fig. 5. Emission intensity as a function of the loss tangent of the phosphor embedding medium.

5100774). The measurements were made with the phosphor and the liquid being in a sample holder with a 0.00584 cm (2.3 mil) gap. An audio oscillator and a high powered amplifier were used as power source. The emission measurements were made with a VISCOR visibility correcting filter-equipped Weston 856 type photocell and a L&N Type E galvanometer. In instances where tan δ was very high, a resistance had to be used in a series with the cell, to limit the current.

Table I contains the measured dielectric properties and the results of the electroluminescent evaluation, together with the calculated values. The phosphor was the identical phosphor used in the earlier parts of the study where it was used in a glass embedding medium. 20% by volume was used, the emission was measured at 1 kc, and the applied field was 27.39 kv/cm. To obtain the values in the "calculated" column of Table I, the value of E_o was calculated and the corresponding brightness value was obtained from the E_o *vs.* brightness curve of the phosphor.

The fact that all experimental data are lower than the calculated ones led to a reexamination of Eq. [5]. Small discrepancies in the values of K_2 and N cannot account for the difference. Only two significant figures were obtained in the measurement of the dielectric constant and loss tangent because the balance of the bridge was rather broad, due to the relatively high loss values. The K'_1 and loss tangent values of most of these liquids are extremely frequency-sensitive. For example, in case of acetone at 10 kc, values were measured of $K'_1 = 23$ and tan $\delta = 0.7$; therefore an inaccurate frequency adjustment may have been a large source of error. The effect of orientation of the phosphor in the liquid medium under the applied field was not considered. In the light of the above considerations, the agreement between the measured and calculated values can be considered good.

Table I. Calculated and measured emission intensities of an electroluminescent phosphor in various phosphor embedding media

Liquid	K'_1	Tan δ	Brightness/ft-L	
			Calculated	Measured
Acetone	1300	25	5.1	4.8
Benzene	2.3	0.01	(<0.4)	(<0.4)
Castor oil	4.7	0.082	0.7	0.6
Glycerol	90	3.7	5.0	3.9

Power Requirement and Efficiency

The calculation of power input and efficiency from the available data can be made with the aid of the following equation:

$$P = 2\,\epsilon_o\, f\, V^2 K'' \frac{A}{D} \qquad [6]$$

A similar formula has been quoted by von Hippel (4).

The results of the power and efficiency calculations are shown in Fig. 6 and 7. It is interesting to note that in case of a dielectric constant of 2.5 there are three different solutions for the same efficiency. This means that a brightness increase by a factor of 25 can be obtained at no loss of efficiency by increasing the tan δ of the embedding medium. With higher dielectric constants that effect rapidly diminishes.

Figures 6 and 7 indicate that the maximum obtainable efficiency, regardless of the brightness, can be obtained with embedding media having a dielectric constant somewhere between 5 and 50. The efficiencies were calculated for a series of dielectric constant values in order to determine the maximum. Figure 8 shows the results of these calculations for a value of tan δ of 0.01 in each case. The curve shows the maximum efficiency is obtained at a point where K'_1 is near 10. At this point the assumed dielectric constant of the phosphor and the dielectric constant of the embedding medium are identical.

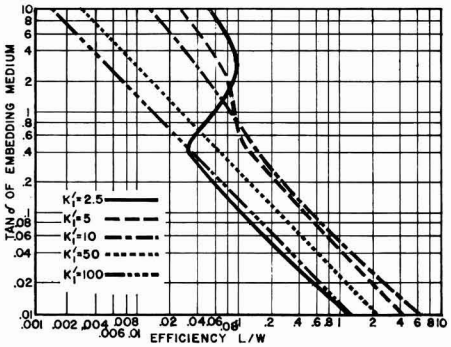

Fig. 6. Effect of the loss tangent of the phosphor embedding medium on the efficiency.

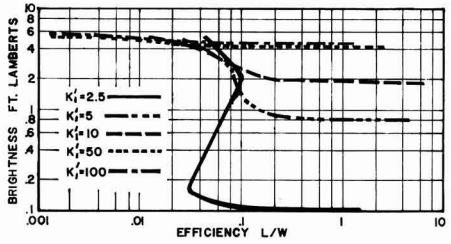

Fig. 7. Efficiency as a function of the emission intensity and the dielectric constant of the embedding medium.

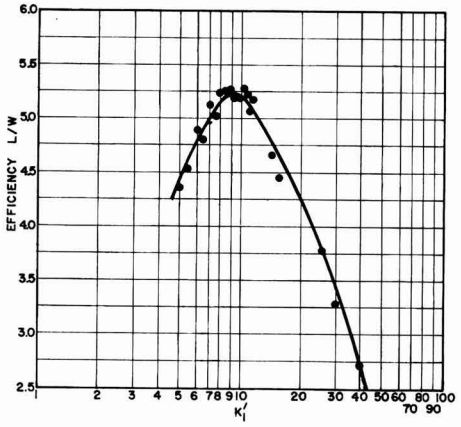

Fig. 8. Maximum efficiency of an electroluminescent cell as a function of the dielectric constant of the phosphor embedding medium.

The incidence of maximum efficiency when the dielectric constants of the phosphor and the embedding medium are identical can be considered only indicative at the most, because the voltage value substituted into Eq. [6] was not the voltage at which peak efficiency (5) can be obtained, but was the same arbitrary voltage used in earlier parts of the study.

Summary

The effect of the dielectric properties of electroluminescent phosphor-embedding media on brightness and efficiency have been examined. Using a formula by Roberts (1), it was established that an increase in the dielectric constant of the embedding medium above a value of 50 does not result in an appreciable gain in emission.

By expanding Roberts' formula to include the loss factor, the effect of the loss tangent of the embedding material was investigated. The results show that from a low loss tangent value of 0.01 to about 0.5, very little change in light emission can be obtained, but above 0.5 a rapid increase in brightness occurs. At successively higher dielectric constant values this increase diminishes. The theoretical calculations were in good agreement with experimental measurements.

In case of a lower dielectric constant embedding media, three different emission values can be obtained at the same efficiency if the loss tangent is varied. Consequently, in such a case the brightness can be increased substantially at no cost in efficiency. Indications are that maximum efficiency can be obtained when the dielectric constant of the phosphor and the embedding medium are identical. In this case the applied field equals the internal field.

Acknowledgments

The valuable suggestions made by Drs. R. V. Harrington and V. D. Mochel and Mr. W. H. Barney are greatly appreciated. Mr. K. R. Kiehl programmed the computer. Miss M. T. Splann has made the dielectric and Mr. J. C. Pinkston the electroluminescent measurements.

Manuscript received March 27, 1961; final revised manuscript received March 16, 1962.

Any discussion of this paper will appear in a Discussion Section to be published in the June 1963 JOURNAL.

REFERENCES

1. S. Roberts, *J. Opt. Soc. Amer.*, **42**, 850 (1952).
2. E. H. Kerner, *Proc. Phys. Soc.*, **69B**, 802 (1956).
3. W. Lehmann, Private communication.
4. A. von Hippel, "Dielectrics and Waves," p. 26, John Wiley & Sons, New York (1959).
5. W. Lehmann, *Illum. Engrg.*, **51**, 684 (1956).

DEFINITION OF SYMBOLS

E_o, Internal electric field, acting on suspended phosphor particles.
E_2, Applied, external electric field.
K_1, Dielectric constant of embedding medium.
K_2, Dielectric constant of phosphor.
N, Volume fraction of embedded phosphor.
K^*, Complex dielectric constant.
K'_1, Real dielectric constant of embedding medium.
$K''_1 = K'_1 \tan \delta$, Loss factor of embedding medium.
$\tan \delta$, Loss tangent (of embedding medium).
V, Voltage, rms.
f, Frequency, cps.
A, Area, cm^2.
D, Thickness, cm.
ϵ_o, Permittivity of free space $= 8.85 \times 10^{-14}$, Farads/cm.
P, power, watts.
Eff., Efficiency, lpw.

Neutron-Activation Study of Gallium Arsenide Contamination by Quartz

Werner Kern

Semiconductor and Materials Division, Radio Corporation of America, Somerville, New Jersey

ABSTRACT

Gallium arsenide crystals were synthesized by the horizontal Bridgman method in neutron-activated boats of natural and synthetic fused quartz. Instrumental radiochemical techniques were applied to determine the silicon concentrations from Si^{31} radioactivity measurements and to identify other trace elements transferred to the gallium arsenide during the process. All crystals were found completely enveloped in an impurity-enriched surface layer containing silicon concentrations up to 1500 ppm. Bulk concentrations of silicon ranged from 1×10^{17} to 3×10^{18} atoms/cm^3 GaAs, and varied in different sections of the crystals within a factor of 1.7. Evidence of several types of transfer mechanisms was obtained. Other impurities that originated from natural fused quartz and were detected in the form of their radioactive isotopes in the crystals include copper, gallium, antimony, and gold at concentrations below 10^{16} atoms/cm^3; the concentrations of these contaminants were effectively decreased by use of high-purity synthetic quartz.

The majority of gallium arsenide crystals made for use in semiconductor devices have been synthesized by the horizontal Bridgman technique (1) using reaction vessels of fused quartz. Experience has indicated that gallium arsenide becomes contaminated by silicon from the quartz during the processes of preparation. In fact, silicon has been detected consistently in gallium arsenide crystals as one of the major impurities and has been recognized as the main electron donor in this semiconductor compound (1). Because the degree of purity is one of the most important quality parameters in semiconductor-grade gallium arsenide, the present investigation was undertaken to provide more knowledge concerning the role of contamination by quartz.

A radiochemical method of analysis appeared to be most promising because of its inherent sensitivity and specificity for trace quantities. Gallium arsenide was synthesized in a neutron-activated quartz boat, and the crystal samples were then analyzed by radiocounting and gamma-ray spectrometry. The experiments were designed primarily to provide information on the extent of silicon contamination. Other impurities originating from the quartz and encountered in the course of this work were identified as a secondary objective.

Bombardment of pure quartz with neutrons in a nuclear reactor leads to several known nuclear transformations (2, 3). Considerations of the relative quantities and half-lives of the product nuclides and the prevailing experimental conditions show that the only reaction of importance in this work is the Si^{30} (n, γ) Si^{31} transformation which takes place between the Si^{30} isotope present in natural silicon and the thermal neutrons from the re-

Table I. Impurity concentrations in fused quartz (ppm, weight/weight)

Impurity element	G.E. Quartz* Found	(4)	(5)	Vitreosil** Found	(5)	(6)	Spectrosil*** Found	(6)
Al		42	20-30		10-100	50-60		<0.02
Ca		16			10	0.4		<0.1
Na	2-6	7		1		4	<0.04	0.04
Fe		4	1		<1-10			<0.1
K		2.5					<0.02	<0.005
Ti		2						
Li		2						
B		0.94				0.5		<0.01
Mg			0.1-1		3-10			
Cu	<0.5		<1-1	<0.2	<1-1	0.01	<0.02	<0.0002
Sb	0.7			<1		0.23	<0.02	<0.0001
Ga							<0.01	<0.004
Mn						0.026		<0.001
P						0.01		<0.001
As								<0.0002

* Clear fused quartz (99.97 to 99.98% SiO_2) from naturally occurring quartz crystals; General Electric Company.
** Ordinary quality transparent fused quartz (99.98% SiO_2) from naturally occurring quartz; Thermal American Fused Quartz Company.
*** Synthetic fused quartz (>99.9999% SiO_2); Thermal American Fused Quartz Company.
(4, 5, 6)—References to literature data.

actor. The Si^{31} decays with a half-life of 2.62 hr to stable P^{31} by emitting one 1.471 Mev negatron per disintegration. In addition, one gamma photon of 1.26 Mev energy is emitted in 0.07% of the disintegrations. Part of the accumulating P^{31} is in turn activated during the bombardment to P^{32}, which transmutes by 1.707 Mev negatron emission with a 14.3-day half-life to stable S^{32}. However, the presence of P^{32} does not conflict in the analysis because of its long half-life with respect to that of Si^{31}.

Possible interference from neutron-activated impurities in fused quartz manufactured from natural sources can be anticipated. Impurity concentrations in three types of quartz from various sources (4-6) are summarized in Table I; also included are some neutron-activation analysis data obtained during this work. A multitude of radionuclides can be expected to arise when these elements are bombarded with nuclear reactor neutrons of thermal and high energies. In the early stages of the radioactivity analysis, the beta activity in the quartz from any of these impurities is relatively small in comparison to the Si^{31} activity. The situation in the gallium arsenide, however, cannot be predicted. One impurity nuclide which could seriously interfere with the radiochemical silicon analysis is Mn^{56}, if it were present in the gallium arsenide crystals. This nuclide has a 2.58-hr half-life and emits beta and gamma rays; it is produced by the thermal-neutron reaction $Mn^{55}(n,\gamma)Mn^{56}$ and by the fast-neutron reaction $Fe^{56}(n,p)Mn^{56}$. The other predictable thermal-neutron activation products have half-lives of either less than 0.5 hr or more than 12 hr and can be resolved from the Si^{31} radioactivity by decay counting.

Experimental

The quartz boats were cleaned before and after activation by submersion in concentrated nitric acid for 20-60 min, followed by extensive rinsings with deionized and doubly quartz-distilled water. The boats were then placed in quartz tubes and irradiated in the water-cooled nuclear reactor of the Industrial Reactor Laboratories, Inc., at Plainsboro, New Jersey. The fluxes employed for the five experiments varied depending on the reactor core position available and ranged between 2×10^{13} and 9×10^{13} thermal neutrons cm^{-2} sec^{-1}, as determined by separate measurements with flux monitor foils and nuclear counters. An irradiation period of 8 hr was chosen to obtain an 88% saturation activity yield of Si^{31}, and to minimize the activation of impurity elements yielding longer-lived nuclides. The activated boats were extracted from the reactor, allowed to "cool off" for 1 hr to decrease the high radiation levels from short-lived nuclides, and were then transferred into the "hot cell" for remote manipulations.

The gallium arsenide synthesis and crystal growth were maintained as close to the normal standard techniques as possible, except that smaller ingots (7g) were prepared and shorter growth periods were employed than usual to minimize radioactivity losses of the rapidly decaying Si^{31}. A weighed quantity of >99.9999% pure gallium as obtained from the manufacturer was placed in the activated quartz boat and introduced in the reaction tube of natural fused quartz. A stoichiometric quantity of >99.999% pure arsenic, plus an excess sufficient to produce an operating pressure of 1 atm, was placed in a second quartz boat, which was not activated, and was positioned in the reaction tube. The tube containing the two boats was first evacuated to 10^{-6} mm Hg and outgassed for purification purposes for 1 hr at temperatures of 200°C for the As and 600°C for the Ga zone. The tube was tipped off in vacuum and introduced into the preheated resistance furnace. A temperature of 1240°C was maintained around the boat zone in which the gallium arsenide crystal was growing during a period of either 3 or 5 hr, while the arsenic reservoir temperature was kept at 600°C. Gallium arsenide crystals were grown at speeds of up to 2 in./hr. The temperature was then reduced to 900°C, the tube was pulled out of the furnace, cooled, and opened on a cutting machine. The vicinity of the radioactive boat was kept closely shielded at all times to minimize radiation hazards. The gallium arsenide crystal was then removed for radioscanning, surface treatments, sectioning, powdering, and radioactivity measurements. Radioactive silicon standards were prepared by crushing and powdering the activated quartz boat and intimately mixing portions weighed on an analytical balance with inactive gallium arsenide powder as diluent; the radiation emitted from the quartz was thereby modified in a similar manner to the radiation from the gallium arsenide samples.

Gas-flow counting was selected as the primary method for beta radioactivity measurements to provide a high sensitivity for the Si^{31} beta radiation and to minimize interfering gamma radiation from activated impurities. The counting rates were normalized and corrected according to radiochemical standard techniques and expressed as relative specific activities, cpm/g GaAs or SiO_2. Survey radiocounting was made with Geiger-Mueller end-window and probe counters connected to a count-rate meter. Integral gamma counting was performed with a scintillation counting unit. Gamma-ray spectrometry was carried out with a heavily shielded 3 x 3 in. thallium-activated sodium iodide crystal as a detector; pulses were transmitted to the linear amplifier of either a 100- or a 200-channel differential pulse-height analyzer. Spectral-data presentation by an automatic programmed printer and an automatic plotter provided scanning curves of differential counting rates *vs.* pulse heights. Energy calibration and counting efficiency of the spectrometers were made with gamma-rays from suitable radionuclide reference sources. Spectra chosen for complete evaluation were plotted in terms of net counting rate per channel as a function of channel number and gamma-ray energy.

The silicon concentrations in gallium arsenide samples were determined from beta radiation counting data which was plotted semilogarithmically as a function of the time. Graphical resolution of the decay curves into the components made it possible to obtain the 2.62-hr Si^{31} activity. The quantity

Table II. Si concentrations in GaAs crystals

Crystal No.	Quartz type of boat	Crystal growth, hr	Surface treatment prior to analysis	Part of crystal analyzed	Si concentration ppm (weight/weight)	Si concentration atoms/cm³
1	G.E. natural fused quartz	3	A	Bottom section	8 ± 4	9.4×10^{17}
2	G.E. natural fused quartz	5	B	Bottom half	20 ± 10	2.3×10^{18}
3	G.E. natural fused quartz	3	C	Surface layer, bottom side	$1{,}500 \pm 150$	1.7×10^{20}
			C	Surface layer, top side	<168	$<2.0 \times 10^{19}$
			C and D	Bulk crystal	<28	$<3.3 \times 10^{18}$
4	Vitreosil natural fused quartz	3	C	Surface layer, bottom side	395 ± 40	4.6×10^{19}
			C	Surface layer, top side	<55	$<6.4 \times 10^{18}$
			C and D	Bulk crystal	1 ± 1	1.2×10^{17}
5	Spectrosil synthetic fused quartz	3	D	Front and rear sections	13 ± 2	1.6×10^{18}
			D	Center section	10 ± 2	1.2×10^{18}

A = lapping; B = sandblasting; C = carborundum paper abrasing; D = chemical etching in H_2O_2-NaOH solution.

of silicon was calculated on the basis of the specific net beta Si^{31} activities in the gallium arsenide samples and the corresponding quartz standards of known silicon contents, analyzed under similar conditions. Determination of the decay half-lives and the maximum beta energies of the resolved components aided in the identification of beta-radiation-emitting nuclides.

Gamma-ray emitters were identified by gamma scintillation spectrometry on the basis of their characteristic energy spectra and decay constants, using standard spectra (7) as comparison. Absolute disintegration rates were calculated by integrating the areas under the characteristic photopeaks resulting from the successive graphical resolution (8) of the spectra into the components. Typical spectra from gallium arsenide and the corresponding quartz standard are shown in Fig. 1 and 2. Concentrations of the detected elements were determined from the total number of disintegrations and the method of absolute neutron-activation calculation (9).

Results

Successive removal of thin surface layers by lapping showed that each of the five gallium arsenide crystals grown in activated quartz boats was completely enveloped in an impurity-enriched surface skin less than 0.02 mm thick. Silicon concentrations in these layers ranged up to 1500 ppm (Table II) for gallium arsenide crystal surfaces that had been in direct contact with the quartz during the preparation. The radioactive impurities in various sections and layers below the surface skin were rather homogeneously distributed, showing variations within a factor of only 1.7. Because of the fast crystal-growth rates necessary, no systematic gradient freeze segregation was expected, and none was detected. The concentrations of silicon inside the five crystals varied from 1 to 28 ppm by weight, as shown in Table II. In some experiments the radioactivity decay measurements of gallium arsenide and quartz standard samples were continued for 30 days following the neutron bombardment of the quartz boat. Resolution of the decay curves obtained identified component activities with half-life and beta-radiation-energy values corresponding closely to those of Si^{31}, Cu^{64}, Na^{24}, Sb^{122}, and P^{32}.

Depending on the time of analysis, different radionuclides were observed by gamma spectrometry. For instance, 30 hr after the quartz boat activation the nuclides indicated in Fig. 1 and 2 dominated the spectra. The maximum at 0.511 Mev in the Cu^{64} spectrum is caused by the annihilation radiation from the positrons associated with the Cu^{64} disintegrations. The unidentified peak at the 1.05 Mev energy position in Fig. 1 had a half-life of 14 hr. Numerous spectra were taken several days and weeks later when the radioactivity of the 15.0 hr-Na^{24}, 12.8 hr-Cu^{64}, and 14.2 hr-Ga^{72} had decreased below the detection limit. The major gamma component in gallium arsenide crystals grown in natural fused quartz boats had a gamma energy peak and a half-life corresponding to Au^{198} (0.412 Mev, 2.69 days). Energy and half-life measurements of other

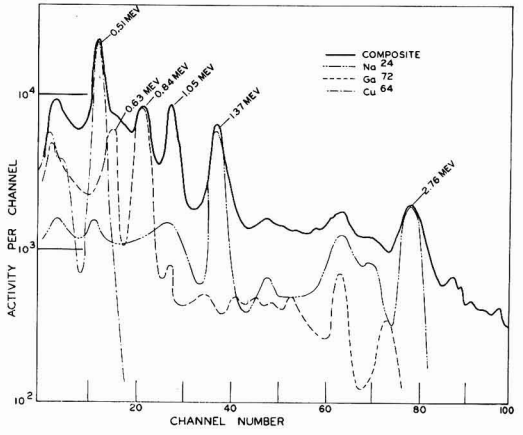

Fig. 1. Resolution of gallium arsenide gamma-ray spectrum. Sample from crystal No. 3 analyzed 30 hr after quartz boat activation. Solid line shows experimental composite spectrum. Normalized standard spectra as defined. Major energy maxima are indicated in Mev.

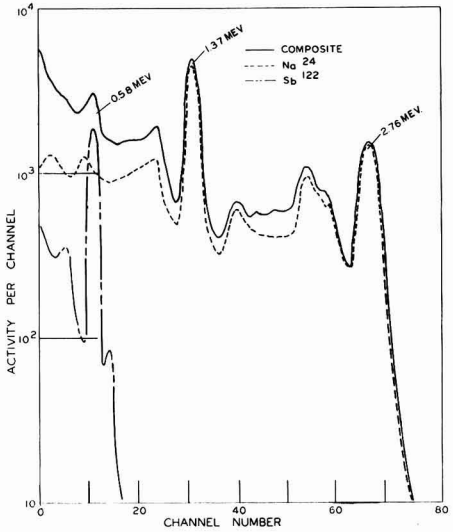

Fig. 2. Resolution of gamma-ray spectrum from quartz. Standard sample from quartz boat No. 3 analyzed 30 hr after neutron activation. Solid line shows experimental composite spectrum. Normalized standard spectra as defined. Major energy maxima are indicated in Mev.

components in these gamma spectra revealed the presence of Sb^{122} (0.564 Mev, 2.75 days), Sb^{124} (0.605 Mev, 60 days), and possibly Cr^{51} (0.323 Mev, 27.8 days). Corresponding gamma spectra from the natural fused quartz were dominated by the full energy photopeaks associated with the disintegration of the Sb^{122} and the Sb^{124} nuclides. The energy peak of the Sb^{124} isotope became observable after the shorter-lived activity from Sb^{122} with a similar energy maximum had disappeared from the spectra. Both radioisotopes were formed by the (n, γ) reaction from natural antimony (57.25% Sb^{121}, 42.75% Sb^{123}) contained in the quartz.

Although the gamma spectra of various gallium arsenide crystals from the natural fused quartz boats were similar in composition, the crystal grown in synthetic fused quartz had considerably more complex spectra which were difficult to resolve by instrumental analysis. Na^{24} and Ga^{72} were positively identified, while the identity of Zn^{65m}, K^{42}, Cu^{64}, Sb^{122}, W^{187}, La^{140}, and Au^{198} was not conclusively established. Concentration levels calculated on the basis of (n, γ) reactions are summarized in Table III. Synthetic fused quartz also has gamma spectra which are different from those of natural fused quartz brands and are characterized by impurity concentrations orders of magnitude lower (Table I).

Discussion

The radioactivity measurements of the gallium arsenide samples could not be started until at least 12 hr after the neutron bombardment of the quartz boats had been terminated because of the necessary manipulations, preparations, and crystal growing. This time delay is the severest of the difficulties in the analysis because of the diminishing sensitivity and accuracy of the Si^{31} radioactivity measurements and cannot be substantially reduced unless the synthesis conditions are altered unrealistically.

Furthermore, an unfavorable change of the radioactivity composition in the gallium arsenide samples takes place. The beta-radioactivity decay curve of natural fused quartz showed that the Si^{31} concentrations during the early stages of radiocounting are about two orders of magnitude greater than the longer-lived background radiation levels; in gallium arsenide samples, however, the relative Si^{31} activity is sharply reduced. These differences in the radioactive impurity concentrations in quartz and gallium arsenide indicate that the contamination process proceeds selectively with respect to different impurities. The transfer is not simply a dissolution process of quartz, but involves diffusion of trace impurities to various degrees. Gamma-ray spectrometry supported these findings and extended them to additional impurity elements. For instance, Au^{198} represented the major radioactive constituent in a "one-week-old" gallium arsenide sample, but could not be detected in the corresponding spectra of the quartz tube from which the boat had been made. In contrast, Sb^{122} and Sb^{124} were taken up by the gallium arsenide to a limited extent only, but represented the major residual radioactivity in the quartz

Table III. Radiochemically detected elements in GaAs transferred from activated quartz boats

Impurity, atoms/cm³	Crystal No. 1 from G.E. natural fused quartz	Crystal No. 2 from G.E. natural fused quartz	Crystal No. 3 from G.E. natural fused quartz	Crystal No. 4 from Vitreosil natural fused quartz	Crystal No. 5 from Spectrosil synthetic fused quartz
Si	9×10^{17}	2×10^{18}	$<3 \times 10^{18}$	1×10^{17}	1×10^{18}
Zn	—	—	—	—	$<2 \times 10^{15}$*
Na	—	$\sim 4 \times 10^{15}$	$\sim 5 \times 10^{14}$	$\sim 5 \times 10^{14}$	$<5 \times 10^{13}$
K	—	—	—	—	$<8 \times 10^{14}$*
Cu	—	—	$<5 \times 10^{14}$	$<5 \times 10^{14}$	$<2 \times 10^{13}$*
Ga	—	—	$\sim 1 \times 10^{14}$	$\sim 2 \times 10^{14}$	$<1 \times 10^{13}$
P	—	$<2 \times 10^{13}$	—	—	—
Sb	—	$\sim 2 \times 10^{12}$	—	—	$<5 \times 10^{12}$*
Cr	—	$<5 \times 10^{12}$*	—	—	—
W	—	—	—	—	$<7 \times 10^{12}$*
La	—	—	—	—	$<5 \times 10^{12}$*
Au	—	$\sim 3 \times 10^{11}$	$<5 \times 10^{11}$	$<3 \times 10^{11}$	$<3 \times 10^{10}$*

— No determination made; * identity not definitely established.

after decay of the shorter-lived nuclides. Controlled etching experiments with activated fused quartz excluded the possibility that the impurities originated from the quartz surface, indicating that they must have diffused from the bulk toward the inner surface of the quartz boat.

The possible sources of error in the analysis were carefully examined. The homogeneity of the neutron flux within the sample area was demonstrated by measuring the induced radioactivity in samples from various positions of the quartz boats. Flux hardening and self-shielding effects (10) by strong absorption of thermal neutrons are considered negligible at the quartz thickness of only a few millimeters. Surface contamination of the quartz boats was minimized by acid cleaning before and after the work at the nuclear reactor facility.

The estimation of impurity elements other than silicon should be considered as semiquantitative because it was not possible to include standards during the neutron activation. Consequently, it was necessary to use theoretical calculation methods which are based on several assumptions. The neutron flux was known with an accuracy of not better than $\pm$ 25%. Nuclear reactions with fast neutrons may contribute to the formation of a particular radioactive nuclide. For instance, besides the main reaction Na^{23} (n, γ) Na^{24}, radiosodium is also formed by the reactions Al^{27} (n, α) Na^{24} and Mg^{24} (n, p) Na^{24}. However, calculations showed that the errors introduced were less than the uncertainties in the neutron flux.

The possibility of changes in the properties of the irradiated quartz used as boat material and their effect on the results were evaluated in the light of present literature (11-13), but seemed to impose no critical complications under the activation conditions used. While all samples of activated natural quartz were typically purple colored from the ionization of impurity-atoms, synthetic fused quartz remained colorless, which is consistent with the extremely low impurity concentrations in this material. Although the formation of color is the most immediately apparent radiation effect, it is easily reversed by annealing at elevated temperature.

Systematic errors in the radioactivity measurements were avoided by use of the usual corrections, calibrations, and statistical treatments of the data. The determination of the silicon concentration in the gallium arsenide was based on a direct comparison with the induced Si^{31} activity in the quartz boat used, so that error factors associated with the activation and the radiocounting were essentially eliminated. The accuracy of the silicon analysis was curtailed by large proportions of extraneous radioactivity from which the Si^{31} had to be resolved. The specificity of the Si^{31} analysis was ascertained by demonstrating the absence of interfering radioactivity levels from other nuclides with half-lives similar to Si^{31}. Mn^{56}, the most critical potential impurity in gallium arsenide, was looked for by both beta-radiation transmission measurements designed to detect the energetic 2.86 Mev beta rays and by gamma-ray spectrometry to discover the characteristic 0.845 Mev major gamma photons emitted by this nuclide. Chemical separation of the silicon from the gallium arsenide was considered, but was avoided after exploratory experiments showed that more work was needed to develop a rapid method.

The radiochemically determined silicon concentrations in the five surface-treated gallium arsenide crystals ranging from 1×10^{17} to 3×10^{18} Si atoms/cm^3 (Table II) checked with the emission spectrographic analyses for total silicon, but are higher than those presently obtained with more refined crystal growing techniques. Additional reasons might be the polycrystallinity of these ingots, their small size which introduced a larger quartz surface area per unit weight of gallium arsenide than in normally grown crystals, and the rapid pulling rate which prevented gradient freeze segregation. For comparison, typical published (1) silicon concentrations compiled from 100 gallium arsenide crystals ranged from 5×10^{15} to 5×10^{18} Si atoms/cm^3, with the majority of data falling between 5×10^{16} and 5×10^{17}.

As shown in Table III, the concentrations of other radiochemically detected impurity elements in the gallium arsenide were in nearly all cases less than 10^{15} atoms/cm^3. Emission spectrographic analysis also showed the usual concentrations of impurities at or below the detection limits, including copper, iron, and magnesium.

The transfer of impurities from the quartz to the gallium arsenide appears to be possible by several routes: (i) adhesion of quartz particles to the crystal, (ii) dissolution of quartz in the melt, (iii) gas phase transport of volatile impurities, and (iv) diffusion of impurities through the quartz and the gallium arsenide.

Adhesion of quartz particles to the ingot was observed with synthetic quartz. Irregular areas of high radioactivity were located by microprobe counting on the bottom side of the crystal prior to surface treatments. A high degree of wetting of the gallium to the boat was observed during the bake-out, and the gallium arsenide crystal adhered to the surface after removal from the furnace. Although this condition cannot be considered typical, it has been observed irregularly in production with Spectrosil boats and may be caused by the high water-vapor content of this quartz, which lowers its softening point (5).

The electrical properties of silicon at concentrations normally encountered in gallium arsenide suggest that this impurity is present in the elemental state. Experimental evidence indicates that silicon is formed by a chemical reaction of gallium with quartz. Silicon dioxide can be reduced by gallium at high temperature to free silicon and volatile gallium suboxide (14). Some of the silicon formed dissolves in the gallium or the gallium arsenide melt. Furthermore, free silicon gives rise to volatile silicon monoxide by reacting with quartz and may subsequently deposit on the exposed gallium arsenide surfaces.

It is clear from the data presented that the exclusive application of synthetic fused quartz for

the preparation of gallium arsenide offers distinct advantages in minimizing the impurity transfer. It is important, however, that the entire surface of the crystals be completely removed before further processing. This removal is best accomplished by abrasive blasting, followed by chemical etching. Other factors which are beneficial include effective surface treatments of the quartz by nitric acid cleaning, water rinsing, and vacuum baking; reduction of the reaction temperature and time as far as permissible; and reduction of the gallium arsenide-quartz contact area by growth of large-diameter crystals.

Acknowledgments

The author wishes to thank L. J. Vieland for his suggestion of neutron activation of quartz boats for investigating crystal contamination; D. A. Ross and R. F. Bailey for their cooperation and contributions in the activation phase, T. H. Baker and W. Oshinsky in the synthesis phase, and H. M. Hyman and G. Hornberger for the emission spectrographic analyses; G. M. Loiacono for his conscientious technical assistance in the project; and A. Mayer for critically reviewing the manuscript.

Manuscript received Jan. 15, 1962; revised manuscript received March 23, 1962. This paper was prepared for delivery before the Detroit Meeting, Oct. 1-5, 1961. The work described in this paper was sponsored by the Electronic Technology Laboratory, Aeronautics Systems Division, Air Force Systems Command, United States Air Force.

Any discussion of this paper will appear in a Discussion Section to be published in the June 1963 JOURNAL.

REFERENCES

1. L. R. Weisberg, F. D. Rosi, and P. G. Herkart, "Properties of Elemental and Compound Semiconductors," Vol. 5, p. 25, Interscience Publishers, New York (1960).
2. D. J. Hughes and R. B. Schwartz, "Neutron Cross Sections," BNL 325 and Supplement No. 1, U.S. AEC, (1958, 1960).
3. G. Friedlander and J. W. Kennedy, "Nuclear and Radiochemistry," John Wiley & Sons, Inc., New York (1957).
4. "Fused Quartz Catalog Q7A," p. 10, General Electric Company, Willoughby Quartz Plant, Willoughby, Ohio (1959).
5. L. R. Weisberg, Private communications.
6. M. H. Robinson, Private communications on data originally reported by C. A. Parker, Admirality Materials Laboratory, England.
7. R. L. Heath, "Scintillation Spectrometry Gamma-Ray Spectrum Catalogue," OTS IDP-16408 TID-4500 (1957).
8. R. E. Connaly, *Anal. Chem.*, **28**, 1847 (1956).
9. T. I. Taylor and W. W. Havens, Jr., "Physical Methods in Chemical Analysis," Vol. III, pp. 447-621, W. G. Berl, Editor, Academic Press, New York (1956).
10. R. C. Plumb and J. E. Lewis, *Nucleonics*, **13** [8], 43 (1955).
11. G. J. Dienes, *J. Phys. Chem. Solids*, **13**, 272 (1960).
12. W. Primak, *J. Phys. Chem. Solids*, **13**, 279 (1960).
13. I. Simon, *J. Am. Ceramic Soc.*, **40**, 150 (1957).
14. L. M. Foster and R. A. Kramer, *This Journal*, **107** [8], 189C (1960).
15. R. T. Sanderson, "Chemical Periodicity," p. 123, Reinhold Publishing Corp., New York (1960).

Evaluation of Germanium Epitaxial Films

J. R. Biard and Stacy B. Watelski

Texas Instruments Incorporated, Dallas, Texas

ABSTRACT

A method has been developed for rapid and accurate determination of the resistivity of p-type epitaxial germanium films deposited on p^+ germanium substrates. Determination of the resistivity is not dependent on a knowledge of film thickness. Data are presented for films with resistivities of 0.05-7.0 ohm-cm deposited on 0.002 ohm-cm substrates; film thicknesses range from 0.15 to 0.6 mil.

Several methods have been proposed and used to determine the resistivity of a p-type epitaxial germanium film deposited on a p^+ germanium substrate. Most of these methods relate breakdown, diffusion depth, or junction capacitance to resistivity and require a lengthy fabrication cycle employing exactly repetitive diffusion runs. The most serious objections to these methods of resistivity determination are the requirements for an optimum surface treatment and a precise junction delineation. In specific instances the resistivity and thickness of the films may also become serious objections. The simultaneous epitaxial deposition on an n-type pilot slice along with the normal p^+ substrate suffers from partial or complete thermal conversion of the pilot slice and yields erroneous results.

The purpose of this investigation was to develop a rapid and accurate technique for measuring the resistivity of p-type epitaxial germanium films deposited on p^+ germanium substrates. This technique, which has been developed, is called the elevated temperature technique and is based on the characteristic variation of resistivity with temperature exhibited by most semiconductors. The use of temperature as a parameter makes it possible to determine the resistivity of an epitaxial film without requiring a knowledge of the film thickness.

The characteristic variation of resistivity with temperature for noncompensated p-type germanium is theoretically calculated using the Brooks-Herring mobility theory. Only lattice and impurity scattering are considered in these calculations; other scat-

tering phenomena such as coulomb, neutral, and dislocation scattering are considered to have no first order effects on the mobilities. The calculated resistivity *vs.* temperature characteristics are compared with those empirically measured using homogeneous p-type germanium and found to be in good agreement. Results of the empirical tests form a standard of comparison for measuring any p-type germanium epitaxial film deposited on a p^+ germanium substrate with an accuracy of ± 20% (95% confidence limits) between 0.1 and 4.0 ohm-cm.

Discussion

The resistance of a semiconductor sample is determined by the size and shape of the sample and its resistivity. Due to the low value of the coefficient of expansion of germanium, variations in the resistance of a semiconductor sample with temperature are almost entirely due to the temperature dependence of resistivity. The equations used for calculating variation of resistivity with temperature are given in the Appendix. As indicated by Eq. [1] of the Appendix, resistivity is controlled by the number of free carriers and their mobilities; a discussion of the theoretical temperature variation of mobility and carrier concentration follows.

Only impurity scattering and lattice scattering mobilities will be considered of prime importance for this discussion. The impurity scattering mobility, Eq. [7], may be simplified for analysis as

$$\mu_I = K_1 T^{3/2} \left[\frac{1}{\ln(1 + K_2 T^2) - \dfrac{K_2 T^2}{1 + K_2 T^2}} \right]$$

At increasing temperatures above 100°K the bracketed expression remains relatively constant and the resulting mobility curve follows the $T^{3/2}$ slope. For temperatures below 20°K the bracketed term is dominant and, in conjunction with the $K_1 T^{3/2}$ term, yields a mobility curve with a $T^{-5/2}$ slope. The lattice scattering mobility Eq. [6], Fig. 1, yields a slope of $T^{-2.33}$. When these two mobilities are combined as in the Brooks-Herring equation (1), Eq. [7] of the Appendix, the resultant mobility curve μ_{LI} is as shown in Fig. 1.

Referring to Eq. [3], as temperatures increase into the intermediate (extrinsic) range, $P_I \rightarrow N_e$. That is, the number of free holes caused by ionization of the impurity atoms approaches the magnitude of the net impurity concentration and remains constant. Since for normal doping ranges $p_i << N_e$, p (the total number of free holes) also approaches N_e and $n << p$. At high temperature (in the intrinsic region) the number of free holes caused by intrinsic ionization, p_i, increases due to the dominant exponential term as does the number of free electrons, n_i, ($n \approx p$). Thus, the total number of free holes, p, is determined by P_I at intermediate temperatures and p_i at high temperatures while the number of minority carrier electrons is negligible at intermediate temperatures and determined by n_i at high temperatures. The curve representing the magnitude of p *vs.* temperature is shown in Fig. 1.

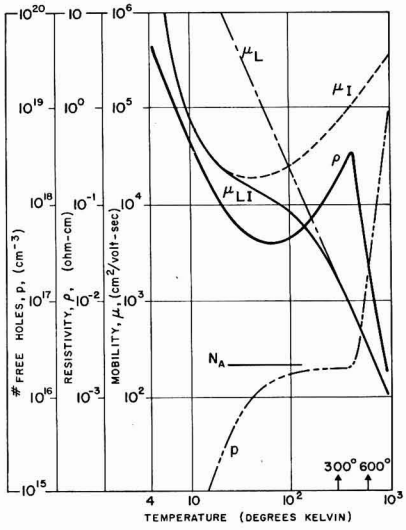

Fig. 1. Calculated mobility, resistivity, and free hole concentration *vs.* temperature, p-type germanium, $N_A = 2 \times 10^{16}$ atoms/cm³.

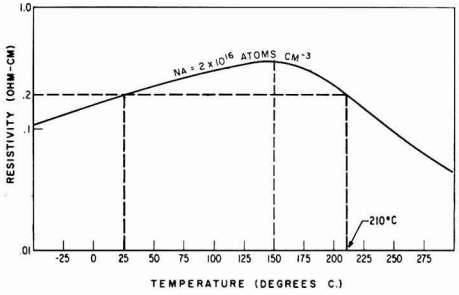

Fig. 2. Resistivity *vs.* temperature, p-type germanium

The variation of resistivity with temperature may be calculated by combining the characteristic curves of p, μ_{LI}, n, and μ_{LN} as dictated by Eq. [1].[1] One such curve of ρ *vs.* T for a wide range of temperature is shown in Fig. 1.

Note that the point at which the total number of free holes, p, begins to increase sharply (≈400°K) corresponds to that point at which the resistivity, ρ, reaches its inflection point, *i.e.*, beginning of intrinsic conduction.

The two arrows at the bottom of Fig. 1 indicate the range of temperature (300°-600°K) with which this report is mainly concerned.

Figure 2 shows the calculated resistivity *vs.* temperature characteristics of 0.2 ohm-cm p-type germanium. A resistor made from this material exhibits the same value of resistance at 25°C (extrinsic

[1] The contribution of the minority carrier electrons is negligible except in the intrinsic range where lattice scattering dominates. Therefore only the lattice scattering mobility, μ_{LN}, is used for electrons in Eq. [1].

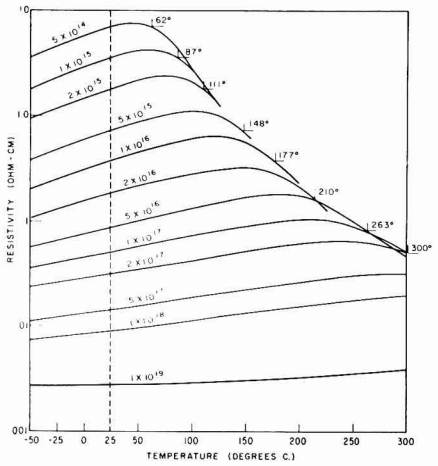

Fig. 3. Resistivity *vs.* temperature, p-type germanium

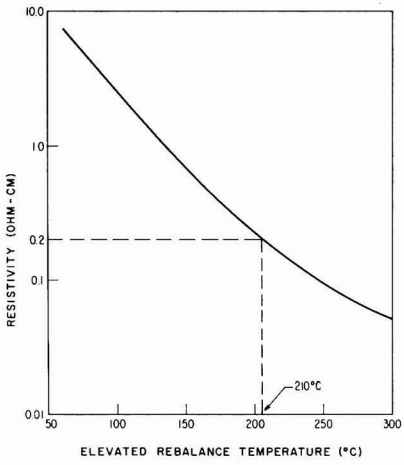

Fig. 4. Calculated resistivity *vs.* elevated rebalance temperature

range) and 210°C (intrinsic range). From Fig. 3 it is seen that the elevated temperature at which the resistivity is equal to the room temperature value is uniquely related to the resistivity. Thus, a resistivity measurement may be made by balancing a germanium resistive element in a low-frequency a-c bridge at room temperature and determining the elevated temperature of the resistive element at which the bridge returns to the balanced conditions.

Note in Fig. 3 the relatively constant resistivity corresponding to a doping level $N_A = 1 \times 10^{19}$ atoms cm^{-3}. This doping level is representative of p^+-type substrate material used in epitaxial depositions.

A calculated curve of resistivity *vs.* elevated rebalance temperature is presented in Fig. 4.

Figure 5 illustrates the construction of the homogeneous germanium resistors used for calibration purposes. The resistance of these ohmic devices is pure spreading resistance, $R = \rho/2d$, where d is the diameter of the contact (2). The resistance of the device is directly proportional to the resistivity as a result of the constancy of the contact diameter

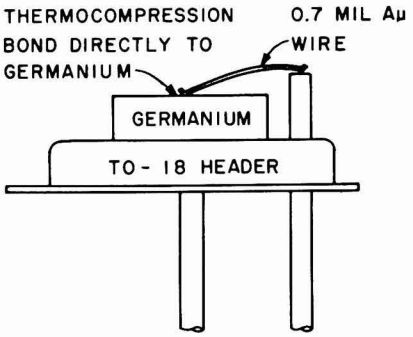

Fig. 5. Ohmic device. Resistance, $R = \frac{\rho}{2d}$, where ρ is the resistivity in ohm-cm and d the diameter of contact in cm; d remains constant throughout temperature range. $\therefore R \propto \rho$.

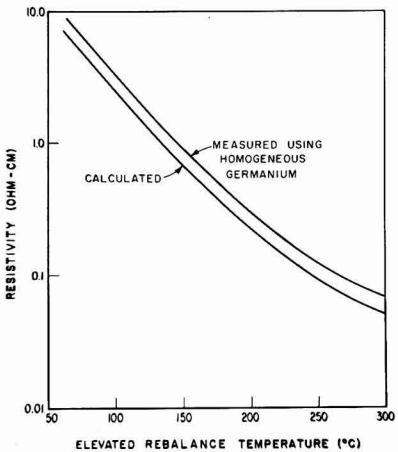

Fig. 6. Calculated and measured resistivity *vs.* elevated rebalance temperature.

throughout the temperature range. Figure 6 compares the measured and calculated curves of resistivity *vs.* elevated rebalance temperature as determined from homogeneous resistive elements of known resistivity. Note that in the experimental case a unique relationship exists between resistivity and elevated rebalance temperature. Thus it is possible to generate an experimental calibration curve for a given test set using known homogeneous samples.

The construction details for epitaxial resistive devices are shown in Fig. 7; this type of mounting is used in determining the resistivity of the epitaxial layer. In order for the elevated temperature technique to give accurate results on epitaxial samples, it is necessary to construct the ohmic devices such that the temperature sensitive part of the total resistance is contributed by the epitaxial layer. Such a construction is possible due to:

(*a*) the use of small contact diameter (≈1.5 mil) to take advantage of spreading resistance in the substrate (substrate resistance is usually less than 2% of the total except for heavily doped thin epitaxial layers where it may approach 15%); (*b*) the fact that the resistivity of the heavily doped sub-

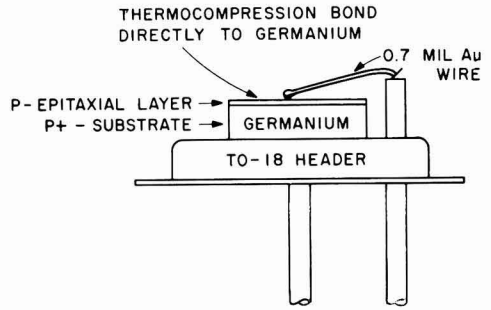

Fig. 7. Ohmic device. Epitaxial layer resistance, $R_E = \frac{\rho t}{A}$; substrate resistance, $R_S = \frac{\rho}{2d}$, where ρ is the resistivity in ohm-cm, t the thickness of epitaxial layer in cm; A the area of contact in cm^2; and d the diameter of contact in cm. t and d remain constant throughout temperature range. $\therefore R \propto \rho$.

strate material (≈0.002 ohm-cm) is nearly independent of temperature (corrections for the substrate may be applied where necessary).

The test set is composed of a temperature chamber, an a-c resistance bridge, and a phase-sensitive detector.

Results

Based on a statistical analysis of resistivity data the accuracy of the test set is ± 20% (95% confidence limits) between 0.1 and 4.0 ohm-cm, with reduced accuracy outside this range. These limits are based on resistive elements constructed from homogeneous material of known resistivity. By exercising extreme care in construction of the temperature chamber and the individual resistive elements it may be possible for an accuracy of ± 10% to be achieved.

It should be pointed out that the elevated temperature resistivity measurement is a destructive test; however, the volume of material required for the resistive element is small. If this technique is to be used as a measure of carrier concentration it is subject, like the 4-point probe, to errors due to compensation and inhomogeneous material.

The indicated rebalance temperature for an inhomogeneous film yields an "average" value for the film resistivity which is a function of the impurity profile within the film. From Fig. 3 it may be seen that the portion of the film having a resistivity higher than the indicated "average" is at a temperature greater than its rebalance temperature, while the lower resistivity portion is at a temperature less than its rebalance temperature. The profile of the film resistivity may be incrementally derived from elevated rebalance temperature vertical profile data. These data may be conveniently obtained by bevel lapping and staggered bonding.

An experiment was performed to determine the quantitative effect of the interfacial diffusion gradient on this measurement technique. A high resistivity (>8 ohm-cm) p-type epitaxial film was deposited on a highly doped p-type substrate; film thickness was 0.25 mil with a diffused gradient width of 0.06 mil as determined by chemical delineation. Consistent rebalance temperature readings were obtained throughout the film thickness, except for those within the interfacial diffused region.

Conclusions

The elevated temperature technique for resistivity measurement is a powerful tool for evaluating p-type germanium epitaxial films deposited on p$^+$ germanium substrates. Aside from routine evaluation of epitaxial film resistivity the technique has also been used to determine resistivity profiles at 5.0 mil increments across the face of epitaxial deposits. Used in conjunction with bevel lapping and staggered bonding, epitaxial deposits may be profiled for resistivity through the thickness of the layer in 0.05 mil increments.

Acknowledgments

The calculated resistivity *vs.* temperature data were supplied by Henry Riser and the statistical analysis of experimental data was performed by Vic Paulos. The test set was built and operated by Jack Leezer. Special fabrication techniques were supplied by Nadene Bedford and O. J. Lewis.

Manuscript received Feb. 12, 1962; revised manuscript received April 4, 1962. This paper was prepared for delivery before the Detroit Meeting, Oct. 1-5, 1961.
Any discussion of this paper will appear in a Discussion Section to be published in the June 1963 JOURNAL.

REFERENCES

1. P. P. Debye and E. M. Conwell, *Phys. Rev.*, **93**, 693 (1954).
2. H. C. Torrey and C. A. Whitmer, "Crystal Rectifiers," MIT Rad Lab Series, Vol. 15, McGraw-Hill Book Co. Inc., New York, Appendix C (1948).

APPENDIX

Equations for calculating resistivity of p-type germanium.

$$\rho = \frac{1}{e(n\mu_{LN} + p\mu_{LI})} \qquad [1]$$

$$e = 1.6 \times 10^{-19} \text{ coulomb}$$

$$n = \sqrt{\frac{P_I^2}{4} + p_i^2} - \frac{P_I}{2}$$

$$p = \sqrt{\frac{P_I^2}{4} + p_i^2} + \frac{P_I}{2} \qquad [2]$$

$$P_I = -\frac{B}{2}\left(1 - \sqrt{1 + \frac{4N_e}{B}}\right) \qquad [3]$$

$$B = 2.4147 \times 10^{15}\left(\frac{m_p}{m}\right)^{3/2} T^{3/2}\, e^{-1.1605 \times 10^4 E_D/T};$$

$$\left(\frac{m_p}{m}\right) = 0.2;$$

T = absolute temperature in °K;

$E_D = 0.0104$ $(N_A < 2 \times 10^{17})$;

$= 0$ $(N_A = 2 \times 10^{17})$; $= -\infty$ $(N_A > 2 \times 10^{17})$

$$N_e = (N_A - N_D)$$

$$P_i = 1.76 \times 10^{16}\, T^{3/2}\, e^{-4550/T} \qquad [4]$$

$$\mu_{LN} = \frac{4.9 \times 10^7}{T^{1.66}}$$

$$\mu_{LI} = \frac{\mu_I\left(1 + 0.556\frac{\mu_I}{\mu_{LP}}\right)}{1 + 2.99\frac{\mu_I}{\mu_{LP}} + 0.556\left(\frac{\mu_I}{\mu_{LP}}\right)^2} \quad [5]$$

$$\mu_{LP} = \frac{1.05 \times 10^9}{T^{2.33}} \quad [6]$$

$$\mu_I = \frac{3.29 \times 10^{15}\, k^2\, T^{3/2}}{\left(\frac{m_p}{m}\right)^{1/2}(P_I + 2N_D)} \cdot \frac{1}{\ln(1+b) - \frac{b}{1+b}}$$

(Brooks-Herring equation) [7]

$$K = 16$$

$$b = \frac{1.29 \times 10^{14}\, K\left(\frac{m_p}{m}\right)T^2}{P_I + \left(1 - \frac{P_I + N_D}{N_A}\right)(P_I + N_D)}$$

EXPLANATION OF SYMBOLS

ρ, Resistivity in ohm-cm
e, Electronic charge in coulombs
n, Number of free electrons
p, Number of free holes
P_I, Number of free holes caused by ionization of impurity atoms
$\left(\frac{m_p}{m}\right)$, Effective mass of hole
E_D, Activation energy in electron volts for Boron dopant
N_e, Net impurity concentration in atoms cm^{-3}
N_A, Majority carrier concentration in atoms cm^{-3}
N_D, Minority carrier concentration in atoms cm^{-3}
p_i, Number of free holes caused by intrinsic ionization if impurity ionization were not present in cm^{-3}
n_i, Number of free electrons caused by intrinsic ionization if impurity ionization were not present in cm^{-3}
μ_{LN}, Lattice scattering (drift) mobility for electrons in cm^2/volt-sec
μ_{LP}, Lattice scattering mobility for holes in cm^2/volt-sec
μ_{LI}, Combined lattice and impurity scattering for holes in cm^2/volt-sec
μ_I, Scattering caused by ionized impurity atoms
K, Dielectric constant for germanium
T, Absolute temperature in °K

Thickness Measurement of Epitaxial Films by the Infrared Interference Method

M. P. Albert and J. F. Combs

Monsanto Chemical Company, St. Louis, Missouri

ABSTRACT

The infrared interference measurement has proved to be an accurate and nondestructive means for evaluating the thickness of epitaxially grown films on silicon. The measuring technique is discussed and the necessary relationships are presented. A fringe wavelength *vs.* film thickness chart is constructed, which enables rapid thickness determination without calculation. The chart is derived for use with silicon films of relatively low carrier concentration deposited on silicon substrates of high carrier concentration (0.007 ohm-cm-N-type). The chart is most useful for low order interference fringes including 12th order. Similar charts are applicable for other semiconductor materials.

Of the various methods examined for making thickness measurements on epitaxial films, the infrared interference method described by Spitzer and Tanenbaum (1) has proved to be best suited for most measuring applications. This method has the advantages of being accurate, quick, nondestructive, and well adapted for routine measurements. Interference fringes are observed only if there is a difference between the optical properties of epitaxially grown film and those of the substrate. This relationship between film thickness and the optical wavelengths of interference fringe maxima is given by a chart which is useful for rapid and accurate data reduction without calculation.

The Beckman spectrophotometers IR-4 and IR-5A equipped with NaCl optics and the Beckman specular reflectance attachment were used for this work. Additional measurements have also been made with KBr and CsBr optics.

Optical Properties of Epitaxial Films on Silicon

The primary requirement for production of interference fringes by reflection from a film is that the optical constants of the film differ from those of the substrate material. The optical constants of a silicon epitaxial film and substrate do not differ significantly unless the free carrier concentration at one side of the interface is very high, approaching degeneracy.

The reflectance at the interface between a nonabsorbing medium (n_1) and an absorbing substrate (n_2,k_o) at normal incidence is

$$R = \frac{(n_1 - n_2)^2 + k_o^2}{(n_1 + n_2)^2 + k_o^2} \quad [1]$$

where R is the reflectance, n is the refractive index, and k_o is the extinction coefficient of the substrate.

$$k_o = \frac{\alpha\lambda}{4\pi} \quad [2]$$

where α is the absorption coefficient and λ is the wavelength.

The influence of the very large free carrier concentration on the electrical susceptibility is such that as the optical wavelength is increased the refractive index decreases, and at still longer wavelengths the absorption effect predominates (2).

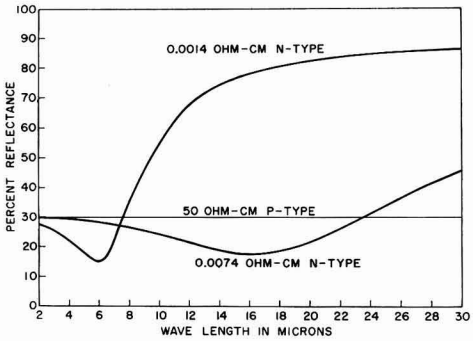

Fig. 1. Reflectance spectra of silicon samples showing the effects of carrier concentration on the optical constants. Decreasing reflectance, below 30%, indicates decreasing refractive index and large increasing reflectance indicates large increasing extinction coefficient.

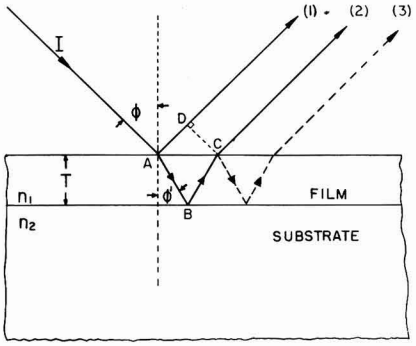

Fig. 2. Ray diagram for reflection from a film deposited on a thick substrate. The amplitudes of rays 1, 2, 3, etc., add vectorially resulting in maxima and minima in the reflectance spectrum.

The reflectance curves of Fig. 1 were obtained from silicon wafers prior to film deposition. The dip and subsequent rise in the reflectance curves for 0.0074 ohm-cm and 0.0014 ohm-cm N-type silicon, similar to reflectance curves shown in a paper by Spitzer and Fan (3), identify the decreasing refractive index and high absorption portions of the spectrum. Contrasted to the very low resistivity samples is the 50 ohm-cm sample which exhibits a nearly constant reflectance indicating a relatively constant refractive index.

Production of Interference Fringes

Figure 2, a ray diagram showing reflection from an epitaxial film at oblique incidence, is used to calculate the optical path difference between the first and second surface reflections. Interference fringes are observed when the first and second surface reflected rays interfere locally as the wavelength is varied.

The optical path difference is

$$\delta = n_1(\mathrm{AB} + \mathrm{BC}) - \mathrm{AD} \qquad [3]$$

The refractive index, n_1, multiplies the apparent optical path in the film, (AB + AC), converting it to an equivalent air path.

Using Snell's law ($\sin \phi = n_1 \sin \phi'$) and Eq. [3] it can be shown that

$$\delta = 2Tn_1 \cos \phi' \qquad [4]$$

where T is the film thickness, ϕ is the angle of incidence, and ϕ' is the angle of refraction.

At point A, in Fig. 2, the reflected ray undergoes a phase change of π or $\lambda/2$ while the transmitted ray remains in phase with the incident ray. These phase relationships apply to reflection from an optically more dense (greater refractive index) dielectric.

At point B the reflected ray undergoes a phase change which may vary from 0 to π depending on the optical constants at the reflecting interface. However, if we limit this discussion to the spectral region where the reflecting substrate is known to have a lower refractive index than the film and also a negligibly small extinction coefficient, k_0, the phase change at point B can be taken as zero.

At point C, both the transmitted and reflected rays are in phase with the incident ray, BC.

For some wavelength, λ_0, the optical path difference will be

$$\delta = \lambda_0/2$$

At this wavelength ray 1 is advanced by $\lambda_0/2$ and ray 2 retarded by $\lambda_0/2$ giving a net difference of λ_0. It is assumed that maxima will occur at wavelengths where ray 2 is in phase with ray 1. The first (zero order) fringe will occur at λ_0, the next fringe (first order) will occur at λ_1, where

$$\delta = \lambda_1 + \frac{\lambda_1}{2} \qquad [5]$$

and the mth order fringe maxima will occur at λ_m where

$$\delta = \left(m + \frac{1}{2}\right)\lambda_m \qquad [6]$$

Minima occur at intermediate wavelengths where $\delta = m\lambda$, (m, an integer).

The additional reflections which occur within the film interfere with the resultant of rays 1 and 2. Each succeeding ray is delayed an additional amount δ relative to the preceding ray. At a fringe maximum these additional reflections alternately aid and oppose with a net result of decreasing the fringe maxima by a small amount. The additional reflections also reduce the values of the fringe minima. The fringes grow in intensity as the difference in refractive index between film and substrate increases. Fringe intensity is observed to increase with both wavelength and doping level of the substrate. These effects are predictable from the influence of wavelength and carrier concentration on the susceptability (1, 3).

Deviations from parallelism within the film and low gradient interfaces are common causes for fringe cancellation when it would appear that there is a sufficient difference of optical constants for fringes to occur.

As the extinction coefficient increases with increasing wavelength it predominates in determining the interface reflectance, Eq. [1]. Relatively high

interface reflectance is characteristic of this spectral region yielding large intensity fringes. The transition between low refractive index and high extinction coefficient is accompanied by a varying phase change upon reflection from the interface. The phase change is nearly zero if k_o is small enough to be neglected in Eq. [1], and it increases approaching π for long wavelengths and large k_o (5).

The transitional region should be avoided when making thickness measurements because of the varying phase change which introduces thickness measuring errors. Successive fringe pairs yield different thickness values in this region.

Thickness Computation

A convenient thickness relationship can be obtained from [4] and [6] utilizing two wavelengths corresponding to fringe maxima, λ_m and λ_{m+x}.

$$T = \frac{x(\lambda_m \lambda_{m+x})}{2n_1 \cos \phi' (\lambda_m - \lambda_{m+x})} \qquad [7]$$

where x is an integer representing the number of fringes occurring from λ_m to λ_{m+x}. An equivalent expression applies to linear wavenumber spectra where the fringe period is uniform.

Equation [7] can be applied to fringe minima as well as maxima and it is also independent of the phase change which may occur at the interface, provided the phase change is constant in the interval λ_m to λ_{m+x}.

The value for the refractive index of the film given by Salzberg and Villa (4) for optical grade silicon at 10μ is 3.4179, which is rounded to 3.42 and assumed constant over the 6-16μ range. The reflectance data also verifies this value.

The angle of incidence, ϕ, for the Beckman specular reflectance attachment is 30°, which corresponds to an angle of refraction of 8.4° and $\cos \phi' = 0.99$. The rays within the film are nearly normal to the surface, which makes the measurement relatively insensitive to ϕ.

The constant, $2n_1 \cos \phi' = 6.77$, when used with Eq. [7] gives film thickness in the same units as those used for wavelength.

The conditions imposed for the development of Eq. [7] were:

1. Fringe maxima occur at wavelengths where the first and second surface reflections are in phase (the phase difference is $2\pi m$, m an integer).

2. The phase change at the interface is zero or constant from λ_m to λ_{m+x}.

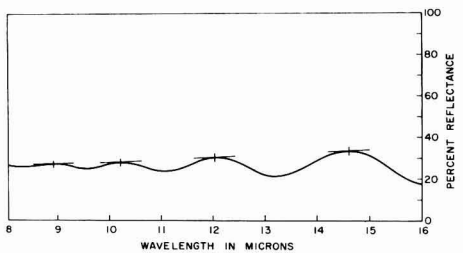

Fig. 3. Reflectance spectrum of a silicon epitaxial film showing the evaluation of fringe maxima.

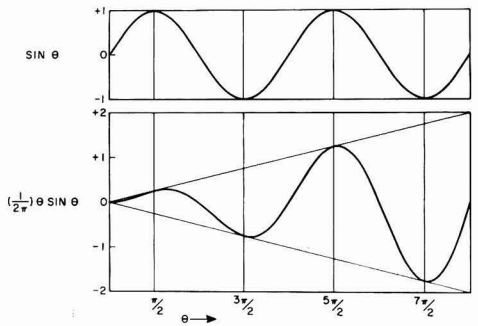

Fig. 4. Fringe model demonstrating the error which can arise by evaluating simple maxima. The desired phase relationship is satisfied at the points of tangency to the fringe envelope.

Evaluation of Fringe Maxima

In the preceding section the interference relationships given were based on wavelength values for which fringe maxima occur, as stated in condition 1. Condition 1 is correct only for equal intensity fringes, and it is incorrect for epitaxial films where the fringes grow in intensity with increasing wavelength. Figure 3 shows a typical reflectance spectrum, obtained from an epitaxial film as described in this paper, illustrating the growing intensity of the fringes.

A simplified model which illustrates the error made in condition 1 is given in Fig. 4. Interference fringes produced by two beams of constant intensity (independent of wavelength) would be of uniform intensity also. However, the second surface reflection from an epitaxial film varies with wavelength, and thus the fringes vary in intensity also. For this condition the simple maxima of the fringe no longer corresponds to the wavelength of $2\pi m$ relative phase shift. The $2\pi m$ relative phase shift can be shown, by differentiation, to correspond to the wavelength for which the fringe curve is tangent to the envelope of the fringes.

The wavelength values needed for the calculation of film thickness utilizing Eq. [7] are obtained by a method of tangents. For each point a tangent line is drawn approximating the slope of the envelope function. The resulting point of tangency is the desired value and will be termed the adjusted maximum. Large intensity fringes can be evaluated at the simple maxima with small error.

Fringe Chart

By using Eq. [4] and [6], it is possible to express film thickness in terms of the fringe order and wavelength of the fringe maxima

$$T = \frac{\left(m + \frac{1}{2}\right) \lambda_m}{2n_1 \cos \phi'} \qquad [8]$$

Equation [8] includes a phase change of π at the first surface but no phase change at the interface, which is the situation for silicon films on 0.007 ohm cm N^+ substrate in the 6 to 16μ range. Plotting Eq. [8], Fig. 5, with thickness as a function of wavelength for

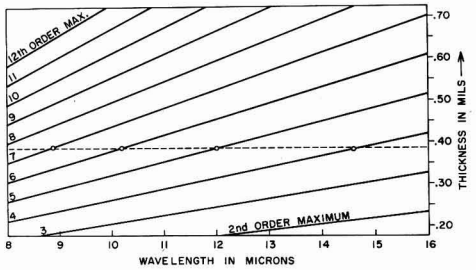

Fig. 5. Fringe chart for silicon epitaxial films, giving the wavelengths of fringe maxima as a function of film thickness. Thickness is determined by fitting fringe maxima data on this chart as shown by the dashed line.

integer values of m, results in a family of straight lines of constant fringe order. A horizontal line, T = constant, intersects the fringe order lines at wavelength values corresponding to the fringe maxima for that thickness.

Use of the Fringe Chart

For low order fringes, through 10th or 12th order, the chart can be used to simplify conversion of fringe wavelength data into accurate film thickness values. An important step is determining the correct fringe wavelength values by the tangent method. This wavelength evaluation method is also important when Eq. [7] is used. Errors up to 5% can occur if simple maximum values are used instead of the adjusted values, especially if only 2 or 3 fringes are available.

The chart will give reliable thickness values with three well-defined fringes. Improved accuracy achieved by use of the chart is due to the fact that all fringe maxima are used, showing up faulty data points.

Once the adjusted maximum values have been determined, a straight edge is positioned horizontally on the fringe chart lining up the wavelength of one of the fringe maxima and a fringe order line for a trial fit of the remaining fringes. Fringe maxima should fall at the intersections of the horizontal line with successive fringe order lines (see Fig. 5). If a good fit of the data is not possible at that thickness, a second trial should be made by moving the initial point up or down to the next fringe order and checking once more to see if the other fringes fit on a horizontal line. When a good fit is obtained, the horizontal line is extended to the right margin to read film thickness.

To aid in using the chart the wavelengths of adjusted maxima can be marked on a calibrated straight edge as they are read from the spectrum. The straight edge is then moved vertically across the chart, maintaining a horizontal position and wavelength reference until a thickness value is found where the marks are located on consecutive fringe order lines. Adjacent solutions should be tried, thicker and thinner, until the best solution is obtained.

Good accuracy will result if four or more fringes are located on the chart. Three fringes will give dependable results through 9th or 10th order. Equation [7] should be used in preference to the chart for fringes of 10th order and higher.

Very thin films are difficult to measure because only one or two fringes are observed. Additional data points can be obtained from the fringe minima which can also be included on the fringe chart. Equations [7] and [8] are converted to equivalent minima expressions by subtracting ½ from the integer values. When using Eq. [7] the interval between a maximum and the next minimum is ½ fringe. The method of tangents also applies to the evaluation of minima.

Experimental Check

An experimental check by an independent thickness measuring method was performed to verify the accuracy of the interference method. The cleavage method was chosen as the most desirable alternate measuring method. The cleaved wafer is etched for 10 to 15 sec in an HF, HNO_3 acetic acid (1-3-10 volume parts) etch and then measured directly with a microscope. The etch delineates the NN^+ interface very well, and the measurement is reasonably easy to make. The major disadvantage of the cleavage method is that it is destructive. This method can be utilized as a periodic check on the interference method and for films which are not sufficiently parallel to produce fringes.

Five different samples were measured by both cleavage and interference methods. The results of these measurements are tabulated.

Sample No.	1	2	3	4	5
T in mils, interference	0.24	0.26	0.33	0.83	0.43
T in mils, cleavage	0.26	0.28	0.32	0.82	0.42
Percentage difference	8%	7%	3%	1.2%	2%

Sample 4 was evaluated by Eq. [7], and the other samples were measured using the chart.

The agreement between the two methods is very good. The cleavage method has been reported to be accurate to ±10%. It is felt that interference methods as described are within a ±5% accuracy range.

Other Materials

Interference methods are applicable to epitaxial films of other semiconductors (1). A similar fringe chart can be constructed for use with materials other than silicon. Equation [8] used to construct the chart includes the refractive index of the film and the angle of refraction. These values must be evaluated for each particular material and reflectance apparatus. Should the refractive index of the film vary over the spectral range, where the fringes are observed, the chart can be constructed to include this variation. The chart would then be a set of curved lines. Should the film have a lower refractive index than the substrate, the chart equation should be rewritten to include the π phase shift at the interface. However, this situation will be very complex due to the attendant high absorption of the film and varying refractive index.

Manuscript received Oct. 5, 1961; revised manuscript received March 16, 1962. This paper was prepared for delivery at the Detroit Meeting, Oct. 1-5, 1961.

Any discussion of this paper will appear in a Discussion Section to be published in the June 1963 JOURNAL.

REFERENCES

1. W. G. Spitzer and M. Tanenbaum, *J. Appl. Phys.*, **32**, 744 (1961).
2. F. A. Jenkins and H. E. White, "Fundamentals of Optics," 3rd ed., pp. 261-264, McGraw Hill, New York (1957).
3. W. G. Spitzer and H. Y. Fan, *Phys. Rev.*, **106**, 882 (1957).
4. C. D. Salzberg and J. J. Villa, *J. Optical Soc. Am.*, **47**, 244 (1957).
5. O. S. Heavens, "Optical Properties of Thin Solid Films," pp. 46-62, Butterworths, London (1955).

Ultrafine Tungsten and Molybdenum Powders

H. Lamprey and R. L. Ripley

Technology Department, Union Carbide Metals Company, Division of Union Carbide Corporation, Niagara Falls, New York

ABSTRACT

A process is described for producing tungsten and molybdenum metal powder of 0.01-0.1μ average particle diameter by hydrogen reduction of the metal chlorides. Some of the physical and chemical properties of this material are discussed, together with data pointing to metallurgical uses of the product. Safety precautions to be observed in handling these fine powders are also described.

There is considerable evidence to indicate that metal compacts made by sintering ultrafine metal powders have improved engineering properties. The pronounced effect of grain size on the mechanical properties of iron and steel (1-5), copper (6), zinc (7), and other metals (8), is clearly shown in the literature. In general, a reduction in grain size is accompanied by an increase in hardness, yield strength, and fracture strength, and by a decrease in the ductile-brittle transition temperature. Ultrafine grain structure is also said to be the key to improving the properties of dispersion-strengthened metal and alloy systems (9,10).

In order to extend our knowledge of such effects to the refractory metals, it was decided to produce tungsten and molybdenum powders for metallurgical evaluation. Theory predicts that the maximum mechanical benefits should be found in sintered products having grain diameters smaller than 0.1μ, and so our efforts were directed toward producing the powders in the 0.01-0.1μ range. This paper will be restricted to describing production by a chemical process, namely, hydrogen reduction of tungsten and molybdenum chlorides in the vapor state.

There are two keys to the production of ultrafine metal powder by chloride reduction processes: one is to carry out the reduction in the vapor phase, whereby, through control of dilution, only a minimum number of atoms or molecules of the reacting species can get together to form agglomerates; the other is to carry out the reaction in free space, away from solid walls on which a continuous metal plating can deposit.

Thermodynamic data compiled by Glassner (11) indicate that the by-product HCl is more stable than any of the tungsten and molybdenum chlorides by 10-20 kcal/g atom of chlorine over the temperature range from 25° to 900°C. Thus, the reaction should proceed readily at elevated temperature, and no back reaction is to be expected as the product is cooled.

The apparatus used for carrying out the reaction is sketched in Fig. 1. Purified hydrogen and tungsten or molybdenum chloride vapors, carried in a stream of argon if desired, are preheated to the chosen temperature and brought together in a large reaction space; the gases react immediately on contact to form submicron metal powder and hydrogen chloride vapor.

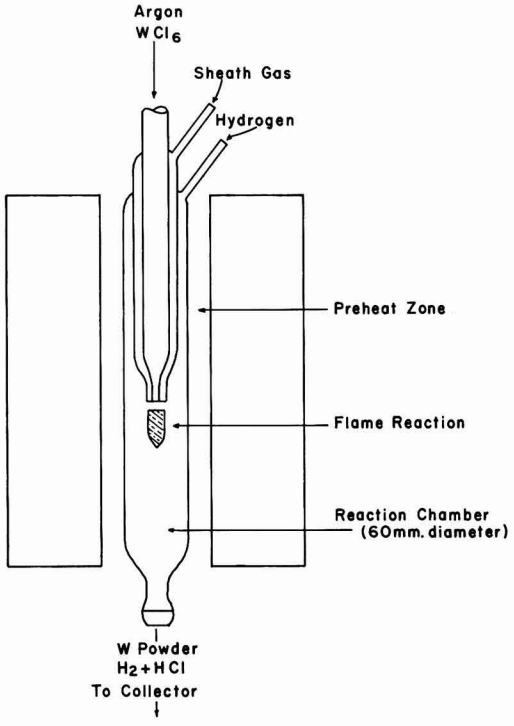

Fig. 1. Quartz apparatus for producing ultrafine tungsten and molybdenum by a flame reaction.

One purpose of flowing argon or chlorine through the sheath gas nozzle in Fig. 1 is to prevent formation of metal at the metal chloride orifice tip, with consequent plugging of the apparatus. Chlorine is somewhat more effective than argon for this purpose. The gases issuing from the concentric tubes react as a flame and the sheath gas serves to position the metal chloride-hydrogen flame at some distance from the orifice.

The metal may be collected by gravity settling with or without the use of an electrostatic precipitator; or the reaction gases may be filtered through a large diameter column of steel wool, the trapped powder shaken free of the wool and separated from small steel fragments by magnetic means. When using electrostatic precipitation, it is necessary to prevent bridging the gap between the electrodes with a conducting film of tungsten powder. When this bridging occurs, the alternating high potential field (20,000-50,000v) is no longer positioned between the collecting electrodes but between the inside and outside walls of the glass sheath over the "hot" electrode. While this over-all process works well for producing submicron powder down to 0.01μ particle size, various chemical and mechanical refinements are necessary to the process in order to control particle sizes within narrow ranges, to operate with high materials efficiency, and to produce powder of high purity.

The quality of the powder produced depends on a number of factors; one of them is the reactant preheat temperature just prior to mixing. As this temperature increases, the powder product becomes somewhat finer (Table I), and the amount of chlorine impurity is reduced.

Runs 1 through 5 were all carried out in the apparatus shown in Fig. 1. The mole ratio of hydrogen to chlorine in the system was maintained at 3 and the inert gas flow was held constant. Ultrafine molybdenum powder was also prepared in the same apparatus at a preheat and reaction chamber temperature of 800°C. This powder contained 0.15% oxygen, 0.35% chlorine, 0.01% silicon, 0.1% carbon, and had a surface area of 11.1 m^2/g corresponding to an average particle size of 0.05μ.

In most of the tests run thus far, the powdered product has analyzed approximately 99.5% metal, the balance being largely chlorine, oxygen, and carbon, with very small amounts, on the order of 0.01% or less, of nitrogen, silicon, and hydrogen. Tungsten and molybdenum chlorides commonly contain oxychlorides, and some of this oxygen finds its way into the powder. The carbon impurity gets into the system during a prior purification of chlorine by passing it over hot carbon to remove oxygenated compounds. This carbon impurity could be reduced or eliminated if necessary.

Table I. Production of ultrafine tungsten powder by the hydrogen reduction of tungsten hexachloride at various temperatures

Run No.	Preheat and reaction chamber temp, °C	% Chlorine in product	Product diam, μ
1	430	1.82	0.029
2	620	0.24	0.025
3	695	0.10	0.031
4	800	0.27	0.026
5	905	0.13	0.021

Oxygen and chlorine impurities in the metal powder products are present as lower valent compounds and as chemisorbed gases.[1] X-ray diffraction patterns show the presence of W_3O in the tungsten powder. Part of the oxygen and chlorine can be removed by post-treatments of various kinds. Vacuum pumping, alone, is relatively ineffective. A product analyzing 0.39% oxygen and 0.24% chlorine with a surface area of 12 m^2/g was heated to 800°C for 24 hr under a flow of dry hydrogen. The oxygen content was reduced to 0.21% and the chlorine content to 0.04%. Simultaneously, the surface area decreased to 6.49 m^2/g as a result of this treatment. Obviously, a tungsten powder product low in oxygen and carbon content is more easily obtained by a careful distillation of the tungsten hexachloride. This distillation removes the oxychlorides and chlorinated hydrocarbons which commonly contaminate tungsten hexachloride made from commercial chlorine.

Powder Properties

The particle sizes of the tungsten powders were determined by surface area measurements (12) and confirmed by electron micrography. Figure 2 shows a typical photomicrograph obtained at a magnification of 50,000 diameters. The particles approach spheres in shape. There is considerable aggregation of particles in this photomicrograph.

The bulk density of the powder as collected was approximately 0.2 g/cc. This is remarkably low for tungsten with a density of 19.3.

The chemical properties of the ultrafine powder are greatly modified by the presence of the chemi-

[1] All oxygen analyses in this study were determined by a vacuum fusion analysis in which the encapsulated sample is dropped into an iron-carbon melt at 1800°C, and the resulting carbon monoxide is measured.

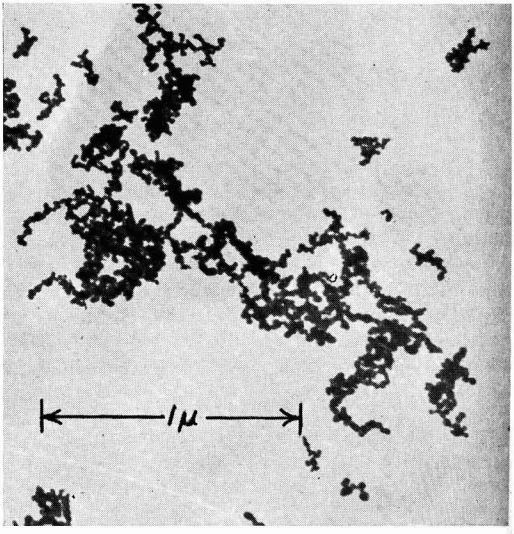

Fig. 2. Photomicrograph of ultrafine tungsten powder. Magnification 40,625X.

sorbed gas films. Powder which is relatively free of chlorine and oxygen appears to be much more reactive than powder made as described above. Finely divided metal powder is sometimes pyrophoric. Great variability in the reactivity of tungsten powder toward air and water has been encountered. Some samples oxidize rapidly on exposure to air. For example, when a sample containing 1.5% of adsorbed chlorine was exposed to air at room temperature, thermocouples embedded in the powder showed temperature rises of 10-20°C due to air reaction, but no ignition occurred. When a red-hot wire was placed in the powder, the material in the vicinity of the wire reacted, turning yellow-green, the color of WO_3, but the remainder of the powder was not affected. Other samples exposed to air have become red hot on the surface within a few seconds' time. Factors such as the rate of heat loss from the powder and the degree of packing of the sample also affect the possibility of ignition.

More usually, however, the tungsten powder is completely inert. For example, a sample of powder analyzing 0.10% oxygen, 0.09% chlorine, 0.01% carbon, and 0.01% silicon, and having an average particle diameter of 0.02μ, was heated in air on a thermogravimetric balance of 1 mg sensitivity, *i.e.*, 0.1% of the weight of the sample. No measurable weight gain occurred until the temperature reached 140°C, when the powder converted rapidly and completely to tungstic oxide. The same result was obtained when oxygen was substituted for air, or when the tungsten powder was pretreated with hydrogen at 800°C, or when it was treated with chlorine until 1% by weight was adsorbed; the ignition temperature in air or oxygen was, in all cases, 130-140°C on the thermogravimetric balance. Powder of the same particle size, from another batch, containing 0.20% chlorine, 0.24% oxygen, 0.16% carbon, and 0.16% silicon, behaved identically.

The submicron tungsten powder physically adsorbs water reversibly at 25°C and does not react appreciably with water up to 1200°C. This powder chemisorbed several per cent of chlorine when exposed to a 20:80 chlorine-argon mixture at room temperature; the chlorine, unlike water vapor, was not driven off by dry argon at room temperature, but was removed, together with a little tungsten chloride, by argon heated to above 350°C.

These tests indicate that the fine tungsten powder can be handled safely if a few simple precautions are taken. However, any finely divided metal powder, mixed with air or other oxidizing agent, is a potential source of uncontrollable reactions. For example, when an operator inadvertently let a small amount of the fluffy tungsten powder come in contact with hot chlorine gas in a large glass receiver, a violent reaction shattered the equipment and could have injured the operators if they had not been wearing safety clothing and goggles. There is a limit to how casually any ultrafine powder can be handled. Currently this problem is being studied further to try to determine the cause of the variability in pyrophoricity of different lots of powder.

Uses

A few tests have been made to determine whether pressed compacts of ultrafine tungsten powder would have improved mechanical properties, as theory predicts. Specimens of rather impure powder (0.6% oxygen and 0.3% chlorine) were pressed at 40 tons/in.^{2}, giving compacts of only about 40% theoretical density, probably because of incomplete removal of entrapped air. The green strength was, however, very good. These specimens sintered poorly at 1750°C, giving compacts of 80% theoretical density. However, grain growth was excessive at these temperatures, *i.e.*, to about 30μ, and it was immediately apparent that low-temperature sintering would have to be possible if the desired fine structure is to be retained. Later, similar green compacts were sintered at 1550°C for 30 min in hydrogen atmospheres to give products of 94% theoretical density.

These results point up a rather remarkable property of ultrafine tungsten powder: that it can be sintered effectively at temperatures nearly a thousand degrees lower than conventional tungsten powder. This seems to be a general phenomenon, not restricted to tungsten. Lowering of the sintering temperature with other ultrafine metal powders has been observed in the same way.

Metallurgical data are currently being collected on these fine powders, including pressing, rolling, extruding, slip casting, dispersion strengthening, and so on. Some of these results should be available soon for publication. The powders, because of their unusual sizes and surface characteristics, may have unique applications as catalysts, fillers, fuels, nucleation agents in alloy production, and other diverse applications.

Acknowledgment

The authors wish to thank Dr. H. V. Seklemian and Mr. R. L. Reddy, who carried out some of the work described in this report.

Manuscript received Oct. 30, 1961. This paper was prepared for delivery before the Indianapolis Meeting, April 30-May 3, 1961.

Any discussion of this paper will appear in a Discussion Section to be published in the June 1963 JOURNAL.

REFERENCES

1. N. J. Petch, *J. Iron Steel Inst.*, **174**, 25 (1953).
2. A. Cracknell and N. J. Petch, *Acta Met.*, **3**, 186 (1955).
3. R. L. Smith, G. Spangler, and R. M. Brick, *Trans. A.S.M.*, **46**, 973 (1954).
4. C. A. Edwards, H. N. Jones, and B. Walters, *J. Iron Steel Inst.*, **139**, 341 (1939).
5. L. D. Jaffe, F. L. Carr, and D. C. Buffum, *Trans. A.I.M.E.*, **197**, 1147 (1953).
6. R. P. Carreker and W. R. Hibbard, *Acta Met.*, **1**, 654 (1953).
7. G. W. Greenwood and A. G. Quarrel, *J. Inst. Met.*, **82**, 551 (1954).
8. L. M. T. Hopkin, *ibid.*, **84**, 102 (1956).
9. N. J. Grant and O. Preston, *Trans. A.I.M.E.*, **209**, 349 (1957).
10. F. V. Lenel, A. B. Backenstro, Jr., and N. V. Rose, *ibid.*, **209**, 124 (1957).
11. A. Glassner, The Thermodynamic Properties of the Oxides, Fluorides, and Chlorides to 2500°K., Argonne National Lab. Report ANL-5750, Supt. of

Documents, U.S. Printing Office, Washington, D. C.
12. P. A. Faeth and C. B. Willingham, Technical Bulletin on the Assembly, Calibration and Operation of a Gas Adsorption Apparatus for the Measurement of Surface Area and Density of Finely Divided Solids, Mellon Institute of Industrial Research, Sept. 1955.

Effect of Adsorbed Anions on Reduction Processes on Passive Stainless Steel

F. A. Posey and R. F. Sympson[1]

Chemistry Division, Oak Ridge National Laboratory,
Operated by Union Carbide Corporation for the U. S. Atomic Energy Commission, Oak Ridge, Tennessee

ABSTRACT

The effects of sulfate, thiocyanate, chloride, and hydroxide ions on the reduction of cupric ion on passive stainless steel have been studied by use of potentiostatic techniques. Specific adsorption of the anions catalyzes the rate of the reduction reaction, and analysis shows that the adsorption follows a potential-dependent Langmuir isotherm. A simple model is proposed, based on electrochemical kinetic theory, which yields isotherms having properties in good agreement with experimental observations.

Studies on the kinetics of electrode processes have shown that anions exert specific effects in many systems. Among numerous contributions to the literature on this subject are papers concerned with the effect of anions on the exchange current of redox systems (1), on the corrosion of metals (2, 3), and on electrode reactions at a mercury surface (4). Frumkin (5, 6) and Piontelli (7) have reviewed anion effects in electrocapillarity and electrode kinetics, and the influence of anions in polarography was the subject of a review by Brdicka (8). Electrode processes occurring on passive metals are also affected by anions, and the sensitivity of the electrode potential of iron passivated in $CrO_4^=$, TcO_4^-, $MoO_4^=$, or $WO_4^=$ to additions of Cl^- or SCN^- was noted by Sympson and Cartledge (9). In a previous paper (10), the reduction of cupric ion on passive stainless steel in sulfate solution was studied by use of potentiostatic, galvanostatic, and tracer techniques. This reaction is catalyzed by the addition to solution of certain anions (11, 12), and the purpose of the present paper is to present results of electrochemical measurements on the effects of Cl^-, $SO_4^=$, OH^-, and SCN^- ions on the kinetics of reduction of Cu^{++} on passive stainless steel.

In order to obtain detailed information on the nature of the anion effects, a series of potentiostatic experiments was performed. The effect of SCN^- on the reduction of Cu^{++} on passive stainless steel was determined in various H_2SO_4-Na_2SO_4 solutions. These results suggested that both sulfate ion concentration and acidity are important variables in the kinetics of the reduction reaction. Hence further experiments were performed in aqueous perchlorate media in order to minimize any effect of complexing of cupric ions by anions in solution. Experiments in perchlorate solutions included the effects of Cl^-, $SO_4^=$, and, in particular, OH^- (acidity) on the kinetics of Cu^{++} reduction as a function of electrode potential and temperature. Since it was desirable to distinguish between complexing and adsorption aspects of the anion effects, accurate values of association quotients were determined spectrophotometrically for the association of Cu^{++} with the anions studied under conditions prevailing in the potentiostatic experiments. The results of the electrochemical measurements are presented below and analyzed on the basis of electrochemical kinetic theory.

[1] Present address: Department of Chemistry, Ohio University. Athens, Ohio.

Experimental

The experimental cell was a five-necked, spherical reaction flask of 500 ml capacity, fitted with a water-cooled condenser for use with heated solutions. Standard taper ports provided space for a thermometer, the entry and egress of gas, a platinum polarizing electrode, the stainless steel electrode assembly, and for additions of aliquots of stock solutions. Temperature was controlled by means of a Glascol heating mantle operated from a Variac supplied with regulated voltage. The constancy of the ambient temperature ensured control of the solution temperature to approximately $\pm 0.5°C$ over long periods of time. Purified helium or nitrogen effused into the solution at a constant rate through a sintered glass disk; the flow was sufficient to ensure vigorous stirring. Residual oxygen was removed from the gas by use of a tube furnace containing heated copper turnings, and columns of Drierite and Ascarite provided further purification.

Electrode potential measurements were made using a L&N *p*H Indicator (No. 7664) as a potentiometer coupled with a Brown recorder. Potentials were measured and recorded with time by the direct method, using a Luggin capillary bridged to a saturated calomel reference electrode maintained at room temperature. The concentration of the electrolyte was such that no significant ohmic potential drop occurred in solution between the electrode and the tip of the reference electrode capillary over the entire range of polarizing currents employed.

Galvanostatic circuitry consisted of high-capacity batteries furnishing 135v output, together with large load resistors in series with the cell. The concentration of cupric ion in solution was always such that comparatively small currents (usually no greater than 10 $\mu a/cm^2$) were sufficient to allow observations over the entire usable potential range of passive stainless steel in the chosen environments. Currents were measured by recording voltage drop across precision resistors in the circuit. The potentiostat used in these studies was developed in this laboratory for the special purpose of providing an all-electronic instrument suitable for precise control of electrode potentials in polarizable systems over extended periods of time. The potentiostat, a single-amplifier type, was constructed using a Reeves Instrument Corporation A-400 Dual D. C. Amplifier (REAC); this is a chopper-stabilized operational amplifier of high gain. Maximum output voltage was ±100v and output current could attain ±20 ma. Electrode potentials were constant to within ±0.1 mv at all times when the potentiostat was controlling, as could be ascertained oscilloscopically. Because of the chopper stabilization, response time was slow compared to potentiostats of the straight-amplifier type, but this was a negligible disadvantage for the present purposes considering the gain in long-term stability and precision afforded by the design adopted.

Electrodes were machined from type 347 stainless steel[2] in cylindrical form with a diameter of 1 cm and a height of 2 cm, thus permitting an exposed geometrical area of 7 cm^2 when mounted on the electrode holder. A Teflon cylinder abutted one end of the steel electrode and was followed by a conical Teflon piece machined to fit the standard taper joint of the cell. The entire assembly was tightened by use of a stainless steel rod which penetrated cylindrical and conical pieces axially and threaded into the steel electrode. A solution-tight seal was easily made, and no further attention was necessary during the life of the electrode. The surface of the stainless steel electrodes was electropolished in a solution of 60% by volume of 85% H_3PO_4 + 20% of 95% H_2SO_4 + 20% of H_2O at 65°C for 3-5 min at a current density of 0.5 amp/cm^2. This procedure produced a mirror-like surface of reproducible polarization characteristics in the solutions studied. Electrodes were stored between measurements in triple-distilled water.

All solutions were prepared using triple-distilled water, obtained by redistilling tap distilled water from the laboratory supply in a two-stage quartz still manufactured by Heraeus-Quarzschmelze. All reagents used were analytical grade. Recrystallization of crystalline reagents was found to be without appreciable effect on the results, and most experiments were performed using analytical grade chemicals without further purification.

In potentiostatic experiments, stainless steel electrodes were allowed to attain steady states at a preselected value of electrode potential. This procedure was time-consuming, as long-term transients are observed on passive stainless steel, especially in perchlorate solutions.[3] After attainment of steady states, aliquots of concentrated stock solutions were added to the experimental solution by micropipettes and the applied current necessary to maintain the chosen potential constant was recorded with time. Most experiments were performed in 0.3*f* $NaClO_4$ acidified with $HClO_4$. Stock solutions of 1*f* Na_2SO_4 and 5*f* NaCl in 0.3*f* $NaClO_4$ were used in experiments on the effects of $SO_4^=$ and Cl^-, respectively. In experiments on the effect of SCN^-, which were performed in dilute H_2SO_4-Na_2SO_4 solutions, freshly prepared stock solutions of 0.25*f* KSCN dissolved in the experimental solutions were used. Experiments on the effect of acidity were performed in $10^{-5}f$ $HClO_4$ + 0.3*f* $NaClO_4$ by adding aliquots of stock solutions of 1*f* $HClO_4$ + 0.3*f* $NaClO_4$ or concentrated $HClO_4$.

Results

Data from a series of potentiostatic experiments on the effect of SCN^- on the reduction of Cu^{++} on passive stainless steel in dilute sulfate solution are shown in Fig. 1. Cupric ion concentration was 2.5 or 5.0 x $10^{-6}f$ in this series; the over-all formal rate constant, $\bar{k}$, was calculated by dividing the current density in amp/cm^2 by the cupric ion concentration in moles/liter. The sigmoid curves observed in Fig. 1 are typical of all the data obtained in experiments on the SCN^- effect. Evidently the rate of reduction of Cu^{++} approaches a limiting value at high $[SCN^-]$. Solid lines drawn through the experimental data of

[2] Commercial type 347 stainless steel, although by no means a simple alloy, was chosen as a working material because its electrochemical behavior is typical of that of a large number of steels of similar composition. In addition, our experience has shown that the kinetics of reduction reactions are relatively insensitive to the type of stainless steel used, provided a standardized method of surface preparation is employed.

[3] The half-times of transients were found to depend greatly on the acidity of the solution, being least (approximately 5 min or less) in solutions of high *p*H (approaching neutrality), and increasing to values of the order of half an hour at low *p*H. The necessity of waiting for true steady states in these passive systems cannot be overemphasized. Whatever the nature of the transients, whether they be due to readjustment of charge distribution in the passive oxide film, to change in the film thickness, or to slow processes akin to a reaction capacity at the oxide-solution interface (or a combination of all of these), considerable charge is required to establish a new steady state. Premature judgment of the existence of steady states or arbitrary selection of times for changing parameters such as added ion concentration, electrode potential, or applied current result in confusion of the desired properties of the Faradaic processes in the system with properties of the non-Faradaic processes occurring during the transients.

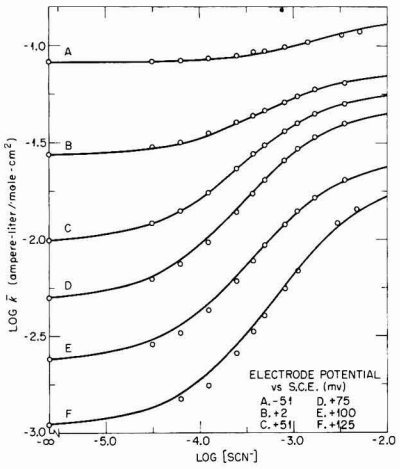

Fig. 1. Effect of SCN^- on the reduction of Cu^{++} on passive stainless steel in 1 x $10^{-3}f$ H_2SO_4 plus 9 x $10^{-2}f$ Na_2SO_4; 65°C, nitrogen atmosphere. Potential *vs.* S.C.E. at room temperature.

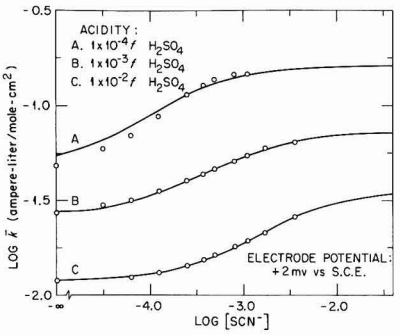

Fig. 2. Effect of acidity and SCN^- on the reduction of Cu^{++} on passive stainless steel in 9 x $10^{-2}f$ Na_2SO_4; 65°C, nitrogen atmosphere. Potential *vs.* S.C.E. at room temperature.

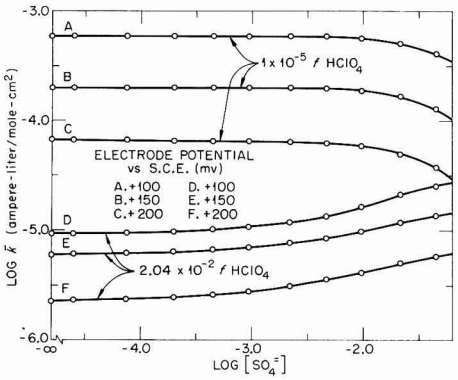

Fig. 3. Effect of $SO_4^=$ on the reduction of Cu^{++} on passive stainless steel in 3 x $10^{-1}f$ $NaClO_4$; 85°C, helium atmosphere. Potential *vs.* S.C.E. at room temperature.

Fig. 1 are least-squares fits of the data with an expression of the form of Eq. [1].

$$\overline{k} = (\alpha + \beta\gamma[X])/(1 + \gamma[X]) \qquad [1]$$

In Eq. [1], the formal electrochemical rate constant, $\overline{k}$, is a function of added anion concentration, [X], and of the three constants, α, β, and λ. The constant α is the rate constant for the reduction reaction in the absence of added anions, β is the limiting rate constant for large [X], and γ may be regarded as an equilibrium quotient for the interaction between anions and system reactants. The meaning of the constants of Eq. [1] is considered further below.

Experiments on the SCN^- effect were run at several acidities and at several over-all concentrations of sulfate ions. The effect of total sulfate ion concentration was found to be slight over the range 10^{-4} to $10^{-2}f$ Na_2SO_4. At constant $[H^+]$, little difference exists between rate constants at $10^{-4}f$ and at $10^{-3}f$ Na_2SO_4; some change of rate constant occurs at $10^{-2}f$ Na_2SO_4, but even here the difference is small. On the other hand, the effect of SCN^- on the reduction of Cu^{++} depends greatly on the acidity of the solution, as shown in Fig. 2. Changing the acidity of the solution not only affects the rate constants but also shifts the curve parallel to the log $[SCN^-]$ axis.

Data on the effect of $SO_4^=$ on the reduction of Cu^{++} on passive stainless steel in perchlorate solutions are shown in Fig. 3. Exploratory experiments had proven that NO_3^- and ClO_4^- ions have no effect on the kinetics of the reduction reaction, so that $0.3f$ $NaClO_4$ was chosen as inert electrolyte for experiments on the effects of $SO_4^=$, OH^-, and Cl^-, and crystalline $Cu(NO_3)_2 \cdot 3H_2O$ was used as the source of cupric ions. Even at $10^{-2}f$ $SO_4^=$, there is little change in the reduction rate of Cu^{++}, especially at lower acidity. These data are not extensive enough to show definitely whether or not a limiting value of rate constant is attained at high $[SO_4^=]$, but the aspect of the curves suggests not only the possibility of a limiting value but also the possibility of a common value independent of acidity.

The effect of acidity on cupric ion reduction is shown in Fig. 4 as a function of electrode potential. In addition to studies at 25°C, potentiostatic experiments were run at 45°, 67°, and 85°C. Figure 5, showing data on the effect of temperature at constant electrode potential, demonstrates that sigmoid curves are also obtained at the higher temperatures. Solid lines in Figs. 4 and 5 are least-squares fits of Eq. [1] to the experimental data. A limiting rate constant is attained at lower acidities in analogy to observations on the SCN^- effect; this effect is more pronounced at higher temperatures as may be seen in Fig. 5. In addition, a limiting rate is observed at the higher acidities (up to $10^{-1}f$ $HClO_4$).

Results of potentiostatic experiments on the effect of Cl^- on the reduction of Cu^{++} are shown in Fig. 6 as a function of electrode potential and acidity. Solid lines through data obtained in $10^{-6}f$ $HClO_4$ are least-squares fits; lines through data referring to $10^{-2}f$ $HClO_4$ are visual fits. The results at low acidity are similar to those shown in Fig. 1 for the effect of SCN^-. However, the experiments at higher acidity revealed a more complex behavior. Curve E of Fig. 6 shows the existence of a minimum in the $\overline{k}$ *vs.* $[Cl^-]$ relationship at ±0 mv *vs.* S.C.E. The influence of the phenomenon responsible for the minimum in curve

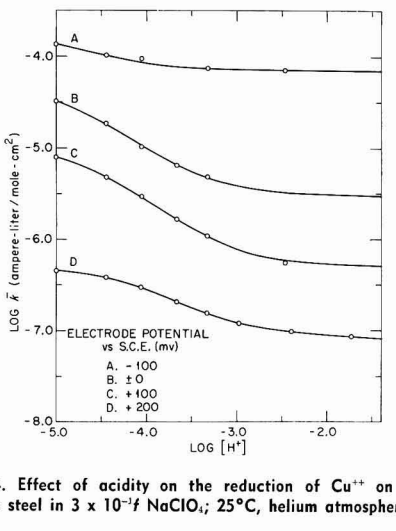

Fig. 4. Effect of acidity on the reduction of Cu^{++} on passive stainless steel in 3 x $10^{-1}f$ $NaClO_4$; 25°C, helium atmosphere.

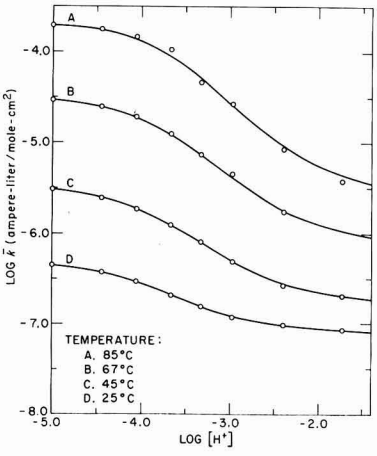

Fig. 5. Effect of temperature on the reduction of Cu^{++} on passive stainless steel in 3 x 10^{-1}f $NaClO_4$; helium atmosphere. Electrode potential: +200 mv vs. S.C.E. at room temperature.

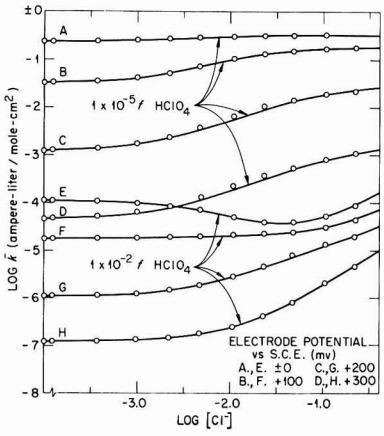

Fig. 6. Effect of Cl^- on the reduction of Cu^{++} on passive stainless steel in 1 x 10^{-5}f $HClO_4$ or 1 x 10^{-2}f $HClO_4$ plus 3 x 10^{-1}f $NaClO_4$; 85°C, helium atmosphere. Potential vs. S.C.E. at room temperature.

E seems to extend also to curve F, the behavior of which is more closely akin to the usual sigmoid relation obtained at lower acidity. Since meaningful data could not be obtained at chloride ion concentrations much larger than those shown in Fig. 6 without drastic changes in the ionic strength of the solution, evidence is insufficient on the question of whether or not rate constants are independent of acidity at high [Cl^-].

Discussion

Attempts to interpret the previous observations quantitatively on the basis of a complexing explanation encountered difficulties. Assuming that cupric ion and the anions studied react to form 1:1 complexes in solution and that rate constants differ for reduction of aquo ion and complex, one may derive an equation for the over-all rate constant which has the form of Eq. [1]. In this instance, the constant γ of Eq. [1] becomes the association quotient for the 1:1 association reaction. Values of γ were calculated from experimental data[4] for comparison with values of the 1:1 association quotients obtained from independent measurements. Examination of the literature showed that measurements of the 1:1 association quotients of Cu^{++} with the anions $SO_4^=$ and SCN^- were not reported for the experimental conditions of this study. Therefore, these quotients were measured spectrophotometrically as a function of temperature at ionic strengths of interest. Comparison of calculated values of γ with measured values of the 1:1 association quotients revealed sharp disagreement between the orders of magnitude. Furthermore, it was found that values of γ vary systematically with electrode potential. These observations forced abandonment of a complexing explanation as the predominant factor in the effect of anions on the reduction of Cu^{++} in the present system.

[4] If log $\bar{k}$ is plotted against log [X], the coordinates of the inflection point of a curve obeying Eq. [1] are given by the following equations; $\bar{k}$ (infl.) = $\sqrt{\alpha\beta}$; [X] (infl.) = $(1/\gamma)\sqrt{\alpha/\beta}$. These equations are useful for estimating γ from graphical data. However, the alternative procedure of calculating γ from a least-squares fit of Eq. [1] to experimental data was used here.

The previous data are better understood if it is assumed that the role of the anions lies in their affinity for the surface of passive stainless steel. The anions may be specifically adsorbed at the surface, thereby affecting the kinetics of rate processes occurring at the oxide-solution interface. An expression of the form of Eq. [1] may be derived by assuming that the number of adsorbed anions is related to anion concentration in solution by a Langmuir isotherm. The Langmuir isotherm is derived from considerations of coverage, without regard to lateral interaction effects or change of adsorption energetics with number of adsorbed particles (13). It can be expected to hold best for localized monolayer adsorption where adsorbed particles are relatively nonmobile and the adsorption bond is relatively nonlabile. At constant electrode potential the data of Fig. 1, 2, 4, 5, and 6 are represented by Eq. [1] to a good approximation, and this suggests that adsorption of anions on passive stainless steel involves strong specific interactions with the substrate. As shown below, combination of Langmuir adsorption model with the formalism of electrochemical kinetics leads to equations which adequately describe the results obtained in this study.

It has been shown previously (10) from analysis of polarization curves that the reduction of Cu^{++} on passive stainless steel proceeds by a two-stage mechanism involving a cuprous intermediate. In order to derive an expression for the effect of anions on the overall reduction rate, we assume for simplicity that three types of surface are available as reaction sites for the reduction of Cu^{++}: (i) the surface present at high acidity, which probably consists of adsorbed H_2O molecules and may be called the "aquo" surface; (ii) the surface present at low acidity because of adsorption of OH^- ions (or because of desorption of H^+ from the aquo surface), which may be called the "hydroxy" surface; and (iii) the surface resulting from specific adsorption of anions, which may be called the "anionic" surface. Equations [2], [3], and [4] show the reaction schemes at aquo, hydroxy, and anionic

surfaces, respectively, together with appropriate formal electrochemical rate constants for the individual charge transfer steps.

$$Cu^{++} \underset{\bar{k}_2}{\overset{\bar{k}_1}{\rightleftharpoons}} Cu^{+} \overset{\bar{k}_3}{\rightarrow} \text{products} \quad \text{(aquo surface)} \qquad [2]$$

$$Cu^{++} \underset{\bar{k}_5}{\overset{\bar{k}_4}{\rightleftharpoons}} Cu^{+} \overset{\bar{k}_6}{\rightarrow} \text{products} \quad \text{(hydroxy surface)} \qquad [3]$$

$$Cu^{++} \underset{\bar{k}_8}{\overset{\bar{k}_7}{\rightleftharpoons}} Cu^{+} \overset{\bar{k}_9}{\rightarrow} \text{products} \quad \text{(anionic surface)} \qquad [4]$$

If the fraction of the total electrode surface existing as hydroxy surface is designated by θ, the fraction as anionic surface by η, and the fraction as aquo surface by $(1-\theta-\eta)$, the total current density for reduction of cupric ion is given by Eq. [5].

$$j/\mathbf{F} = K_1(1-\theta-\eta) + K_2\theta + K_3\eta \qquad [5]$$

K_1, K_2, and K_3 are the rates of reduction on aquo, hydroxy, and anionic surfaces, respectively, in units of equivalents/cm^2-sec, $\mathbf{F}$ is the Faraday, and j is current density in amp/cm^2. K_1, K_2, and K_3 are given by Eq. [6], [7], and [8], respectively.

$$K_1 = \bar{k}_1 C_0(a) + (\bar{k}_3 - \bar{k}_2) C_R(a) \qquad [6]$$

$$K_2 = \bar{k}_4 C_0(\theta) + (\bar{k}_6 - \bar{k}_5) C_R(\theta) \qquad [7]$$

$$K_3 = \bar{k}_7 C_0(\eta) + (\bar{k}_9 - \bar{k}_8) C_R(\eta) \qquad [8]$$

$C_0(a)$ and $C_R(a)$ refer to concentrations of cupric and cuprous ions, respectively, at the interface of the aquo surface, with analogous definitions for $C_0(\theta)$, $C_R(\theta)$, $C_0(\eta)$, and $C_R(\eta)$.

The flux of each of the six species in Eq. [6], [7], and [8] may be related to the bulk concentration of cupric ions in solution by using the Nernst diffusion layer approximation to Fick's first law. When this is done, the results may be substituted into Eq. [6], [7], and [8] to give explicit expressions for rates of reduction on the several types of surface; these are given in Eq. [9], [10], and [11].

$$K_1 = C^\circ \frac{\bar{k}_1(D_0/\delta_0)(2\bar{k}_3 + D_R/\delta_R)}{\bar{k}_1(\bar{k}_3 + D_R/\delta_R) + (D_0/\delta_0)(\bar{k}_2 + \bar{k}_3 + D_R/\delta_R)} \qquad [9]$$

$$K_2 = C^\circ \frac{\bar{k}_4(D_0/\delta_0)(2\bar{k}_6 + D_R/\delta_R)}{\bar{k}_4(\bar{k}_6 + D_R/\delta_R) + (D_0/\delta_0)(\bar{k}_5 + \bar{k}_6 + D_R/\delta_R)} \qquad [10]$$

$$K_3 = C^\circ \frac{\bar{k}_7(D_0/\delta_0)(2\bar{k}_9 + D_R/\delta_R)}{\bar{k}_7(\bar{k}_9 + D_R/\delta_R) + (D_0/\delta_0)(\bar{k}_8 + \bar{k}_9 + D_R/\delta_R)} \qquad [11]$$

In these equations, C° is the concentration of cupric ions in the bulk of the solution, and D_0/δ_0 and D_R/δ_R are ratios of diffusion coefficient to thickness of Nernst diffusion layer for cupric ions and cuprous ion intermediates, respectively.

The pertinent adsorption equilibria are given by Eq. [12], [13], and [14].

$$OH^- + \text{aquo surface} \underset{\bar{k}_\beta}{\overset{\bar{k}_\alpha}{\rightleftharpoons}} \text{hydroxy surface} \qquad [12]$$

$$X + \text{aquo surface} \underset{\bar{k}_\delta}{\overset{\bar{k}_\gamma}{\rightleftharpoons}} \text{anionic surface} \qquad [13]$$

$$X + \text{hydroxy surface} \underset{\bar{k}_\alpha'}{\overset{\bar{k}_\gamma'}{\rightleftharpoons}} OH^- + \text{anionic surface} \qquad [14]$$

Since charge is transferred during adsorption or desorption of anions, it is necessary to use formal electrochemical rate constants to allow for the potential dependences of the several processes. Equation [14] represents an anion exchange process which is possible when more than one kind of anion is available for adsorption on the surface. In the cases of $X = SCN^-$ or Cl^-, this process probably is only slightly potential dependent since no net charge transfer is involved.

Equations relating the rate of change of hydroxy and anionic surface fractions to adsorption process rate constants and concentrations of OH^- and X in solution may be solved for θ, η, and $(1-\theta-\eta)$ at equilibrium. These are given by Eq. [15], [16], and [17].

$$\theta = (1/\Delta)\left\{(\bar{k}_\alpha/\bar{k}_\beta)[OH^-] + \bar{k}_\alpha'/\bar{k}_\delta[OH^-]\cdot\left[(\bar{k}_\alpha/\bar{k}_\beta)[OH^-] + (\bar{k}_\gamma/\bar{k}_\beta)[X]\right]\right\} \qquad [15]$$

$$\eta = (1/\Delta)\left\{(\bar{k}_\gamma/\bar{k}_\delta)[X] + (\bar{k}_\gamma'/\bar{k}_\beta)[X]\cdot\left[(\bar{k}_\alpha/\bar{k}_\delta)[OH^-] + (\bar{k}_\gamma/\bar{k}_\delta)[X]\right]\right\} \qquad [16]$$

$$1-\theta-\eta = (1/\Delta)\left\{1 + (\bar{k}_\alpha'/\bar{k}_\delta)[OH^-] + (\bar{k}_\gamma'/\bar{k}_\beta)[X]\right\} \qquad [17]$$

The denominator Δ which is common to all three equations is given explicitly by Eq. [18].

$$\Delta = 1 + (\bar{k}_\alpha/\bar{k}_\beta)[OH^-] + (\bar{k}_\gamma/\bar{k}_\delta)[X] + (\bar{k}_\alpha'/\bar{k}_\delta)[OH^-]\left[1 + (\bar{k}_\alpha/\bar{k}_\beta)[OH^-]\right] + (\bar{k}_\gamma'/\bar{k}_\beta)[X]\left[1 + (\bar{k}_\gamma/\bar{k}_\delta)[X]\right] + \left[(\bar{k}_\alpha\bar{k}_\gamma' + \bar{k}_\alpha'\bar{k}_\gamma)/\bar{k}_\beta\bar{k}_\delta\right][OH^-][X] \qquad [18]$$

Finally the equation for the over-all rate constant is obtained by combining Eq. [5], [9], [10], [11], [15], [16], [17], and [18] and dividing through by C° to give $\bar{k} \equiv j/\mathbf{F}C^\circ$.

The quantity Δ occurring in the denominators of Eq. [15], [16], and [17] is also the denominator of the general equation for $\bar{k}$. When the theoretical expression for $\bar{k}$ is put into the form of Eq. [1], we find that the equilibrium quotient γ takes the form of Eq. [19], provided [X] of Eq. [1] is taken to be the same as the added ion concentration [X] of Eq. [18], etc.[5]

$$\gamma = \frac{\dfrac{\bar{k}_\alpha[OH^-]}{\bar{k}_\beta[X]}\left(1 + \dfrac{\bar{k}_\alpha'}{\bar{k}_\delta}[OH^-]\right) + \dfrac{\bar{k}_\gamma}{\bar{k}_\delta} + \dfrac{\bar{k}_\gamma'}{\bar{k}_\beta}\left(1 + \dfrac{\bar{k}_\gamma}{\bar{k}_\delta}[X]\right) + \left(\dfrac{\bar{k}_\alpha\bar{k}_\gamma' + \bar{k}_\alpha'\bar{k}_\gamma}{\bar{k}_\beta\bar{k}_\delta}\right)[OH^-]}{1 + \dfrac{\bar{k}_\alpha'}{\bar{k}_\delta}[OH^-]} \qquad [19]$$

[5] [X] in Eq. [1] may be [Cl$^-$], [$SO_4^=$], [SCN$^-$], or [OH$^-$], while [X] of Eq. [18], etc., may be [Cl$^-$], [$SO_4^=$], or [SCN$^-$].

For certain special cases, γ becomes much simpler. If no anions other than OH^- are present, the equation for the over-all rate constant as a function of $[OH^-]$ possesses the form of Eq. [20].

$$\bar{k} = \frac{K_1 + K_2\bar{k}_a[OH^-]/\bar{k}_\beta}{C^o(1 + \bar{k}_a[OH^-]/\bar{k}_\beta)} \qquad [20]$$

γ for this special case is simply the ratio $\bar{k}_a/\bar{k}_\beta$, the equilibrium quotient for the adsorption reaction of Eq. [12]. On the other hand, the theoretical form of $\bar{k}$ for experiments performed in strong acid solution on the effect of X is given by Eq. [21].

$$\bar{k} = \frac{K_1 + K_3\bar{k}_\gamma[X]/\bar{k}_\delta}{C^o(1 + \bar{k}_\gamma[X]/\bar{k}_\delta)} \qquad [21]$$

Under these conditions γ is the simple ratio $\bar{k}_\gamma/\bar{k}_\delta$, which is the equilibrium quotient for the adsorption reaction of Eq. [13]. Evidently the complications of Eq. [19] arise when the exchange reaction of Eq. [14] is important.

Values of a quantity proportional to the equilibrium quotient for adsorption of OH^- on passive stainless steel are shown in Fig. 7 plotted against electrode potential. The quantity γ of Fig. 7 is related to $\bar{k}_a/\bar{k}_\beta$, the true adsorption quotient (cf. Eq. [20] and [12]), by Eq. [22].

$$\gamma = (\bar{k}_a/\bar{k}_\beta)K_w{}^c \qquad [22]$$

$K_w{}^c$ of Eq. [22] is the ion product of water ($K_w{}^c = [H^+]\,[OH^-]$) expressed in concentration units. Use of Eq. [22] is convenient since values of γ were determined by least-squares fits of Eq. [1] to experimental data with $[X] \equiv 1/[H^+]$.

The potential dependence of the equilibrium quotient $\bar{k}_a/\bar{k}_\beta$ is assumed to be given explicitly by Eq. [23], where $\Delta\phi_{ads}$ is the inner potential difference between the layer of specifically adsorbed hydroxide ions and the solution and λ is the absolute value of the charge on the adsorbed ions ($\lambda = 1$ for OH^- adsorption).

$$\bar{k}_a/\bar{k}_\beta = (k_a/k_\beta)\exp(+\lambda\mathbf{F}\Delta\phi_{ads}/RT) \qquad [23]$$

$\Delta\phi_{ads}$ may be assumed to vary with changes in the over-all inner potential difference between metal and solution, $\Delta\phi_T$, the latter being composed additively of the potential difference between metal and oxide layer, the potential drop across the passive film, the potential between the oxide layer and the position of the adsorbed ions, and the potential difference $\Delta\phi_{ads}$. Changes of the equilibrium quotient, $\bar{k}_a/\bar{k}_\beta$, with the over-all potential $\Delta\phi_T$ depend on the variation of the specific rate constants for adsorption and desorption steps of the reaction of Eq. [12] with $\Delta\phi_{ads}$, the latter being some fraction of $\Delta\phi_T$. Combination of Eq. [22] and [23] and differentiation with respect to $\Delta\phi_T$ leads to Eq. [24].

$$\frac{d\ln\gamma}{d\Delta\phi_T} = \frac{\lambda\mathbf{F}}{RT}\left(\frac{d\Delta\phi_{ads}}{d\Delta\phi_T}\right) \qquad [24]$$

The slope of the line in Fig. 7 is $+6.75 \times 10^{-3}$ (mv^{-1}) and $2.303\,RT/\mathbf{F} = 71$ mv at 85°C, so that $(d\Delta\phi_{ads}/d\Delta\phi_T) = 0.48$. On the basis of the stated assumptions, this result suggests that a change in $\Delta\phi_{ads}$, which affects adsorption processes, accounts for only approximately half of the total change in those components of the over-all interfacial potential difference ($\Delta\phi_T$) which change their values appreciably during polarization.

The temperature dependence of $\bar{k}_a/\bar{k}_\beta$, the equilibrium quotient for adsorption of OH^-, is shown in the Arrhenius-type plot of Fig. 8. Values of $\bar{k}_a/\bar{k}_\beta$ were computed from Eq. [22] using values of $K_w{}^c$ calculated according to the method given by Harned and Owen (14). The solid lines of Fig. 8 are least-squares fits of the data; in spite of scatter, which is expected because of the approximate nature of the model used, the slopes of the lines are roughly the same. Evaluation of the ratio k_a/k_β of Eq. [23] in terms of thermodynamic quantities leads to Eq. [25],

$$k_a/k_\beta = \exp(+\Delta S^\circ_{ads}/R)\exp(-\Delta H^\circ_{ads}/RT) \qquad [25]$$

where ΔS°_{ads} and ΔH°_{ads} are standard entropy and enthalpy of adsorption, respectively. Combination of

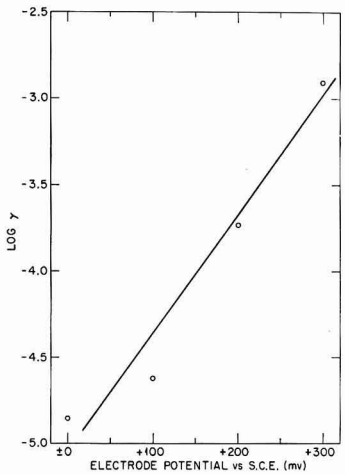

Fig. 7. Potential dependence of equilibrium quotient for adsorption of OH^- on passive stainless steel in 3 x $10^{-1}f$ $NaClO_4$ at 85°C. Potential vs. S.C.E. at room temperature.

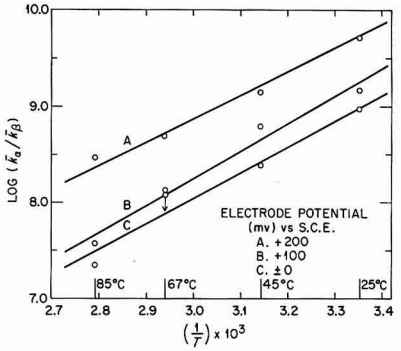

Fig. 8. Temperature dependence of equilibrium quotient for adsorption of OH^- on passive stainless steel in 3 x $10^{-1}f$ $NaClO_4$. Potential vs. S.C.E. at room temperature.

Eq. [23] and [25], followed by differentiation, leads to Eq. [26] relating the slope of the lines in Fig. 8 to the apparent standard enthalpy of the adsorption reaction (ΔH°_{app}).

$$\Delta H^\circ_{app} \equiv \Delta H^\circ_{ads} - \lambda \mathbf{F} \Delta\phi_{ads}$$
$$-(\lambda \mathbf{F}/T)[d\Delta\phi_{ads}/d(1/T)]_{\Delta\phi_T}$$
$$= -R[d \ln (\bar{k}_a/\bar{k}_\beta)/d(1/T)]_{\Delta\phi_T} \quad [26]$$

Use of Eq. [26] with the data of Fig. 8 leads to $\Delta H^\circ_{app} = -11.3$, -13.0, and -12.3 kcal/mole for curves A, B, and C, respectively. Therefore the adsorption reaction is exothermic. Using an average value of $\Delta H^\circ_{app} = -12.2$ (± 0.6) kcal/mole and neglecting the potential dependence of the apparent enthalpy of adsorption (cf. Eq. [26]), calculation of the standard entropy of the adsorption reaction from the data in Fig. 8 leads to $\Delta S^\circ_{ads} = +1.7$ (± 1.4) e.u. Instead of adsorption of OH^- onto an aquo surface as in Eq. [12], an alternative and electrochemically equivalent reaction scheme is given in Eq. [12′].

$$\text{aquo surface} + H_2O \rightleftharpoons \text{hydroxy surface} + H_3O^+ \quad [12']$$

The low value of standard entropy of adsorption calculated from these data is consistent with the mechanism of Eq. [12′], since proton transfer from an aquated surface probably involves less configurational entropy change than a process involving adsorption of hydroxide ion.

Results shown in Fig. 2 on the SCN^- *effect receive* qualitative explanation on the basis of Eq. [19]. For most choices of rate constants, the numerator of Eq. [19] essentially determines the effect of acidity, and γ increases with $[OH^-]$ as observed. Evidently SCN^- displaces adsorbed OH^- more readily than adsorbed H_2O, although information is needed on the relative magnitudes of the ratios $\bar{k}_\gamma/\bar{k}_\delta$ and $\bar{k}_\gamma'/\bar{k}_a'$, the equilibrium quotients of the reactions in Eq. [13] and [14], before definite conclusions can be made. As seen in Fig. 3, the opposite situation appears to hold with $SO_4^=$ higher $[SO^=_4]$ being required to produce a significant change in rate constant at low acidity than at high acidity.

Under certain conditions, the over-all rate constant $\bar{k}$ varies with added ion concentration [X] in the manner shown in curve E of Fig. 6. Analysis of the theoretical model shows that this behavior is possible provided the association quotients of Eq. [12], [13], and [14] have appropriate values. Specifically, these quotients must satisfy the inequality of Eq. [27].

$$\left(\frac{\bar{k}_\gamma}{k_\delta} - \frac{\bar{k}_a}{k_\beta} \cdot \frac{\bar{k}_\gamma'}{k_a'}\right) << 0 \quad [27]$$

The left-hand side of Eq. [27] must be sufficiently negative to compensate for positive terms appearing in the equation for the slope of a plot of over-all rate constant against added ion concentration. Mechanistically, the ratio of aquo to hydroxy surface increases to a maximum at low added ion concentrations before decreasing at higher [X] because of the peculiarities of the mixed isotherm when the echanism of Eq. [14] is important. Since $K_1 << K_2 < K_3$ in the present system ($[X] = [Cl^-]$), the over-all rate constant goes through a minimum with increasing [X]. Analysis further shows that no minimum should be observed at very high or very low acidity, and this is in accord with experimental observation.

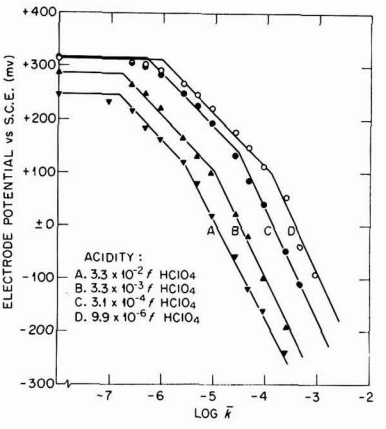

Fig. 9. Effect of acidity on polarization curves for reduction of Cu^{++} on passive stainless steel in 3 x 10^{-1}f $NaClO_4$; 67°C, helium atmosphere. Potential vs. S.C.E. at room temperature.

Polarization curves for the reduction of Cu^{++} on stainless steel in perchlorate medium are similar to those observed previously (10) in dilute sulfuric acid solution. A typical set of curves is shown in Fig. 9; closely analogous results were obtained from galvanostatic measurements at other temperatures. The change of slope of the polarization curves results from a change with potential of the rate-determining step in the mechanisms of Eq. [2] and [3]. Examination of Eq. [9] shows that, neglecting diffusion ($D_o/\delta_o >> \bar{k}_1$ and $D_R/\delta_R << \bar{k}_2 + \bar{k}_3$), the rate of reduction of Cu^{++} on the aquo surface reduces to the form of Eq. [28].

$$K_1 = C^\circ 2\bar{k}_1\bar{k}_3/(\bar{k}_2 + \bar{k}_3) \quad [28]$$

At low potentials $\bar{k}_3 >> \bar{k}_2$ and K_1 is proportional to $\bar{k}_1$, the rate constant for the reduction of Cu^{++} to the cuprous intermediate. At high potentials, $\bar{k}_2 >> \bar{k}_3$ and K_1 becomes proportional to $\bar{k}_1\bar{k}_3/\bar{k}_2$, implying that in this potential region there is virtual equilibrium between cupric and cuprous species and that reduction of the cuprous intermediate is rate determining. *Rate control by diffusion (plus convection in stirred* solution) becomes important at potentials more negative than those shown in Fig. 9. The results of Fig. 9 show that the transition between high and low potential regions of the polarization curve is essentially independent of acidity. Since the transition occurs when $\bar{k}_2 = \bar{k}_3$, this observation supports the assumption implicit in the derivation of the isotherm that the rate constants of the charge transfer steps in the mechanisms of Eq. [2], [3], and [4] are independent of acidity. When plotted as a function of temperature at constant acidity, polarization curves show that the potential of the transition region increases with temperature, implying different ener-

getics for the alternative modes of decomposition of the cuprous intermediate.

Values of differential capacity for the present system were estimated by analysis of recordings of the initial potential-time transients observed during the establishment of new steady states in galvanostatic measurements. Although this manual procedure is inexact, reasonably reproducible numbers were obtained. In units of microfarads/cm^2, the capacity of the interface was 35 to 40 at +300 mv *vs* SCE., 40 to 50 at +200 mv, 60 to 80 at +100 mv, 90 to 120 at ±0 mv, and 110 to 160 at −100 mv. Slight increases of capacity with temperature were observed, the range of values in the above listing corresponding to measurements at 25° and 85°C. Values of capacity were found to be independent of the current density of the Cu^{++} reduction reaction at the oxide-solution interface. A slight acidity effect was detected; values of capacity increased with acidity at constant potential, but in no case did the capacity change by more than a factor of two over the acidity range, 10^{-5} to 10^{-2} *f* $HClO_4$. Capacities were also essentially independent of added anion concentration, so that measurements of capacity in the present system did not appear to include a contribution from the reaction capacity of the adsorption processes. The foregoing observations allow the speculation that the capacity of the interface is determined largely by the properties of the passive oxide; *i.e.*, the smallest capacity in the interfacial system depends on the thickness and the charge distribution within and on each side of the oxide layer.

We conclude from the evidence presented that the rates of reduction reactions on passive stainless steel are sensitive to specific adsorption of anions from solution. To a good approximation this specific adsorption follows a potential-dependent Langmuir isotherm. Analysis of data on the adsorption of hydroxide ion yields results in good agreement with theory, thus permitting calculation of the energetics of the adsorption reaction. Adsorption of anions other than hydroxide follows a similar, although much more complex isotherm, the properties of which allow qualitative interpretation of salient observations. Similar anion effects undoubtedly occur for other reduction reactions and in other passive systems, for which the foregoing analysis may also prove to be useful.

Acknowledgment

The authors wish to express appreciation to their colleagues, Dr. G. H. Cartledge and Dr. R. E. Meyer, for stimulation and encouragement during the course of this work.

Manuscript received Dec. 6, 1961; revised manuscript received March 5, 1962. This paper was prepared for presentation at the Los Angeles Meeting, May 6-10, 1962.

Any discussion of this paper will appear in a Discussion Section to be published in the June 1963 JOURNAL.

REFERENCES

1. H. Gerischer, *Z. Elektrochem.*, **54**, 366 (1950).
2. J. M. Kolotrykin, *This Journal*, **108**, 209 (1961).
3. K. E. Heusler and G. H. Cartledge, *ibid.*, **108**, 732 (1961).
4. J. Heyrovsky, *Discussions Faraday Soc.*, **1**, 212 (1947).
5. A. N. Frumkin, *Uspekhi Khim.*, **24**, 933 (1955).
6. A. N. Frumkin, *Trudy 4-go Soveshchaniya Po Elektrokhimii, Moscow, 1956*; trans. Consultants Bureau, N. Y., 1961, p. 39.
7. R. Piontelli, *Compt. rend. C.I.T.C.E.*, **2**, 185 (1950).
8. R. Brdicka, *Chem. Listy*, **38**, 252 (1944).
9. R. F. Sympson and G. H. Cartledge, *J. Phys. Chem.*, **60**, 1037 (1956).
10. F. A. Posey, G. H. Cartledge, and R. P. Yaffe, *This Journal*, **106**, 582 (1959).
11. R. F. Sympson and F. A. Posey, "Chem. Div. Ann. Prog. Rept. June 20, 1959," ORNL-2782, p. 57.
12. R. F. Sympson and F. A. Posey, "Chem. Div. Ann. Prog. Rept. June 20, 1960," ORNL-2983, p. 54.
13. R. H. Fowler and E. A. Guggenheim, "Statistical Thermodynamics," p. 426, Cambridge (1952).
14. H. S. Harned and B. B. Owen, "The Physical Chemistry of Electrolytic Solutions," p. 643, Reinhold Publishing Co., New York (1958).

A Solid Electrolyte Fuel Cell

J. Weissbart and R. Ruka

Chemistry Department, Research Laboratories, Westinghouse Electric Corporation, Pittsburgh, Pennsylvania

ABSTRACT

A high-temperature oxide electrolyte galvanic cell of the type H_2/H_2O, Pt || $(ZrO_2)_{0.85}(CaO)_{0.15}$ || Pt, O_2 is described. Experimental data for reaction of oxygen with hydrogen-water and methane-water mixtures are given. Open-circuit voltages for the hydrogen-oxygen reaction are close to theoretical, and current-voltage curves show that the output of the cell is limited essentially by the resistance of the electrolyte. The data suggest that solid oxide electrolyte cells of this general type may offer attractive possibilities as fuel cells for utilizing hydrocarbons as fuel and oxygen or air as oxidant.

High-temperature galvanic cells with solid oxygen ion conducting electrolytes have features which may make them attractive as fuel cells. Catalytic problems are reduced at high temperatures, and a mechanically stable electrode-electrolyte interface is possible with an all-solid construction.

Schottky (1) discussed the problem of solid electrolytes from the theoretical point of view in 1935 and two years later Baur and Preis (2) constructed the first solid oxide-electrolyte fuel cell. The electrolyte was in the form of a ceramic tube of $(ZrO_2)_{0.85}(Y_2O_3)_{0.15}$, a material which Nernst had previously

shown to possess a relatively high ionic conductivity. The tube was filled with coke to form the anode and surrounded with iron oxide in an air atmosphere to form the cathode. An output of less than 1 ma/cm^2 of electrolyte area at 1050°C and 0.65v was obtained and it was concluded that sufficient cation conductivity[1] was occurring to damage the cell.

A number of researches have contributed information on the physical and chemical properties of ceramics with high oxygen ion mobility. Nernst (3) observed qualitatively the electrolytic evolution of oxygen from a rod of $(ZrO_2)_{0.85}$ $(Y_2O_3)_{0.15}$ (Nernst glower). More recently Weininger and Zemany (4) made a quantitative measurement of the electrolytic evolution of oxygen from a Nernst glower of similar composition and found that 7-80% of the current could be accounted for by ionic conduction, depending on temperature, current flow, and previous history of the material.

Wagner (5) proposed in 1943 that oxide solid solutions such as $(ZrO_2)_{1-x}$ $(CaO)_x$ or $(ZrO_2)_{1-x}$ $(Y_2O_3)_x$ contain vacant oxygen ion sites, one vacancy occurring for each Ca^{+2} or two Y^{+3} ions that substitute for Zr^{+4} ions in the fluorite-type crystal structure. He assumed that this would lead to high oxygen ion conductivity. Hund (6) determined the density of these oxides by x-ray and pycnometric methods. The data are consistent with the oxygen ion vacancy model.

Kingery (7) and co-workers calculated the oxygen ion mobility in $(ZrO_2)_{0.85}$ $(CaO)_{0.15}$ from the Nernst-Einstein relation[2] and the diffusion coefficient obtained from measurements of the rate of exchange of oxygen in the oxide with O^{18}. Comparing this data with measurements of electrical conductivity of the oxide they concluded that the conductivity is wholly ionic and that the transference number is near unity for the oxygen ion.

Kiukkola and Wagner (8) and several other authors have obtained high temperature thermodynamic data using galvanic cells with electrolytes of zirconia of thoria containing CaO, Y_2O_3, La_2O_3, and other oxides.

Weissbart and Ruka (9, 10) have constructed vacuum tight cells of the type

$$O_2\ (p_1), Pt \mid\mid (ZrO_2)_{0.85}(CaO)_{0.15} \mid\mid Pt, O_2(p_2)$$

in which the electrode reactions at temperatures above 600°C were shown to correspond closely to the reversible reaction

$$O_2 + 4e^- \rightleftharpoons 2\,O^= \qquad [1]$$

The voltages obtained are in good agreement with the theoretical emf E calculated from the thermodynamic relationship for reversible transfer of oxygen from cathode to anode at the given pressures.

$$E = \frac{RT}{4F} \ln \frac{P_{O_2}\ (\text{cathode})}{P_{O_2}\ (\text{anode})} \qquad [2]$$

This shows that the cells act as oxygen concentration cells.

[1] Cation conductivity is undesirable since it results in transfer of electrolyte from anode to cathode of the galvanic cell. This would damage the electrode-electrolyte interfaces.

[2] $D_i = B_i kT$ where D_i is the self-diffusion coefficient and B_i is the absolute mobility of the i-th species.

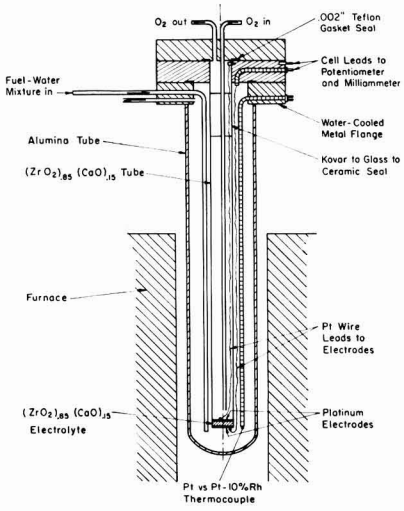

Fig. 1. Schematic diagram of galvanic cell with solid oxide electrolyte.

Faraday's laws were found to be obeyed closely for current flow through a cell of this type as determined by microweighing of the oxygen transferred. The electronic contribution to the total conductivity was found to be less than 0.5% near 1000°C in an oxygen atmosphere.

Experimental

The construction of the galvanic cell is illustrated schematically in Fig. 1. It is similar to that previously described (9) except that it is arranged to flow gases past both electrodes.

The essential elements of the cell are the flat bottom portion of the $(ZrO_2)_{0.85}(CaO)_{0.15}$ tube, which acts as the electrolyte, and two porous platinum electrodes (9) of less than 0.001 in. thickness. Cell dimensions were of the order of 2.5 cm^2 area and 0.15 cm thickness. For these cells contact resistances of the order of 1-2 ohms were encountered depending on the thickness of the porous platinum films.

For all experiments pure oxygen at atmospheric pressure flowed slowly past the cathode, and the various water-hydrogen or water-methane mixtures flowed at a faster rate through the anode chamber. The experimental arrangement of the cell is designed for current-voltage measurements rather than for optimum conversion of fuel. An appreciable fraction of the total gas flowing through the anode chamber does not come in contact with the electrode. Consequently a high flow rate of gas was used to minimize concentration polarization and thermal diffusion effects. The volume of preheated gas flowing per minute into the anode chamber was about 3.7 times the volume of the chamber. For a decrease in flow rate to one-third of this value the temperature of a thermocouple placed near the anode changed less than 1°C.

The hydrogen or methane was first passed through water bubblers and the effluent gas from the anode chamber was analyzed for H_2, H_2O, CO, CO_2, and

CH_4. Calculations of the theoretical emf for the experiments are based on these analyses.

Results and Discussion

When current is drawn from a galvanic cell the voltage may be lower than the open-circuit value due to (*a*) activation polarization, (*b*) concentration polarization, (*c*) ohmic resistance of the cell. The voltage drop due to each of these is a function of the current density. (*a*) depends on the particular rate-determining chemical and electrochemical reactions at the electrodes, (*b*) involves mass transfer of reactants and products, and (*c*) ordinarily depends largely on electrolyte resistance.

Activation polarization is frequently encountered in low temperature cells, and significant reaction of hydrocarbons at the fuel electrode is particularly difficult to attain. In addition, the oxygen electrode reaction proceeds by a peroxide mechanism which even in the presence of peroxide decomposing catalysts results, according to Kordesch (11), in a lower voltage than the ideal oxygen electrode value.

At higher temperatures the mechanism at the oxygen electrode is different. Thus the peroxide reaction is not detected in a fused carbonate cell which has been shown to act as an oxygen-carbon dioxide concentration cell by Chambers and Tantram (12).

The present solid oxide cell involves even less complicated electrode reactions since it acts as a simple oxygen concentration cell (9). If hydrogen is present at the anode, we write the cell diagrammatically as

$$H_2/H_2O, Pt \,||\, (ZrO_2)_{0.85}(CaO)_{0.15} \,||\, Pt, O_2$$

The emf E is given by the standard thermodynamic relation

$$E = E^{\circ} + \frac{RT}{4\mathbf{F}} \ln P_{O_2}\ (\text{cathode}) + \frac{RT}{2\mathbf{F}} \ln \frac{P_{H_2}}{P_{H_2O}}\ (\text{anode}) \qquad [3]$$

Figure 2 shows a comparison of experimental and theoretical open-circuit voltage values *vs.* the $H_2/(H_2 + H_2O)$ ratio for a constant oxygen pressure at the cathode. The theoretical curve is calculated from Eq. [3]. The experimental points are based on the measured emf and the analytically determined $H_2/(H_2 + H_2O)$ mole ratio. Agreement is within 5 mv of the theoretical value. This is within the error of the H_2 and H_2O analyses.

Figure 3 shows current-voltage curves for the hydrogen-oxygen reaction in the cell at four temperatures at approximately constant $H_2/(H_2 + H_2O)$ ratios and oxygen pressure. The curves are all straight lines with slopes $\Delta E/\Delta I$ agreeing within 5% of the values of resistance determined directly by 1000 cycle a-c resistance measurements. Figure 4 shows further current-voltage curves at two temperatures for two different water-hydrogen ratios. The two sets of parallel lines indicate that the d-c resistance was the same at the same temperature. Although the internal resistance of a cell stayed nearly constant during measurements of individual current-voltage curves, variations in either direction were found over longer periods of time, even

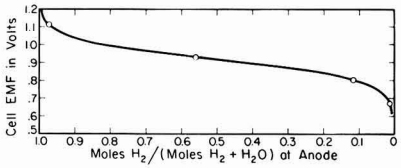

Fig. 2. Comparison of measured voltage with theoretical emf of cell,

O_2, Pt||$(ZrO)_{0.85}$ $(CaO)_{0.15}$||Pt, H_2/H_2O

------ Theoretical line; ○ experimental point; temperature 1015°C, O_2 pressure at cathode 731.2 mm.

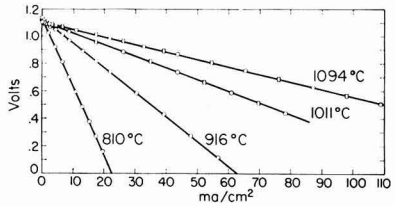

Fig. 3. Current-voltage behavior of cell,

O_2, Pt||$(ZrO_2)_{0.85}$ $(CaO)_{0.15}$||Pt, H_2/H_2O

at O_2 pressure ≅ 730 mm and $H_2/(H_2+H_2O)$ ≅ 0.973 for four temperatures. ○ Increasing current; □ decreasing current.

on open circuit. Open-circuit voltages were reproducible to about 1 mv in duplicate runs, independent of this effect, while the slopes of the current-voltage curves changed in accordance with the measured resistance changes. According to Dietzel and Tober (13) the lower temperature limit for existence of the fluorite phase in the zirconium-calcium mixed oxide lies in the neighborhood of 850°C, but phase boundaries are very uncertain since equilibrium was not attained over a wide temperature range. This suggests that resistance changes under open-circuit conditions encountered in the present work could possibly be associated with slow phase changes occurring as a function of temperature, composition and homogeneity of the mixed oxide.

Figure 5 shows the current-voltage curve obtained for a mixture of 3.8% methane, 2.1% water and 94.1% N_2 as fuel. The rate of fuel flow was sufficiently rapid that chemical equilibrium was not attained for the reforming reaction and 80% of the methane remained undecomposed by passage through the cell. The open-circuit voltage of 0.945v

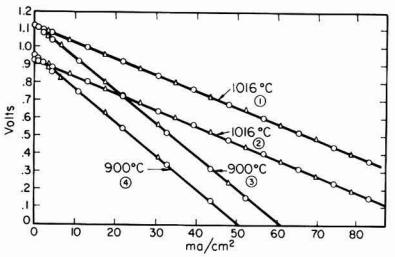

Fig. 4. Current-voltage behavior of the cell,

O_2, Pt||$(ZrO_2)_{0.85}$ $(CaO)_{0.15}$||Pt, H_2/H_2O

at two temperatures for two H_2/H_2O ratios. ○ Increasing current; △ decreasing current; O_2 pressure ≅ 731 mm. $H_2/(H_2+H_2O)$ ≅ 0.97 for curves 1 and 3; $H_2/(H_2 + H_2O)$ ≅ 0.54 for curves 2 and 4.

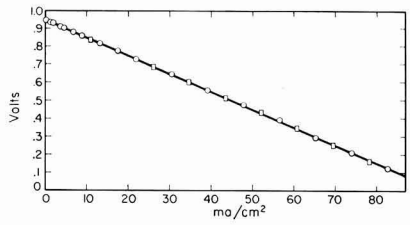

Fig. 5. Current-voltage behavior of the cell, O_2, Pt||$(ZrO_2)_{0.85}$ $(CaO)_{0.15}$||Pt, CH_4/H_2O
Composition of inlet fuel gas: CH_4 3.8%, H_2O 2.1%, N_2 94.1%; temperature 1015°C. ○ Increasing current; □ decreasing current; O_2 pressure 731 mm.

is within 5 mv of the value calculated for the simple hydrogen-oxide reaction and approximately 50 mv lower than the value for the carbon monoxide-oxygen reaction. The calculations are based on the H_2/H_2O and CO/CO_2 ratios in the effluent gas from the anode chamber and the known oxygen pressure at the cathode. At slower flow rates a higher percentage of methane was converted, probably largely by the reforming reaction $CH_4 + H_2O \rightarrow CO + 3H_2$. This results in higher H_2/H_2O and CO/CO_2 ratios and thus higher open-circuit voltages. The data indicate that the major electrochemical reactions probably involve the reformed gases, H_2 and CO rather than CH_4. The moles of CH_4 and H_2O decomposed is consistent with the CO, CO_2, and H_2 formed as determined from the analysis of the exit gases. This shows that carbon formation did not occur within the cell. However, analysis of exit gases indicated that carbon formation did occur in some other experiments at similar low H_2O/CH_4 ratios.

The ultimate life expectancy of the cell under optimum conditions has not been determined, although an individual cell of this type using a 30 to 1 H_2/H_2O mixture as fuel has been operated continuously at 10 ma/cm² of electrolyte area for two months at temperatures between 1000° and 1200°C. Some platinum loss from electrodes by evaporation, possibly as an oxide, occurs at these temperatures.

The current-voltage data indicate that the cell has an output for the hydrogen-oxygen reaction which is essentially resistance limited and thus should be capable of higher output by simply decreasing the thickness of the electrolyte, provided contact resistances are low.

The studies necessary to improve the cell include investigations of the cation conductivity and phase stability of the electrolyte, the electrode structure, properties of thin films of the electrolyte and substitution of other electrodes and electrolytes.

Acknowledgment

The authors wish to thank W. Hickam and coworkers for the mass spectrometric analyses of the gas samples. Helpful discussions were held with Y.L. Sandler and S. Barnartt.

Manuscript received Nov. 6, 1961. This paper was prepared for delivery before the Los Angeles Meeting, Oct. 6-10, 1962.

Any discussion of this paper will appear in a Discussion Section to be published in the June 1963 JOURNAL.

REFERENCES

1. W. Schottky, Wiss. *Veröffentl. Siemens-Werken*, **14**, 1 (1935).
2. E. Baur and H. Preis, *Z. Elektrochem.*, **43**, 727 (1937).
3. W. Nernst, *ibid.*, **6**, 41 (1900).
4. J. L. Weininger and P. D. Zemany, *J. Chem. Phys.* **22**, 1469 (1954).
5. C. Wagner, *Naturwissenschaften*, **31**, 265 (1943).
6. F. Hund, *Z. physik. Chem.*, **199**, 142 (1952).
7. W. D. Kingery, J. Pappis, M. E. Doty, and D. C. Hill, *J. Am. Chem. Soc.*, **42**, 394 (1959).
8. K. Kiukkola and C. Wagner, *This Journal*, **104**, 379 (1957).
9. J. Weissbart and R. Ruka, *Rev. Sci. Instr.*, **32**, 593 (1961).
10. J. Weissbart and R. Ruka, Paper presented at the Electrochemical Society Fall Meeting, Detroit, Mich. (Oct. 2-5, 1961) (Extended Abstract No. 44, Battery Division).
11. K. Kordesch, *Ind. Eng. Chem.*, **52**, 296 (1960).
12. H. H. Chambers and A. D. S. Tantram, *ibid.*, **52**, 295 (1960).
13. A. Dietzel and H. Tober, *Ber. deut. keram. Ges.*, **30**, 47 (1953).

Studies of the Electrochemical Kinetics of Indium

I. Kinetics of Deposition and Dissolution in the Indium + Indium Sulfate System

B. Lovrecek and V. Markovac

Institute of Electrochemistry and Electrochemical Technology, Faculty of Technology, University of Zagreb, Zagreb, Yugoslavia

ABSTRACT

The kinetics of the deposition and dissolution of indium (from indium amalgam) in indium sulfate solutions at *p*H 2.5 have been studied by observing variations of overpotential during individual constant current pulses. The electrode was in the form of a hanging drop of the amalgam, which was renewed for each pulse. The steady-state activation overpotential was reached approximately 1 msec after application of the pulse, which corresponds to a mean value of double layer capacity of 25.4 μF/cm^2. Plots of the activation overpotential *vs.* log current density show good Tafel relations in both the cathodic and anodic regions. Analysis of these data shows the mechanism to consist of three consecutive electron transfer steps

$$In^{3+} \underset{e^-_0}{\overset{+e^-_0}{\rightleftarrows}} In^{2+} \underset{e^-_0}{\overset{+e^-_0}{\rightleftarrows}} In^{1+} \underset{e^-_0}{\overset{+e^-_0}{\rightleftarrows}} In^0$$

The rate-determining step for both anodic and cathodic polarization is

$$In^{3+} \underset{e^-_0}{\overset{+e^-_0}{\rightleftarrows}} In^{2+}$$

for which the transfer coefficient α was determined to be approximately 0.83.

The mechanism of electrochemical deposition and dissolution of metals, because of its great theoretical and practical importance, has been the subject of numerous studies and discussions. This paper deals with the mechanism of deposition and dissolution of indium, in which studies methods similar to those used by Gerischer (1), Berzins and Delahay (2), and Mattsson and Bockris (3) have been applied. Kangro and Weingärtner (4), and Duić, Kovac, and Lovrecek (5) have already established that the deposition of indium(III)-ion and the dissolution of metallic indium, respectively, follow in a "many step" electrode process over an ion of lower valency, but have not determined either the electrochemical step in question or the rate-determining step. The kinetics of the system have been studied[1] on basis of theoretical expressions for the kinetics of "many step" electrode reactions (6), with due consideration to possible reaction steps in the electrochemical deposition and dissolution of indium.

Experimental

Apparatus.—The apparatus (Fig. 1) comprised an electrolytical cell with nitrogen purification unit and electrical device.

The electrolytic cell resembles those used earlier (1, 2) and comprises a main compartment and a reference electrode compartment. The main compartment is shaped like a vessel with a cap through which a carrier for measuring electrode, a capillary with an amalgam reservoir on the top, a spoon for catching of the amalgam drops, and a bubbler are fixed. The carrier is a glass tube with a thin platinum wire sealed into the top. After sealing the wire was cut level with the glass and electrolytically gold-plated. The measuring electrode is a hanging drop of amalgam, of determined surface area, on which the polarization takes place. The carrier for the measuring electrode passes through the center of the cap into the cell following its vertical axis. The capillary resembles those used in polarography. The capillary with reservoir is connected to the mercury pressure system by means of a tygon tube. The pressure system regulates the pressure in the reservoir and thus regulates the rate of dropping through the capillary. The spoon for catching drops

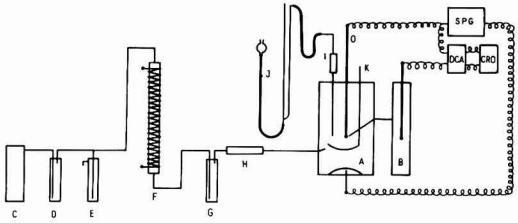

Fig. 1. Schematic diagram of apparatus: A, main compartment of electrolytic cell; B, reference electrode compartment; C, nitrogen tank; D, washing bottle; E, mercury security valve; F, electric furnace with active copper; G, washing bottle; H, drop collector containing glass wool; I, capillary with amalgam reservoir; J, pressure system; K, glass spoon; SPG, square pulse generator; DCA, direct current amplifier; CRO, cathode-ray oscilloscope; O, hanging drop electrode; P, reference electrode (S.C.E.).

[1] Further experiments with this system and description of details of the apparatus and procedure will be found in the Ph.D. thesis of V. Markovac.

is fastened by its handle to the cap by a cylindrical ground glass joint and revolves freely in the direction and around its vertical axis. It catches the drop of amalgam from under the capillary and hangs it on the tip of the carrier.

The main compartment of the cell has in its side a tube for the introduction of nitrogen, which is introduced before the electrolysis so as to remove the dissolved oxygen from the electrolyte, and immediately proceeding each measurement, to level the concentration. In the opposite side of the main compartment of the cell an electrolytical bridge is built in, connecting this compartment with the reference electrode compartment. The electrolytical bridge is executed so that one end enters the main compartment of the cell approximating the form of a capillary to the hanging drop of the measuring electrode (distance of 3 mm). At the bottom of the cell there is a quantity of amalgam of the same composition as the hanging drop, *i.e.*, the measuring electrode. This quantity of amalgam is continually increased by the drops discharged from the carrier of measuring electrode. In the reference electrode compartment there is a standard saturated calomel electrode in the electrolyte of the same composition as that in the main compartment of the cell. During the pre-electrolysis, a platinum electrode is put into this compartment to serve as an anode instead of the calomel electrode.

Before the electrolysis and immediately proceeding each measurement, purified nitrogen is forced through the cell and the electrolyte. The ordinary tank nitrogen is purified (oxygen removed) in the manner introduced by Meyer and Ronge (7), by forcing the gas through a column filled with active copper, spread on the infusorial earth. The column is heated to 200°C by an electric heater in the sheath around the column. The electrolytic cell and purification units are made of Pyrex glass. All joint and stopcocks are made in the ground glass technique and sealed with distilled water.

The electrical device (Fig. 2) has three main components: a square-wave pulse generator SPG, a direct current amplifier DCA, and a cathode-ray oscilloscope CRO.

A relay RE built into the generator synchronizes the beginning of the square-wave pulse and the time

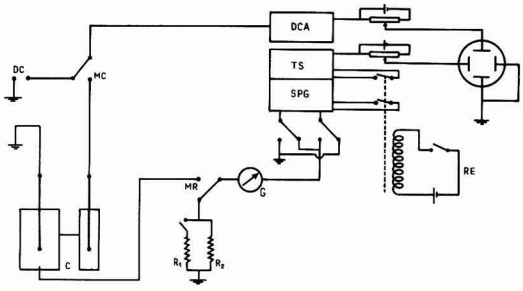

Fig. 2. Schematic diagram of electrical arrangement: RE, relay; SPG, square pulse generator; TS, time sweep; DCA, direct current amplifier; CRO, cathode-ray oscilloscope; AC, switch anodic-cathodic polarization; G, galvanometer; MR, switch measurement regulation; R_1 and R_2, resistors (5.6 KΩ and 56Ω); MC, switch measurement-calibration; DC, calibration device; C, electrolytical cell.

sweep TS, so that the time sweep begins a little earlier, for safety's sake. The time sweep, built into the generator, regulates the recording time in a 0.3 msec to 3 sec range. The square-wave pulse is electronically stabilized by means of a penthode, so that changes in the resistance of the cell do not influence the constant current of a pulse. Pulses obtained cover the range of 2.0×10^{-6}-8.0×10^{-3} amp. The switch AC serves to change the direction of the pulse current. Before the measurement the selected current is read on the galvanometer G by passing the current through a combination of resistors R_1 and R_2, instead of through the cell. The rise time of a pulse is less than 10 μsec.

The direct current amplifier DCA is constructed to let pass a 10 MHz span of frequencies, which makes possible the observation of pulses with rise time up to 1 μsec. The factor of amplification is up to 1.700. The switch MC and a device DC serve for the calibration of the amplifier.

Procedure.—Before the experiments the glass apparatus was washed in chrom-sulfuric acid (16 hr), washed out in running water, and then washed in distilled water (16 hr).

The composition of the electrolyte used was $0.116N$ $In_2(SO_4)_3$ in $0.5N$ K_2SO_4, $pH = 2.5$ solution. The electrolyte was prepared by the dissolution of a wire of very pure indium[2] in the calculated amount of H_2SO_4 with regard to indium sulfate and potassium sulfate. Once the dissolution was completed the corresponding amount of KOH solution was added successively until a certain pH value was reached. Chemicals used were of the analytical reagent grade.

As the measuring electrode a hanging drop of 0.3% by weight In-amalgam was used. In-amalgam in such concentrations has the physical properties of liquids (8). It is prepared in the reservoir of the capillary, covered by electrolyte in the stream of nitrogen. The rate of dropping is regulated by the change of pressure of nitrogen in the pressure system. The presence of nitrogen eliminates the possibility of oxidation of In-amalgam (9). The size of the drop in the electrolyte depends on the diameter of the capillary. It was determined by weighing a number of drops, and from the weight the surface of a drop was set at 2.78×10^{-2} cm².

The electrolyte is in the main compartment of the cell and in the reference electrode compartment. Before the experiments purified nitrogen is forced through the cell (12 hr). Pre-electrolysis with the current of 0.32 ma is undertaken as a last purification step (10 hr). The mass of amalgam on the bottom of the main compartment of the cell serves as a cathode. A platinum electrode in the reference electrode compartment serves as an anode.

Single d-c square-wave pulses of selected intensity pass through the hanging drop as the measuring electrode and the amalgam mass as the counter electrode. Resulting overpotential changes are recorded in relation to the reference electrode (S.C.E.) over the d-c amplifier, on the screen of the

[2] For the preparation of electrolyte and In-amalgam a wire with the guaranteed minimum purity of 99.95% of indium was used (Dr. E. Durrwächter, DODUGO K.G. Pforzheim, West Germany).

cathode-ray oscilloscope as the overpotential-time ($\eta_t - t$) curves. The duration of pulses and the degree of amplification is suited to the intensity of current so that the overpotential can reach a constant value before the concentration polarization sets in. Measurements were made from low current densities to higher ones. For each pulse a new drop of amalgam was used. All the cathodic transients were taken first and then the anodic ones, covering the current density range of 8.1×10^{-5} to 2.1×10^{-1} amp/cm^2.

The overpotential-time curves on the screen of the cathode-ray oscilloscope were photographed on Ilford-HPS 6 x 9 cm film with a Rolleicord camera.

Results

Overpotential-time relationship.—An example of experimentally obtained $\eta_t - t$ curve for anodic polarization is shown in Fig. 3. The ohmic overpotential η_Ω is represented by the gap at the initial part of the curve, as has already been done by other authors (3, 10). In cathodic curves the part of the ohmic overpotential is very small in relation to the total overpotential η_t, which is not the case in anodic $\eta_t - t$ curves, so it is very difficult to obtain exact and precise values by experimentation. To obtain the values, the sensitivity of the measuring device was increased and only the initial part of the $\eta_t - t$ curve was recorded, regardless of the fact

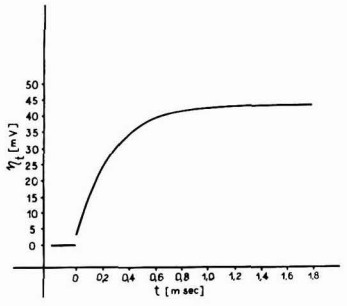

Fig. 3. Curve $\eta_t - t$ for anodic current density 3.6×10^{-3} amp/cm^2.

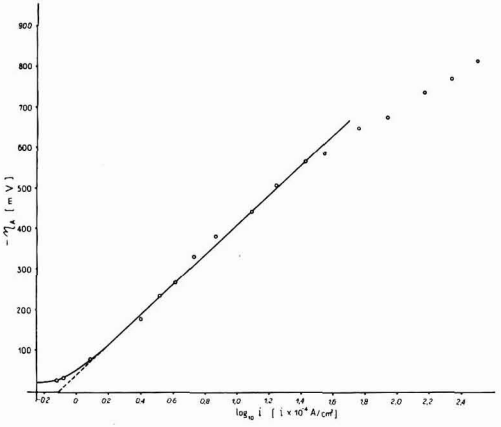

Fig. 4. Tafel line for cathodic polarization, $\alpha = 0.844$

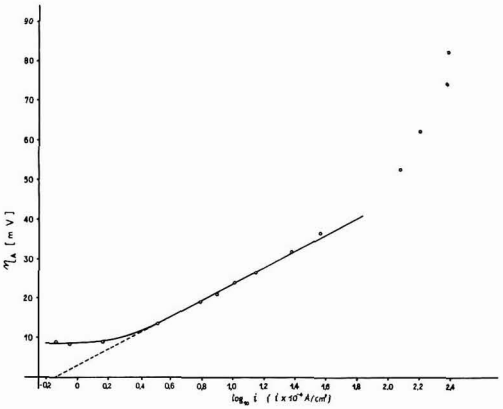

Fig. 5. Tafel line for anodic polarization, $\alpha = 0.800$

that overpotential did not build up to its steady-state value.

The change of potential, minus the ohmic overpotential, until the building up to the steady-state value, represents activation overpotential η_A.

The linear part of the curve $\eta_t - t$ (Fig. 3) corresponds to the charging of double layer, and from the slope of this part of the curve the double-layer capacity can be calculated (11).

$$C = i \left(\frac{dt}{d\eta} \right)_{t \to 0} \qquad [1]$$

The mean value, obtained from the experimental data, is 25.4 μF/cm^2.

Activation overpotential-current density relationship.—When the experimental values of activation overpotential η_A were plotted against the logarithm of c.d. $\log_{10} i$, curves obtained of cathodic and anodic polarization (Fig. 4, 5) show in one region Tafel's linear relation.

Further, experimental Tafel lines were treated with an earlier developed method (6) using expression for the slowest reaction step, *i.e.*, rate-determining step.

$$\frac{\partial \log i_-}{\partial V} = -\frac{\mathbf{F}}{2{,}303\,RT}(n_c^* - \alpha) \qquad [2]$$

$$\frac{\partial \log i_+}{\partial V} = \frac{\mathbf{F}}{2{,}303\,RT}(n_a^* - 1 + \alpha) \qquad [3]$$

i_- and i_+ being parts of the total cathodic and anodic c.d. used in the slowest reaction step, ∂V the change of potential, n_c^* and n_a^* the ordinal numbers of the slowest reaction step for the cathodic and anodic polarization (small integer), α the transfer coefficient ($0 < \alpha < 1$), $\mathbf{F}$ the Faraday, R the gas constant, and T the absolute temperature.

As mentioned earlier (6) the left sides of the Eq. [2] and [3] represent the slopes of the experimental Tafel lines, so out of the experimental data it was possible to obtain α, n_c^*, and n_a^*.

The calculations indicate that the slowest reaction step for the cathodic polarization is the first, and for the anodic the third; for results see Table I.

Table I. Parameters for the deposition and dissolution of indium in 0.116*N* $In_2(SO_4)_3$ + 0.5*N* K_2SO_4, pH 2.5

Experiment	$\frac{\partial \log i}{\partial V}$ cathodic	$\frac{\partial \log i}{\partial V}$ anodic	α transfer coefficient cathodic	α transfer coefficient anodic
1	3.00	49.7	0.826	0.880
2	2.69	47.8	0.844	0.775
3	2.92	49.2	0.831	0.855
4	2.69	48.3	0.844	0.800
5	2.54	47.8	0.853	0.773
Mean of experiments 1-5.	2.77	48.6	0.840	0.817

Discussion

Overpotential-time curves.—Ohmic overpotential η_Ω plotted against the current for individual measurements shows, as was expected, a linear relation (Fig. 6). The corresponding resistance R represents the slope of the line and has the mean value of 33.04 ohms. The general expression for the calculation of resistance between the Haber-Luggin capillary and the electrode, given by Mattsson and Bockris (3), is

$$R = \frac{1}{4 \cdot \pi \cdot \kappa} \left(\frac{1}{r} - \frac{1}{x} \right) \qquad [4]$$

where κ is the specific conductance of the solution, r the radius of the electrode, and x the distance between the tip of the Haber-Luggin capillary and the center of the electrode. Using in our case the κ-value (for 0.116*N* $In_2(SO_4)_3$ + 0.5*N* K_2SO_4, pH = 2.5) 4.45 x 10^{-2} mhos/cm, the radius of the amalgam drop r = 4.7 x 10^{-2} cm, x = 3 mm, the value of R = 32.1 ohms, in agreement with the experimental values.

The double-layer capacitance is calculated from the slope of the initial linear part of the curve η_t —t. The experimentally obtained value of 25.4 μF/cm^2 is within the limits of expected values for similar systems.

The slope of the curve $\eta_t - t$ gradually levels off, and after some time, t_A, the potential value becomes almost constant. This value diminished by ohmic overpotential represents the activation overpotential η_A. The state of the "constant" potential, in relation to the duration of the pulse, is defined as $t_A < \tau$, τ[12] being the transition time (for flat surfaces)

$$\tau^{1/2} = \frac{\pi^{1/2} \cdot n \cdot \mathbf{F} \cdot C \cdot D^{1/2}}{2\, i} \qquad [5]$$

n being the number of electrons involved, **F** the Faraday, C the concentration of In^{3+} in mole/cm^3, D the diffusion coefficient of In^{3+} with the value set at 0.5 x 10^{-5} cm^2/sec, and i the c.d. in amp/cm^2.

Only after a time t_c, t_c being $t_c > \tau$, more marked concentration polarization occurs, which manifests itself in the rise of the potential. Considering the short duration of the current pulse (Fig. 3) there is hardly any concentration polarization, consequently it can be considered that the buildup to the constant values of the potential indeed does represent the activation overpotential.

Activation overpotential-logarithms of current density curves.—When the experimental values of activation overpotential η_A were plotted against the logarithms of c.d. $\log_{10} i$ the curves (Fig. 4, 5) of the cathodic and anodic polarization were obtained. Both curves show in the c.d. range 2.5 x 10^{-4}-2.5 x 10^{-3} amp/cm^2 a marked Tafel linear relation.

Considering Eq. [2] and [3] and the theoretical discussion (6) it is clear that the slope of the Tafel line is directly indicative of the determination of the parameters of the electrode kinetics of electrochemical processes with several reaction steps.

The slope of the linear part of the curve of the cathodic polarization (Fig. 4) is some 20 times more steep than the slope of the anodic curve (Fig. 5), and it can be shown easily that small experimental errors, while having a negligible influence on the slope of cathodic curves, can seriously influence the slope of anodic curves. Besides, the Tafel line of anodic polarization forms itself in a narrow region of the activation overpotential (η_A = 10 — 40 mv) and in the expression

$$i = i_a - |i_c| \qquad [6]$$

the corresponding cathodic part of c.d. i_c must not be neglected. From expression [6] it follows that

$$i_a = i + |i_c| \qquad [7]$$

which means that to get the correct anodic c.d. under these conditions the measured value i ought to be corrected by the corresponding cathodic c.d. i_c. The cathodic c.d. which would correspond to individual measuring points of the anodic polarization can be obtained graphically if the Tafel line of the cathodic polarization is extrapolated to corresponding anodic overpotentials. The execution of this procedure has shown, as is expected, that the correction values i_c for the measuring points of low anodic overpotentials are such that correction is justified, while for the higher values of the anodic overpotential the corrective i_c are so small, that correction is of no essential importance, *i.e.*, that the second element on the right side of Eq. [6] can be ignored. Such corrections of the measuring points of the low overpotentials of the anodic polarization prove the correctness of the extrapolation of the Tafel line, because the corrected measuring points fall just into

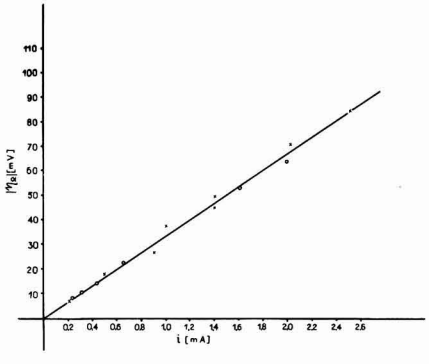

Fig. 6. Curve $\eta_\Omega - i$. Slope — R = 33.04 ohms
x — cathodic data; ○ — anodic data

the extrapolated line. This of course enables a more accurate determination of the linear part of the Tafel line, especially if it is formed in the narrow area of low overpotentials.

Considering the fact that in our case the experimental errors influence the anodic curves more, the use of values obtained by extrapolation from the cathodic curves is justified, while the reverse is not the case.

For the electrochemical process of deposition and dissolution of indium in an aqueous solution the following reactions are assumed

$$In^{3+} \xrightarrow{+e^-_o} In^{2+} \xrightarrow{+e^-_o} In^{1+} \xrightarrow{+e^-_o} In^{0} \qquad [8]$$

$$In^{0} \xrightarrow{-e^-_o} In^{1+} \xrightarrow{-e^-_o} In^{2+} \xrightarrow{-e^-_o} In^{3+} \qquad [9]$$

On grounds of expressions [2], [3], [8], and [9] and the experimentally obtained slope of the linear part of Tafel line for the cathodic and anodic polarization, calculations indicate that the slowest reaction step for the cathodic polarization is the first, and for the anodic the third.

Consequently

$$In^{3+} + e^-_o \xrightarrow{\text{slow}} In^{2+} \qquad [10]$$

and

$$In^{2+} - e^-_o \xrightarrow{\text{slow}} In^{3+} \qquad [11]$$

From this it follows that the reaction step

$$In^{3+} \underset{-e^-_o}{\overset{+e^-_o}{\rightleftharpoons}} In^{2+} \qquad [12]$$

is the rate-determining step for the over-all electrochemical process of deposition and dissolution of indium.

Experiments have shown that when c.d. is increased above 2.5 x 10^{-3} amp/cm^2 the measuring points do not follow Tafel line, but show reproducible deviations. There are indications that in this current region there may be some other processes which interfere in the processes described above. The phenomena will be treated in detail in further investigations.

Manuscript received Aug. 25, 1961; revised manuscript received March 1, 1962.

Any discussion of this paper will appear in a Discussion Section to be published in the June 1963 JOURNAL.

REFERENCES

1. H. Gerischer, *Z. physik. Chem.*, **202**, 302 (1953).
2. T. Berzins and P. Delahay, *J. Am. Chem. Soc.*, **77**, 6448 (1955).
3. E. Mattsson and J. O'M. Bockris, *Trans. Faraday Soc.*, **55**, 1586 (1959).
4. W. Kangro and Fr. Weingärtner, *Z. Elektrochem.*, **58**, 505 (1954).
5. LJ. Duić, Z. Kovac, and B. Lovrecek, *Croat. Chem. Acta*, **32**, 213 (1960).
6. B. Lovrecek, *J. Phys. Chem.*, **63**, 1795 (1959).
7. F. R. Meyer and G. Ronge, *Z. angew. Chem.*, **52**, 637 (1939).
8. N. Sunden, *Z. Elektrochem.*, **57**, 100 (1953).
9. M. v. Stackelberg and V. Toome, *Z. Elektrochem.*, **58**, 226 (1954).
10. A. R. Despić and J. O'M. Bockris, *J. Chem. Phys.*, **32**, 389 (1960).
11. G. Kortüm, "Lehrbuch der Elektrochemie," (2 Aufl.) S.354. Verlag Chemie GmbH, Weinheim/ Bergstr. (1957).
12. P. Delahay, "New Instrumental Methods in Electrochemistry," p. 184. Interscience Publishers, Inc., New York (1954).

Technical Notes

A Continuous Flow Cell for Electrochemical Synthesis

M. J. Allen

Chemical Research Department, Electro-Optical Systems, Inc., Pasadena, California

One of the more important aspects of organic electrochemistry which has received little attention in the literature, is the design, construction, and performance of electrolytic cells. Two cells have been described which utilize porous carbon electrodes (1) and a third designed for use with a mercury cathode (2). Unfortunately neither of the designs can be used with solid or amalgam type electrodes. Therefore a cell was developed (Fig. 1) which was not only suitable for the type of electrodes mentioned, but also had in common with the previously reported cells the advantages of continuous flow operation for extended periods.

This cell consists of 22 compartments constructed of "annealed" polystyrene, ½ in. thick x 5 in. wide x 6 in. high. A center section is removed leaving a chamber 2 in. wide x 4½ in. high. A ¼ in. hole is drilled on one side so that it is flush with the bottom of the center section, and on the other side so that the hole is 2⅜ in. to center from the top. Approximately ½ in. of the outside portion of each of these holes is bored out (approximately 13/32 in.) so as

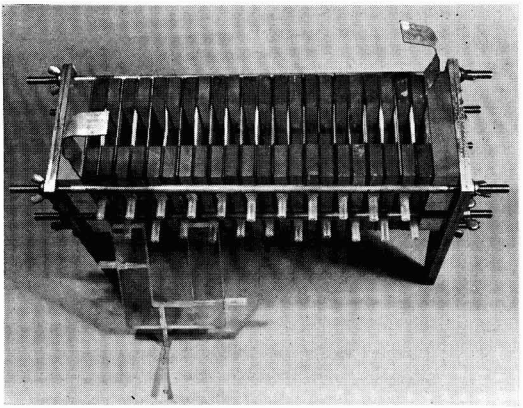

Fig. 1. Cell for continuous flow operation

to loosely accept a 1½ in. length of ¼ in. ID polystyrene tubing. These are cemented in place by dropping methylene chloride with a hypodermic syringe and fine needle in the space between the polystyrene tubing and the plate. The bond is quite solid and leak-free within an hour. A bottom outlet for drainage of each compartment is fabricated in the same manner.

The end plates consist of ½ in. stock steel through which seven holes have been drilled to accommodate 21 in. lengths of ⅜ in. rod, threaded on each end. Next to the inner face of these end plates is placed a 1 in. thick x 5 in. wide x 6 in. high polystyrene sheet, followed by an electrode (approximately 1/16 in. thick) with a connector flap, a neoprene gasket (1/16 in. thick), a polystyrene compartment, an ion-exchange type membrane between 2 neoprene gaskets, another compartment, a floating electrode between 2 neoprene gaskets, another compartment, etc. Each compartment contains approximately 54.5 ml. The active electrode area was 32.26 cm^2.

In practice the opposing electrolyte, *e.g.*, catholyte and anolyte, are pumped through alternate tygon tube connected compartments, utilizing a Sigmamotor pump. The rate of flow is so adjusted that when the electrolyte containing the depolarizer comes from the last compartment, the reaction is complete. If cooling is found necessary in the process, it is possible to place glass cooling coils within each compartment. It is, of course, obvious that the surface of the first floating electrode facing the cathode, for example, will be positive, its reverse surface negative, and so on to the power connected anode.

Experimental

In order to study the operational characteristics of this cell, the reduction of p-hydroxybenzaldehyde to its corresponding hydrobenzoin was investigated at a tin cathode. For comparison purposes, batch-type experiments were performed under controlled potential, as well as constant current density conditions. In each batch-type experiment the catholyte consisted of 12g (0.098 mole) p-hydroxybenzaldehyde dissolved in 100 ml 2*N* NaOH. The anolyte consisting of 2*N* NaOH was separated from the catholyte by an "Alundum"[1] membrane. The tin electrode area was 93.3 cm^2. A platinum anode was used in these experiments and the temperature maintained between 24°-26°. The reference potential used in the controlled potential experiments was similar to that previously reported in the literature (3). At a potential of −1.8v *vs.* SCE the initial current density was 0.064 amp/cm^2. The current plateaued at 0.0048 amp/cm^2, and during the course of the reaction 1.14 times the theoretical current (10,850 coulombs) was passed, yield 9.8g (81.3%), mp 214°-215° (3), current efficiency 71%. Utilizing constant current density conditions (0.064 amp/cm^2) for 1.14 times theory in order to duplicate the 10,850 coulombs passed in the previous typical controlled potential experiment gave a yield of 7.9g (65.6%), current efficiency 57.3%. The lower efficiency of the constant current density experiments was due to the partial use of the current toward the latter part of the experiment for hydrogen production. This was indicated by gas evolution at the cathode during this period. An experiment was performed at the lower current density of 0.0048 amp/cm^2. After the passage of 10,850 coulombs the catholyte was examined and found not to contain any detectable amount of the desired hydrobenzoin.

The catholyte for a typical continuous flow cell experiment consisted of 244g (2.0 mole) p-hydroxybenzaldehyde dissolved in 2000 ml 2*N* NaOH. The anolyte was a solution of 2*N* NaOH. The 11 cathode compartments were filled with approximately 600 ml of the catholyte from the reservoir; the anode compartments were filled with the 2*N* NaOH. A current density of 0.064 amp/cm^2 (2.1 amp/electrode) was used. The probe, a saturated calomel electrode placed at the surface of the first and last cathode, initially indicated a reference potential of −1.8v. The catholyte was recirculated through the cathode compartments at the rate of 25 ml/min until the reference potential at the last cathode reached a potential of −2.0v, at which time the reacted catholyte was delivered to a receiver and fresh unreacted catholyte permitted to enter the cell. The rate of flow was then so adjusted that the potential and the last cathode did not go above −2.0v *vs.* SCE. The flow rate for the catholyte was 12.5 ml/min and for the anolyte 5 ml/min. The applied voltage varied from 30-36v. After 162 min a total of 224,000 coulombs (1.16X theory) has been passed. Yield 184.7g (75.7%), mp 214°-215°, current efficiency 65%.

Discussion

From the results obtained a continuous flow cell appears to be more efficient than a batch type cell operating under the same constant current density conditions. This increased efficiency can be attributed to the fact that, in a flow cell operation of the type described, the potential at the electrode surface does not reach destructive heights which might result in undesirable side reactions; the depolarizer is being replenished at the electrode surface at such a rate as to enable maximum use of the electric

[1] Norton Company, Worcester, Mass.

current for the reduction process; we are dealing essentially with a flowing film in which the path the depolarizer must travel to reach the electrode is shorter than in a stirred solution.

Manuscript received Oct. 13, 1961; revised manuscript received Feb. 8, 1962. This paper was prepared for delivery before the Detroit Meeting, Oct. 1-5, 1961.

Any discussion of this paper will appear in a Discussion Section to be published in the June 1963 JOURNAL.

REFERENCES

1. G. W. Heise and N. M. Winslow, *Trans. Electrochem. Soc.*, **75**, 164 (1939); D. R. Allen and A. S. Allen, *Res. and Dev.*, **12**, 91 (1961).
2. P. C. Condit, *Ind. Eng. Chem.*, **48**, 1252 (1956).
3. M. J. Allen, *J. Am. Chem. Soc.*, **72**, 3797 (1950).

Thermal Oxidation of GaAs

Henry T. Minden[1]

General Electric Company, Syracuse, New York

Oxide masking (1) is the key technique in the fabrication of modern silicon semiconductor devices. If a silicon single crystal wafer is exposed to oxygen under controlled conditions an amorphous layer of silica will form (2). This layer is impervious to the diffusion of doping impurities into the wafer. By etching holes in the silica, diffusion can be localized for the purposes of device preparation, and the oxide protects the p-n junctions from attack by ambients.

To determine whether this technology can be carried over to gallium arsenide, a brief study of the thermal oxidation of this material was undertaken. Wafers were placed in a simple tube furnace through which gas flowed in the conventional manner. Best results in terms of the evenness of the oxide were obtained with pure oxygen, and a flow rate of about 1.3 l/min was used in the runs reported here. Temperatures between 600° and 900°C were used. Below 600° the oxidation was negligible, while above 900° the sample tended to burn up. In general, increasing the temperature merely increased the rate of oxidation, while the character of comparable films was the same.

Films of intermediate thickness (1000Å to ~6000Å) showed typical interference colors. Films which were either too thin or too thick to show interference colors were gold or brown. Even thicker films were transparent and glassy in appearance. The thickest films which were formed at 900°C were white, obviously crystalline, and somewhat waxy in texture. In some experiments water vapor was introduced into the oxygen stream. This had no discernable effect at temperatures below about 800°. Above 800° white, hard crystalline spots formed; these spots grew to cover almost the whole surface. This oxide could easily be flaked off the wafer, whereas the thinner layers were quite adherent.

Oxidation on the (110) surface of gallium arsenide was slower and more uniform than on either (111) surface. Fine white pits tended to form under the oxide on the latter surfaces, whereas even, gold films could readily be produced on the (110) surface by oxidation at 700° for ½ hr. Thicker films tended to have extensively pitted and irregular surfaces under the oxide layer. The extent of oxidation on polycrystalline surfaces varied markedly from grain to grain. No difference was noted between the oxidation of n and p material.

Electron diffraction pictures consisted of sharp rings which had spots characteristic of partial orientation of the crystallites in the film. Indexing of the rings showed unequivocably that the film consisted of β Ga_2O_3, the commonest form of gallium oxide. This was the only phase found in all the films investigated, regardless of the thickness of the film and the temperature of oxidation. In none of the samples investigated were there any electron diffraction rings which could be attributed to an arsenic containing phase. The white oxide formed in the presence of water vapor was flaked off and examined by powder x-ray diffraction. This too revealed the presence of only β Ga_2O_3.

Several samples of n GaAs were oxidized on the (110) face at 700° for ½ hr to form an attractive, uniform gold film. Part of the surface was covered with black wax, and the oxide on the exposed surface was dissolved in warm concentrated hydrochloric acid. The wax was removed, and the sample was sealed in an evacuated tube with a trace of zinc metal. The zinc was diffused into the wafer at 800° for ½ hr. After diffusion the remaining oxide was removed with warm hydrochloric acid and the surface probed with a hot point. The surface was p at both the masked and unmasked areas. The penetration of the zinc through the oxide could not be correlated with any macroscopic imperfection in the film. It is presumed that the microcrystalline nature of the oxide film allowed extensive grain boundary diffusion to the surface of the gallium arsenide. Finally an oxidized and an unoxidized wafer were simultaneously heated to 950° in an argon atmosphere overnight; both samples were reduced to a droplet of gallium. It is felt that the oxide does not prevent the outdiffusion of arsenic from gallium arsenide.

From these discouraging but fairly clear results, it does not appear that thermal oxide masking is readily applicable to gallium arsenide.

Acknowledgment

The author wishes to thank Mr. C . V. Bielan who did the electron diffraction and x-ray diffraction studies.

Manuscript received March 7, 1962; revised manuscript received April 25, 1962.

Any discussion of this paper will appear in a Discussion Section to be published in the June 1963 JOURNAL.

REFERENCES

1. C. J. Frosch and L. Derick, *This Journal*, **104**, 547 (1957).
2. M. M. Atalla, E. Tannenbaum, and E. J. Scheibner, *Bell Syst. Tech. J.*, **38**, 749 (1959).

[1] Present address: Sperry Rand Research Center, Sudbury, Massachusetts.

Solid Solubilities of Antimony, Arsenic, and Bismuth in Germanium from a Saturation Diffusion Experiment

F. A. Trumbore, W. G. Spitzer, R. A. Logan, and C. L. Luke

Bell Telephone Laboratories, Incorporated, Murray Hill, New Jersey

In the course of growing arsenic-doped germanium crystals for Esaki diodes, it was noted (1) that anomalously low carrier concentrations were obtained in crystals grown from the more heavily doped melts. Minden (2) and Cardona and Sommers (3) also have reported that only a fraction of the arsenic present in heavily doped material is electrically active. Furthermore, it has been shown (4) that appropriate heat treatment and quenching procedures can lead to significant increases in carrier concentrations, thus indicating a precipitation effect. Even after quenching, however, there remained a discrepancy of about a factor of two between the carrier concentrations and the arsenic concentrations expected from available solidus curve data (5). As pointed out previously (5), the evaporation technique used to determine this solidus curve was quite conducive to the formation of occlusions containing arsenic and hence could lead to high results.

In order to obtain an unambiguous check on the solidus curve a long term saturation diffusion experiment has been carried out at a temperature where a solid solubility of arsenic in germanium in excess of 1×10^{20} atoms/cc would be expected from the solidus curve. By using a diffusion technique the presence of germanium arsenide occlusions, formed in grown crystals by trapping of the melt during growth, should be eliminated. In addition to arsenic, antimony and bismuth were also diffused into germanium in the same experiment. The purpose of the present paper is to present the results of chemical, optical, and electrical measurements on the resulting samples.

Experimental

Available diffusion coefficient data (6) indicated that at a temperature of about 865°C one might obtain essentially complete saturation of germanium samples of a reasonable thickness in a reasonable length of time. Accordingly, the samples were diffused for 97 days at a temperature of 865° ± 5°C.

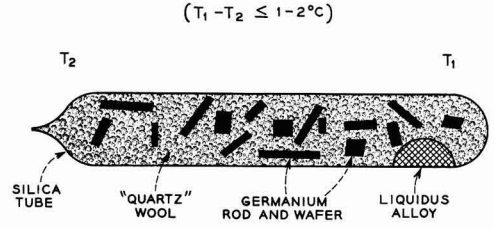

Fig. 1. Schematic diagram of the experimental arrangement during the diffusion run.

Square wafers and rods of single crystal undoped germanium were sealed, together with high-purity (> 99.9999%) arsenic, antimony, or bismuth, in evacuated ($\sim 10^{-6}$ mm Hg) vitreous silica tubes. The wafers [150 x 150 x (10-25) mils] and rods [500 x (15-25) x (15-25) mils] were of various thicknesses to permit a check for saturation at the end of the experiment. As shown in Fig. 1 "quartz" wool (99.9% pure) was used to separate the various samples to permit free access of the impurity vapor. To prevent random melting of the germanium samples the tubes were placed in a slight thermal gradient (only $\lesssim$ 1-2° over the length of the sample tube). The amounts of the group V impurity elements contained in the tubes were sufficient to form and maintain a liquidus alloy with some of the germanium in the hotter ends of the tubes during the course of the experiment. Since the partial pressure of arsenic (and, in this temperature range, probably that of antimony) over the liquidus alloys decreases with increasing temperature (4) no melting of the germanium should occur in the cooler portions of the tube. In the case of bismuth where the predominant vapor species is the monomer, instead of the tetramer or dimer, as in the case of the other two impurities, it is doubtful whether the bismuth partial pressure behaves in the same way. In fact, there was evidence of random melting in the tubes containing bismuth.

One striking feature of this experiment was the presence of a considerable amount of transport of germanium through the vapor phase, especially in the tube containing arsenic. This is illustrated in Fig. 2 which shows two examples of deposition of germanium on the germanium wafers. The presence of this vapor transport caused some difficulty since the rods became tapered and were unsuitable for Hall effect or resistivity measurements. The mechanism responsible for this transport is not known. One interpretation of the present results is that transport in the slight thermal gradient via a volatile Ge-As species was a factor since the amount of transported material was so much greater in the tubes containing arsenic. However, the presence of oxygen and transport via GeO(g) is a distinct possibility and perhaps either or both mechanisms were operative. Holonyak, Jillson, and Bevacqua (7) have observed a similar transport of silicon with group V impurities and do not believe that oxygen is responsible.

The arsenic- and antimony-doped germanium samples were analyzed chemically for the impurity concentration by using spectrophotometric methods. (The concentration of bismuth was too low for

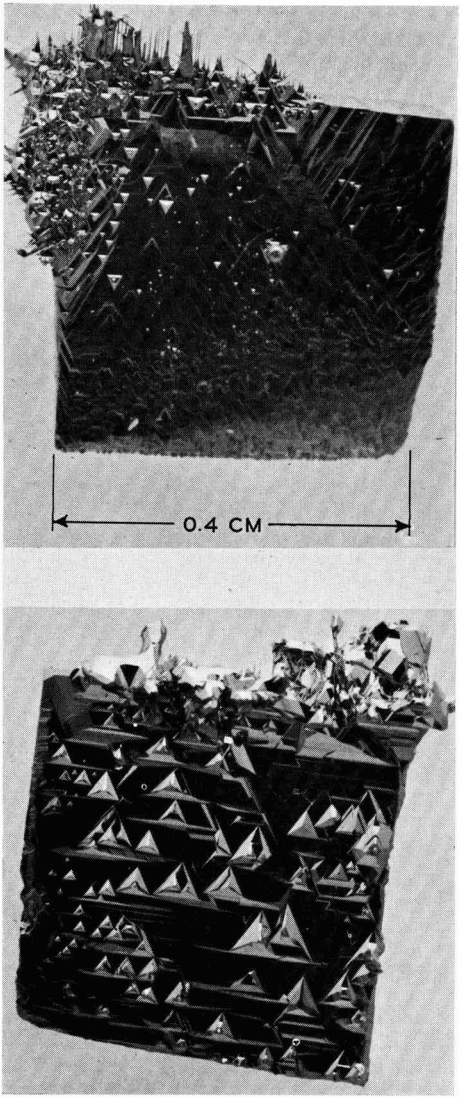

Fig. 2. Two examples of vapor transported germanium deposited on the Ge wafers. The major faces of the wafers are {111} surfaces.

analysis by these techniques.) In both cases the germanium was removed by distillation as the chloride. The antimony and arsenic contents were then determined by the iodoantimonite and heteropoly molybdenum blue methods (8, 9), respectively. In order to insure that only diffused material was analyzed, the wafers were lapped to eliminate any trace of vapor deposited germanium (Fig. 2). The samples were then etched to remove any contaminants introduced in the lapping process and analyzed. In the case of arsenic one of thickest and one of the thinnest wafers were analyzed to determine whether sufficient time had elapsed for saturation of the germanium by arsenic.

Optical reflectivity measurements were made on the arsenic- and antimony-doped samples by using the same techniques described previously (4). The carrier concentrations were determined from the known variation of the reflectivity minimum with carrier concentration in heavily doped materials (4). (The optical method is not applicable to the bismuth-doped samples because of the low concentration of bismuth.) To test for saturation in the antimony-doped samples one wafer was measured near the surface and then lapped down for a measurement near the middle of the sample. One arsenic sample was heated to 850° ± 5°C for 30 min and quenched in a jet of nitrogen as described previously (4), following which the reflectivity was measured.

By using van der Pauw's method (10) room temperature Hall effect and resistivity measurements were made on disks cut from the wafers. The carrier concentration, n, was calculated from the Hall coefficient assuming a Hall to drift mobility ratio of unity. As a check on the resistivity measurements, two-point probe measurements were made on some rods cut from the wafers. The results agreed to within 3% or better with the data obtained by the disk method.

Results and Discussion

The most important results of the various measurements are summarized in Table I which gives n and C_I^s, the concentration of the impurity. A more detailed discussion of the individual systems is given below.

Antimony.—Saturation of the germanium by the antimony was achieved as evidenced by the fact that within experimental error the positions of the reflectivity minima at the surface (14.2-14.5μ) and near the middle (14.3-15.1μ) of a 23 mil thick wafer were identical. (The attenuation distance for the optical measurement is $\lesssim$ 1 mil for these samples.) The chemical analyses, performed on two sets of four wafers each, yielded identical results of 0.036 w/o antimony, believed to be accurate to better than ±5% of the antimony content. The agreement among the impurity and carrier concentrations summarized in Table I is well within experimental error. The most likely value of the equilibrium solid solubility is believed to be (1.00 ± 0.05) x 10^{19} atoms/cc.

The available solid solubility data (4, 5, 11-13) are presented in Fig. 3 in the form of a log k *vs.* $1/T$ plot, where k is the distribution coefficient, based on the liquidus data of Thurmond and Kowalchik (14). Included in this plot is a point obtained from resistivity measurements on a polycrystalline sample grown at ~ 708°C by the sealed tube ther-

Table I. Summary of chemical, optical, and electrical data

Impurity	n (cm^{-3}) (reflectivity)	n (cm^{-3}) (Hall effect)	C_I^s (atoms/cc) (chemical)
Antimony	$1.08 \pm 0.07 \times 10^{19}$	1.02×10^{19}	9.5×10^{18}
Bismuth	—	3.5×10^{16}	—
Arsenic	5.0×10^{19}	4.8×10^{19}	7.3×10^{19}
Arsenic*	7.5×10^{19}*	7.4×10^{19}*	—

* Heat treated at 870°C and quenched.

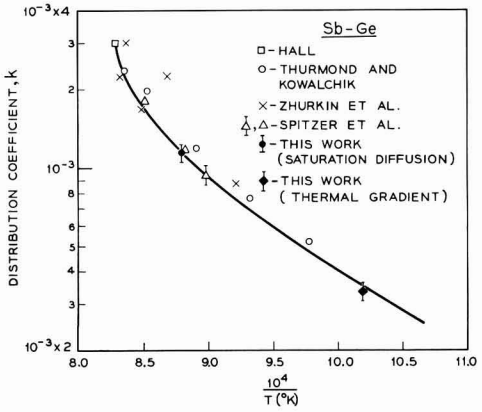

Fig. 3. Plot of log k as a function of $1/T$ for antimony in germanium.

mal gradient technique described previously (15).[1] With the exception of a few of the points due to Zhurkin *et al.* (13), there is good agreement among the various sets of data which were obtained by crystal pulling (12, 13) radiotracer diffusion profile (11), solvent evaporation and cooling (4), thermal gradient, and saturation diffusion methods. Since the saturation diffusion technique should yield an unambiguous equilibrium solid solubility and since the agreement with an adjacent solvent evaporation-cooling data point is very good, the curve has been revised from that given in ref. (4) to favor the lower values of k obtained from these experiments and from the thermal gradient experiment.[2] This results in a relatively slight modification of the previous solidus curve (5). The revised solidus curve, shown in Fig. 4, is based on the log k *vs.* $1/T$ plot in Fig. 3 and on the liquidus curve (14).

Arsenic.—Chemical analyses on two wafers of different thicknesses (10-15 and 20-25 mils) gave identical values of the amount of arsenic (0.17 w/o) indicating saturation had been achieved. (The chemical analysis is believed to be accurate to better than ±10% of the arsenic content.) This fact and the excellent agreement between the value of n in the quenched sample and the arsenic concentration indicate that a reliable value of the equilibrium solid solubility has been obtained.[3] The saturation diffusion value obtained here is about a factor of two lower than expected from the solidus curve reported previously. Hence, the latter is in error, probably due to failure to eliminate arsenide occlusions.[4] A revised solidus curve is plotted in Fig. 4 based on available liquidus data (14) and on the log k *vs.* $1/T$ plot shown in Fig. 5 which includes the crystal pulling data of Jillson and Scheckler (18) and the radiotracer diffusion profile data of Thurmond and Kowalchik (19).[5]

These experiments also indicate that the presence of micro-occlusions of germanium arsenide is not necessary for nucleation of the precipitation of arsenic as postulated earlier (4). The probability is that dislocations serve as nucleation sites. In the present samples the dislocation density of the original wafers was the order of 10^3-10^4 cm^{-2}. However, even if one should start with dislocation free germanium, Prussin (20) has shown that dislocations may be introduced in the process of diffusion.

Bismuth.—Since no chemical analyses were made, the identification of n in Table I with the bismuth

[1] This sample contained small amounts of occluded antimony which could not be separated chemically from the antimony-doped germanium so that no reliable chemical analyses could be run. However, two rods were cut from sections which appeared to contain no significant number of occlusions. The resistivities of these two rods were 1.25 × 10^{-3} and 1.42 × 10^{-3} ohm-cm corresponding to a carrier concentration of (8.8 ± 0.5) × 10^{18} cm^{-3}.

[2] The agreement between the saturation diffusion point and the adjacent solvent evaporation-cooling point of Spitzer *et al.* in Fig. 3 indicates that equilibrium data were also obtained from the latter experiments and also supports the earlier conclusion that no significant "facet" effect (16, 17) was present in the crystal growth work (4).

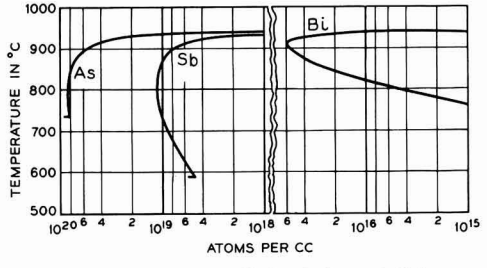

Fig. 4. Solidus curves for the Sb-Ge, As-Ge, and Bi-Ge systems calculated from the log k *vs.* $1/T$ plots in Fig. 3, 5, and 6, respectively.

[3] The fact that the Hall effect and resistivity measurements on the arsenic- and antimony-doped samples are consistent with our earlier resistivity *vs.* n curves (4) demonstrates conclusively that the difference in mobility between antimony- and arsenic-doped material is an inherent property and is not due to the presence of occluded material such as germanium arsenide.

[4] One further observation remains to be explained, namely, the apparent attainment of a very small amount of 0.0003-0.0004 ohm-cm material in a thermal gradient crystal (4). From the present work it would seem that this was just a spurious result. However, it is possible that this small region grew on a {111} facet and by the facet effect trapped in a nonequilibrium amount of arsenic. A facet effect of about a factor of two has been reported for arsenic in germanium (17).

[5] The curvature in the log k *vs.* $1/T$ plot derives from the results of the quenching experiments on As-doped samples prepared by thermal gradient crystallization reported earlier (4). The present quenching experiments indicate that the total arsenic in solid solution can be quenched in the electrically active state. Therefore, it was assumed that the maximum figure for the quenched-in carriers, 8.1 × 10^{19} cm^{-3}, represented the arsenic concentration corresponding to a melt composition between 25 and 40 mole % arsenic [see Table I, ref. (4)]. The points joined by the dashed tie line in Fig. 5 represent the values of k and $1/T$ corresponding to the melt compositions of 25 and 40 mole % arsenic, the true value lying somewhere along the tie line. If the 8.1 × 10^{19} cm^{-3} figure was not the total arsenic concentration, then a minimum value should lie somewhere on the tie line.

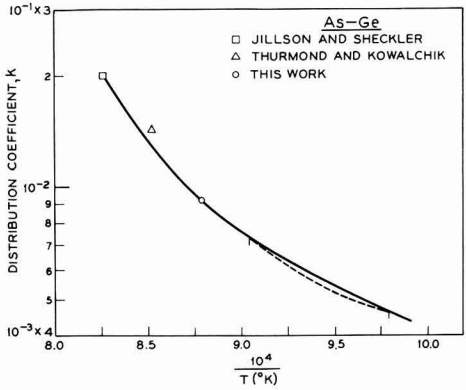

Fig. 5. Plot of log k *vs.* $1/T$ for arsenic in germanium. The dashed curve is a tie line on which one point is located (see footnote 5).

concentration is obviously not as certain as in the arsenic and antimony experiments due to the possibility of impurity contamination. However, the likelihood of significant contamination is slight in view of (*a*) the relatively low concentrations of the more soluble impurities in the silica and bismuth, (*b*) the low diffusion coefficient of these impurities (*e.g.*, Al and B) and (c) perhaps most important, the "gettering" action of the liquid Bi-Ge phase. Thus, we believe the value of n may be taken as equal to the bismuth concentration. Except for a value of the distribution coefficient at the melting point of germanium, no other solid solubility data have been reported for bismuth.

Utilizing these two data points, an approximate estimate of the temperature dependence of the distribution coefficient, k, may be obtained as shown in Fig. 6. This estimate is based on considerations of the departures from ideality in the liquid and solid phases as discussed previously for the Al-Ge and Ga-Ge systems (15). Specifically, the distribution coefficient is given by $k = \gamma^L/\gamma_n^S F_n$ where γ^L is the activity coefficient of the impurity in the liquidus alloy, γ_n^S is the activity coefficient of the neutral impurity species in the solid (both referred to the same standard state), and F_n is the fraction of the impurity atoms which remain neutral in the solidus alloy. It is reasonable to assume that log γ_n^S is a linear function of $1/T$. Thus, by plotting log k'' *vs.* $1/T$, where $k'' \equiv kF_n/\gamma^L = 1/\gamma_n^S$, for the two available data points and extrapolating one can obtain k'' and hence k at a lower temperature if one knows F_n and γ^L. The values of F_n were obtained from the treatment of Blakemore (21) while γ^L was approximated from the data of Thurmond and Kowalchik (14). In the temperature range covered only a small departure from linearity is predicted as shown in Fig. 6. An estimate of the solidus curve based on this approximation is plotted in Fig. 4. It should be stressed that there are several possible sources of error in this approximation which is carried out here in lieu of other experimental data.

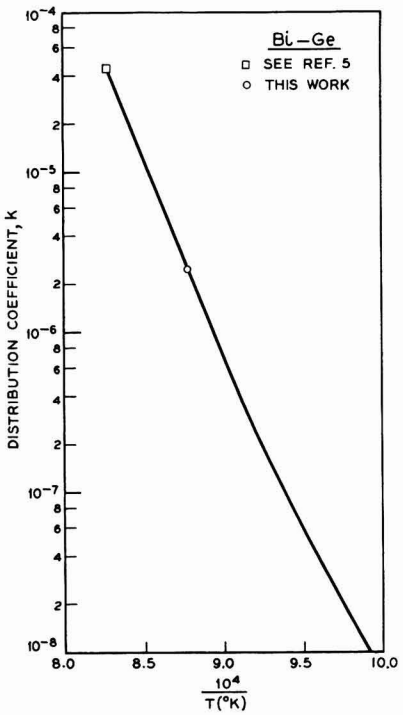

Fig. 6. Plot of log k *vs.* $1/T$ for bismuth in germanium

Summary

The present work has yielded unambiguous determinations of the equilibrium solid solubilities of arsenic and antimony at one temperature. It is believed that these data represent the most definitive equilibrium solid solubility measurements to date for any impurity in germanium or silicon except perhaps for fast diffusers such as copper, lithium, etc., where saturation is readily achieved. While the antimony result agrees well with previous measurements, the arsenic value indicates the previous solidus data are in error by about a factor of two. An estimate of the Bi-Ge solidus curve has been made based on a solid solubility measurement which was not quite as conclusive as the arsenic and antimony results.

Acknowledgments

The authors are indebted to J. F. Gilbert for the Hall effect measurements and for performing the quenching experiment, to L. Howarth for some of the reflectivity measurements, to M. Kowalchik for assistance in carrying out the diffusion experiment, to Miss A. Mills for some of the resistivity measurements, and to A. A. Tartaglia for the photographs.

Manuscript received Feb. 12, 1962; revised manuscript received April 12, 1962. This paper was prepared for delivery before the Detroit Meeting, Oct. 1-5, 1961.

Any discussion of this paper will appear in a Discussion Section to be published in the June 1963 JOURNAL.

REFERENCES

1. F. A. Trumbore in "Metallurgy of Elemental and Compound Semiconductors," R. Grubel, Editor, p. 15, Interscience Publishers, New York—London (1961).
2. H. T. Minden, *ibid.*, p. 35.
3. M. Cardona and H. S. Sommers, Jr., *Phys. Rev.*, **122**, 1382 (1961).
4. W. G. Spitzer, F. A. Trumbore, and R. A. Logan, *J. Appl. Phys.*, **32**, 1822 (1961).
5. F. A. Trumbore, *Bell System Tech. J.*, **39**, 205 (1960).
6. H. Reiss and C. S. Fuller in "Semiconductors," N. B. Hannay, Editor, p. 244, Reinhold Publishing Corp., New York (1959).
7. N. Holonyak, Jr., D. C. Jillson, and S. F. Bevacqua in "Metallurgy of Elemental and Compound Semiconductors," R. Grubel, Editor, p. 81, Interscience Publishers, New York-London (1961).
8. ASTM Methods of Chemical Analysis of Metals, p. 419, Am. Soc. Testing Materials, Philadelphia (1960).
9. C. L. Luke and M. E. Campbell, *Anal. Chem.*, **25**, 1590 (1953).
10. L. J. van der Pauw, *Philips Res. Repts.*, **13**, 1 (1958).
11. C. D. Thurmond and M. Kowalchik, see ref. (5).
12. R. N. Hall, *Fortschritte der Hochfrequenztechnik*, **4**, 129 (1958).
13. B. G. Zhurkin, V. S. Zemskow, D. A. Petrov, and

A. D. Suchkova, *Izvestia Akad, Nauk SSSR*, OTN, MiT, No. 5, 86 (1959).
14. C. D. Thurmond and M. Kowalchik, *Bell System Tech. J.*, **39**, 169 (1960).
15. F. A. Trumbore, E. M. Porbansky, and A. A. Tartaglia, *J. Phys. Chem. Solids*, **11**, 239 (1959).
16. K. F. Hulme and J. B. Mullin, *Phil. Mag.*, **4**, 1286 (1959).
17. J. A. M. Dikhoff, *Solid State Electronics*, **1**, 202 (1960).
18. D. C. Jillson and A. C. Sheckler, *Phys. Rev.*, **98**, 229 (1955).
19. C. D. Thurmond and M. Kowalchik, Private communication.
20. S. Prussin, *J. Appl. Phys.*, **32**, 1876 (1961).
21. J. S. Blakemore, *Proc. Phys. Soc.*, **71**, 692 (1958).

A Simple Technique for Seeding and Growing Oriented, Relatively Unstrained, Single Crystal Antimony, Square-Sectioned Rods

Seymour Epstein[1]

U. S. Army Signal Research and Development Laboratory, Fort Monmouth, New Jersey

Systematically preparing oriented, square-sectioned, long, single crystal rods of antimony and its dilute alloys with tin, having uniform and reproducible electrical properties and dimensions, presents many difficulties. For example, mechanical cutting, in addition to cold working the crystal, usually introduces fissures; these frequently cause large changes in the resistivity or break the specimen, according as the principal plane is parallel or not parallel to the rod's longest dimension. Acid cutting, on the other hand, is characterized by nonuniform rod faces. These difficulties can be avoided by growing oriented crystals in the desired shape, a technique first used by Kapitza (1) for bismuth and soon after by others (2) for bismuth and higher melting point materials. In principle, any one of these modified apparatuses are directly applicable to antimony, and Rausch (3), using Hasler's modification, has grown circular-sectioned antimony rods in the two principal orientations. However, our experience with these modifications and the conditions implied or specified (slow rates) is that we were able to seed and grow only rods in which the c-plane is parallel to the rod axis. The same result was obtained with our own modified apparatus only until both a fast rate of crystallization, not less than 2 cm/min, and a crucible material of low thermal conductivity relative to antimony were used. Under these conditions seeding and growing single crystal antimony rods, whose axes are at either 0°, 45°, and 90° with the <111> direction, becomes almost a routine operation. The rods are 6 cm or more long and have nearly square, 3 mm × 3 mm, cross sections.

Our modified apparatus also allows for easy control of the binary axis orientation, and the growth of rods seeded in arbitrary orientations appears possible. The fast rate of growth also minimizes the segregation of added impurities and does not appear to strain the rods.

In these experiments the undoped antimony is nominally 99.997% pure and is used as supplied by the Bradley Mining Company, San Francisco, California.

[1] Most of this material is included in a Dissertation on the "Galvanomagnetic Effects and Band Structure of Pure and Tin-Doped Antimony Single Crystals," submitted in partial fulfillment of the requirements for the Doctor of Philosophy (in Physics) degree at the Polytechnic Institute of Brooklyn (1961), to be submitted for publication.

Description of Apparatus and Procedure

The technique combines many of the desirable features of the earlier ones (1, 2). It consists of seeding and recrystallizing precast rods in a partly enclosed crucible mold. The motion of the temperature gradient through the rod is obtained by cutting off the heater power; both furnace and crucible are stationary. The latter can be taken apart, permitting strain free removal of the recrystallized rod. The furnace, crucible mold, seed orienting jigs and procedure, and seeding and growing procedure are next described.

Furnace.—By not insulating the furnace from its ambient room temperature, rapid heat dissipation and cooling rates are made possible. Simple in design and construction, it consists of two concentric, clear Vycor tubes, 1 and 3 in. in diameter, with a continuous nichrome heater element uniformly wound on the outside of the inner tube. The spacing between adjacent turns is about ⅜ in. so that the furnace charge can be seen. Two temperature zones, one 40° above the other, are used; a slight gradient exists within each. The two zones and their gradients are obtained by stretching the heater element, initially, a close wire-wound helix. For a wire diameter of 0.062 in. and a total zone length of 5 in. the heater resistance is 12 ohms; about 600 watts are sufficient to melt antimony. The gradient, the furnace and rod axes, and the growth direction are parallel.

Crucible mold.—Square cross sections are obtained in the manner prescribed by Hasler (2). Square precast rods are recrystallized in a crucible chamber of the same shape and dimensions as the rod. This technique also serves to minimize straining of the single crystal rod due to antimony's expansion upon solidification. Straining while removing the rod from the mold is avoided by designing the mold so that it can be taken apart.

The basic crucible, Fig. 1, is made up of two thin slats for side walls, a thin bottom slat, a top cover (not shown), and two channeled holding blocks. It is taken apart by axially sliding the hold-

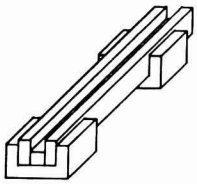

Fig. 1. Basic crystal growing crucible. The crucible is held together by the two channelled blocks. After the rod is recrystallized it is separated from the crucible by taking the latter apart.

ing blocks away from the slats, which, if they do not adhere to the rod, simply fall away. The slats are 1/16 in. thick; their remaining dimensions are determined by the size of the rod. The top cover is about ¼ in. thick for added weight.

Many crucible materials exist which neither adhere to nor react with antimony at temperatures below 700°C in the argon atmosphere used. In addition, a suitable material must have a low heat conductivity relative to the substance being crystallized (4). One such material is the mineral pyrophyllite.[2] Its advantage over most other materials is that it can be easily machined before it is fired, and it was chosen because of this additional property. (With carbon crucibles, we were able to obtain only the 90°-oriented rods, where the growth direction is the preferred one, and at lower yield.)

Seed orienting jigs and procedure.—Three orienting jigs, schematically shown in Fig. 2, have been conveniently used, although with truly perpendicular rod faces only one is required. A holding block is part of each jig and positions it accurately in relation to the rod chamber. The remaining parts of the jigs are, of course, used to orient the principal and binary crystallographic axes. The jig of Fig. 2(a) provides a flat horizontal surface which is parallel to and at the same level as the bottom of the crucible chamber; that of Fig. 2(b) provides an inclined plane at 45°; the third jig, Fig. 2(c), aligns a screw, on which a 90°-vee is grooved, along the crucible axis.

The initial seed is a single crystal chip cleaved in the principal plane. The binary directions are known from the directions of three lines in the principal plane which make acute angles of 60° with one another. To seed a 90°-oriented rod, the cleaved plane is placed in contact with the flat of jig 2(a) and the binary axis direction at the desired angle with the crucible axis. Because the resulting 90° rod's vertical faces may not be precisely at right angles to the bottom surface, jig 2(b) is used for generating seeds in the 45°- and 0°-orientations. The bottom surfaces of the 90° rod and, in turn, of the 45° rod it seeds, are placed on the incline. Alignment of the seed rod and crucible axes is assured if a part of each seed rod is inserted into the mold chamber. To change the binary axis orientation of the 0°-oriented rods, jig 2(c) is used. The seed is placed in the groove and the screw turned through an appropriate angle.

Once a set of accurately oriented square-sectioned seed rods is obtained, each orientation is reproduced by innoculating other rods. No special jig is required. Each seed rod is simply placed in the crucible chamber with its bottom face referenced against the bottom of the mold.

Seeding and growing procedure.—Successful seeding is not difficult. It is neither necessary to fuse the seed to the precast rod with a reducing flame prior to melting in the crucible nor to use freshly cleaved or etched surfaces, as some of the earlier researchers found necessary for bismuth (2). Satisfactory contact is obtained simply by pushing one against the other. The rod and seed are joined by melting the former back to the latter at the time the single crystal is to be grown. As a general rule, a minimum of the seed is melted; usually 3 mm or less is satisfactory. However, the amount appears not to be critical because seeding was successful when lengths up to 15 mm were inadvertently used. For a given heater power the position of the seed junction in the furnace determines the amount of the seed melted. This position also appears to be a factor which influences the frequency of successful seeding. The optimum location is the region of the steep gradient between the zones.

In order not to stress the junction and to watch the wetting process, about 2 mm of the precast rod and the seed are not covered. Because of this, surface tension may act to form a blob at the junction. If the blob extends too far above the crucible walls, the seed orientation frequently does not survive.

The procedure for melting and resolidifying the precast rod is simple, once the optimum position and the corresponding heater power are determined. With the seed junction properly placed the system is flushed with argon; a positive pressure is maintained and the heater circuit is closed. Melting begins in nearly 10 min and is completed in about 2 min. A few seconds after the seed is wetted, the heater circuit is opened. Although the growth rate could not be determined accurately, it is not less than the 2 cm/min rate mentioned nor greater than 10 cm/min; more than likely, it is about 6 cm/min. The resulting rods are either thermally etched or etched in dilute aqua regia to bring out any gross grain structure.

[2] Spectroscopic analysis of the recrystallized rods does not show contamination.

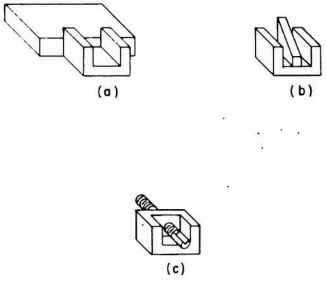

Fig. 2. Schematic representation of orienting jigs. Jig (a) can be used to obtain arbitrary orientations, jig (b) to obtain the 45° and 0° orientations, or multiples of the inclination angle, from 90°-oriented rods; jig (c) to adjust secondary axis orientation of 0° rods. Each jig is attached and referenced to the crucible by the channelled holding block which is an integral part of each jig.

Evaluation of Crystals

A measure of the quality of the rods is obtained by describing some of their physical properties and, where possible and meaningful, by comparing these with those of both slow-grown cast single crystal antimony rods and other single crystal specimens cut from large slow-grown ingots. The properties examined are their room temperature mechanical behavior, their ability to recrystallize in the solid, their room temperature galvanomagnetic coefficients, the segregation of added impurity due to normal freezing, their fine structure, the variation of one of the two principal resistivity coefficients with temperature, and the liquid helium-room temperature resistivity ratio. Our characterization is for the most part qualitative.

Allowing for anisotropy in mechanical behavior, the unworked undoped antimony rods are invariably more plastic than correspondingly oriented machined specimens. Unworked rods of the 45° and 90° orientation can be bent and twisted easily; the 0° rods are brittle. For orientations where it is not parallel to the rod axis, the c-plane is the one along which the rods break when dropped or otherwise stressed. Where the principal plane is very close to being parallel, the rods almost invariably break along secondary cleavage planes whose traces on the c-plane are the lines giving the binary axes directions. The cleavages and breaks are sharp and well-defined as shown in Fig. 3. Alloy rods are in general less plastic than their undoped antimony counterparts and appear to become brittle as tin is added.

Before breaking, not all rods of a given orientation deform to the same extent. This nonuniformity may be due to the fact that the one rate of growth used, or some unspecified factor(s), unknowingly and uncontrollably varied slightly. An exceptionally plastic rod, which we have not been able to reproduce, has been bent through nearly 95° and twisted. The rod is a single crystal in the region of deformation whose <111> axis is neither parallel to the lateral faces nor makes an angle of 0°, 45°, or 90° with the rod axis. Another interesting difference between our cast and cut single crystal rods is that many of the latter recrystallize in the solid at temperatures just below the melting point and none of the former do.

The nonuniformity also extends to the room temperature electrical properties in the form of spurious fluctuations about an average value for a given alloy. An example of this is the spread in ρ_{11}, the resistivity in the c-planes, and ρ_{33}, the resistivity across the c-planes. Values for these are, respectively, 43-46 x 10^{-6} ohm-cm and 32-36 x 10^{-6} ohm-cm for pure antimony and 38-39 x 10^{-6} ohm-cm and 42-45 x 10^{-6} ohm-cm for nominally 0.8% tin-doped specimens. These numbers show the percentage fluctuation to be orientation dependent, and, indeed, the spread in resistivity for 45° oriented rods of a given alloy is almost midway between the spreads for the 0° and 90° rods. On this basis it can be concluded that the nonuniform qualities of the rods are caused by minor flaws and inhomogeneities associated with the principal planes, probably the same ones which determine the planes of highest stress, or the weakest ones, at which a rod will break. The numbers, together with the spread in resistivities for our 0.2% alloys, also show the fluctuations to decrease on the addition of tin in amounts up to 0.8%.

Compared to independently obtained published values measured on specimens cut from Bridgman grown ingots of the same nominal and probably lower purity stock (5), our average values for ρ_{11} and ρ_{33} at room temperature agree to within 3% but our Hall coefficients and most of the magnetoresistance coefficients are lower by 10% and 20%, respectively. This agreement for the ρ's and the disagreement for the Hall and magnetoresistance coefficients, the latter larger than the former, cannot be accounted for by differences in purity and are compatible with different states of strain in the unworked and cut rods. A positive assignment is not possible from our data. Theory, however, does point to strain dependent coefficients (6).

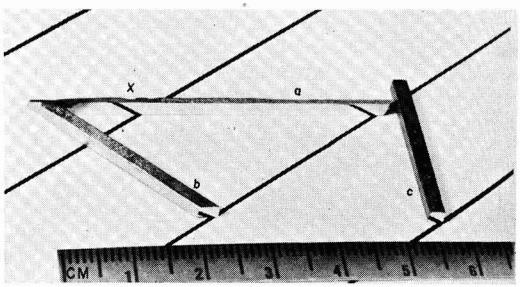

Fig. 3. Oriented single crystal antimony rods cleaved in the principal plane. The cleaved surfaces are unpolished and mirror the black stripes. Rod a has been grown in the 0° orientation; rods b and c in the 45° and 90° orientations, respectively. The region marked x is the seeding junction. The 45° and 90° specimens are cleaved by placing the tip of a thin blade on the edge of the rod and, with the blade parallel to the cleavage plane, pressing the blade into the rod; rod a is split by inserting the blade into a small crack obtained in the way just described and then sliding the blade, which is parallel to the cleavage plane, along the rod. A secondary cleavage plane on which fracture takes place bounds the right end of rod a.

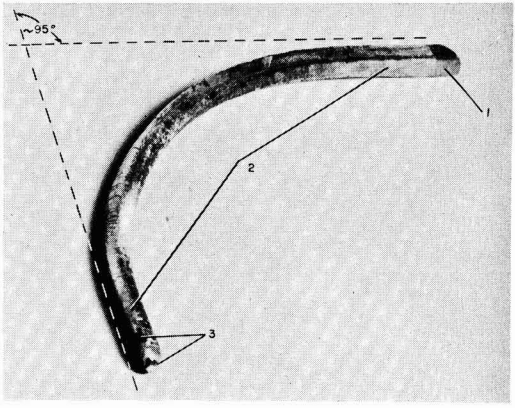

Fig. 4. An exceptionally plastic antimony rod. In response to a slight torque, the rod has simultaneously bent and twisted in the large single crystal region shown by the number 2. The traces of slip planes can be seen at the bend. Differently oriented grains at the ends of the rod, marked by 1 and 3, are clearly visible.

The segregation of tin due to normal freezing in the rods was checked by measuring ρ_{11} or ρ_{33} and spectroscopic sampling along the rod. On some long specimens where the resistivities did vary with length, the end-to-end change is less than 1% and orientation independent. Spectroscopic sampling shows some local fluctuations in doping, but these can be minimized by using zone-levelled starting stock.

As to fine structure, the dislocation density on a (111) plane appears to be about the $10^4/cm^2$ value recently reported by Wernick and co-workers for zone-refined, 99.999% pure, slowly grown, antimony crystals (7). We also find, in agreement with their observations, low-angle grain boundaries on some principal plane surfaces. Because our etching techniques are rather crude and not reproducible, our agreement and disagreement may not be significant.

Consistent with low-angle grain boundaries but not necessarily directly related to them are slightly split back reflection Laue spots. The amount of splitting is less than that obtained from specimens grown by Bridgman and horizontal techniques at slow rates and slightly more than that obtained from one carefully selected slow-grown Czochralski specimen. The slight degree of misorientation does not prevent the rods, as we have stated before, from being sharply cleaved at room temperature, nor does it distort the image mirrored in the principal cleavage plane, Fig. 3.

A complete evaluation should include extensive data on their electronic properties at low temperatures. In this connection our remarks are limited to the general features of the temperature variation of resistivity between room temperature and 77°K and to a brief discussion of known values for $\rho_{11}(4.2°K)/\rho_{11}(\sim 295°K)$. Our undoped and 0.2% tin-doped crystals respectively reproduce Lane and Dodd's (8) curves for cast, 3 mm diameter (9), undoped and 0.25% tin-doped, slow-grown, single crystal rods, and our 0.8% alloy data fall on their 0.5% alloy curve. Also in good agreement with the cast undoped antimony curve are a few of our undoped specimens cut from large slow-grown ingots. The remainder, however, have the same temperature coefficient of resistivity but prescribe curves which are shifted upward by constant arbitrary amounts. Although a detailed definitive explanation of these observations is not warranted because the possible variables involved were not systematically controlled, it would appear that the amount of defects in the cast slow- and fast-grown rods, and in selected specimens cut from large slow-grown ingots, is about the same. We would also expect to reproduce Browne and Lane's (9) value of 0.0012 for $\rho_{11}(4.2°K)/\rho_{11}(297°K)$ even though their nominal purity is 99.94%, for Steele (5), on cut specimens of about 0.5 mm x 2 mm, obtained a value of 0.014 on what appears to be the same antimony stock as ours but zone-refined to 99.999%. With higher purity materials a value of 0.0017 (10) has been reported for roughly 2 mm thick specimens (11). Using ultrapure antimony, less than 1 part in 10^7, Datars (11), who, incidentally, gives 0.0017 as the upper limit for cyclotron resonance in antimony, reports a value of 0.0005. This marked dependence of the 4.2°K resistivity on low-level impurity content plus our tentative conviction about the internal condition of our cast rods suggest that the technique described can yield low resistivity ratio crystals.

Conclusion

From the observed properties, the unworked single crystal antimony rods grown at a fast rate appear to be relatively unstrained compared to rods prepared by most other techniques. Their properties are reproducible within specifiable limits, and, although some properties differ from those of cut rods, the differences appear to reflect favorably on the technique. The rods are adequate for measuring the room temperature galvanomagnetic coefficients of pure and tin-doped antimony, the purpose for which this technique was developed, and ought to be satisfactory for cyclotron resonance and anomalous skin effect experiments where a long mean free path is necessary provided sufficiently pure starting material is used. The technique is applicable to the bismuth-antimony alloy system, and antimony-rich alloy rods have been grown in the nonpreferred, 0° orientation with the conditions optimum for pure antimony.

Acknowledgments

The author wishes to thank J. W. Mellichamp of the Institute for Exploratory Research at this Laboratory, for the spectroscopic analyses, and H. Jacobs, Deputy Director of the Laboratory's Solid State and Frequency Control Division, and H. J. Juretschke, of the Polytechnic Institute of Brooklyn, for their encouragement.

Manuscript received Jan. 25, 1962; revised manuscript received April 12, 1962. This paper was prepared for delivery before the Detroit Meeting, Oct. 1-5, 1961.

Any discussion of this paper will appear in a Discussion Section to be published in the June 1963 JOURNAL.

REFERENCES

1. P. Kapitza, *Proc. Roy. Soc.*, **A119**, 358 (1928).
2. Some of these are: L. Schubnikow, *K. Acad. Amst. Proc.*, **33**, 327 (1930); A. Goetz, *Phys. Rev.*, **35**, 193 (1930); E. Donat and O. Stierstadt, *Ann. Physik* (Leipzig), **17**, 897 (1933); M. F. Hasler, *Rev. Sci. Instr.*, **4**, 656 (1933).
3. K. Rausch, *Ann. Physik*, **1**, 190 (1947).
4. B. Chalmers, *Can. J. Phys.*, **31**, 132 (1953). This reference qualitatively presents the factors to be controlled in growing, seeding, and orienting metallic single crystals in horizontal containers.
5. P. W. Bridgman, *Proc. Am. Acad. Arts Sci.*, **60**, 305 (1924); M. C. Steele, *Phys. Rev.*, **99**, 1751 (1955); S. J. Freedman and H. J. Juretschke, *ibid.*, **124**, 1379 (1961).
6. R. W. Keyes, "Solid State Physics," Vol. 11, F. Seitz and D. Turnbull, Editors, Academic Press, Inc., New York (1960).
7. J. H. Wernick, J. N. Hobstetter, L. C. Lovell, and D. Dorsi, *J. Appl. Phys.*, **29**, 1013 (1958).
8. C. T. Lane and W. A. Dodd, *Phys. Rev.*, **61**, 183 (1942).
9. S. H. Browne and C. T. Lane, *ibid.*, **60**, 895 (1941).
10. W. R. Datars and R. N. Dexter, *ibid.*, **124**, 75 (1961).
11. W. R. Datars, Private communication.

Steady-State Evaporation Method for Composition Control of Thin Films Prepared by Halide Reduction

H. C. Theuerer

Bell Telephone Laboratories, Incorporated, Murray Hill, New Jersey

A widely used method for the preparation of thin films of elemental and compound semiconductors or metals is the hydrogen reduction of the appropriate halides. The inherent flexibility of this method makes it possible to prepare films with a large variety of compositions by appropriate adjustments of the vapor phase introduced to the reduction vessel. However, the precise composition control required for research and device purposes has, heretofore, made it necessary to meter accurately the very small amounts of halide vapors required in the reduction process. Metering of components is eliminated with the steady-state evaporation method, herein discussed. In essence, this is a simple and efficient method for maintaining a fixed vapor phase composition during the evaporation of binary or multicomponent solutions, the composition obtained being that of the starting liquid used.

The objective in steady-state evaporation is to promote evaporation from the surface of a liquid column using a carrier gas such as hydrogen with thermal and mechanical agitation of the liquid eliminated. Under these conditions, the surface layers of the liquid become enriched in the constituents with lower vapor pressures. Diffusion in the liquid results in an exponential concentration gradient in the region near the surface. Steady state is reached when the composition at the liquid surface is such that the gas phase in equilibrium with this liquid is that of the bulk liquid. For an ideal binary system, steady state is realized when the liquid surface has the composition $N_a p_b^\circ / N_b p_a^\circ$ where N_a/N_b is the mole ratio of the constituents initially, with p_a° and p_b° being the vapor pressures of the pure constituents.

Using this evaporation method, once steady state has been established, the gas phase composition will remain invariant so long as the gas flow rate, temperature, and the composition gradient near the liquid surface are not changed significantly. Conventional means of maintaining temperature and gas flow are adequate, and control of the liquid concentration gradient can be realized by containing the liquid in a porous medium such as a glass frit filter. The fine capillaries in such filters effectively block thermal and mechanical agitation. Moreover since the quantity of liquid held in the frit is small and the rate of liquid transport through the capillaries is high the diffusion gradient is restricted to a small region near the frit surface. In consequence, this evaporator design is insensitive to minor fluctuations in temperature and gas flow rate. A major change in either temperature or flow rate will result in a large transient change in composition of the evaporating liquid. It should be noted that as soon as the new steady state is established the evaporating liquid will revert to its original composition. Since the same steady state is achieved for any temperature at which the solution remains liquid and for any maintainable evaporation rate, control of these variables makes it possible to vary the quantity of vapors introduced to the reaction vessel over a wide range.

The apparatus for steady-state evaporation and halide reduction is shown in Fig. 1. With this apparatus it is possible to carry out all operations required to obtain steady state by proper manipulation of the stop cocks. Initially, the halide mixture is forced above the glass frit by applying hydrogen pressure to the reservoir. The pressure within the reservoir and evaporation chamber is then equalized which allows the liquid to drain back into the reservoir. Due to capillarity, the liquid column will remain in contact with the frit, and the upper surface of the frit will be uniformly wet. The liquid level in the reservoir should be below the frit, but other control of this height is not required since capillarity and the cohesive strength of the liquid will support the column in contact with the frit against an appreciable gravity head. After these preliminary operations, the desired hydrogen flow is maintained for a period of 10 min which is adequate to establish steady-state conditions. Following this, the gaseous mixture can be introduced to the reduction chamber for film deposition.

While this evaporator has been designed primarily to maintain a uniform vapor phase composition for the preparation of films with uniform composition, it is possible when desired to produce temporarily sharp concentration gradients by perturbing the evaporation rate. With an increase in

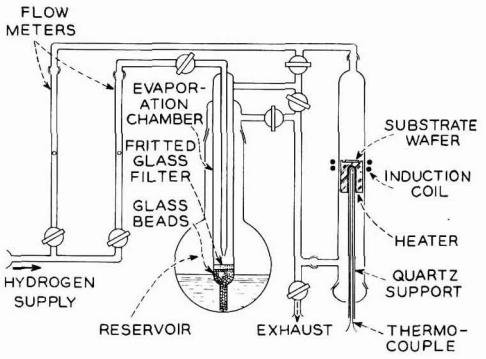

Fig. 1. Apparatus for steady-state evaporation and halide reduction.

evaporation rate, solutes with lower vapor pressure than the solvent will increase in concentration, the effect being greater the larger the difference between the solute and solvent vapor pressures. Solutes with higher vapor pressures than the solvent similarly decrease in concentration for an increase in evaporation rate. A decrease in evaporation rate from the initial steady-state rate results in solute concentration changes the opposite of those stated above. Since the composition of the vapor differs from that of the liquid only during the transient period while steady state is being reestablished, it is possible to produce sharp gradients in the deposited films. In the case of semiconductors, with the proper balance of donor and acceptor halides, in for example $SiCl_4$, it should be possible to produce p-n junctions. The mechanism here is analogous to that for rate grown junctions from the melt. The mathematics for solute distribution during solidification has been developed by Smith, Teller, and Rutter (1) and this may be used as a guide in utilizing the perturbed steady-state evaporator.

Acknowledgment

The author gratefully acknowledges the fruitful discussions and assistance of his colleagues J. J. Hauser, J. E. Kunzler, W. G. Pfann, and D. D. Bacon.

Manuscript received March 2, 1962. This paper was prepared for delivery before the Los Angeles Meeting, May 6-10, 1962.

Any discussion of this paper will appear in a Discussion Section to be published in the June 1963 JOURNAL.

REFERENCE

1. V. G. Smith, W. A. Tiller, and J. W. Rutter, *Can. J. Phys.*, **33**, 723 (1955).

Nature of the Damaged Layer on Abraded Silicon Specimens

R. Stickler and G. R. Booker

Research and Development Center, Westinghouse Electric Corporation, Pittsburgh, Pennsylvania

The damaged layer associated with semiconductor surfaces after abrasive treatments has been investigated extensively during the last few years; for a review see ref. (1). However, most of the work was directed toward determining the depth of the layer rather than the nature of the layer. Several investigators (2-5) hold the view that the damaged layer consists of a narrow outer region of cracked material together with a wide inner region of high dislocation density material. On the other hand, Pugh and Samuels (6) recently concluded that the entire layer consists of cracked material, and that dislocations are not present. However, both groups of investigators(6, 7) found that dislocations were formed if abraded specimens were subsequently annealed. We have investigated the damaged layer associated with abraded Si specimens by chemically thinning the specimens and examining them by transmission electron microscopy. Some preliminary results are described.

Procedure and Results

Silicon slices were cut, chemically polished with CP4 to remove the surface damage arising from the cutting, and abraded unidirectionally for a few minutes on one side using a No. 400 SiC paper with water as a lubricant. The slices were then chemically polished from the unabraded side using an HNO_3/HF solution (8) until portions of the slices were only a few 1000Å thick. These specimens were then mounted on a tilting specimen stage, and the thin portions were examined in transmission in the electron microscope.

The micrographs show areas corresponding to regions below the Vs of grooves gouged out of the surface by the abrasive particles. Directly beneath the Vs, two types of structure were observed. The less common type (Fig. 1) consisted of numerous single, and sometimes superposed, electron interference fringe systems. The fringes were in general curved and were not oriented along crystallographic directions. These fringes are of the kind which would result if small blocks of material located directly above one another were slightly misaligned, as in cracking.

The second more common type of structure (Fig. 2) consisted of an irregular network running along the length of the grooves. The structure comprised intersecting lines oriented along crystallographic directions and appears to be a severely strained dislocation network.

The regions directly adjacent to these two types of structure mainly exhibited only a surface texture structure. The appearance of this structure sug-

Fig. 1. Silicon abraded with No. 400 SiC paper. Electron interference fringes arising from cracked material are present. Transmission electron micrograph 50,000X.

Fig. 2. Silicon abraded with No. 400 SiC paper. Severely strained dislocation network is present. Transmission electron micrograph 100,000X.

gested that it arose during the abrasion process by small pieces of material being chipped away from the surface.

If the type of structure shown in Fig. 2 does consist of strained dislocation networks, then one would expect the dislocations to rearrange themselves during an annealing treatment and to assume a more equilibrium form, ideally a hexagonal network. Accordingly, Si slices were abraded with No. 400 SiC paper, annealed at 850°C for 1 hr in a hydrogen atmosphere and then prepared for transmission electron microscope examination as previously described.

The annealing treatment had two effects. First, a rearrangement of the dislocations in the networks occurred (Fig. 3), many areas adopting an approximately hexagonal form. Second, single dislocation lines ran outward from the edges of the networks (Fig. 3) into the surrounding, previously dislocation-free, regions. It is presumably this latter type of dislocation which was revealed by Faust (7) and Pugh and Samuels (6).

Summary and Conclusions

When silicon specimens were abraded with No. 400 SiC paper, the regions directly beneath the grooves gouged out by the abrasive particles were heavily damaged. The damage consisted of severely strained dislocation networks and cracks. Annealing of the abraded specimens at 850°C caused the dislocations within the networks to rearrange themselves into an approximately hexagonal form, and

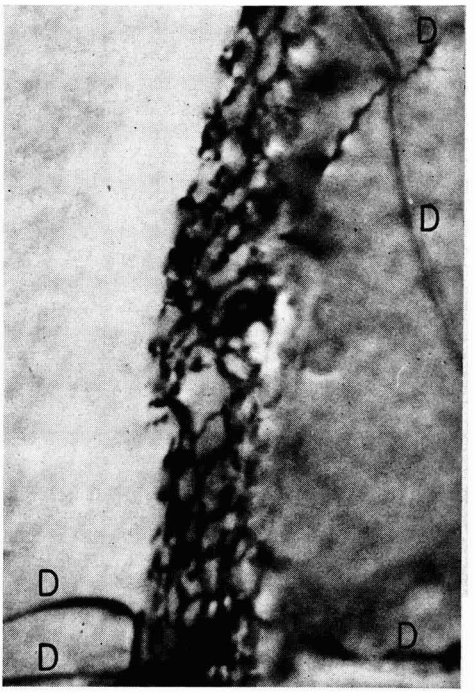

Fig. 3. Silicon abraded with No. 400 SiC paper and annealed at 850°C for 1 hr. Dislocations within the network have rearranged themselves into an approximately hexagonal form, and single dislocations (D) have propagated from the network into the surrounding regions. Transmission electron micrograph 50,000X.

single dislocation lines to propagate outward from both networks and cracks into the surrounding regions.

Conventional metallographic techniques would in most instances not reveal the individual dislocations of such networks because of the small distance between the dislocations (<1000Å). Moreover, such networks would etch as grooves, and hence would not be distinguishable from cracks. However, the single dislocations formed during annealing are relatively widely spaced, and are readily revealed.

Manuscript received April 12, 1962.

Any discussion of this paper will appear in a Discussion Section to be published in the June 1963 JOURNAL.

REFERENCES

1. T. M. Buck in "The Surface Chemistry of Metals and Semiconductors," H. C. Gatos, Editor, p. 107, John Wiley & Sons, Inc., New York (1960).
2. J. W. Faust, Jr., Paper presented before the Buffalo Meeting, October 1957.
3. R. L. Hopkins, *Phys. Rev.*, **98**, 1567 (1955).
4. D. Baker and H. Yemm, *Brit. J. Appl. Phys.*, **8**, 302 (1957).
5. J. W. Allen, *Phil. Mag.*, **4**, 1046 (1959).
6. E. N. Pugh and L. E. Samuels, *This Journal*, **108**, 1043 (1961).
7. J. W. Faust, ASTM Symposium on Cleaning of Electronic Device Components and Materials, Special Tech. Publ. No. 246.
8. G. R. Booker and R. Stickler, To be published.

Silver-Silver Chloride Electrodes Using Optical Silver Chloride Crystals

J. Greyson

Thomas J. Watson Research Center, International Business Machines Corporation, Yorktown Heights, New York

For a current investigation of membrane potentials, we require silver-silver chloride electrodes which can maintain stability for long time periods even when subjected to frequent moves from one dilute (less than 1M) aqueous chloride solution to another. A very simple preparation which requires only routine laboratory precautions and yields electrodes with excellent stability is described in this note.

Electrode Preparation

Silver chloride optical crystal sheet,[1] 1 mm thick, is cut into small sections about 0.5 cm on an edge. A piece of 0.030-in. silver wire[2] is heated over a bunsen flame until the end melts to a small sphere and while hot is pressed into an edge of one of the sections. The wire must be hot enough to melt the crystal around itself to secure an adequate electrical and mechanical connection. A piece of glass tubing, somewhat shorter than the silver wire, and previously filled with Apiezon W is warmed to soften the filling. The wire is pushed through the tube drawing the crystal as close to the end as possible. After the assembly has cooled, the crystal is rinsed several times successively and briefly in reagent grade concentrated nitric acid, water, and concentrated ammonium hydroxide, and is finally washed for several minutes in distilled water. Using the crystal as the cathode and platinum wire or foil as the anode, a deposit of metallic silver is developed on the crystal surface by immersing it in a 0.05-0.1*N* redistilled hydrochloric acid solution and then slowly withdrawing it while passing about 10 ma of current. The silver deposit forms at the contact of the crystal and the wire and grows down the surface in a thin jagged line. After obtaining the initial deposits, a group of electrodes are cathodized in the same solution for 30-40 min at a current of 2-3 ma per electrode. During this period the initial deposits broaden and become more diffuse. The current is reversed on completion of cathodizing and the electrodes are anodized at 0.2-0.3 ma/electrode for 2-3 min. They are then washed for a few minutes in distilled water and can be used.

Electrode Performance

Taniguchi and Janz (1) have defined "bias potential" as the difference in potential between a pair of identical electrodes immersed in a uniform solution. The term is used throughout the following to characterize electrode performance.

Bias potentials of all electrode pairs were measured, initially and for one week thereafter, in 0.1*N* HCl. After the first week, the medium was changed periodically. No attempt was made to stir the solutions or free them of oxygen. Potential measurements were made with negligible current flowing by using a microvoltmeter with a 6 megohm input impedance or a Rubicon Portable Potentiometer in conjunction with a Keithley 151R Null Detector with an input impedance of 100,000 ohms.

Three groups of electrodes were prepared at different times, the second group four hours after the first and the third, four days later. Of the first group of four, two were removed and used for measurements of cell potentials. All possible pairs in the second two groups, each composed of six electrodes, and the remaining two of the first group were compared at regular time intervals. The two in use for cell potential measurements were periodically returned to the bias potential cell and compared with all the rest.

Within any of the groups of electrodes which were prepared simultaneously, the bias potentials never exceeded ±0.1 mv (and frequently were less than ±0.05 mv) within 30 min after completion of anodizing. The average of the absolute values of the bias potentials for electrode pairs within a simultaneously prepared group was about 0.07 mv initially. After 100 hr in hydrochloric acid this average value decreased to about 0.05 mv. Changes in media (*i.e.*, 0.01*N* lithium chloride, 0.1*N* sodium chloride) caused an initial rise in bias potentials, but within 30 min the average of the absolute values reduced to that in the hydrochloric acid. The electrodes which were periodically returned to the bias cell always compared to those of the same group within 0.1 mv within 30 min.

A newly prepared electrode was usually about 1 mv negative with respect to an old one. This value increased to −0.15 mv in about 100 hr with a half time of about 15 hr. Changes in the nature of the surrounding solutions did not affect the magnitude of the potentials between new and old electrodes. It is interesting to note that in using standard preparative techniques, new electrodes are positive with respect to older ones. Janz (2) has discussed this effect and has pointed out that it may arise from a depletion of solute in the electrode pores during long anodizing periods. In the present technique the ratio of cathodization to anodization is high, and solute may concentrate in the electrode pores giving rise to a reversal in polarity.

We have examined several other characteristics of these electrodes. The electrical resistance of a pair is approximately 500 ohms. In dilute ethanol-HCl solutions, bias potentials were larger by an

[1] Harshaw Chemical Company, Cleveland, Ohio.

[2] Spectroscopically analyzed grade, Jarrell-Ash Co., Newtonville, Mass.

order of magnitude (> 1.0 mv) than in aqueous solutions. Over the temperature range 5°-100°C, bias potentials remained less than 0.1 mv. After passing 10 μa for 1 min, the bias potential reduced to the prepolarizing value in under 60 min with a half time of about 1 min.

These electrodes are used as probes to measure membrane potentials between chloride solutions. Within 15 min after cell assembly the potential reaches a value (P_1) which remains steady within 20 μv for 30 min or more. The electrodes are interchanged, and a potential P_2 is determined in the same way. The cell potential is taken as $\frac{1}{2}(P_1 + P_2)$ while $\frac{1}{2}(P_1 - P_2)$ may be compared with the bias potential B for the same electrodes in a mixture of the solutions in the two cell compartments. We find $\frac{1}{2}(P_1 - P_2) - B$ is at most 40 μv. A slow variation in bias potential has been noted in moving the probes through a succession of solutions of varying composition and concentration but the absolute magnitude has never exceeded 0.15 mv even after several weeks of use.

Acknowledgment

The author wishes to thank P. R. Mackey for his assistance and H. P. Charbnau for contributing the silver chloride crystals.

Manuscript received Dec. 11, 1961; revised manuscript received April 24, 1962.

Any discussion of this paper will appear in a Discussion Section to be published in the June 1963 JOURNAL.

REFERENCES

1. H. Taniguchi and G. J. Janz, *This Journal*, **104**, 123 (1957).
2. J. G. Ives and G. J. Janz, Editors, "Reference Electrodes," Academic Press, New York (1961).

Ionic Conductivity of Zirconium Phosphate

R. P. Hamlen

General Engineering Laboratory, General Electric Company, Schenectady, New York

Ion exchange membrane hydrogen-oxygen fuel cells employing proton or hydroxyl ion conducting membranes as the electrolyte and gas barrier are under development at present (1-4). The organic ion exchange membranes employed in these cells have high conductivities (5), so that the internal resistances of these cells are relatively low. However, it would be desirable in some cases to employ solid electrolytes with greater thermal stability, oxidation resistance, and resistance to ionizing radiation. The operation of a cell employing such an electrolyte, zirconium phosphate, has been reported by Dravnieks and Bregman (6).

Since ionic solids in general are noted for being relatively poor ionic conductors at low temperatures when compared with aqueous electrolyte solutions, it is pertinent to mention the desired conductivity, and the order of magnitude of the conductivity observed for some types of ionic conduction in solids. Broers (7) has estimated that the specific resistance should be no higher than 10 ohm-cm in order that the ohmic voltage drop in the electrolyte will not be too great. Ionic conduction by lattice vacancy migration usually yields room temperature specific resistances of the order of 10^5 to 10^{11} ohm-cm. It is possible to increase the number of vacancies, and also the conduction, by doping with the proper impurity, but in general the maximum conductivity observed at room temperature is of the order of 10^{-6} $ohm^{-1}cm^{-1}$. Doped oxides of Zr, W, etc., have been employed in fuel cells (7) as oxide ion conductors, but in order to increase the conductivity to a reasonable value the temperature must be maintained at or above 1000°C.

In a few isolated cases the conductivities encountered in interstitial ion migration are very high. AgI undergoes a phase transition at 146°C wherein the silver ions become almost completely mobile in a fixed lattice of iodide ions (8), and batteries have been designed around this property (9). However, measurement of the proton conductivity in solid hydrated acetylene dicarboxylic acid, which has a high density of acid groups (although a weak acid), yields a specific resistance of 3 x 10^6 ohm-cm at 50°C (10). Ice has been doped with HF to increase the proton density, thereby producing a mode of conduction somewhat analogous to that of aqueous solutions, but in so doing the specific resistance was decreased to only about 10^5 ohm-cm (11).

The specific resistances of hydrated organic ion exchange membranes can run as low as 10 ohm-cm. Because of the large difference between this value and the values mentioned above, reasonable conductivities might be attained only in a material which conducts by a similar aqueous mechanism, such as in zirconium phosphate (6). The amorphous aluminosilicates and the zeolites also show cation exchange properties (12), but they are relatively unstable in acids, so that they are not readily hydrogen-exchanged to form proton-conducting solid electrolytes.

Recent investigations of inorganic ion exchangers for use in nuclear reactor water purification have dealt with the phosphates, arsenates, tungstates, and molybdates of zirconium, thorium, and titanium (13). Amphlett (14) has made an extensive study of the properties of zirconium phosphate, which appears to be one of the more stable hydrogen exchangers. He reports that it can be refluxed in water for several weeks without appreciable breakdown. It is an amorphous solid formed by the precipitation of a soluble zirconyl salt with phosphoric acid, consisting essentially of an O-Zr-O-Zr chain with $-O-PO(OH)_2$ groups attached to each Zr atom. Naturally the number of phosphate groups per Zr atom is going to depend on the conditions under

which it is made, and the cross linkage between adjacent phosphate groups by dehydration is going to depend on the thermal treatment of the product. Zirconium phosphate prepared using an excess of phosphoric acid and not subjected to high temperature has a high density of replaceable protons and is relatively insoluble.

Experimental

Preparation of zirconium phosphate.—The zirconium phosphate employed in these conductivity measurements was prepared as follows: 20g of $ZrO(NO_3)_2 \cdot 2H_2O$ were dissolved in 500 cm^3 of water. To this a solution of 50 cm^3 of 86.3% phosphoric acid in 250 cm^3 of water was added rapidly. The solution was stirred rapidly during the addition of the reagents, and the stirring was continued for about 5 min. Water was added so that the total volume was increased to 3.5 liters, and the solids were allowed to settle. The solids were washed by decantation several times, and were finally filtered and dried overnight at 60°C. More water was added to the solid product, and the gel particles broke apart with audible crackling to a final product having a particle size in the range 0.1-0.5 mm.

During the preparation the ratio of phosphorus to zirconium in the starting solutions was high, approximately 10, so that the solid product would be the normal phosphate $ZrO(H_2PO_4)_2$, which has the maximum hydrogen content.

Preparation of powder compacts for conductivity measurements.—Since there were no particles of the product large enough for use in conductivity measurements, it was necessary to employ powder compacts. These were 17.0 mm in diameter and about 3 mm thick. The densities of the compacts fell in the range 2.0-2.2 g/cm^3. On soaking in water, the pellets were observed to undergo a 20-30% increase in volume, although the pellets retained their shape and appeared to suffer no degradation of mechanical properties. Because of this expansion conventional electrodes, such as those made from conducting paints, could not be employed. In order to overcome this difficulty, 100 mg of finely divided zirconium phosphate and 50 mg of platinum black were mixed, and one half of this mixture was spread over each face of the compact after it had been formed at a pressure of 13,000 psi. After a final pressing at 33,000 psi the electrode layers showed no tendency to peel off when the pellets were soaked in water. The electrodes so formed showed a resistance of only a few ohms from one point to another on each face.

Conductivity measurements.—For measurements of conductivity *vs.* temperature the apparatus shown in Fig. 1 was placed in an oven. Platinum disks were pressed against each face of the compact, and silicone rubber gaskets prevented the escape of water vapor from the apparatus. Therefore, the measurements were conducted under conditions of constant water content. A General Radio Company type 1650A Impedance Bridge was used for the measurements, with a variable capacitor across one leg of the bridge to balance out capacitive effects in the sample.

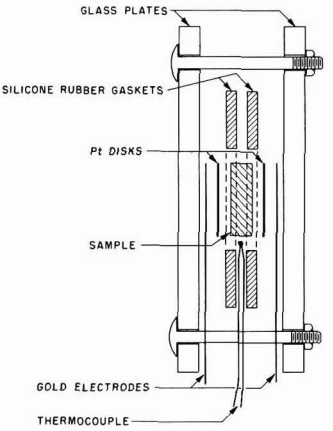

Fig. 1. Conductivity apparatus

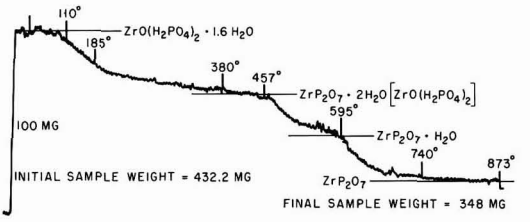

Fig. 2. Thermogram for zirconium phosphate

The frequency dependence of the conductivity was low, as is seen in Table I, an indication that electrode polarization effects were absent (15).

Results and Discussion

Thermogravimetric analysis.—In order to obtain a rough idea as to the thermal stability of the zirconium phosphate a thermogravimetric analysis was conducted on the material as dried at 60°C at a heating rate of 5°C/min. This is shown in Fig. 2. When prepared in the manner described previously it should have a composition near $ZrO(H_2PO_4)_2 \cdot XH_2O$. If one assumes that the final product has the empirical formula ZrP_2O_7, as is done in the standard phosphate analysis for zirconium, the two breaks in the curve correspond closely to the loss of one water molecule at 470°C and another at 600°C by the condensation of adjacent phosphate groups. The water lost at lower temperatures is water originally retained in the gel structure, and the initial composition is then approximately $ZrO(H_2PO_4)_2 \cdot 1.6H_2O$.

On soaking in water the volume of the compact used for the conductivity measurements increased

Table I. Frequency dependence of conductivity

Frequency, cps	Resistance, ohms × 10^{-4}
2000	3.98
1000	4.00
500	4.00
200	4.02
100	4.02
50	4.02
25	4.02

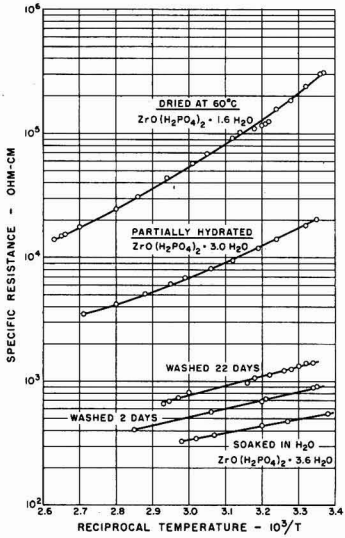

Fig. 3. Specific resistance of zirconium phosphate *vs.* 1/*T*

by 22%. Assuming the increase in volume was due to the addition of water with a density of 1.0, and since the density of the compact initially was 2.0, the composition of the soaked compact should be approximately $ZrO(H_2PO_4)_2 \cdot 3.6H_2O$.

Conductivity measurements.—Measurements of conductivity *vs.* temperature were carried out on a pellet immediately after pressing from zirconium phosphate dried at 60°C, and on the same pellet after partial and complete hydration. The temperature dependence of resistivity ρ can usually be expressed over narrow ranges by an equation of the form $\rho = \rho_0 e^{E/RT}$, where E is an activation energy for the conduction process. Therefore, E can be obtained from the slope of a plot of log ρ *vs.* $1/T$. Figure 3 contains plots of log ρ *vs.* $1/T$ for the samples in each of the three states of hydration. It is seen that the activation energy decreases from 9.8 kcal/mole to 2.6 kcal/mole as the sample becomes more hydrated. The activation energy for the soaked pellet falls in the range normally found for conduction in aqueous solutions (5). If the assumption is made that there is a solution of $2H_2PO_4$ units for every $3.6H_2O$ molecules, a rough calculation of the expected conductivity can be made using the second ionization constant of phosphoric acid. The above ratio of H_2PO_4/H_2O corresponds to a 75% solution of phosphoric acid, which would have a density of 1.58 g/cm³. K_2 for phosphoric acid at 25°C is 6.2 x 10^{-8} (16), and this would result in a proton concentration of about 9 x 10^{-4}g equivalent/liter. Since each cubic centimeter of solid would contain about 0.80 cm³ of the above solution, and since the equivalent ionic conductance of protons is about 350 ohm^{-1}-cm^2, the conductance would be of the order of 3 x $10^{-4}ohm^{-1}$. This would correspond to a specific resistance for the solid of about 3000 ohm-cm. This is about a factor of 5 greater than the specific resistance of 550 ohm-cm observed on this material at 25°C. Considering the assumptions involved, especially the assumption that K_2 for the phosphoric acid is not affected by reaction with the hydrated zirconium oxide, the agreement is within reason. It has already been observed by Amphlett that a titration curve of zirconium phosphate *vs.* NaOH does not give two inflection points characteristic of K_2 and K_3 for phosphoric acid, but gives a relatively smooth curve.

Activation energies were calculated from the slopes of the three curves at the low end of the temperature range. They are 9.8, 6.4, and 2.6 kcal/mole for increasing degrees of hydration. The last value corresponds to the temperature variation observed in aqueous solutions as a result of the decrease in viscosity with increasing temperature.

Effect of continuous washing on the conductivity.—Because of the nature of the zirconium phosphate, it would be expected that continuous washing would hydrolyze the solid, releasing phosphoric acid and eventually converting the zirconium phosphate to zirconium hydroxide (hydrous zirconium oxide). The compact employed in the measurements above was washed continuously, and the conductivity was measured after 2 and 22 days. These results are also shown in Fig. 3. The figure shows that the conductivity decreased, although the slope of the plot remained relatively constant. This would indicate that the mode of conduction remained the same, namely, transport of H^+ ions in an aqueous system, but that the number of current carriers (H^+ ions) decreased as a result of the hydrolysis mentioned above.

Fuel cell using a zirconium phosphate membrane.—A cell similar to that of Dravnieks and Bregman was prepared by pressing a 1 mm thick disk from 90% zirconium phosphate and 10% powdered Teflon at a pressure of 35,000 psi. This was soaked in water, each face was sprinkled with Pt black, and a Pt screen was placed against this in a simple hydrogen-oxygen fuel cell configuration. The polarization curve for this cell is shown in Fig. 4. The resistance of the membrane as calculated from the slope of the polarization curve was 110 ohms, which agrees roughly with the measured value of 150 ohms. This value of 110 ohms corresponds to a specific resistance of about 6000 ohm-cm, showing that the Teflon binder in this case decreased the conductivity sub-

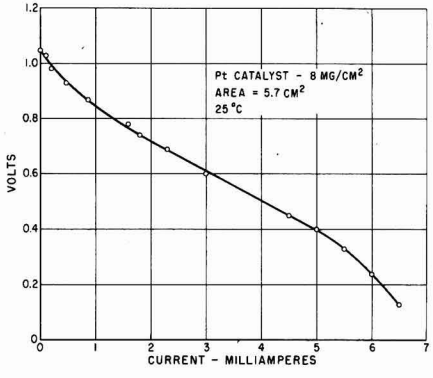

Fig. 4. Polarization curve for H_2-O_2 fuel cell with zirconium phosphate membrane.

stantially. Obviously, it is desirable to increase the conductivity by better membrane construction and by the use of higher temperatures. Because of the aqueous mechanism of ion transport pressurization would be required above 100°C.

It is evident that such a membrane has two major drawbacks from the standpoint of fuel cell applications: (*A*) Low conductivity. This might be partially overcome if sufficiently thin membranes could be fabricated. (*B*) Changes due to hydrolysis.

Manuscript received Nov. 13, 1961; revised manuscript received March 16, 1962.

Any discussion of this paper will appear in a Discussion Section to be published in the June 1963 JOURNAL.

REFERENCES

1. W. T. Grubb and L. W. Niedrach, *This Journal*, **107**, 131 (1960).
2. E. Joachim and W. Vielstich, *Electrochim. Acta*, **3**, 244 (1960).
3. H. F. Hunger, *Proc.* 14th Annual Power Sources Conference, Atlantic City, May 17, 1960.
4. R. M. Lurie, C. Berger, and R. J. Shuman, American Chemical Society Symposium on Recent Advances in Fuel Cells, Chicago, September 3, 1961.
5. W. T. Grubb, *J. Phys. Chem.*, **63**, 55 (1959).
6. A. Dravnieks and J. I. Bregman, Fuel Cell Symposium of the Electrochemical Society, Detroit, Oct. 1, 1961. (See also *Chem. and Eng. News*, Oct. 16, 1961, p. 40.)
7. G. H. J. Broers, "High Temperature Fuel Cells," Dissertation, University of Amsterdam (1958).
8. R. C. Evans, "An Introduction to Crystal Chemistry," Cambridge University Press (1948).
9. J. L. Weininger, *This Journal*, **106**, 475 (1959).
10. J. M. Pollack and A. R. Ubbelohde, *Trans. Faraday Soc.*, **52**, 1112 (1956).
11. H. Granicher, C. Jaccard, P. Scherrer, and A. Steinemann, *Discussions Faraday Soc.*, **23**, 50 (1957).
12. R. Kunin, "Ion Exchange Resins," 2nd ed., John Wiley & Sons, Inc., New York (1958).
13. H. F. Walton, *Ann. Rev. Phys. Chem.*, **10**, 123 (1959).
14. C. B. Amphlett, L. A. McDonald, and M. J. Redman, *J. Inorg. and Nuclear Chem.*, **6**, 220 (1958).
15. G. Kortum and J. O'M. Bockris, "Textbook of Electrochemistry," Elsevier, New York (1951).
16. C. D. Hodgman, Handbook of Chemistry and Physics, 42nd ed., Chemical Rubber Publishing Co., Cleveland.

Brief Communications

The Chemical Polishing of Rare Earth Tellurides

P. Bro

Research and Advanced Development Division, Avco Corporation, Wilmington, Massachusetts

There is a growing interest in the semiconducting compounds of the rare earth metals, and several compounds have been reported (1) with interesting thermoelectric properties. One of the problems associated with the electrical measurements on these compounds is the preparation of reproducible surfaces. Mechanical polishing can be employed, but it generates a strained surface which gives rise to anomalies in the surface properties of the samples. A chemical or electrochemical method generally is preferred in the preparation of semiconductor surfaces for electrical and optical measurements.

We have investigated a variety of chemical etches for the rare earth tellurides and the main problem was that of finding a reactive medium that could dissolve the metal and the tellurium at comparable rates under conditions which would produce a polished surface. A satisfactory chemical polish was found for the sesqui- and higher tellurides, and it consisted of 10 ml glacial acetic acid and 1 ml bromine. It gave an etch rate on La_2Te_3 at room temperature of 0.84 g/sec m^2 when freshly prepared. An etching period of 20-60 sec appeared satisfactory. The etch rate could be increased by the addition of ethyl alcohol, and an etch rate of 1.63 g/sec m^2 was obtained with 5 ml HAc, 5 ml EtOH, and 1 ml Br. The gradual heating of the latter etch due to the exothermic Br/EtOH reaction also increased the etch rate. An inferior polish was obtained in the presence of excess amounts of alcohol or when the etch was not strictly fresh.

An interesting observation was obtained with La_2Te_3 in etches composed of HBr, H_2O, and Br, *e.g.*, 10 ml fuming HBr, 30 ml H_2O, 1 ml Br. Initially, the sample acquired a high apparent polish, but a continued exposure to the etch under quiescent conditions led to the formation of long, twisted tellurium whiskers which grew profusely and very rapidly from the surface of the sample. The initial polish was found to be due to the formation of a tellurium phase on the surface which could be removed quite readily. The growth of the tellurium whiskers appeared to depend on the formation of highly mobile tellurium atoms in the crystal lattice by the preferential dissolution of the rare earth metal, and it is a phenomenon which lends itself to experimentation in the interesting field of crystal growth mechanisms.

Acknowledgments

The synthesis of the rare earth tellurides was carried out by W. Mularz and his assistance is gratefully acknowledged.

Manuscript received March 15, 1962.

Any discussion of this paper will appear in a Discussion Section to be published in the June 1963 JOURNAL.

REFERENCE

1. J. F. Miller, F. J. Reid, and R. C. Himes, *This Journal*, **106**, 1043 (1959).

Gallium Phosphide Crystal Growth by Vapor Phase Iodide Transport

A. S. Roy[1]

Bell Telephone Laboratories, Incorporated, Murray Hill, New Jersey

The growth of small GaP crystals from the vapor phase has been reported by Antell and Effer by mixing GaI and phosphorus and slowly cooling from 1050°C in a quartz tube (1). Gershenzon and Mikulyak (2) allowed Ga_2O to react with phosphorus at about 1000°C in a sealed quartz tube and obtained thin whiskers and filaments of GaP up to 0.2 mm in width. Epitaxial films of GaP have been grown by Frosch and Foy (3) and by Moest and Shupp (4). Holonyak reported growth of massive polycrystals of GaP using halides as transport agents (5).

[1] Present address: Israel Atomic Energy Commission, Rehovoth, Israel.

The experiments reported here describe the growth of GaP single crystals whose sizes were up to 2 mm in each dimension. Growth was from the vapor phase at temperatures between 780° and 935°C and about atmospheric pressure in a sealed quartz tube containing a polycrystalline GaP source (about 0.5g), H_2, and I_2, with initial mole ratios of 8:7:1. The tube was 18 cm long and of 2 cm inside diameter. A temperature gradient provided the potential for the net reaction of transferring GaP from the source to a lower tempera-

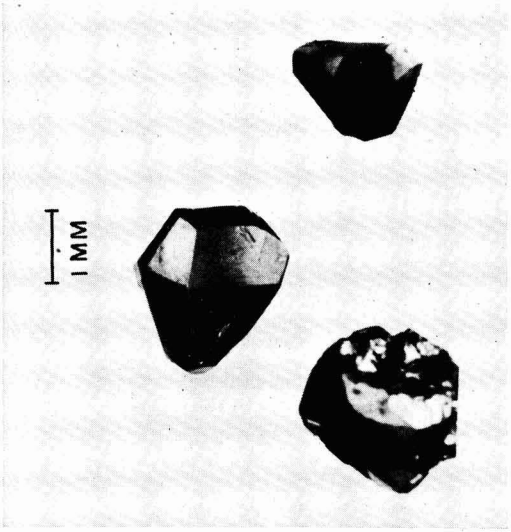

Fig. 1. GaP single crystals grown at 946°C at a point of 5°C below source temperature.

ture. Larger crystals were obtained when the gradient along the tube was small. The largest crystals were, in general, found at the middle of the tube rather than at the coolest end. Figure 1 shows several crystals over 2 mm in size grown at 946°C at a point 5°C below the temperature of the source material. Smaller crystals were obtained with larger gradients. When the cold end was reduced to 780°C with the source at 950°C, aggregates of crystallites approximately 0.02 mm in size deposited at the cold end. In one case, a similar gradient produced GaP needles with typical dimensions of 0.1x0.4x2 mm. The transport rate increased with the source temperature. For a temperature difference of 50°C between the source and the colder end of the tube and with the source at 850° and 950°C, the transport rates were 25 and 75 mg/hr, respectively.

The crystals adhered strongly to the quartz. The contact area was observed by reversing the temperature gradient and transferring the GaP to a cooler region of the tube. Gallium phosphate and α-quartz crystals ~0.1 mm in size were side reaction products. These were identified by x-ray diffraction measurements. Typical GaP crystals were analyzed spectrographically after removing the regions adhering to the quartz by etching. The concentrations of detectable impurities, Ca, Mg, Al, Si, Fe, and Ni, were less than 50 ppm. The crystals were always *n*-type, suggesting that Si was the dominant electrically active impurity.

The results of these preliminary experiments indicate the feasibility of relatively rapid growth of large GaP crystals at comparatively low temperature and pressure.

Manuscript received March 22, 1962.

Any discussion of this paper will appear in a Discussion Section to be published in the June 1963 JOURNAL.

REFERENCES

1. G. P. Antell and D. Effer, *This Journal*, **106**, 509 (1961).
2. M. Gershenzon and R. M. Mikulyak, *ibid.*, **108**, 548 (1961).
3. C. J. Frosch and P. W. Foy, Electrochem. Soc. Meeting Abstract No. 142, Detroit, October 1961, *This Journal*, **108**, 177C (1961).
4. R. Moest and B. R. Shupp, *ibid.*, Abstract No. 143, **108**, 178C (1961).
5. N. Holonyak, Jr., Scientific Report No. 2b (GE Company, Syracuse, New York) AF 19 (604)-6623, October 1960.

Monographs of The Electrochemical Society

ECS Series

The following are books developed and sponsored by The Electrochemical Society and published by John Wiley & Sons, Inc., 440 Park Ave. South, New York 16, N. Y. Members of The Electrochemical Society can receive a 33 1/3% discount by ordering volumes from Society Headquarters, 30 East 42 St., New York 17, N. Y. Book and invoice will be mailed by John Wiley & Sons. Nonmembers (including subscribers) should order direct from Wiley.

Corrosion Handbook. Edited by Herbert H. Uhlig. Published 1948, 1188 pages, **$16.00**

Modern Electroplating. Edited by Allen G. Gray. Published 1953, 563 pages, **$8.50** (Out of print; new edition to be published sometime in 1962)

Abstracts of the Literature on Semiconducting and Luminescent Materials and Their Applications. Compiled by Battelle Memorial Institute.

Vol. I, 1953 Issue—published 1955, 169 pages, **$5.00** (soft cover)

Vol. II, 1954 Issue—published 1955, 200 pages, **$5.00** (soft cover)

Vol. III, 1955 Issue—Edited by E. Paskell; published 1957, 322 pages, **$10.00** (hard cover)

Vol. IV, 1956 Issue—Edited by E. Paskell; published 1959, 456 pages, **$12.00** (hard cover)

Vol. V, 1957 Issue—Edited by C. S. Peet; published 1960, 449 pages, **$12.00** (hard cover)

Vol. VI, 1958 Issue—Edited by J. J. Bulloff and C. S. Peet; published 1961, 528 pages, **$14.00** (hard cover)

Vol. VII, 1959 Issue—Edited by J. J. Bulloff and C. S. Peet; published 1962, 728 pages, **$20.00** (hard cover)

Electrochemistry in Biology and Medicine. Edited by Theodore Shedlovsky. Published 1955, 369 pages, **$11.50**

Vapor Plating (The Formation of Metallic and Refractory Coatings by Vapor Deposition), by C. F. Powell, I. E. Campbell, and B. W. Gonser, Published 1955, 158 pages, **$6.00**

High-Temperature Technology (Materials, Methods, and Measurements). Edited by I. E. Campbell. Published 1956, 526 pages, **$15.00** (Out of print; new edition to be published sometime in 1962)

***Stress* Corrosion Cracking and Embrittlement.** Edited by W. D. Robertson. Published 1956, 202 pages, **$7.50**

Arcs in Inert Atmospheres and Vacuum. Edited by W. E. Kuhn. Published 1956, 188 pages, **$7.50**
(Papers Presented at the Symposium on Arcs in Inert Atmospheres and Vacuum of the Electrothermics and Metallurgy Division of The Electrochemical Society, April 30 and May 1, 1956, San Francisco, Calif.)

Technology of Columbium (Niobium). Edited by B. W. Gonser and E. M. Sherwood. Published 1958, 120 pages, **$7.00**
(Papers Presented at the Symposium on Columbium—Niobium of the Electrothermics and Metallurgy Division of The Electrochemical Society, May 15 and 16, 1958, Washington, D. C.)

The Structure of Electrolytic Solutions. Edited by Walter J. Hamer. Published 1959, 441 pages, **$18.50**
(Based on a Symposium held in Washington, D. C., in May 1957, sponsored by The Electrochemical Society, New York, and The National Science Foundation, Washington, D. C.)

Mechanical Properties of Intermetallic Compounds. Edited by J. H. Westbrook. Published 1959, 435 pages, **$9.50**
(A Symposium, Sponsored by the Electrothermics and Metallurgy Division of The Electrochemical Society, May 4, 5, and 6, 1959, Philadelphia, Pa.)

The Surface Chemistry of Metals and Semiconductors. Edited by Harry C. Gatos, with the assistance of J. W. Faust, Jr., and W. J. La Fleur. Published 1960, 526 pages, **$12.50**
[Proceedings of an International Symposium Sponsored Jointly by the Office of Naval Research and The Electrochemical Society, Inc. (Corrosion and Electronics Divisions), October 19, 20, and 21, 1959, Columbus, Ohio]

Transactions of the Symposium on Electrode Processes. Edited by Ernest Yeager. Published 1961, 374 pages, **$20.00**
(The papers and discussions of the Symposium on Electrode Processes, sponsored jointly by the U. S. Air Force, Office of Scientific Research, and The Electrochemical Society, Inc., Philadelphia, Pa., May 1959)

Iodide Metals and Metal Iodides, by Robert F. Rolsten. Published 1961, 441 pages, **$17.50**

Vacuum Metallurgy

Vacuum Metallurgy, third printing, 1958. Edited by J. M. Blocher, Jr.; 216 pages; **$5.00,** less a 20% discount to ECS members only. Available from Electrochemical Society Headquarters, 30 East 42 St., New York 17, N. Y.
(Papers Presented at the Vacuum Metallurgy Symposium of the Electrothermics and Metallurgy Division of The Electrochemical Society held in Boston, Mass., October 6 and 7, 1954)

FUTURE MEETINGS OF
The Electrochemical Society

★ ★ ★

Boston, Mass., September 16, 17, 18, 19, and 20, 1962

Headquarters at the Statler-Hilton Hotel
Sessions will be scheduled on
Batteries (General Sessions on primary and secondary batteries, and fuel cells), Battery—Theoretical Electrochemistry Joint Symposium on Porous Electrodes, Corrosion, Corrosion—Electronics Joint Symposium on Phenomena at Interfaces, Electrodeposition (including a Symposium on Alloy Electrodeposition), Electrodeposition—Electronics Joint Symposium on Electrochemical Processes for Semiconductor Devices, Electronics—Semiconductors (including a Symposium on Semiconductor Phenomena), Electrothermics and Metallurgy (including a Symposium on Hot Pressing), Electrothermics and Metallurgy—Corrosion Joint Symposium on High-Temperature Corrosion

★ ★ ★

Pittsburgh, Pa., April 14, 15, 16, 17, and 18, 1963

Headquarters at the Penn Sheraton Hotel
Sessions probably will be scheduled on
Electric Insulation, Electronics (including Luminescence and Semiconductors), Electrothermics and Metallurgy, Industrial Electrolytics, and Theoretical Electrochemistry

★ ★ ★

New York, N. Y., September 29, 30, and October 1, 2, and 3, 1963

Headquarters at the New Yorker Hotel

★ ★ ★

Toronto, Ont., Canada, May 3, 4, 5, 6, and 7, 1964

Headquarters at the Royal York Hotel

★ ★ ★

Washington, D. C., October 11, 12, 13, 14, and 15, 1964

Headquarters at the Sheraton-Park Hotel

Papers are now being solicited for the meeting to be held in Pittsburgh, Pa., April 14, 15, 16, 17, and 18, 1963. **Triplicate copies of the usual 75-word abstract, as well as of an extended abstract of 500-1000 words** (*see* notice on following page), are due at Society Headquarters, 30 East 42 St., Rm. 1806, New York 17, N. Y., *not later than December 14, 1962* in order to be included in the program. *Please indicate on abstract for which Division's symposium the paper is to be scheduled, and underline the name of the author who will present the paper.* No paper will be placed on the program unless one of the authors, or a qualified person designated by the authors, has agreed to present it in person. An author who wishes his paper considered for publication in the JOURNAL or in ELECTROCHEMICAL TECHNOLOGY should send triplicate copies of the manuscript to the Managing Editor of the appropriate publication, 30 East 42 St., Rm. 1806, New York 17, N. Y.

Presentation of a paper at a technical meeting of the Society does not guarantee publication in the JOURNAL or in ELECTROCHEMICAL TECHNOLOGY. However, all papers so presented become the property of The Electrochemical Society, and may not be published elsewhere, either in whole or in part, unless permission for release is requested of and granted by the Editor. Papers already published elsewhere, or submitted for publication elsewhere, are not acceptable for oral presentation except on invitation by a Divisional program Chairman.

Extended Abstract Booklet Publication Program Being Instituted for Society's 1963 Spring Meeting in Pittsburgh

The Board of Directors has provided that the National Office shall assist Divisions with the mechanics of publishing Extended Abstracts for sessions involving 15 or more papers at our National Meetings.

This program is being instituted at our 1963 Spring Meeting in Pittsburgh, and all Divisions which will hold Technical Sessions will participate in this publication program. The Divisions will handle the technical editing of the abstracts following which the Society Office will arrange for the printing and distribution of the booklet, thus relieving Division representatives of this responsibility. Each Division program will be the subject of a separate Extended Abstract Booklet covering papers presented at its Technical Sessions.

This means that each author who submits a paper for presentation at our meeting should do three things:

1—Submit *three* **copies of the usual 75-word abstract of the paper for publication in the printed program of the meeting;**

2—Simultaneously submit *three* **copies of an extended abstract of the paper of 500-1000 words; and**

3—Send the 75-word abstract and the 500-1000-word extended abstract to Society Headquarters, 30 East 42 St., New York 17, N. Y., *not later than December 14, 1962.*

The Extended Abstract Booklets will be published by photo-offset reproduction *from typewritten copy submitted by the author.* Special care should be given to the following typing instructions so as to establish some uniformity in printing:

1—Abstracts are to be 500-1000 words in length.

2—Use white bond paper, size 8½ x 11 inches.

3—Abstracts should be typed single space.

4—Use 1 inch margin top and bottom of the page, and 1½ inches on each side.

5—Figures should be pasted in within the typing dimensions indicated. Captions should be typed not wider than figure dimensions and pasted in proper place in the abstract. Figure captions should appear at bottom of figure. Table titles should appear at top of tables.

6—Wherever possible, avoid use of halftones.

7—Title of paper should be in capital letters. Author(s) name and affiliation should be typed immediately below.

8—Mail to Society Headquarters *unfolded.*

Members and JOURNAL subscribers will receive notice of Extended Abstracts Booklets to be scheduled for publication. The notices will be accompanied by order blanks for the copies desired. Orders must be submitted with remittance. The advance orders will be necessary for estimating numbers of booklets to be printed and will be mailed to purchasers prior to the meeting. Some extra copies will be available at the meeting but the advance-paid order is the only way to be assured of getting copies.

Boston Meeting

THE ELECTROCHEMICAL SOCIETY

September 16, 17, 18, 19, and 20, 1962

Sunday through Thursday

CONDENSED TECHNICAL PROGRAM

Monday, September 17, 1962

Battery—Theoretical Electrochemistry (Abstracts 1-12) 9:00 A.M.-12:00 M.; 2:00-5:05 P.M. (Ballroom Assembly)
Corrosion (Abstracts 50-61) 9:00 A.M.-12:00 M.; 2:00-4:30 P.M. (Parlors A and B)
Corrosion—Electronics (Abstracts 77-89) 9:00-11:50 A.M.; 2:00-5:10 P.M. (Imperial Ballroom)
Electrodeposition—Electronics (Abstracts 103-110) 8:55 A.M.-12:00 M.; 2:00-3:00 P.M. (Georgian Room)
Electrodeposition (Abstracts 111-114) 3:00-5:00 P.M. (Georgian Room)
Electronics—Corrosion (Abstracts 77-89) 9:00-11:50 A.M.; 2:00-5:10 P.M. (Imperial Ballroom)
Electronics—Electrodeposition (Abstracts 103-110) 8:55 A.M.-12:00 M.; 2:00-3:00 P.M. (Georgian Room)
Electronics—Semiconductors, 7:00-8:30 P.M. (Imperial Ballroom)
Electrothermics & Metallurgy (Abstracts 165-175) 9:00-11:50 A.M.; 2:00-4:55 P.M. (Parlor C)
Theoretical Elect.ochemistry—Battery (Abstracts 1-12) 9:00 A.M.-12:00 M.; 2:00-5:05 P.M. (Ballroom Assembly)

Tuesday, September 18, 1962

Battery—Theoretical Electrochemistry (Abstracts 13-19) 9:00 A.M.-12:15 P.M. (Ballroom Assembly)
Battery (Abstracts 20-24) 2:30-4:40 P.M. (Ballroom Assembly)
Corrosion (Abstracts 62-71) 9:00-11:30 A.M.; 2:00-4:30 P.M. (Parlors A and B)
Corrosion—Electronics (Abstracts 90-102) 9:00-11:50 A.M.; 2:00-4:50 P.M. (Imperial Ballroom)
Electrodeposition (Abstracts 115-127) 9:00 A.M.-12:00 M.; 2:00-5:00 P.M. (Georgian Room)
Electronics—Corrosion (Abstracts 90-102) 9:00-11:50 A.M.; 2:00-4:50 P.M. (Imperial Ballroom)
Electrothermics & Metallurgy (Abstracts 176-180) 2:00-5:00 P.M. (Parlor C)
Theoretical Electrochemistry—Battery (Abstracts 13-19) 9:00 A.M.-12:15 P.M. (Ballroom Assembly)

Wednesday, September 19, 1962

Battery (Abstracts 25-37) 9:00 A.M.-12:00 M.; 2:00-4:50 P.M. (Ballroom Assembly)
Corrosion (Abstracts 72-76) 9:00-11:30 A.M. (Parlors A and B)
Corrosion—Electrothermics & Metallurgy (Abstracts 181-192) 9:00-11:55 A.M.; 2:00-4:55 P.M. (Georgian Room)
Electronics—Semiconductors (Abstracts 129-146) 9:00 A.M.-12:00 M.; 2:00-5:00 P.M. (Imperial Ballroom)
Electrothermics & Metallurgy—Corrosion (Abstracts 182-192) 9:00-11:55 A.M.; 2:00-4:55 P.M. (Georgian Room)

Thursday, September 20, 1962

Battery (Abstracts 38-49) 9:00 A.M.-12:00 M.; 2:00-4:40 P.M. (Ballroom Assembly)
Corrosion—Electrothermics & Metallurgy (Abstracts 193-204) 9:00 A.M.-12:05 P.M.; 2:00-4:55 P.M. (Georgian Room)
Electronics—Semiconductors (Abstracts 147-164) 9:00 A.M.-12:00 M.; 2:00-5:00 P.M. (Imperial Ballroom)
Electrothermics & Metallurgy—Corrosion (Abstracts 193-204) 9:00 A.M.-12:05 P.M.; 2:00-4:55 P.M. (Georgian Room)

GENERAL INFORMATION

Convention Headquarters is the Statler Hilton Hotel, Park Square at Arlington St., Boston 17, Mass.

Rates per day for rooms are; single $10.00-15.50; double-bed room $16.00-21.00; twin-bed room $18.50-22.00.

Requests for room reservations should be mailed to the Statler Hilton Hotel, Park Square at Arlington St., Boston 17, Mass. If accommodations are not available at the Statler Hilton, the hotel will make suitable reservations for you at a nearby hotel at a comparable price.

BE SURE to state that you will be attending the Electrochemical Society Meeting. If your wife will be attending, be sure so to indicate on your request for reservations.

The office of the Secretary is Parlor D, Ballroom floor.
The Boston Local Section office is Parlor E, Ballroom floor.
The Press and Publicity Office is Parlor F, Ballroom floor.
Ladies' Headquarters is the Hancock Room, Ballroom floor.

REGISTRATION

The Registration Desk will be on the Mezzanine floor Sunday, September 16, through Thursday, September 20, 1962.

The registration schedule is:

Sunday, September 16—2:00-9:00 P.M.
Monday, September 17—7:30 A.M.-5:00 P.M.
Tuesday, September 18—8:00 A.M.-4:00 P.M.
Wednesday, September 19—8:00 A.M.-4:00 P.M.
Thursday, September 20—9:00 A.M.-12:00 M.

Registration fees are:

Technical Session Registration (Men and Women)	
Members	$ 7.00
Nonmember Speakers and Coauthors	7.00
Nonmembers	20.00*
Student Members	Complimentary
Student Nonmembers	2.00
Thursday only	5.00
Ladies' Registration Fee for Social Events	5.00

* If a nonmember fills out an application form and subsequently is elected to membership in the Society, the difference between the nonmember and member registration fee will be applied to his first year's dues. If his membership begins on January 1, he is entitled to the entire differential; if his membership begins on July 1, he is entitled to half the differential.

All of the technical sessions will be held in various rooms on the Mezzanine floor.

INFORMATION ABOUT BOSTON

Boston abounds with thousands of points of interest. It is the birthplace of liberty and has many historic shrines. The famous Freedom Trail provides an opportunity to view many of the historic sights in and around Boston, including Boston Common, the State House, Park Street Church, Kings Chapel, Benjamin Franklin's birthplace, the Boston Massacre, Old Faneuil Hall, Paul Revere House, Old North Church, Old Ironsides, Bunker Hill Monument, to name a few. The suburbs of Boston provide additional historical shrines in Plymouth, Salem, Marblehead, Cambridge, Lexington, Concord, Rockport, Gloucester, Sudbury, and many others.

Boston is famous for its sea food. As the country's largest fish-shipping port, it can choose the "best of the catch" that the cold, flavor-heightened North Atlantic waters yield. By making use of the old-fashioned Yankee cooking and "handed-down" recipes, Boston restaurants have developed many distinctive ways of preparing lobster, shellfish, and salt water fish dishes.

Boston is also one of the cultural centers of the country, with its 200 universities, colleges, and schools, its Public Library, Symphony Orchestra, Museum of Fine Arts. Several summer stock theaters will be concluding their programs during the week of the meeting. In addition, there is ample evening entertainment at many hotels and night clubs.

SYMPOSIA

The Battery—Theoretical Electrochemistry Divisions have scheduled a Joint Symposium on Porous Electrodes all day Monday and Tuesday morning in the Ballroom Assembly.

The Battery Division has scheduled a General Session on Storage Batteries Tuesday afternoon and Wednesday morning, one on Secondary and Primary Batteries Wednesday afternoon and one on Fuel Cells all day Thursday, all in the Ballroom Assembly.

The Corrosion Division has scheduled a session on Passivation and Inhibition Monday morning, one on Light Metal Corrosion Monday afternoon, one on General Corrosion Tuesday morning, one on Electrode Processes Tuesday afternoon, and another general session Wednesday morning, all in Parlors A and B.

The Corrosion—Electronics Divisions have scheduled a Joint Symposium on Phenomena at Interfaces all day Monday and Tuesday in the Imperial Ballroom.

The Electrodeposition—Electronics Divisions have scheduled a Joint Symposium on Electrochemical Processes for Semiconductor Devices all day Monday in the Georgian Room.

The Electrodeposition Division has scheduled a Symposium on Alloy Electrodeposition all day Tuesday in the Georgian Room.

The Electronics—Semiconductor Division has scheduled Recent News Papers from 7:00-8:30 P.M. on Monday in the Imperial Ballroom. Wednesday morning there will be a session on Semiconductor Materials, Wednesday afternoon on Semiconducting Compounds, Thursday morning on Semiconductor Surfaces, Thursday afternoon on Semiconducting Techniques, all in the Imperial Ballroom.

The Electrothermics and Metallurgy Division has scheduled a Symposium on Hot Pressing Monday morning and afternoon, closing the afternoon with a general session, and a Symposium on Studies in Electrolytic Cells, all in Parlor C.

The Electrothermics & Metallurgy—Corrosion Divisions have scheduled a Joint Symposium on High-Temperature Corrosion all day Wednesday and Thursday in the Georgian Room.

BOARD AND COMMITTEE MEETINGS

Sunday, Sept. 16, 2:00 P.M.—**Board of Directors,** Hancock Room, Mezzanine floor.

Monday, Sept. 17, 5:00 P.M.—**Council of Local Sections,** Hancock Room, Mezzanine floor.

Monday, Sept. 17, 5:00 P.M.—**Editorial Staff of *The Journal of The Electrochemical Society,*** Parlor F, Mezzanine floor.

Tuesday, Sept. 18, 5:00 P.M.—**Editorial Staff of *Electrochemical Technology,*** Parlor F, Mezzanine floor.

Tuesday, Sept. 18, 5:00 P.M.—**Membership Committee,** Hancock Room, Mezzanine floor.

Wednesday, Sept. 19, 12:15 P.M.—Luncheon Meeting of the **General Chairmen of Future Meetings,** Parlor C, Mezzanine floor.

Wednesday, Sept. 19, 4:00 P.M.—**Technical Committee,** Hancock Room, Mezzanine floor.

LUNCHEONS, SOCIAL AFFAIRS, AND BUSINESS MEETINGS OF DIVISIONS

Monday, Sept. 17, 5:00 P.M.—**Electrothermics & Metallurgy Division** Cocktail party, Bay State Room, lower level of the lobby floor.

Tuesday, Sept. 18, 12:30 P.M.—**Battery Division** Luncheon and Business Meeting, Ballroom Assembly.

Tuesday, Sept. 18, 12:15 P.M.—**Electrodeposition Division** Luncheon and Business Meeting, Georgian Room.

GENERAL FUNCTIONS

Symposia Chairmen Breakfasts

Special breakfasts will be held for Symposia Chairmen Monday through Thursday, Sept. 17-20. On the day on which he presides at a technical session, each Symposium Chairman should be in the Cafe Rouge, Lobby floor, at 7:45 A.M.

Sunday Evening Social Hour

There will be a Sunday evening social hour in Parlors B and C, Mezzanine floor, from 8:00 to 10:00 P.M. All those registered for The Electrochemical Society Meeting ore invited to attend.

Monday Evening Mixer

Between 8:00 and 11:00 P.M. on Monday, Sept. 17, there will be a get-acquainted evening in the Georgian Room, Mezzanine floor. Everyone registered for the meetings is welcome.

The Electrochemical Hall of Fame—The Story of the Men Who Built the Electrochemical Industry with Niagara Power by F. L. Koethen

A special lecture will be given by F. L. Koethen at 4:15 P.M. on Tuesday, Sept. 18, in Parlor C, Mezzanine floor. While sponsored by the Electrothermics and Metallurgy Division, everyone registered at the meeting is cordially invited to attend. Mr. Koethen, who has been associated with the electrochemical industry in the Niagara Falls area for over fifty years, is a well-known historian of the region and its industrial electrochemical development.

Tuesday Acheson Medal Reception and Banquet

On Tuesday evening, Sept. 18, a reception and banquet will be held for the Acheson Medalist, Dr. Charles L. Faust. Cocktails will be served at 6:30 P.M. in Parlors A, B, and C, the banquet in the Georgian Room at 7:15 P.M. Dr. Faust will deliver the Acheson Medal address.

Wednesday Clambake at Plymouth

Buses will leave the main entrance of the Statler Hilton Hotel from 5:00 to 6:00 P.M. for the clambake at Plymouth, Mass., rain or shine. If you've been to a clambake, you know what fun one is; if you haven't, here's your chance to find out.

PLANT TRIPS

Tuesday morning.—A trip for 40 is planned for Tuesday, Sept. 18, to the High Voltage Engineering Corp., Burlington,

1963 SPRING MEETING
at the
Penn Sheraton Hotel
PITTSBURGH, PENNSYLVANIA
April 14, 15, 16, 17, and 18, 1963

Sessions probably will be scheduled on

Electric Insulation
Electronics—Including Luminescence and Semiconductors
Electrothermics and Metallurgy
Industrial Electrolytics
Theoretical Electrochemistry

Papers are now being solicited for the meeting to be held in Pittsburgh, Pa., April 14, 15, 16, 17, and 18, 1963. Triplicate copies of each abstract (*not exceeding 75 words in length*) are due at Society Headquarters, 30 East 42 St., New York 17, N.Y., not later than December 14, 1962 in order to be included in the program. Please indicate on abstract for which Division's symposium the paper is to be scheduled, and underline the name of the author who will present the paper. No paper will be placed on the program unless one of the authors, or a qualified person designated by the authors, has agreed to present it in person. An author who wishes his paper considered for publication in the JOURNAL should send triplicate copies of the manuscript to the Managing Editor of the JOURNAL, 30 East 42 St., New York 17, N.Y.

Also on **December 14,** 1962, a **500-1000-word abstract** of each paper to be included in the Technical Program must be at The Electrochemical Society headquarters. Details on preparing these 500-1000-word abstracts for offset appear in the August 1962 issue of the JOURNAL, page 184C.

Presentation of a paper at a technical meeting of the Society does not guarantee publication in the JOURNAL. However, all papers so presented become the property of The Electrochemical Society and may not be published elsewhere, either in whole or in part, unless permission for release is requested of and granted by the Editor. Papers already published elsewhere, or submitted for publication elsewhere, are not acceptable for oral presentation except on invitation by a Division program Chairman.

Mass., the world's leading manufacturer of particle acceleration types. These units produce high-energy charged particles whose applications embrace nearly every major category of science and industry. A short movie "High Energy Radiation for Mankind" will be shown.

Tuesday afternoon.—Tuesday afternoon, Sept. 18, a tour for 40 people has been arranged to visit the Avco Research and Advanced Development Division at Wilmington, Mass. Avco is engaged in research in phenomena of re-entry, preparation of prototypes of long-range missiles, development of new materials for high temperatures of re-entry and materials for orbiting outer-space vehicles. Facilities to be shown include high-temperature plasma arcs, ballistic range, Material Development laboratories, solar furnaces, and shock tubes for hypervelocity simulation. U.S. citizenship required.

Wednesday morning.—On Sept. 19, a morning trip is scheduled for the Western Electric Company Merrimack Valley Works, North Andover, Mass. The principal product of the Works is telephone transmission carrier equipment and includes products such as radio relays and repeaters used to increase the capacity of existing telephone voiceways across America. The shop tour will visit Printed Wiring Board, Plating, Ferrite, Heat Treating, Tape Core, Precision Ground Transformer, Quartz Crystal, and the Engineering of Manufacture Laboratory areas. U.S. citizenship required.

LADIES' PROGRAM

Ladies' Headquarters for the Boston Meeting is the Hancock Room, Mezzanine floor, Statler Hilton Hotel. Every morning, Monday through Thursday, there will be a coffee hour at 9:00 in the Hancock Room.

Sunday, Sept. 16—Registration from 2:00 to 9:00 P.M. and a social hour from 8:00 to 10:00 P.M. in Parlors B and C, Mezzanine floor.

Monday, Sept. 17—Coffee hour from 9:00 to 10:00 A.M. No specific plans have been made for the day. Members of the Ladies Committee will be on hand to make suggestions and take small groups on trips. Monday evening the ladies are welcome to attend the mixer from 8:00 to 11:00 P.M. in the Ballroom, Mezzanine floor.

Tuesday, Sept. 18—Coffee hour from 9:00 to 10:00 A.M. A bus tour of Boston to be conducted by the Museum of Fine Arts is scheduled for 10:00 A.M. Luncheon will be served in the Tapestry Room of the Museum, and the afternoon can be spent in the Museum. Ladies are invited to attend the Acheson Medal Reception and Banquet at 6:30 P.M.

Wednesday, Sept. 19—Coffee hour from 9:00 to 10:00 A.M. At 10:00 a trip to the Adams Mansion in Quincy is planned. Luncheon will be served at the Toll House in Whitman. The afternoon will be spent in Plymouth. An old-fashioned New England clambake is scheduled for the evening.

Thursday, Sept. 20—Coffee hour from 9:00 to 10:00 A.M.

COST OF VARIOUS FUNCTIONS

(other than registration)

Please buy tickets as early as possible.

Symposia Chairmen Breakfasts	Standard menu prices
Sunday Evening Social Hour	Complimentary
Electrothermics & Metallurgy Cocktail Party	$3.00
Monday Evening Mixer	Complimentary
Division Luncheons	4.25
Tuesday Acheson Medal Reception and Banquet:	
Men	9.00
Ladies	7.00
Ladies Social Events:	
Tuesday Museum trip, including luncheon	2.00
Wednesday trip including bus fare, luncheon, tour, and clambake	8.00
Plant trips	Bus fare

JOURNALS

Copies of the June, July, and August issues of "The Journal of The Electrochemical Society" will be available at the Registration Desk. The price of a single copy of the Journal is $1.70 to members and $2.25 to nonmembers.

EXTENDED ABSTRACTS

The Battery Division is making available an extended abstract booklet containing 1000-word abstracts of most of the papers presented at the Division's Boston Meeting. Copies of the booklet may be obtained from C. H. Clark, 34 Pleasant Way, Deal, N. J., after Sept. 1 for $2.00 each.

DISCUSSION

No recordings will be made of oral discussion. Those contributing to the discussion of a paper and desiring their remarks to be published will be supplied by the Symposium Chairman with a printed form on which any discussion may be written. These forms should be given to the Symposium Chairman or to the Managing Editor of the JOURNAL after the session; or they can be mailed to the Managing Editor of the JOURNAL, 30 East 42nd Street, New York 17, N. Y. The discussion will then be referred to the author for reply. Publication of the discussion and the comments of the author depends on publication of the article in the JOURNAL.

Written discussion of a published paper should be submitted within two months following publication of the article in the JOURNAL. A Discussion Section is published semiannually in the JOURNAL.

EMPLOYMENT POSTERS

Companies which desire to recruit employees at the Boston Meeting will have posters to this effect on a Bulletin Board

MEETING ROOM SCHEDULE

Meeting of:	Monday		Tuesday		Wednesday		Thursday	
	A.M.	P.M.	A.M.	P.M.	A.M.	P.M.	A.M.	P.M.
Battery				B	B	B	B	B
Battery—Theoretical Electrochemistry	B	B	B					
Corrosion	DE	DE	DE	DE	DE	DE	DE	
Corrosion—Electronics	A	A	A	A				
Electrodeposition—Electronics	C	C						
Electrodeposition			C	C				
Electronics-Semiconductors					A	A	A	A
Electrothermics & Metallurgy	F	F		F				
Electrothermics & Metallurgy—Corrosion					C	C	C	C

A—Imperial Ballroom
B—Ballroom Assembly
C—Georgian Room
D—Parlor A
E—Parlor B
F—Parlor C
G—Bay State Room

adjacent to the Registration Desk. Companies are requested to confine their announcements to this Bulletin Board.

NOTE

Photographing of lantern slides, charts, etc., will be permitted unless specifically prohibited by the speaker. Photo flash and photo floods are prohibited.

Technical Program—Boston Meeting

Monday A.M., September 17, 1962

BATTERY—THEORETICAL ELECTROCHEMISTRY

Joint Symposium on Porous Electrodes, with Ernest Yeager presiding

(BALLROOM ASSEMBLY)

9:00 A.M.—Welcoming Remarks
9:05 A.M.—Introductory Remarks
9:15 A.M.—"The Importance of Liquid-Phase Diffusional Processes in Operation of a Hydrogen Electrode" by E. N. Lightfoot and M. R. Anderson (Abstract No. 1)
9:45 A.M.—"Theoretical Analysis of Current Distribution in Porous Electrodes" by J. S. Newman and C. W. Tobias (Abstract No. 2)
10:30 A.M.—Five-minute intermission
10:35 A.M.—"Improved Calculation of Polarization of Porous Electrodes" by A. W. Winsel (Abstract No. 3)
11:10 A.M.—"Statistical Descriptions of Porous Solids" by E. A. Flood (Abstract No. 4)
11:35 A.M.—"The Characterization of Platinum-on-Carbon Catalysts" by L. J. Hillenbrand (Abstract No. 5)

CORROSION

Passivation and Inhibition, with Henry Leidheiser, Jr., presiding

(PARLORS A and B)

9:00 A.M.—"Kinetics of Anodic Formation of Passive Films on Iron in a Neutral Solution" by Norio Sato and Morris Cohen (Abstract No. 50)
9:30 A.M.—"Effect of *p*H, Chlorides, and Sulfates on the Behavior of Chromates and Other Passivators as Corrosion Inhibitors for Steel" by S. Matsuda and H. H. Uhlig (Abstract No. 51)
10:00 A.M.—"On the Passivity of Titanium and Tantalum" by Rikuro Otsuka (Abstract No. 52)
10:30 A.M.—"Effect of Velocity on Corrosion of Iron in Aerated and Deaerated Sulfuric Acid" by Z. A. Foroulis and H. H. Uhlig (Abstract No. 53)
11:00 A.M.—"Activation Characteristics of Passive Stainless Steels in Sulfuric Acid Solutions" by Tatsuo Ishikawa and Go Okamoto (Abstract No. 54)
11:30 A.M.—"Corrosion Inhibition of Iron by Methyl Pyridines in 6N HCl" by R. C. Ayers and Norman Hackerman (Abstract No. 55)

CORROSION—ELECTRONICS

Joint Symposium on Phenomena at Interfaces, I, with H. C. Gatos presiding

(IMPERIAL BALLROOM)

9:00 A.M.—Introductory Remarks
9:10 A.M.—"Adsorption at Interfaces" by J. H. de Boer (Abstract No. 77)
10:00 A.M.—"Epitaxial Growth of Silicon by Vacuum Sublimation" by E. Tannenbaum Handelman and E. I. Povilonis (Abstract No. 78)
10:20 A.M.—Ten-minute intermission
10:30 A.M.—"Vapor Growth of Germanium-Silicon Alloy Films on Germanium Substrates" by R. C. Newman and J. Wakefield (Abstract No. 79)
10:50 A.M.—"Masking of Epitaxial Germanium by Fluorocarbons" by C. Z. LeMay and J. C. Marinace (Abstract No. 80)
11:10 A.M.—"The Evaporation Kinetics of Iron-Chromium Alloys" by L. A. Morris and W. W. Smeltzer (Abstract No. 81)
11:0 A.M.—"Effects of Alloying Elements on the Oxidation of Tin" by W. E. Boggs, R. H. Kachik, and G. E. Pellissier (Abstract No. 82)

ELECTRODEPOSITION—ELECTRONICS

Joint Symposium on Electrochemical Processes for Semiconductor Devices, with D. R. Turner presiding

(GEORGIAN ROOM)

8:55 A.M.—Introductory Remarks
9:00 A.M.—"A Review of Semiconductor Device Cleaning Technology" by H. M. Cleveland (Abstract No. 103)
9:30 A.M.—"Surface Research and Its Relation to Device Technology" by S. S. Baird (Abstract No. 104)
10:00 A.M.—"A New Chemical Polish for Gallium Arsenide" by M. V. Sullivan and G. A. Kolb (Abstract No. 105)
10:30 A.M.—"Plating of Metals on Semiconductors" by G. L. Schnable and W. J. Hillegas, Jr. (Abstract No. 106)
11:00 A.M.—"Jet Electrolytic Etching and Plating" by W. M. Lilker and G. L. Schnable (Abstract No. 107)
11:30 A.M.—"Method for Producing Diodes and Transistors by Electrodeposition" by W. P. Alina, M. A. Blumenfeld, and R. A. Straight (Abstract No. 108)
12:15 P.M.—Electrodeposition Division Luncheon and Business Meeting, Georgian Room

ELECTRONICS—CORROSION

Joint Symposium on Phenomena at Interfaces

(IMPERIAL BALLROOM)

See Corrosion—Electronics program, morning and afternoon.

ELECTRONICS—ELECTRODEPOSITION

Joint Symposium on Electrochemical Processes for Semiconductor Devices

(GEORGIAN ROOM)

See Electrodeposition—Electronics program, morning and afternoon.

ELECTROTHERMICS & METALLURGY

Symposium on Hot Pressing, with J. H. Westbrook presiding

(PARLOR C)

9:00 A.M.—Introductory Remarks
9:05 A.M.—"Variations in Hot-Pressing Techniques" by W. W. Beaver and R. S. Truesdale (Abstract No. 165)
9:45 A.M.—"Relationship of the Yield Pressure to the Hot-Pressed Density of Metal Powders" by G. W. Cunningham (Abstract No. 166)
10:15 A.M.—"The Continuous Hot Pressing of Refractory Materials" by B. Best (Abstract No. 167)
10:35 A.M.—Twenty-five minute intermission
11:00 A.M.—"The Effect of Hot-Pressing Variations on the Properties of Zirconium and Titanium Diboride" by R. A. Alliegro and A. R. Schultz (Abstract No. 168)
11:30 A.M.—"Gas Evolution during Consolidation of Carbothermic TiB_2 Powders to High Density" by R. D. Holliday, R. Mogstad, and J. L. Henry (Abstract No. 169)

THEORETICAL ELECTROCHEMISTRY—BATTERY

Joint Symposium on Porous Electrodes

(BALLROOM ASSEMBLY)

See Battery—Theoretical Electrochemistry program, morning and afternoon.

Monday P.M., September 17, 1962

BATTERY—THEORETICAL ELECTROCHEMISTRY

Joint Symposium on Porous Electrodes (cont'd), with C. W. Tobias presiding

(BALLROOM ASSEMBLY)

2:00 P.M.—Introductory Remarks
2:05 P.M.—"Measurements of Pore Size and Surface Area of Porous Electrodes by Nondestructive Means" by A. J. Salkind, M. L. Block, and H. J. Canning (Abstract No. 6)
2:30 P.M.—"Graded Boundary Electrode" by F. G. Reick (Abstract No. 7)

2:55 P.M.—"A-C Capacitance Measurements of a Porous Electrode" by J. Batelaan and P. L. Bourgault (Abstract No. 8)
3:20 P.M.—"Surface Area Measurements of Platinized-Platinum Electrodes" by M. J. Joncich and Norman Hackerman (Abstract No. 9)
3:45 P.M.—Five-minute intermission
3:50 P.M.—"Migration of Adsorbed Species on an Electrode" by H. B. Urbach (Abstract No. 10)
4:15 P.M.—"An Equation for Battery Discharge Curves" by C. M. Shepherd (Abstract No. 11)
4:40 P.M.—"Investigation of Justi-Type Gas Diffusion Electrodes" by P. J. Clemm (Abstract No. 12)
5:10 P.M.—"The Application of Radiography to the Study of the Operation of Porous Electrodes" by M. Bonnemay (Abstract No. 12A)

CORROSION

Light Metal Corrosion, with Fred Fink presiding

(PARLORS A and B)

2:00 P.M.—"The Oxidation of Aluminum in Contact with Mercuric Iodide" by D. A. Jackson, Jr., and Henry Leidheiser, Jr. (Abstract No. 56)
2:25 P.M.—"Photomicrographical Observations of Mercurous Halide Films" by D. C. Cornish, S. N. Das, D. J. G. Ives, and R. W. Pittman (Abstract No. 57)
2:50 P.M.—"An Infrared Study of the Hydration of Anodic Coatings on Aluminum" by C. E. Michelson and J. F. Murphy (Abstract No. 58)
3:15 P.M.—"Disintegration of Magnesium While Dissolving Anodically in Neutral and Acidic Solutions" by M. E. Straumanis and B. K. Bhatia (Abstract No. 59)
3:40 P.M.—"A Radiotracer Study of Sulfate Ion Behavior in Aluminum Anodic Coatings" by C. E. Michelson and J. F. Murphy (Abstract No. 60)
4:05 P.M.—"The Difference Effect on Magnesium Dissolving in Acids" by W. J. James, M. E. Straumanis, and B. K. Bhatia (Abstract No. 61)

CORROSION—ELECTRONICS

Joint Symposium on Phenomena at Interfaces (cont'd), II, with W. A. Tiller presiding

(IMPERIAL BALLROOM)

2:00 P.M.—"Imperfections at Interfaces" by W. Dekeyser (Abstract No. 83)
2:50 P.M.—"Morphology Control of the Solid-Melt Interface" by W. A. Tiller (Abstract No. 84)
3:20 P.M.—"Studies of the InSb Crystal-Melt Interface" by N. Albon (Abstract No. 85)
3:40 P.M.—Ten-minute intermission
3:50 P.M.—"Formation of Conical Hillocks on Crystals" by S. E. Miller and N. Albon (Abstract No. 86)
4:10 P.M.—"The Travelling Solvent Method of Crystal Growth, Part II" by A. I. Mlavsky and Martin Weinstein (Abstract No. 87)
4:30 P.M.—"Growth Processes of Three Twin Germanium Dendrites" by R. G. Seidensticker and D. R. Hamilton (Abstract No. 88)
4:50 P.M.—"Preferred Orientation in the Growth of Refractory Metals from the Melt" by L. G. Tensmeyer (Abstract No. 89)

ELECTRODEPOSITION—ELECTRONICS

Joint Symposium on Electrochemical Processes for Semiconductor Devices, with D. Gardner Foulke presiding

(GEORGIAN ROOM)

2:00 P.M.—"Electroless Palladium on Semiconductor Materials" by R. N. Rhoda (Abstract No. 109)
2:30 P.M.—"Immersion Gold Plating Semiconductor Materials" by G. I. Edson (Abstract No. 110)

General Session

3:00 P.M.—"Some Observations on Electrodeposited Dendrites" by H. F. John and J. W. Faust, Jr. (Abstract No. 111)
3:30 P.M.—"Electrocrystallization, I. Electron Tunnelling and Crystal-Face Work Function in Electrocrystallization" by Ram Mohan Mallya (Abstract No. 112)
4:00 P.M.—"A Study of the Electroreduction of Chromic Ion at the Mercury Cathode" by M. E. McLain, Jr. (Abstract No. 113)
4:30 P.M.—"Radiochemical Studies of Thiourea in the Electroless Deposition Process" by J. S. Sallo, J. Kivel, and F. C. Albers (Abstract No. 114)

ELECTROTHERMICS & METALLURGY

Symposium on Hot Pressing (cont'd), with L. H. Juel presiding

(PARLOR C)

2:00 P.M.—Introductory Remarks
2:05 P.M.—"Furnaces Used in Hot Pressing" by D. T. Lapp and G. R. Watson (Abstract No. 170)
2:45 P.M.—"Thermal-Pressing Analysis" by B. Best (Abstract No. 171)
3:15 P.M.—"The Influence of Gravity in Sintering" by F. V. Lenel, H. H. Hausner, O. V. Roman, and G. S. Ansell (Abstract No. 172)
3:35 P.M.—"The Hot Pressing of Carbides, Metal-Ceramic Composites, and Oxides" by W. B. Crandall and J. R. Tinklepaugh (Abstract No. 173)

General Session

4:05 P.M.—"Vaporization of Zinc Antimonide" by Chikara Hirayama (Abstract No. 174)
4:35 P.M.—"Correlation between Ferromagnetic Tape Material Structure and the Magnetic Behavior of the Tape Material" by P. Kuttner (Abstract No. 175)
5:00 P.M.—Electrothermics and Metallurgy Division Cocktail Party, Bay State Room (lower level of lobby floor)

Monday Evening, September 17, 1962

ELECTRONICS—SEMICONDUCTORS

(IMPERIAL BALLROOM)

7:00-8:30 P.M.—Recent News Papers. Titles and short abstracts will be available at the meeting.

Tuesday A.M., September 18, 1962

BATTERY—THEORETICAL ELECTROCHEMISTRY

Joint Symposium on Porous Electrodes (cont'd), with P. Ruetschi presiding

(BALLROOM ASSEMBLY)

9:00 A.M.—Introductory Remarks
9:05 A.M.—"Porous Carbon Electrodes for Low-Temperature Fuel Cells" by R. R. Paxton, J. F. Demendi, G. J. Young, and R. B. Rozelle (Abstract No. 13)
9:30 A.M.—"Performance Studies with Porous Electrodes" by M. B. Clark (Abstract No. 14)
9:55 A.M.—"Porous Carbon Fuel Cell Electrodes" by W. E. Parker and R. W. Marek (Abstract No. 15)
10:20 A.M.—Five-minute intermission
10:25 A.M.—"The Role of Porosity in the MnO_2 Cathode of the Leclanche Cell" by N. C. Cahoon (Abstract No. 16)
10:50 A.M.—"Polarization Studies of Molten Carbonate Fuel Cell Electrodes" by Isaac Trachtenberg (Abstract No. 17)
11:15 A.M.—"Theoretical Treatment of a Model for a Gas Diffusion Electrode" by F. G. Will (Abstract No. 18)
11:45 A.M.—"Theory of Separation by Gaseous Diffusion through a Bed of Spheres" by D. Massignon, J. P. Breton, R. Broise, and Soubbaramayer (Abstract No. 19)
12:30 P.M.—Battery Division Luncheon and Business Meeting, Ballroom Assembly.

CORROSION

General Corrosion, with E. Koehler presiding

(PARLORS A and B)

9:00 A.M.—"The Anodic Behavior of Zinc in Potassium Hydroxide Solution" by N. A. Hampson and M. J. Tarbox (Abstract No. 62)
9:30 A.M.—"A Polarization Method for Determining the Corrosion Rate of Tin Plate" by T. J. Butler and P. R. Carter (Abstract No. 63)
10:00 A.M.—"On the Etching Characteristics and Capacitor Properties of Zone Refined Aluminum" by R. Bakish, R. Kornhaas, and E. Z. Borders (Abstract No. 64)
10:30 A.M.—"Chromate Ion Inhibition of the Differential Oxygen Corrosion of Zinc" by M. M. Wright (Abstract No. 65)
11:00 A.M.—"Dissolution of Brass in Sulfuric Acid Solutions, I. 85/15 Brass" by J. Bumbulis and W. F. Graydon (Abstract No. 66)

CORROSION—ELECTRONICS

Joint Symposium on Phenomena at Interfaces (cont'd), III, with D. Vermilyea presiding

(IMPERIAL BALLROOM)

9:00 A.M.—"Electrical and Optical Properties of Semiconductor Surfaces" by E. Mollwo (Abstract No. 90)
9:50 A.M.—"Surface Energy of Germanium and Silicon" by R. J. Jaccodine (Abstract No. 91)
10:20 A.M.—Ten-minute intermission
10:30 A.M.—"The Surface-Barrier Photovoltaic Effect on Silicon, I" by A. H. A. Pampanini, Maryjane MacLaren, and A. I. Mlavsky (Abstract No. 92)
10:50 A.M.—"The Surface-Barrier Photovoltaic Effect on Silicon, II" by A. H. A. Pampanini and Georg Rupprecht (Abstract No. 93)
11:10 A.M.—"Effect of Light on the Electrochemical Behavior of the Zn-ZnO Electrode" by W. R. Ware, R. A. Powers, and G. K. Johnson (Abstract No. 94)
11:30 A.M.—"The Oxide Films Formed on Copper Single Crystal Surfaces in Water, III. Effect of Light" by Jerome Kruger and J. P. Calvert (Abstract No. 95)

ELECTRODEPOSITION

Alloy Electrodeposition, with L. D. McGraw presiding

(GEORGIAN ROOM)

9:00 A.M.—Introductory Remarks
9:05 A.M.—"Alloy Plating—Scientific Curiosity or Useful Technology?" by M. E. Browning (Abstract No. 115)
9:30 A.M.—"Russian Research on Alloy Electrodeposition" by George Dubpernell (Abstract No. 116)
9:55 A.M.—"Electrodeposition of Nickel-Molybdenum Alloys" by N. W. Hovey, Albertine Krohn, and G. M. Hanneken, Jr. (Abstract No. 117)
10:20 A.M.—"Electrodeposition of Zinc-Molybdenum Alloys" by Albertine Krohn, N. W. Hovey, and H. L. Lewis (Abstract No. 118)
10:45 A.M.—"The Production of Thick Cobalt-Molybdenum Alloy Deposits" by P. C. Rydel and S. C. Barnes (Abstract No. 119)
11:10 A.M.—"Deposition Mechanism of a Gold-Tungsten Codeposit" by R. F. Walton (Abstract No. 120)
11:35 A.M.—"On the Theory of Simultaneous Discharge of Metal Ions in Real Conjugated Systems" by A. T. Vagramyan and T. A. Fatueva (Abstract No. 121)

ELECTRONICS—CORROSION

Joint Symposium on Phenomena at Interfaces

(IMPERIAL BALLROOM)

See Corrosion—Electronics program, morning and afternoon.

THEORETICAL ELECTROCHEMISTRY—BATTERY

Joint Symposium on Porous Electrodes

(BALLROOM ASSEMBLY)

See Battery—Theoretical Electrochemistry program, morning and afternoon.

Tuesday P.M., September 18, 1962

BATTERY

General Session, Storage Batteries, with E. J. Ritchie presiding

(BALLROOM ASSEMBLY)

2:30 P.M.—"Further Studies on the Crystallogenesis of the Positive Plate Active Material" by A. C. Simon (Abstract No. 20)
3:00 P.M.—"Morphology of PbO_2 Crystals in the Positive Plate of Some Lead Calcium Cells" by Jeanne Burbank (Abstract No. 21)
3:20 P.M.—"Analysis of Volatile Acids in Lead-Acid Storage Batteries" by Frank Spagnolo and J. P. Cestaro (Abstract No. 22)
3:45 P.M.—Five-minute intermission
3:50 P.M.—"Electrical Resistance of Battery Separators" by R. L. Wentworth (Abstract No. 23)
4:15 P.M.—"Battery Mathematics" by W. C. Arsem (Abstract No. 24)

CORROSION

Electrode Processes, with C. V. King, presiding

(PARLORS A and B)

2:00 P.M.—"Dissolution of Oxygen Layers on Platinum in Chloride Solutions" by M. W. Breiter and J. L. Weininger (Abstract No. 67)
2:30 P.M.—"The Cathodic Reduction of Oxygen at a Rotating Disk" by G. Butler and S. C. Shome (Abstract No. 68)
3:00 P.M.—"Electrochemical Mechanism of Hydrogen Embrittlement of Steel" by Walter Beck, Alfred Glass, and Edward Taylor (Abstract No. 69)
3:30 P.M.—"Time Dependency of Anodic Polarization Currents" by O. L. Riggs, Jr. (Abstract No. 70)
4:00 P.M.—"Effect of Acetylenic Molecules on Cathodic Overvoltage on Steel in Acid Solutions" by E. J. Duwell (Abstract No. 71)

CORROSION—ELECTRONICS

Joint Symposium on Phenomena at Interfaces, (cont'd), IV, with W. W. Harvey presiding

(IMPERIAL BALLROOM)

2:00 P.M.—"The Anodic Dissolution Reaction at Semiconductor Electrodes" by W. W. Harvey (Abstract No. 96)
2:40 P.M.—"On the Etching of III-V and II-VI Compounds" by G. A. Wolff, J. J. Frawley, and J. R. Hietanen (Abstract No. 97)
3:00 P.M.—"Gallium Arsenide Etch Rate Characteristic" by Allen Owen, J. F. Delord, and W. C. Myers (Abstract No. 98)
3:20 P.M.—Ten-minute intermission
3:30 P.M.—"The Movement of Ions during the Oxidation of Metals" by R. C. Plumb, J. W. Swaine, Jr., and J. E. Boggio (Abstract No. 99)
3:50 P.M.—"Becquerel Effect of Victoria Blue B on Platinum" by S. A. Greenberg and H. P. Silverman (Abstract No. 100)
4:10 P.M.—"Exchange of Silver Ions at Single Crystal-Solution Interfaces" by I. I. Tingley (Abstract No. 101)
4:30 P.M.—"On the Formation of Electrochemical Etch Pits on the (111) Face of Copper" by Ugo Bertocci, L. D. Hulett, L. H. Jenkins, and F. W. Young, Jr. (Abstract No. 102)

ELECTRODEPOSITION

Alloy Electrodeposition (cont'd), with M. E. Browning presiding

(GEORGIAN ROOM)

2:00 P.M.—"Magnetic Co-Ni Electrodeposition; Characterization of the Deposit as a Function of Process Parameters" by J. D. Kresge, M. A. Sanborn, and S. Simoliunas (Abstract No. 122)
2:25 P.M.—"Magnetic Co-Ni Electrodeposition; Study of Solutions with Stable and Unstable Additives" by J. D. Kresge, M. A. Sanborn, and S. Simoliunas (Abstract No. 123)
2:50 P.M.—"Compositional Studies of Electrodeposited Fe-Ni Alloys" by I. M. Croll (Abstract No. 124)
3:15 P.M.—"Electrodeposition of Iron-Nickel-Phosphorus Thin Films for Computer Memory Use" by W. O. Freitag, G. DiGuilio, and J. Mathias (Abstract No. 125)
3:40 P.M.—"Tensile Strength and Ductility of Electrodeposited Brass" by H. J. Read and W. A. Nystrom (Abstract No. 126)
4:15 P.M.—"Thorium Fused Salt Electrodeposition into a Molten Zinc Cathode" by R. E. Johnson (Abstract No. 127)
4:35 P.M.—"Electrodeposition of Bright Aluminum Coatings from Fused Salt Baths" by L. W. Austin, M. G. Vucich, and E. J. Smith (Abstract No. 128)

ELECTROTHERMICS AND METALLURGY

Symposium on Studies in Electrolytic Cells, with W. E. Kuhn presiding

(PARLOR C)

2:00 P.M.—Introductory Remarks
2:05 P.M.—"Thermodynamic Studies of Ternary Liquid Metallic Systems Containing Miscibility Gaps, I. The Alumi-

num-Bismuth-Lead System" by T. C. Wilder and J. F. Elliott (Abstract No. 176)
2:35 P.M.—"Thermodynamic Properties of the Manganese-Lead-Bismuth System" by M. Weinstein and J. F. Elliott (Abstract No. 177)
3:05 P.M.—"EMF Response of Strained Nickel, Molybdenum, and Titanium Electrodes" by S. M. Toy and Ken Nobe (Abstract No. 178)
3:35 P.M.—"Electrodeposition of Dispersion-Hardened Ni-Al_2O_3 Alloys" by F. K. Sautter (Abstract No. 179)
4:15 P.M.—"The Electrochemical Hall of Fame—The Story of the Men Who Built the Electrochemical Industry with Niagara Power" by F. L. Koethen (Abstract No. 180)

Wednesday A.M., September 19, 1962

BATTERY

General Session, Storage Batteries (cont'd), with Jeanne Burbank presiding

(BALLROOM ASSEMBLY)

9:00 A.M.—Introductory Remarks
9:05 A.M.—"The Design and Performance of High Capacity Sealed Silver Cadmium Batteries" by P. L. Howard (Abstract No. 25)
9:25 A.M.—"Evaluation of Silver-Cadmium Batteries for Satellite Applications" by T. R. Beck, J. T. MacLean, and C. B. Whitney (Abstract No. 26)
9:50 A.M.—"The Silver-Cadmium Couple in Sealed Cells for Space" by R. C. Shair and Guy Rampel (Abstract No. 27)
10:15 A.M.—"Improvement in Cycle Life of the Silver Zinc Secondary Battery" by Frank Solomon (Abstract No. 28)
10:40 A.M.—Five-minute intermission
10:45 A.M.—"The Silver-Silver Oxide Electrode, II. Anodization at 0° and 25°C in Alkaline Solutions" by C. P. Wales (Abstract No. 29)
11:05 A.M.—"Sealed Alkaline Secondary Battery Systems" by J. T. Arms and J. C. Duddy (Abstract No. 30)
11:30 A.M.—"Oxide Formation and Reduction on Single Crystals of Nickel" by J. L. Weininger and M. W. Breiter (Abstract No. 31)

CORROSION

General, with J. F. Murphy, presiding

(PARLORS A and B)

9:00 A.M.—"Surface Layers Associated with the Electropolishing of Copper in H_3PO_4" by F. H. Giles, Jr. (Abstract No. 72)
9:30 A.M.—"The Copper Etching Characteristics of Ammonium Persulfate Solutions" by T. D. Schlabach and B. A. Diggory (Abstract No. 73)
10:00 A.M.—"The Rate of Growth of Electrochemical Etch Pits at Dislocations on (111) Copper Surfaces" by L. D. Hulett and F. W. Young, Jr. (Abstract No. 74)
10:30 A.M.—"Some Effects of Metal Defect Structure on the Anodic Dissolution of Single Crystalline Copper" by L. H. Jenkins and Ugo Bertocci (Abstract No. 75)
11:00 A.M.—"Electrochemical Behavior of Nickel Intermetallic Compounds" by A. K. M. Shamsul Huq and M. A. Loud (Abstract No. 76)

CORROSION—
ELECTROTHERMICS & METALLURGY

Joint Symposium on High-Temperature Corrosion

(GEORGIAN ROOM)

See Electrothermics and Metallurgy—Corrosion program, morning and afternoon.

ELECTRONICS—SEMICONDUCTORS

Semiconductor Materials, with F. H. Horn presiding

(IMPERIAL BALLROOM)

9:00 A.M.—"Synthesis of Semiconducting Black Phosphorus" by R. C. Ellis and D. M. Warschauer (Abstract No. 129)
9:20 A.M.—"Properties of Semiconducting Black Phosphorus" by D. M. Warschauer (Abstract No. 130)
9:40 A.M.—"Conversion and Resistivity Changes in Floating Zone Silicon" by S. N. Levine and H. Goldberg (Abstract No. 131)
10:00 A.M.—"Preparation and Electrical Properties of Bismuth Trisulfide" by A. C. Glatz and V. F. Meikleham (Abstract No. 132)
10:20 A.M.—"A New Method of GaP Growth and Purification" by G. A. Wolff and J. D. Broder (Abstract No. 133)
10:40 A.M.—"Electrical Properties of Some Peritectic Compounds from the CdTe-In_2Te_3 System" by D. F. O'Kane and D. R. Mason (Abstract No. 134)
11:00 A.M.—"X-Ray Studies of Twinned GaAs Blades Grown from the Vapor Phase" by R. R. Monchamp, W. J. McAleer, and P. I. Pollak (Abstract No. 135)
11:20 A.M.—"High-Temperature Electrical Conduction in $CuInTe_2$" by S. M. Zalar (Abstract No. 136)
11:40 A.M.—"Hall Effect and Electrical Conductivity of Single Crystal Cuprous Oxide" by M. R. Wright, R. S. Toth, and Dan Trivich (Abstract No. 137)

ELECTROTHERMICS & METALLURGY—
CORROSION

Joint Symposium on High-Temperature Corrosion, I. Steam-Water Corrosion, with A. Dravnieks presiding

(GEORGIAN ROOM)

9:00 A.M.—Introductory Remarks
9:05 A.M.—"Solution and Diffusion of Corrosion Oxide Film in Zircaloy" by R. M. Treco (Abstract No. 182)
9:35 A.M.—"Reaction of Lithium with Water Vapor" by W. R. Irvine and J. A. Lund (Abstract No. 183)
10:05 A.M.—"High-Temperature Oxidation of Iron-Chromium Alloys in Water Vapor" by C. T. Fujii and R. A. Meussner (Abstract No. 184)
10:35 A.M.—"Corrosion of Al in Steam at 540°C and 60 psi" by R. K. Hart (Abstract No. 185)
11:05 A.M.—"Reaction of Boron Carbide with Steam at Elevated Temperatures" by L. M. Litz and R. A. Mercuri (Abstract No. 186)

Wednesday P.M., September 19, 1962

BATTERY

General Session, Secondary and Primary Batteries, with Charles Clark presiding

(BALLROOM ASSEMBLY)

2:00 P.M.—Introductory Remarks
2:05 P.M.—"Kinetic Studies of the Reversible Potentials of the Nickel Oxide Electrode as a Function of Degree of Oxidation" by B. E. Conway and E. Gileadi (Abstract No. 32)
2:35 P.M.—"Systematized Concepts of Manganese Dioxide Dry Cells" by Masataro Fukuda, Taketsugu Hirai, and Haruo Manabe (Abstract No. 33)
3:05 P.M.—"Thermal Dissociation of Manganese Dioxides" by Earl Otto (Abstract No. 34)
3:30 P.M.—Five-minute intermission
3:35 P.M.—"The Transient Impedance of Leclanche Cells, II. Current Drain Dependence" by Aladar Tvarusko (Abstract No. 35)
4:00 P.M.—"Silver, Silver Iodide, Vanadium Pentoxide, Carbon Solid Electrolyte Cell" by D. V. Louzos (Abstract No. 36)
4:25 P.M.—"Lithium Nonaqueous Secondary Battery" by J. E. Chilton, Jr., and G. M. Cook (Abstract No. 37)

ELECTRONICS—SEMICONDUCTORS

Semiconducting Compounds, with J. M. Whelan presiding

(IMPERIAL BALLROOM)

2:00 P.M.—"Mixed Conduction Measurements in $Zr_{0.85}Ca_{0.15}O_{1.85}$" by R. W. Vest and N. M. Tallan (Abstract No. 138)
2:20 P.M.—"Solubility of 3-5 Compound Semiconductors in Column 3 Liquids" by R. N. Hall (Abstract No. 139)
2:40 P.M.—"Magnesium Diffusion in Gallium Arsenide and Prevention of Surface Evaporation" by D. C. Gupta and S. R. Shortes (Abstract No. 140)
3:00 P.M.—"Segregation of Silicon in Gallium Phosphide" by Martin Rubenstein (Abstract No. 141)

3:20 P.M.—"Electrical Properties of Mg_2Sn Crystals Grown from Nonstoichiometric Melts" by B. D. Lichter (Abstract No. 142)
3:40 P.M.—"Rare Earth Nitride and Hexaboride Semiconductors" by Nathan Sclar (Abstract No. 143)
4:00 P.M.—"The Hall Effect in Semiconducting Glasses" by W. F. Peck, Jr., and J. F. Dewald (Abstract No. 144)
4:20 P.M.—"Carrier Compensation in Germanium Telluride" by M. S. Lubell and R. Mazelsky (Abstract No. 145)
4:40 P.M.—"Semiconducting Nature of Stannic Oxide" by L. D. Loch (Abstract No. 146)

ELECTROTHERMICS & METALLURGY—CORROSION

Joint Symposium on High-Temperature Corrosion (cont'd), II. High-Temperature Oxidation, with L. M. Litz presiding

(GEORGIAN ROOM)

2:00 P.M.—Introductory Remarks
2:05 P.M.—"Some Studies on the Oxidation of Graphite at Temperatures of 600°-1500°C and at Pressures of 2-76 Torr of Oxygen" by E. A. Gulbransen, K. F. Andrew, and F. A. Brassart (Abstract No. 187)
2:35 P.M.—"Kinetics and Mechanism of the Oxidation of Uranium Dioxide Sintered Pellets" by Tennyson Smith (Abstract No. 188)
3:05 P.M.—"High-Pressure Oxidation of Metals; Nickel in Oxygen" by J. P. Baur, R. W. Bartlett, J. N. Ong, Jr., and W. M. Fassell, Jr. (Abstract No. 189)
3:35 P.M.—"A Method for the Determination of Composition of Microgram Quantities of Oxides of Platinum" by G. C. Fryburg and D. A. Otterson (Abstract No. 190)
4:05 P.M.—"Oxidation of Molybdenum at High Temperatures and Low Pressures" by J. Engelke, A. Buchler, and J. B. Berkowitz-Mattuck (Abstract No. 191)
4:35 P.M.—"Oxidation of Molten High-Purity Aluminum in Dry Oxygen" by W. C. Sleppy (Abstract No. 192)

Thursday A.M., September 20, 1962

BATTERY

General Session, Fuel Cells, with M. W. Breiter presiding

(BALLROOM ASSEMBLY)

9.00 A.M.—Introductory Remarks
9:05 A.M.—"A High-Rate High-Output Thermal Battery System" by S. M. Selis, J. P. Wondowski, and R. F. Justus (Abstract No. 38)
9:30 A.M.—"An Application of Thermodynamic Methods to the Determination of Reactions and Voltages in Liquid Ammonia Electromotive Cells" by W. F. Meyers (Abstract No. 39)
9:55 A.M.—"The Bubbling Gas Electrode. Reduction of Oxygen on Graphite" by W. J. Subcasky and M. Shaw (Abstract No. 40)
10:20 A.M.—Five-minute intermission
10:25 A.M.—"On the Potential-Determining Reactions in the Au-O_2-Acid System" by J. P. Hoare (Abstract No. 41)
11:00 A.M.—"Anodic Oxidation of Molecular Hydrogen at Platinum Electrodes" by Akiya Kozawa (Abstract No. 42)
11:30 A.M.—"A Study of the Adsorption of Carbon Monoxide and Oxygen on a Platinum Electrode—Significance of the 'Polarization Curve' " by S. Gilman (Abstract No. 43)

CORROSION—ELECTROTHERMICS & METALLURGY

Joint Symposium on High-Temperature Corrosion

(GEORGIAN ROOM)

See Electrothermics and Metallurgy—Corrosion program, morning and afternoon.

ELECTRONICS—SEMICONDUCTORS

Semiconductor Surfaces, with R. L. Petritz presiding

(IMPERIAL BALLROOM)

9:00 A.M.—"Surface Damage Associated with Abraded Silicon Specimens" by R. Stickler and G. R. Booker (Abstract No. 147)
9:20 A.M.—"Formation of Organo-Silicon Surfaces" by J. A. Cunningham and L. E. Sharif (Abstract No. 148)
9:40 A.M.—"Formation of Thermal Oxides of Silicon" by H. W. Cooper, H. C. Evitts, and S. S. Flaschen (Abstract No. 149)
10:00 A.M.—"Electrical Evaluation of Passivating Coatings on Silicon" by H. W. Cooper, R. W. Rader, and S. S. Flaschen (Abstract No. 150)
10:20 A.M.—"Etching Characteristics of Degenerately Doped P-N Junctions" by L. Varettoni, E. T. Casterline, and R. Glicksman (Abstract No. 151)
10:40 A.M.—"Some Comments on Thermal Etching of Silicon Surfaces Treated in Sealed Quartz Tubes" by A. N. Knopp (Abstract No. 152)
11:00 A.M.—"Gettering of Silicon Planar Diodes" by S. W. Ing, Jr., R. E. Morrison, L. L. Alt, and R. W. Aldrich (Abstract No. 153)
11:20 A.M.—"Effect of Adsorbed Molecules on Electrooptical Properties of Zinc Oxide" by Eiichi Inoue (Abstract No. 154)
11:40 A.M.—"A Novel Technique for Preparing Low-Temperature Alloyed Gold Contacts to Silicon and Germanium" by H. F. Gossenberger, E. Helpert, and W. Mehl (Abstract No. 155)

ELECTROTHERMICS & METALLURGY—CORROSION

Joint Symposium on High-Temperature Corrosion (cont'd), III. Liquid Bismuth Corrosion, with C. Hampel presiding

(GEORGIAN ROOM)

9:00 A.M.—Introductory Remarks
9:05 A.M.—"Liquid Bismuth Corrosion—A Review" by A. L. Lowe, Jr. (Abstract No. 193)
9:45 A.M.—"Dissolution of Nuclear Fuel Additions in Molten Bismuth" by A. F. Weinberg and R. J. Van Thyne (Abstract No. 194)
10:15 A.M.—"Capsule Evaluation of Structural Materials for Liquid Bismuth Service" by E. J. Rozic, Jr., and A. L. Lowe, Jr. (Abstract No. 195)
10:45 A.M.—"Evaluation of Liquid Bismuth Corrosion in Dynamic Systems" by O. H. Baker, A. L. Lowe, Jr., and W. Markert, Jr. (Abstract No. 196)
11:15 A.M.—"The Investigation of Container Materials for Bi and Pb Alloys, I. Thermal Convection Loops" by A. J. Romano, C. J. Klamut, and D. H. Gurinsky (Abstract No. 197)
11:45 A.M.—"Possible Correlations between Thermoelectric Potentials and Liquid Metal Corrosion" by J. R. Weeks and S. G. Epstein (Abstract No. 198)

Thursday P.M., September 20, 1962

BATTERY

General Session, Fuel Cells (cont'd), with A. Fleischer presiding

(BALLROOM ASSEMBLY)

2:00 P.M.—Introductory Remarks
2:05 P.M.—"The Fuel Cell Central Station: An Appraisal" by J. R. Dafler (Abstract No. 44)
2:30 P.M.—"The Hydrazine-Oxygen Fuel Cell, I. The Mechanism and Kinetics of the Hydrazine Electrode" by B. Baker and M. Eisenberg (Abstract No. 45)
2:55 P.M.—"The Performance of a Compact Design Butane-Air Fuel Cell" by M. Eisenberg and B. Baker (Abstract No. 46)
3:20 P.M.—Five-minute intermission
3:25 P.M.—"Vacuum Depolarized Hydrogen Concentration Cells for Space Power" by H. Krupp, G. Sandstede, G. Walter, and R. McJones (Abstract No. 47)
3:50 P.M.—"New High-Performance Methanol Fuel Cell Electrodes" by D. B. Boies and Andrew Dravnieks (Abstract No. 48)
4:15 P.M.—"An Aluminum-Air Fuel Cell" by R. A. Foust, Jr. (Abstract No. 49)

ELECTRONICS—SEMICONDUCTORS

Semiconducting Techniques, with W. C. Dunlap presiding

(IMPERIAL BALLROOM)

2:00 P.M.—"Operation of a Pilot Scale Vertical Epitaxial Silicon Reactor" by J. M. Fairfield and E. G. Grochowski (Abstract No. 156)
2:20 P.M.—"Disproportionation of Silicon Iodide in an Open-Tube Process" by J. J. Oberly and A. Adams, Jr. (Abstract No. 157)

2:40 P.M.—"Measurement of Silicon Epitaxial Layer Resistivity with a Four-Point Probe" by P. A. Schumann, Jr., and J. F. Hallenback, Jr. (Abstract No. 158)
3:00 P.M.—"The Epitaxial Growth of Silicon Carbide" by V. J. Jennings, Armin Sommer, and Hung-Chi Chang (Abstract No. 159)
3:20 P.M.—"The Vapor Growth of Epitaxial Germanium Multijunction Structures" by R. E. Gonzales, D. L. Malcuit, and J. W. Sprague (Abstract No. 160)
3:40 P.M.—"The Diffusivity of Arsenic in Silicon" by W. J. Armstrong (Abstract No. 161)
4:00 P.M.—"Investigation of Effects of Process Variables in Gaseous P_2O_5 Diffusion" by C. M. Lutfy, W. M. Gegg, J. E. Reynolds, and S. S. Flaschen (Abstract No. 162)
4:20 P.M.—"Optical and Electrical Properties of Semiconducting Cadmium Oxide Films" by T. K. Lakshmanan (Abstract No. 163)
4:40 P.M.—"Electrical Properties of Thin Organic Films" by Arthur Bradley and J. P. Hammes (Abstract No. 164)

ELECTROTHERMICS & METALLURGY—CORROSION

Joint Symposium on High-Temperature Corrosion (cont'd), IV. Nonconventional Media, with R. Foley presiding

(GEORGIAN ROOM)

2:00 P.M.—Introductory Remarks
2:05 P.M.—"High-Temperature Hydrogen Attack of Steels" by P. C. Rosenthal and F. H. Vitovec (Abstract No. 199)
2:35 P.M.—"Corrosion of Carbon Steel by High-Temperature Mercury" by A. H. Fleitman, A. J. Romano, and C. J. Klamut (Abstract No. 200)
3:05 P.M.—"Corrosion and Inhibition of Titanium and Titanium Alloys in Mercury at Elevated Temperatures" by J. Y. N. Wang (Abstract No. 201)
3:35 P.M.—"Accelerated High-Temperature Corrosion of Alloys Contaminated by Salt Deposits" by J. J. Moran, J. R. Mihalisin, and B. E. Hopkinson (Abstract No. 202)
4:05 P.M.—"Compatibility of Commercial Chromium-Nickel Alloys with Several Nitrogenous Atmospheres at 1750°F" by J. S. Brunhouse and G. W. Titus (Abstract No. 203)
4:35 P.M.—"Prestressed Ceramic Linings" by R. R. Pierce (Abstract No. 204)

Abstracts

BATTERY—THEORETICAL ELECTROCHEMISTRY

Abstract No. 1

The Importance of Liquid-Phase Diffusional Processes in Operation of a Hydrogen Electrode

E. N. Lightfoot, Dept. of Chemical Engineering, University of Wisconsin, Madison, Wis. and **M. R. Anderson,** New Product Development Dept., A. O. Smith Corp., Milwaukee, Wis.

A simplified analysis of a hydrogen electrode considers the electrochemical reactions to take place in the electrolyte phase and treats the heterogeneous electrode-electrolyte region as a single phase. The semiquantitative development of the model half-cell performance uses the relationships, namely, an equation of continuity for hydrogen being essentially a modified Fick's law, an equation of continuity for ionic constituents being essentially the Nernst-Planck equation, Kirchoff's law, and Tafel's equation. Numerical examples are given for palladium.

Abstract No. 2

Theoretical Analysis of Current Distribution in Porous Electrodes

J. S. Newman and **C. W. Tobias,** Dept. of Chemical Engineering, University of California, Berkeley 4, Cal.

General equations describing the behavior of porous electrodes are developed. These equations are used to determine the initial and the steady-state conditions in one-dimensional porous electrodes of uniform geometry and polarization parameters. In particular, it is shown that the current and reaction distributions in the depth of the electrode are strongly influenced by the type of activation polarization and by mass transport of the reacting ionic species, in addition to the effective conductivities of the two phases. It is found that a linear approximation to a Tafel curve leads to an inadequate description of actual behavior when the reaction is distributed nonuniformly in the depth of the electrode.

Abstract No. 3

Improved Calculation of Polarization of Porous Electrodes

A. W. Winsel, c/o E. Justi, Pockelstrasse 4, (33) Braunschweig, Germany

To calculate the total polarization of a gas diffusion electrode it is useful to distinguish four different regions within its pores. The first region contains the electrolyte in front of the pore mouth and contributes a constriction resistance. Region 2 is filled with electrolyte, which is flowing due to the production and consumption of water by the electrochemical process and the evaporation from the meniscus, respectively. This region is governed both by ohmic and concentration polarization. Section 3 includes the neighborhood of the three phase boundary, effecting reaction, concentration, and activation polarization. Section 4 contains gas and contributes concentration polarization due to accumulation of inert gases. All these polarization effects are discussed and calculated in detail. Methods to recognize, localize, and overcome the slowest step are described. The theoretical aspects are checked by some experimental results.

Abstract No. 4

Statistical Descriptions of Porous Solids

E. A. Flood, Pure Chemistry Div., National Research Council, Ottawa, Ont., Canada

Physical properties of porous systems are often controlled by many small contributions from the microscopic parts of the systems concerned. Frequently these small individual contributions are not directly measurable, and we must resort to describing them statistically. A statistical model porous system of fairly wide applicability is presented, together with illustrations of its use and limitations.

Abstract No. 5

The Characterization of Platinum-on-Carbon Catalysts

L. J. Hillenbrand, Battelle Memorial Institute, Columbus 1, Ohio

In one aspect of the fuel cell program at Battelle, an attempt has been made to determine the relationship between the chemical state of the surface and the electrochemical activity of catalytic electrodes. For this purpose, nonelectrochemical methods are being used in an attempt to characterize the platinum-on-carbon catalysts used in some electrodes. In this paper the gas adsorption methods for estimation of metal surface areas in such preparations are discussed.

Abstract No. 6

Measurements of Pore Size and Surface Area of Porous Electrodes by Nondestructive Means

A. J. Salkind, M. L. Block, and **H. J. Canning,** Electric Storage Battery Co., Carl F. Norberg Research Center, Yardley, Pa.

A BET surface area apparatus has been modified so that the surface area and pore size distribution of porous electrodes can be measured nondestructively. Experiments have been conducted with sintered electrodes from nickel-cadmium cells, with porous graphites, fuel cell electrodes, and nonmetallic porous materials.

Abstract No. 7

Graded Boundary Electrode

F. G. Reick, Diversified Technology Inc., P.O. Box 973, Syracuse 1, N. Y.

Description is made of an electrode system consisting of a main carbon conductor to which an inorganic fiber

mat has been cemented by a carbonaceous binder in a manner that forms a graded or diffuse boundary on the surface of the electrode. This electrode has been found to have resistance to polarization at high d-c current densities, no polarization at all at low d-c currents and excellent capacity for handling very high a-c currents.

Abstract No. 8

A-C Capacitance Measurements of a Porous Electrode

J. Batelaan and **P. L. Bourgault,** Johnson Matthey & Mallory Ltd., 110 Industry St., Toronto, Canada

The distributive arrangement of resistance and of capacitance within a porous electrode is analyzed with regard to its effects on the measurement of capacitance by a-c methods. Both planar and cylindrical electrode structures are discussed. Under certain conditions (*e.g.*, low frequency) the equivalent circuit of a porous electrode reduces to that of a simple resistor in series with a capacitor. At higher frequencies a more elaborate treatment is required to account for the observed behavior.

Abstract No. 9

Surface Area Measurements of Platinized-Platinum Electrodes

M. J. Joncich (present address: Northern Illinois University, DeKalb, Ill.) and **Norman Hackerman,** University of Texas, Austin 12, Texas

Platinized-platinum electrodes were prepared under varying conditions of geometry, composition of the plating solution, time of plating, and current density. The surface areas of the electrodes were determined by krypton adsorption using the B.E.T. method as well as by the method of Bowden-Rideal. It was determined that the specific surface areas of the platinum deposits were functions of all of the measured variables.

Abstract No. 10

Migration of Adsorbed Species on an Electrode

H. B. Urbach, Research Labs., United Aircraft Corp., East Hartford 8, Conn.

A mathematical model for current flow and mass transport in a stagnant fluid adjacent to a flat plate electrode has been formulated. This model includes specifically the transport by surface migration of adsorbed species under the influence of coulombic forces as well as transport by diffusion. The assumed form of the relationship between the transport rate and the force involves a migration velocity coefficient which is reducible from experimental data under ideal conditions. An experimental approach to the measurement of this parameter is described.

Abstract No. 11

An Equation for Battery Discharge Curves

C. M. Shepherd, U.S. Naval Research Lab., Washington 25, D. C.

The discharge of a porous plate battery is described by a simple, theoretically derived equation which has been fitted empirically to a wide range of discharge curves. The cell potential during discharge is a function of time, current density, internal resistance, polarization, available active material, and a correction for diffusion. The watt hour and ampere hour capacities can be determined readily from this equation. The practical application is based on a few simple arithmetical operations.

Abstract No. 12

Investigation of Justi-Type Gas Diffusion Electrodes

P. J. Clemm, Chemical & Metallurgical Engineering Lab., General Engineering Lab., General Electric Co., 1 River Rd., Schenectady 5, N. Y.

This paper describes an exploration of the methods described by E. Justi and co-workers to produce porous nickel electrodes incorporating Raney nickel catalyst. The performance of both the single and double layer type of electrode in the anodic decomposition of hydrogen in KOH is described and is related to fabrication variables, mean pore size and gas pressure variations. Problems associated with scale-up of this type of electrode are also described.

Abstract No. 12A

The Application of Radiography to the Study of the Operation of Porous Electrodes

M. Bonnemay, Laboratoire d'Electrolyse de C.M.R.S., 1 Place Aristide Briand, Bellevue, (S. et O.) France

(Abstract delayed)

Abstract No. 13

Porous Carbon Electrodes for Low-Temperature Fuel Cells

R. R. Paxton and **J. F. Demendi,** Pure Carbon Co., St. Marys, Pa., and **G. J. Young** and **R. B. Rozelle,** Surface Processes Research and Development Corp., Dallas, Pa.

Porous carbon materials of widely differing properties were evaluated as gas diffusion fuel electrodes. The fuel gases were hydrogen, ethane, propane, and isobutane. Graphitized electrodes performed as well as nongraphitized electrodes. Performance of carbons with larger pore diameters could be improved as much as tenfold by wetproofing or by operating at high enough gas pressure to cause bubbling; however, the ultimate concentration polarization limitations appeared related only to the micropore structure. A simple method of measuring the micropore volume was developed. Limiting current densities with hydrocarbons were substantially less than with hydrogen under identical cell conditions. Chemical attack, including electrochemical oxidation of some of the carbons, was observed.

Abstract No. 14

Performance Studies with Porous Electrodes

M. B. Clark, Research Lab., Union Carbide Consumer Products Co., Parma 30, Ohio

Gross permeability of porous electrodes cannot be used as a sole criterion for estimating concentration polarization. The important role of the structure of the electrode surface is discussed. Observed limiting currents appear to be determined not only by the porous structure of the electrode, but also by specific mass transfer phenomenon related to reaction product accumulation. The extent to which the presence of nitrogen in air interferes with the diffusion of oxygen to the active sites is shown.

Abstract No. 15

Porous Carbon Fuel Cell Electrodes

W. E. Parker and **R. W. Marek,** Speer Carbon Co., Niagara Falls, N. Y.

The effects of the physical parameters of porous carbons on their electrochemical behavior as electrodes in hydrogen-oxygen fuel cell systems have been studied. The influence of total porosity and pore size distribution on electrode electrochemical utility has been examined. A high degree of total porosity has been found to be a requirement for achievement of high current density. Optimum pore size range appears to be larger for the oxygen electrode than for the hydrogen electrode.

Abstract No. 16

The Role of Porosity in the MnO_2 Cathode of the Leclanché Cell

N. C. Cahoon, Development Div., Union Carbide Consumer Products Co., P.O. Box 6056, Cleveland 1, Ohio

The cathode of the Leclanché dry cell is probably one of the oldest types of porous electrochemical electrodes in use today. The porosity in the cathode is developed (*a*) as interparticle spaces filled with electrolyte and (*b*) as intraparticle pores which may or may not be filled with electrolyte. The relationships between the intraparticle pores, the total surface area, and the electrochemical activity of specific types of manganese dioxide are presented and discussed. Data on two recently introduced types of synthetic MnO_2 are presented.

Abstract No. 17

Polarization Studies of Molten Carbonate Fuel Cell Electrodes

Isaac Trachtenberg, Corporate Research and Engineering, Texas Instruments Inc., P.O. Box 5474, Dallas 22, Texas

Polarization measurements have been made on individual electrodes in operating molten carbonate fuel

cells by using a third idling electrode. Overvoltages as a function of time from 10^{-6} to 100 sec have been recorded. Analyses of these curves indicate that total electrode polarization is the result of several factors; (*a*) ohmic and/or activation, (*b*) electrode coverage by reactants and products, (*c*) concentration gradients of potential determining species in the electrolyte.

Abstract No. 18

Theoretical Treatment of a Model for a Gas Diffusion Electrode

F. G. Will, Research Lab., General Electric Co., Schenectady, N. Y.

The mechanism of the anodic oxidation of molecular hydrogen on partially immersed platinum electrodes in acidic solutions, serving as an idealized model for a gas diffusion electrode, has been treated theoretically. The assumed mechanism consists in the slow diffusion of molecular hydrogen through the upper edge of the electrolyte meniscus and a thin liquid film covering the electrode surface above the intrinsic meniscus. On the basis of this model, the relationship $I = K_1[E_a - K_2(1 - e^{-K_3 E} a)]^{1/2}$ between current and applied potential is derived which agrees with experimental data over a potential range from zero to 1.8v. The relative contributions of meniscus and film to the total current are calculated. The reaction takes place mainly at a few tenths of a millimeter length of the electrode close to the upper meniscus edge. The true current density at this narrow band and the thickness of the liquid film are calculated. The surface diffusion of hydrogen atoms as transport mechanism has also been treated, and it is shown that the results of this treatment are not in agreement with the experimental data.

Abstract No. 19

Theory of Separation by Gaseous Diffusion through a Bed of Spheres

D. Massignon. J. P. Breton, R. Broise, and **Soubbaramayer,** Dept. of Physical Chemistry, Commissariat a l'Energie Atomique, Centre d'Etudes Nucleaires de Saclay, Boite Postale No. 2, Gif-sur-Yvette (Seine-et-Oise), France

The paper will be mainly theoretical showing a derivation of a new theory from approximate solutions of the Boltzmann equation. Other theories will be discussed, and experimental material will illustrate the new theory.

BATTERY

Abstract No. 20

Further Studies on the Crystallogenesis of the Positive Plate Active Material

A. C. Simon, U.S. Naval Research Lab., Washington 25, D. C.

Microscopic examination has revealed several species of crystals present in the microstructure of the positive plate active material used in the lead-acid storage battery. Photomicrographs will be presented that illustrate features of interest in this microstructure that may influence battery performance. An attempt will be made to enlarge on the theory previously presented that the microstructure bears a relationship to paste retention.

Abstract No. 21

Morphology of PbO_2 Crystals in the Positive Plate of Some Lead Calcium Cells

Jeanne Burbank, U.S. Naval Research Lab., Washington 25, D. C.

The PbO_2 crystals comprising the positive active material in some commercial lead calcium cells were examined by electron microscopy. Some positive pastes were entirely made up of prismatic crystals with many side arms, possible twins. The particles in the positive pastes from other cells showed no evidence of the prismatic habit, but were nondescript pebble-like masses. The durability of the positive paste is believed to be related to the morphology of these crystals.

Abstract No. 22

Analysis of Volatile Acids in Lead-Acid Storage Batteries

Frank Spagnolo and **J. P. Cestaro,** Research Center, National Lead Co., Hightstown, N. J.

The volatile acids formed at various stages of the battery life cycle have been analyzed by chemical and infrared means. Formic and acetic acids are formed by decomposition of the organic separators. Sulfurous acid is formed by a redox reaction between sulfate ion and organic matter. The distribution and the amounts of these acids at each cycle have been measured. Experimental data for various separator types are given.

Abstract No. 23

Electrical Resistance of Battery Separators

R. L. Wentworth, Dewey and Almy Chemical Div., W. R. Grace & Co., Cambridge 40, Mass.

Measurements of the electrical resistance of separators for lead-acid batteries by both alternating and direct current techniques are presented and compared. The salient factors of test cell configuration which affect precision of results are discussed. The relationship of the separator electrical resistance measured by these techniques to the internal resistance of batteries is demonstrated.

Abstract No. 24

Battery Mathematics

W. C. Arsem, Consulting Chemical Engineer, 6405 Maiden Lane, Bethesda 14, Md.

Mathematical interrelations are developed for the operating characteristics of batteries. The subjects covered are: internal resistance, load resistance, electromotive force or open-circuit voltage, operating or closed circuit voltage, power lost in battery, power available in load, maximum available power, power efficiency, energy efficiency, and current density. The relations developed are applied to the problems of designing and operating batteries, including fuel cells, and also to methods of testing cells for life and performance.

Abstract No. 25

The Design and Performance of High Capacity Sealed Silver Cadmium Batteries

P. L. Howard, Yardney Electric Corp., 40-52 Leonard St., New York, 13, N. Y.

Our requirements for military and commercial applications in which the sealed Silcad cell are required have resulted in the development of cells ranging in capacity from the 1 AH size to the 150 AH size. The problems involved in obtaining larger cells with the same performance characteristics and re-combination rates necessitate special considerations. Both plastic case and metallic case designs have been made. The results of this work and performance characteristics are reported.

Abstract No. 26

Evaluation of Silver-Cadmium Batteries for Satellite Applications

T. R. Beck, J. T. MacLean, and **C. B. Whitney,** Aero-Space Div., Physics Technology Dept., The Boeing Co., Seattle, Wash.

Silver-cadmium cells were evaluated in a test satellite power system with a simulated silicon solar cell charger and a 65/35 min charge/discharge cycle. Batteries at 25%, 35% and 50% depth of discharge operated for over a year. Analyses of electrical characteristics, efficiency, heat generation and mode of failure, were related to power system design. It is expected that silver-cadmium cells will have a significant place in satellite power systems because of their high energy density and long life.

Abstract No. 27

The Silver-Cadmium Couple in Sealed Cells for Space

R. C. Shair and **Guy Rampel,** Gulton Industries, Inc., 212 Durham Ave., Metuchen, N. J.

Hermetically sealed silver-cadmium cells utilizing a unique electrode construction, ceramic-to-metal seals, and a continuous sealed overcharge capability present new possibilities for the use of these cells in space applications. The new electrodes permit 50% of the total cell capacity to be delivered at 1.30v. The ceramic seals provide reliable operation without leakage for many years, and the built-in overcharge mechanism allows complete charging of the cells without the buildup of high internal gas pressures.

Abstract No. 28

Improvement in Cycle Life of the Silver Zinc Secondary Battery

Frank Solomon, Yardney Electric Corp., 40-52 Leonard St., New York 13, N. Y.

The rechargeable silver-zinc alkaline cell, which is especially applicable for uses where light weight and small volume are required, was introduced by Yardney Electric Corporation about 12 years ago. At that time cycle life was short and unreliable being in the range of 10 to 30 cycles, and capacity maintenance was quite poor. Since then, a great deal of research and development has been carried out to improve this condition. At present, production models have achieved over 150 cycles, and laboratory units now in evaluation have reached 300 deep cycles and as many as 450 partial cycles (30% depth). Capacity loss of less than 30% in 250 cycles has been attained. A discussion is given of the problems encountered and resultant solutions. Performance characteristics are summarized.

Abstract No. 29

The Silver-Silver Oxide Electrode, II. Anodization at 0° and 25°C in Alkaline Solutions

C. P. Wales, U. S. Naval Research Lab., Washington 25, D. C.

Capacity decreased when a silver electrode was cycled in 20% KOH at 25°C due to loss of active material. In 35% KOH the results at 0° were close to those at 25°, although charge-discharge efficiency was 100% only at low rates of current and polarization had increased. In 50% KOH at 0° charge acceptance was poor, under certain conditions a silver peroxy compound may form, and the electrode discharged even less readily than it charged.

Abstract No. 30

Sealed Alkaline Secondary Battery Systems

J. T. Arms and **J. C. Duddy,** Carl F. Norberg Research Center, Electric Storage Battery Co., Yardley, Pa.

Electrode fabrication techniques developed in recent years yield thin flexible electrochemically reversible structures which can be convolutely wound into cylindrical cell packs for insertion into metallic containers. The systems Ag-Cd, Ag-Zn, and Ni-Cd have been evaluated in the conventional "D" size configuration and comparisons are made there between. System advantages and disadvantages which accrue from fixation of cell geometry are presented.

Abstract No. 31

Oxide Formation and Reduction on Single Crystals of Nickel

J. L. Weininger and **M. W. Breiter,** Research Lab., General Electric Co., Schenectady, N. Y.

The formation of $Ni(OH)_2$ and higher oxides of nickel on different crystal faces and on polycrystalline nickel in alkaline solution was studied with a potentiostat. The number of molecular layers of oxide was small, varying from less than 1 to about 12. It was possible in some cases to elucidate the role of the metallic substrate in the anodization and reduction reactions. This is discussed in connection with the charge-discharge mechanism of a nickel anode in a battery system.

Abstract No. 32

Kinetic Studies of the Reversible Potentials of the Nickel Oxide Electrode as a Function of Degree of Oxidation

B. E. Conway and **E. Gileadi,** Dept. of Chemistry, University of Ottawa, Ottawa, Canada

The real reversible potential of the nickel oxide (Ni^{II}-Ni^{III}) electrode has been the subject of controversy for some years, and previously reported values are shown to be misleading since they are not based on well-defined equilibrium conditions or a well-defined state of the system. Electrochemical kinetic studies have been carried out at the nickel oxide electrode showing that the reversible potential for the Ni^{II}-Ni^{III} system is independent of the state of oxidation of the bulk oxide in the electrode over a wide range of degrees of oxidation. The properties of the electrode are shown to be determined by the state of a surface phase, which is completely charged when the bulk oxide material in the electrode has been charged to 10% of its total charge capacity. Experiments on sparingly charged electrodes have proved that charging of the bulk oxide does not commence significantly until the electrode is charged to about 1.5%. Consecutive electrochemical reactions possibly involved in the charging process are discussed.

Abstract No. 33

Systematized Concepts of Manganese Dioxide Dry Cells

Masataro Fukuda (present address: Dept. of Chemistry, University of Michigan, Ann Arbor, Mich.), **Taketsugu Hirai** and **Haruo Manabe,** Central Research Lab., Matsushita Electric Industrial Co., Osaka, Japan

This is a conclusion of a series of studies. The depolarizing activities of various manganese dioxides, the so-called γ-MnO_2 samples in particular, were related to their physical and chemical properties. These relations were schematically explained. Moreover, the discharge characteristics of the cells (which were principally different in $ZnCl_2$ concentrations) were clearly systematized in terms of the correlations between cell compositions, discharge drains, chemical and physical phenomena, internal resistances, and electropotential distributions. This concept can be fundamentally applied to any case of discharges.

Abstract No. 34

Thermal Dissociation of Manganese Dioxides

Earl Otto, National Bureau of Standards, Washington 25, D. C.

Oxygen equilibrium pressures have been determined experimentally for pyrolusite from 440° to 640°C. Constants have been calculated for the equation: $p(O_2) = a + b/T$. ΔH_o for the dissociation has been obtained. Reversibilitv of the dissociation reaction has been considered. Data are quoted from the literature and are examined. Calculated $p(O_2)$ and ΔH_o values based on the best available thermodynamic tables show marked disagreement with results obtained in the present work. African ore and electrolytic gamma MnO_2 have been brought near to pressure-temperature equilibria. Pyrolusite-MnO reactions have been studied and are reported.

Abstract No. 35

The Transient Impedance of Leclanché Cells, II. Current Drain Dependence

Aladar Tvarusko, Carl F. Norberg Research Center, Electric Storage Battery Co., Yardley, Pa.

A milliohmmeter, using 100 cps square wave, was employed to study the transient impedance of Leclanché cells. The transient impedance remained constant up to a certain current drain, after which it steadily decreased and approached the internal resistance of the cell. The larger the current drain the faster the decrease of the transient impedance. The influence of the composition and size of the Leclanché cell on the transient impedance was investigated.

Abstract No. 36

Silver, Silver Iodide, Vanadium Pentoxide, Carbon Solid Electrolyte Cell

D. V. Louzos, Research Lab., Union Carbide Consumer Products Co., Div. of Union Carbide Corp., Parma 30, Ohio

Solid electrolyte cells of the type silver, silver iodide, vanadium pentoxide, carbon are described. Such cells have been found to be capable of providing extremely stable potentials at fractional microampere drains over the temperature range of −75° to +200°F. Shelf life in excess of 20 years is estimated in view of the essentially stoichiometric silver iodide that is used as the solid electrolyte.

Abstract No. 37

Lithium Nonaqueous Secondary Battery

J. E. Chilton, Jr., and **G. M. Cook,** Lockhead Missile and Space Co., Dept. 52-30, Bldg. 102B, Sunnyvale, Calif.

Lithium-nickel chloride and lithium-silver chloride couples in a nonaqueous organic solvent-electrolyte system have been studied. These cells are shown to have theoretical values of 455 and 250 watt-hours per pound of active material and open circuit voltages of 2.8 and 3.0 volts respectively. Electrical conductivity and transference numbers of ions in the electrolyte system have been studied. Electrochemical properties of the cells such as electrode reaction reversibility and behavior on charge-discharge cycling are summarized. (This work is sponsored by the A.S.D. of the U.S.A.F.)

Abstract No. 38

A High-Rate High-Output Thermal Battery System

S. M. Selis, J. P. Wondowski, and **R. F. Justus,** Research Labs., General Motors Corp., Warren, Mich.

The system is $Ca/LiCl-KCl-AgCl-K_2CrO_4/Ag$. At the positive electrode silver ion is reduced to silver metal; silver ion is regenerated through the oxidation of silver by chromate ion. A calcium chromite is formed on discharge of the negative electrode. Cells are discharged at 400°-500°C. Terminal voltage is 2.65v at zero current, and with a current density of 800 ma/cm^2 it is 1.85v. Most of the difference is due to mass transfer polarization at the calcium electrode. Internal resistance is relatively small and remains constant during discharge.

Abstract No. 39

An Application of Thermodynamic Methods to the Determination of Reactions and Voltages in Liquid Ammonia Electromotive Cells

W. F. Meyers, Research Lab., G. & W. H. Corson, Inc., Plymouth Meeting, Pa.

A semi-empirical method for estimating the potentials of ammonia electromotive cells is proposed. This method is applied to a number of heavy metal sulfate-tvpe cells, and correlation to within 0.06v average deviation was obtained. The technique is extended to $AgCl,PbO_2$ and MnO_2 depolarizers. Finally the method is used to elucidate the performance of sulfur in ammonia batteries.

Abstract No. 40

The Bubbling Gas Electrode. Reduction of Oxygen on Graphite

W. J. Subcasky and **M. Shaw,** Electrochemical Research Div., The Electric Autolite Co., Toledo 1, Ohio

A new electrochemical technique which gives essentially time independent polarization curves is described. This technique gives reproducible concentration gradients at the electrode surface by controlled intermittent stirring by means of electronically pulsed gas bubbles. The method has been applied to the reduction of oxygen on catalyzed and uncatalyzed graphite electrodes. At uncatalyzed electrodes stepwise reduction of oxygen to perhydroxyl and then to hydroxyl ions was observed. At silver catalyzed electrodes, the enhanced decomposition of perhydroxyl ions was observed.

Abstract No. 41

On the Potential-Determining Reactions in the Au-O_2-Acid System

J. P. Hoare, Research Labs., General Motors Corp., Warren, Mich.

The rest potential of a clean gold bead in clean oxygen-saturated 2N sulfuric acid solution was studied as a function of time, partial pressure of oxygen, pH, and the history of electrode preparation. The 4-electron oxygen reaction is much more irreversible on gold than on platinum because the oxygen layers on gold are poor electronic conductors while those on platinum are good ones. Also, it is for this reason that oxide layers grow on gold surfaces with anodic polarization while they do not do so on platinum surfaces.

Abstract No. 42

Anodic Oxidation of Molecular Hydrogen at Platinum Electrodes

Akiya Kozawa, Dept. of Chemistry, Western Reserve University, Cleveland 6, Ohio

Ionization of dissolved hydrogen in alkaline and acid solutions was studied at smooth and platinized platinum electrodes by a voltametric method in a potential range between hydrogen and oxygen evolution potentials in those solutions. By surface voltammetry at least four redox couples on the platinum surface were found, and their redox potentials were determined. It was found that ionization of hydrogen at platinum electrodes was closely connected with the redox couples on the electrode surface.

Abstract No. 43

A Study of the Adsorption of Carbon Monoxide and Oxygen on a Platinum Electrode—Significance of the "Polarization Curve"

S. Gilman, Research Lab., General Electric Co., P. O. Box 1088, Schenectady, N. Y.

The adsorption of carbon monoxide on smooth platinum immersed in 1*N* $HClO_4$ has been examined by means of anodic linear voltage pulses. Carbon monoxide was determined both in the presence and absence of dissolved gas, and the extent and nature of saturation coverage was ascertained. The technique was further utilized to determine the extent of carbon monoxide and oxygen coverage during a slow triangular sweep. The characteristics of the current-voltage curves were interpreted with the aid of the adsorption data.

Abstract No. 44

The Fuel Cell Central Station: An Appraisal

J. R. Dafler, Central Research Div., Research and Development Dept., Continental Oil Co., P. O. Drawer 1267, Ponca City, Okla.

The conversion capacities of model fuel cell central stations are investigated. Three of the models considered refer to gasification plants associated with high-temperature cells. A fourth consists of a high-temperature cell fueled with hydrocarbons and steam. All are consumers of conventional fuels. The potentialities of these models are examined in terms of the enthalpy changes of the pertinent reactions, thermal demands of the model plants, and fuel cell efficiencies of 65% and over.

Abstract No. 45

The Hydrazine-Oxygen Fuel Cell, I. The Mechanism and Kinetics of the Hydrazine Electrode

B. Baker and **M. Eisenberg,** Electrochimica Corp., Menlo Park, Calif.

The hydrazine-oxygen electrochemical system represents an interesting basis for fuel cells operating at room temperature. The anodic oxidation of hydrazine in alkaline media proceeds at a relatively high rate with small polarization losses. The active nature of the reactant helps in the maintenance of relatively poison-free anode surface. Kinetic data are analyzed to determine the nature of the anodic processes and the mech-

anisms are derived. The chemical decomposition of the hydrazine and its effect on the over-all faradaic efficiency as a function of current density are discussed and pertinent data presented.

Abstract No. 46

The Performance of a Compact Design Butane-Air Fuel Cell

M. Eisenberg and **B. Baker,** Electrochimica Corp., Menlo Park, Calif.

Open and closed circuit potentials of a butane-air fuel cell of compact high energy design are presented. Attention is given to individual electrode polarization. Other operational characteristics of the system such as mass and heat transfer calculations are also given.

Abstract No. 47

Vacuum Depolarized Hydrogen Concentration Cells for Space Power

H. Krupp, G. Sandstede, and **G. Walter,** Battelle Institut e. V., Frankfurt (Main), Germany, and **R. McJones,** 529 Via del Monte, Palos Verdes Estates, Calif.

The proposed hydrogen concentration cell uses the vacuum of space to maintain a low concentration at one electrode. A thin palladium membrane permits the hydrogen to leave the cell while retaining the electrolyte. Cell performance appears to be limited both by hydrogen diffusion rates within the palladium membrane and by the maximum rate at which hydrogen molecules can be propelled into space from the outer electrode. Such a cell may become competitive with fuel cells and other space power systems.

Abstract No. 48

New High-Performance Methanol Fuel Cell Electrodes

D. B. Boies and **Andrew Dravnieks,** Armour Research Foundation of Illinois, Institute of Technology, Technology Center, Chicago 16, Ill.

Compact electrodes were manufactured by electrochemical deposition of noble metals on thin porous layers of Raney nickel. Such structures were simple to prepare, and the amount of the noble metals and nickel needed per unit area was minimal. Fast electrochemical oxidation of methanol and formaldehyde occurred at these electrodes in alkaline solutions. At 80°C electrolyte temperature the polarization from open circuit was 0.07v and 0.27v at 10 and 500 ma/cm², respectively.

Abstract No. 49

An Aluminum-Air Fuel Cell

R. A. Foust, Jr., Philco Scientific Lab., Philco Corp., Blue Bell, Pa.

A low-temperature fuel cell utilizing a consumable aluminum anode and a porous nickel cathode operating on ambient air has been developed. 10-cell batteries, specifically designed to deliver 5 amps at 12v, have been fabricated. Operating characteristics are presented and discussed, as are operating parameters and design flexibility which permit modifying the method of operation for different specific applications, such as portable *vs.* stationary and cyclical *vs.* continuous uses.

CORROSION

Abstract No. 50

Kinetics of Anodic Formation of Passive Films on Iron in a Neutral Solution

Norio Sato and **Morris Cohen,** Division of Applied Chemistry, National Research Council, Ottawa, Ont., Canada

The rate of growth of passive films on iron was measured in neutral boric/borate solutions by using a potentiostatic method and a galvanostatic method. It was found that the rate of growth of the oxide changed with film thickness as well as potential and could be expressed as

$$i = k \exp(\beta E) \exp\left(-\frac{Q_T}{B}\right)$$

where i is the rate of growth, E the potential, Q_T the total amount of charge accumulated in the film, and k, β, and B are constants. The constant β was close to $F/2RT$, and the constant B was a linear function of temperature. k is related to the exchange current of the rate-determining reaction. The mechanism of film growth is discussed.

Abstract No. 51

Effect of pH, Chlorides, and Sulfates on the Behavior of Chromates and Other Passivators as Corrosion Inhibitors for Steel

S. Matsuda (present address: ILIKON Corp., Natick Industrial Center, 10 Strathmore Rd., Natick, Mass.) and **H. H. Uhlig,** Corrosion Lab., Dept. of Metallurgy, Massachusetts Institute of Technology, Cambridge, Mass.

Corrosion rates of Armco iron foil were determined by a sensitive electric resistance method. Chromates inhibit within the pH range 3-6 in presence of ClO_4^-, but are not as effective in presence of SO_4^{--} or Cl^-. The critical minimum concentration C for inhibition at room temperature follows the equation $\log C = 1.18 \log (Cl^-) + 1.4$ where concentrations are in molarity. In absence of Cl^-, the critical concentration is $5 \times 10^{-4}M$ in agreement with data published by other investigators. Sulfates are more damaging than chlorides, whereas for nitrites the reverse situation applies. Critical concentrations of passivators in absence of extraneous anions were measured for molybdates, tungstates, iodates, and vanadates, the first two requiring dissolved oxygen for inhibition, but not the others. For chromates, an initial higher corrosion rate (1 mdd) lasting about 1 hr precedes the final rate (0.1 mdd) in aerated solutions. In deaerated solutions the final rate appears from the very first. At 100°C, the initial reaction rate in aerated solutions increases (53 mdd), but not the final rate (0.0 mdd). These results are interpreted in terms of O_2 corrosion before the passive film is established by reduction of the passivator, and by competitive adsorption by various anions for sites on the metal surface.

Abstract No. 52

On the Passivity of Titanium and Tantalum

Rikuro Otsuka, Institute of Physical and Chemical Research, Hongo, Tokyo, Japan

The surfaces of titanium and tantalum passivated in acid and base (HCl, H_2SO_4, and NaOH) included their hydrides. This is consistent with the fact that the Flade potentials of these metals are much less noble than the reversible hydrogen potential. The presence of these hydrides was indispensable to promote passivation and rendered these metals more resistant to acid and base. This phenomenon could be comprehended by taking account of the fact that there exists a remarkable difference between the hydrogen overpotential of these pure metals and those of their hydrides.

Abstract No. 53

Effect of Velocity on Corrosion of Iron in Aerated and Deaerated Sulfuric Acid

Z. A. Foroulis (present address: Engineering Div., Esso Research and Engineering Co., P. O. Box 209, Madison, N. J.) and **H. H. Uhlig,** Corrosion Lab., Dept. of Metallurgy, Massachusetts Institute of Technology, Cambridge, Mass.

In aerated $0.33N$ H_2SO_4, relatively pure iron (0.009%C) corrodes first at a rate which increases and later decreases with velocity. For 0.24%C and 1.05%C steels, the rate first decreases, reaching a minimum, and then increases with velocity. Oxygen or Fe^{+++} in small concentrations at the metal surface were found to act as inhibitors apparently increasing anodic polarization and decreasing the rate; in higher concentrations they act as cathodic depolarizers and increase the rate. In

deaerated 0.33*N* H_2SO_4, the corrosion rate of 0.009%C iron is independent of velocity up to the maximum velocity of the test (200 meters/min). This is in accord with lack of dependence of activation polarization involving H^+ discharge, which is the controlling reaction on velocity.

Abstract No. 54

Activation Characteristics of Passive Stainless Steels in Sulfuric Acid Solutions

Tatsuo Ishikawa and **Go Okamoto,** Physico-Chemical and Electrochemical Lab., Faculty of Engineering, Hokkaido University, Sapporo, Japan.

The behavior of self-activation of passive stainless steels has been observed by measuring potential decay curves in 30% H_2SO_4 free from oxidizing agents. Passivation was established in 5% H_2SO_4 by polarizing the specimen anodically with a potentiostat or by adding an oxidizing agent to the solution. Judging from the behavior of passivation and activation, the passivators used were classified into two groups: (*a*) one which produces passive films similar to that obtained by anodic passivation (metallic ions such as Ce^{4+}, Hg^{2+}, and Cu^{2+}), and (*b*) one which forms comparatively imperfect films due to the slow rate of its reduction (oxidizing anions including oxygen such as O^{2-}, HO_2^-, $S^2O_8^{2-}$, and CrO_4^{2-}). This grouping coincides with that obtained from the previous measurements on the characteristics of cathodic reduction of the passivators on the passive stainless steels. Discussion is made especially in terms of the properties of passive films.

Abstract No. 55

Corrosion Inhibition of Iron by Methyl Pyridines in 6N HCL

R. C. Ayers and **Norman Hackerman**, Dept. of Chemistry, University of Texas, Austin 12, Texas

A series of methyl pyridines have been examined with regard to their corrosion inhibition properties in an attempt to relate inhibition to molecular structure. Experiments were performed with Armco iron in 6*N* HCl at 35°C. Corrosion rates were determined colorimetrically and electrode potentials *vs.* S.C.E. were also measured. The results are explained on electronic and steric grounds.

Abstract No. 56

The Oxidation of Aluminum in Contact with Mercuric Iodide

D. A. Jackson, Jr., and **Henry Leidheiser, Jr.,** Virginia Institute for Scientific Research, 2820 Grove Ave., Richmond 21, Va.

The rate of air oxidation of pure aluminum in contact with mercuric iodide increased greatly with increase in relative humidity. Rates equivalent to 0.6 mg of oxygen/cm²/min were observed at 30°C and 100% relative humidity on bulk samples. The water content of the oxide conformed approximately to that expected for $Al_2O_3 \cdot 3H_2O$. X-ray diffraction analyses were made of the product after various treatments.

Abstract No. 57

Photomicrographical Observations of Mercurous Halide Films

D. C. Cornish, S. N. Das, D. J. G. Ives, and **R. W. Pittman,** Dept. of Chemistry, Birkbeck College, Malet St., W. C. 1, London, England

Because of their high birefringence, extremely thin films of mercurous halides can be observed under the polarizing, reflecting microscope. This has been adapted to observation of the growth of such films on mercury, with results that are correlated with previous studies of the galvanostatic anodization of mercury in halide solutions, of the mechanism of the reversible calomel electrode, and of the properties of passivating films of mercurous halides.

Abstract No. 58

An Infrared Study of the Hydration of Anodic Coatings on Aluminum

C. E. Michelson and **J. F. Murphy,** Metals Div., Olin Mathieson Chemical Corp., P. O. Box 906, New Haven 4, Conn.

Techniques of preparing "window" specimens of anodic coatings for infrared transmission studies have been developed. Reduction of the normal interference fringes due to first surface reflection has permitted the study of the spectrum over the 1-15μ range using the as-formed oxide specimens rather than mulls or pellets. The infrared spectra of hydrated anodic oxide were found to resemble those reported for the trihydrate rather than the monohydrate of alumina regardless of the conditions under which hydration occurred. The effect of phosphates and chromates on the hydration of the oxide was also examined and was found to modify the extent of hydration.

Abstract No. 59

Disintegration of Magnesium While Dissolving Anodically in Neutral and Acidic Solutions

M. E. Straumanis and **B. K. Bhatia,** Dept. of Metallurgical Engrg., University of Missouri School of Mines and Metallurgy, Rolla, Mo.

The closer investigation of the dark deposits, which separate from the magnesium anode in form of leaflets in neutral and even in acidic solutions, showed that the Mg dispersion theory (Baborovsky, 1905) is correct. A great multitude of the particles of about 6×10^{-5} to 7×10^{-4} mm in diameter were visible in the flakes. In perchloric acid the magnesium anodes turned slightly dark. Beautiful patterns of deformation twins appeared. At still higher current densities flakes separated from the anode containing innumerable metallic particles. The latter broke out at places of the anode where the bonding of the metal was weakened leaving series of dark holes.

Abstract No. 60

A Radiotracer Study of Sulfate Ion Behavior in Aluminum Anodic Coatings

C. E. Michelson and **J. F. Murphy,** Metals Div., Olin Mathieson Chemical Corp., P. O. Box 906, New Haven 4, Conn.

The effect of sealing and various chemical treatments on the adsorption and exchange of sulfate ions in anodic coatings has been studied using radiotracer techniques. Radio-autographs of the anodized aluminum surfaces have demonstrated large local variations in adsorption and exchange reactions. Results have shown that the tendency toward adsorption of ions from solution is greatly reduced by very short exposures to boiling water.

Abstract No. 61

The Difference Effect on Magnesium Dissolving in Acids

W. J. James, M. E. Straumanis, and **B. K. Bhatia,** Dept. of Chemical and of Met. Engrg., University of Missouri School of Mines and Metallurgy, Rolla, Mo.

The difference (Δ) effect on Mg metal was measured in HCl, $HClO_4$ and H_2SO_4 of concentrations between 0.05 and 0.5*N* at 25°C. Generally the effect was positive, but departed from linearity at high current densities and with decreasing acid concentrations. In sulfuric acid the positive effect changed to the negative at increased current densities. Disregarding the difference effect the departure from Faraday's law can be attributed to the anodic expulsion of uncommon valency Mg-ions. Very smooth but unrealistic curves are obtained.

Abstract No. 62

The Anodic Behavior of Zinc in Potassium Hydroxide Solution

N. A. Hampson and **M. J. Tarbox,** Dept. of Applied Chemistry, College of Technology, Loughborough, England

A study of the anodic behavior of horizontal zinc electrodes in KOH solution has shown that the equation

$(i - i_1)\ t^{1/2} = k$ holds for concentrations in the range 1-13.8M and passivation times in the range 10-800 sec. The constant k depends on the KOH concentration and attains a maximum value in the region of 8.5M KOH; i_1 from a least squares fit is very near zero in all cases. From the linear parts of the curves connecting anode potential and time, values of dE/dT indicate that the conductivity of the anodic product prior to passivation depends on the concentration of the KOH electrolyte. This conductivity attains a maximum value, of approximately 100 times that of pure zinc oxide, in electrolyte of 9M concentration.

Abstract No. 63

A Polarization Method for Determining the Corrosion Rate of Tin Plate

T. J. Butler and **P. R. Carter,** Applied Research Lab., U. S. Steel Corp., Monroeville, Pa.

A corrosion test for tin plate based on polarization measurements is described. In this test a specimen is polarized, and the current, I, and potential, E, are measured simultaneously. Two parameters, the polarization resistance R and the corrosion current Ic, both related to the corrosion rate, are determined from graphs of E *vs.* I and of E *vs.* log I, respectively. The theoretical relationship between R and Ic was found to hold for alloy-layer ($FeSn_2$ on a steel base) samples polarized in citric acid, grapefruit juice, tomato juice, and prune juice. Both R and Ic determined in grapefruit juice using alloy-layer samples had a good correlation with ATC test values. R and Ic also rank the three food juices, prune, grapefruit, and tomato, in the same order of corrosivity as do pack tests and couple current tests.

Abstract No. 64

On the Etching Characteristics and Capacitor Properties of Zone Refined Aluminum

R. Bakish, Alloyd Electronics Corp., 35 Cambridge Parkway, Cambridge 42, Mass., and **R. Kornhaas,** and **E. Z. Borders,** Republic Foil, Inc., Triangle St., Danbury, Conn.

Zone refined aluminum was subjected to electrochemical etching under a variety of experimental conditions. Capacitance and leakage currents for material so processed and formed at different voltages are presented. These results are compared with similar data obtained on lower purity aluminum.

Abstract No. 65

Chromate Ion Inhibition of the Differential Oxygen Corrosion of Zinc

M. M. Wright, Consolidated Mining and Smelting Co. of Canada Ltd., Trail, B. C., Canada

Chromate ion, in 0.1 to 100 ppm Cr^6 concentration, produces marked effects at the zinc electrodes of a differential oxygen cell. The anode potential is shifted in a positive direction, compensating for the like depolarizing action of oxygen at the cathode, and cathodic reduction of oxygen is inhibited. When chromate is added to a corroding cell, there is an instant response; when initially present, current and potentials change over hours. A chromium oxide film forms on the zinc surface which provides protection even after removal of soluble chromate.

Abstract No. 66

Dissolution of Brass in Sulfuric Acid Solutions, I. 85/15 Brass

J. Bumbulis (present address: Research Dept., Imperial Oil Ltd., Sarnia, Ont., Canada) and **W. F. Graydon,** Dept. of Chemical Engineering and Applied Chemistry, University of Toronto, Toronto, Canada

The dissolution of 85/15 brass from rotating cylindrical samples by aerated dilute sulfuric acid solutions was investigated over the range of 15°-35°C. The reaction was found to proceed in three successive steps: dezincification of the brass surface, dissolution of the redeposited copper and etching of the brass surface, dissolution of the dezincified surface. The rate of the last step was determined by the rate of dissolution of copper, zinc being dissolved as fast as it is uncovered by the dissolving copper. The mechanism of dissolution of copper from 85/15 brass was found to be similar to that of pure copper, controlled by the rate of oxidation of cuprous ions to cupric. Equations were developed that describe the effect of experimental variables on the apparent dissolution rate of copper for each stage. A general kinetic equation was developed that describes the rate of dissolution of copper for all stages. Hydrogen peroxide was found to be a reaction product.

Abstract No. 67

Dissolution of Oxygen Layers on Platinum in Chloride Solutions

M. W. Breiter and **J. L. Weininger,** Res. Lab., General Electric Co., Schenectady, N. Y.

Oxygen layers on platinum are dissolved at open circuit in electrolytes containing chloride ions. The dissolution of layers formed at 1.4 and 1.6v in 1N H_2SO_4 was investigated in two solutions with different concentrations of chloride ions at 25° and 85°C, and it is shown that the dissolution occurs by the following mechanism. The electrode is the seat of simultaneous cathodic and anodic reactions, in which the sum of the partial currents of anodic platinum dissolution on the free surface is equal to the cathodic partial current of the oxygen reduction.

Abstract No. 68

The Cathodic Reduction of Oxygen at a Rotating Disk

G. Butler and **S. C. Shome,** National Chemical Lab., Teddington, Middlesex, England

The use of a rotating disk electrode in the study of electrode processes is discussed. Rates of reduction of oxygen have been measured at cathodes of various sizes in acid, near-neutral, and alkali solutions.

Abstract No. 69

Electrochemical Mechanism of Hydrogen Embrittlement of Steel

Walter Beck, Alfred Glass, and **Edward Taylor,** Naval Air Material Center, Aeronautical Materials Lab., Philadelphia 12, Pa.

Hydrogen overvoltage, hydrogen coverage, and the radiochemically determined surface concentration of C^{14} on high strength steel, polarized cathodically in $NaC^{14}N$ solutions, increase with rising concentration of this compound as rapidly as ductility decreases. The cyanide is chemisorbed, and electrochemical and radiochemical desorption studies proved it to be tenaciously adherent to the steel. Results are discussed in the light of a mechanism in which presence of cyanide on the steel surface retards the rates of the electrochemical and catalytic hydrogen desorption reactions. Hydrogen accumulates on the cathode, creating favorable conditions for fast diffusion of embrittling H atoms into the steel.

Abstract No. 70

Time Dependency of Anodic Polarization Currents

O. L. Riggs, Jr., Continental Oil Co., P. O. Drawer 1267, Ponca City, Okla.

Anodic polarization studies were used to determine current densities necessary for the passivation of 304, 316, 410 stainless steel and 1020 carbon steel in 20.0N H_2SO_4 at 25°C. Polarization data were obtained on Armco iron (99.99%) in both 20.0N H_2SO_4 and 1.0N NaOH at 25°C. Along the anodic polarization curve the potential was held constant at 20 mv increments, and the current was recorded as a function of time (at intervals of 1, 3, 20, and 60 min). When the anodic polarization curve was plotted for the 60-min interval, minimum currents were observed for specific potentials. These potentials at which the minima were observed were defined as inversion peaks. It was suggested that they correspond to various oxidation states of iron.

Abstract No. 71

Effect of Acetylenic Molecules on Cathodic Overvoltage on Steel in Acid Solutions

E. J. Duwell, Minnesota Mining and Manufacturing Co., 2301 Hudson Rd., St. Paul 19, Minn.

An apparatus was constructed for accurately measuring changes in electrode potential at constant current

density. Large increases in cathodic overvoltage were noted when acetylenic molecules were adsorbed on a steel cathode. Thus, it can be concluded that these molecules slow down the oxidation of steel in acid solutions by inhibiting the cathodic reactions. The most effective adsorbates are characterized by steric availability of acetylenic bond, nonionic character, and large molecular size.

Abstract No. 72

Surface Layers Associated with the Electropolishing of Copper in H_3PO_4

F. H. Giles, Jr., Physics Dept., University of South Carolina, Columbia, S. C.

Copper anodes will electropolish in 50% H_3PO_4 (throughout either of two ranges of applied voltage). Investigation reveals no evidence of an adherent surface layer during polishing in the lower voltage range, whereas in the higher range such a layer is evident. Also, further insight into possible reactions occurring at the surface has been obtained from schlieren photographs made during electrolysis. (Supported by the Office of Army Research, Grant DA-ORD-9).

Abstract No. 73

The Copper Etching Characteristics of Ammonium Persulfate Solutions

T. D. Schlabach and **B. A. Diggory**, Bell Telephone Labs., Inc., Murray Hill, N. J.

The etching of copper by ammonium persulfate was studied over a range of temperatures and solution concentrations. The influence of already dissolved copper on the rate was examined as well as the added presence of various salts in very low concentrations. Silver, mercury, and gold salts were found to accelerate the corrosion rate markedly. This may, in part, be explained by plating out on local cathode areas. Ammonium persulfate etching of copper was also compared with that of chromic acid, cupric and ferric chloride.

Abstract No. 74

The Rate of Growth of Electrochemical Etch Pits at Dislocations on (111) Copper Surfaces

L. D. Hulett and **F. W. Young, Jr.,** Solid State Div., Oak Ridge National Lab., Oak Ridge, Tenn.

Copper crystals with $\sim 10^3$ dislocations per cm^2 were etched electrochemically on a (111) surface in solutions containing HCl and HBr under conditions such as to form pits at dislocations. The surface was photographed as the reaction proceeded. The rate of growth of etch pits and of other surface features was determined, and the results are presented in terms of the variables $[Br^-]$, $[Cl^-]$, current density and crystal orientation.

Abstract No. 75

Some Effects of Metal Defect Structure on the Anodic Dissolution of Single Crystalline Copper

L. H. Jenkins and **Ugo Bertocci,** Solid State Div., Oak Ridge National Lab., Oak Ridge Tenn. Operated for the U.S.A.E.C. by Union Carbide Corp.

Studies of the effect of metal defect structure on the anodic dissolution of single crystals of copper in acidic copper sulfate solutions have been extended to include observations on (111) and (110) oriented surfaces. Results obtained at low current densities ($\sim 10\ \mu a\ cm^{-2}$) are correlated with data previously reported for the (100) orientation. Similarities and differences of current-potential data and topographic changes on surfaces of different orientations are discussed.

Abstract No. 76

Electrochemical Behavior of Nickel Intermetallic Compounds

A. K. M. Shamsul Huq and **M. A. Loud**, Tyco Labs., Inc., Waltham, Mass.

A number of intermetallic compounds containing nickel together with an electronegative element from groups IV-B, V-B, VI-B of the periodic table have been synthesized and their electrochemical behavior studied. Anodic and cathodic current-potential measurements were made on NiO, NiS, NiAs, NiSb, and NiSi, and elemental nickel in the massive form in N_2, O_2, and H_2 atmospheres in alkaline and acid perchlorate media. Galvanostatic and potentiostatic techniques were used. Results are discussed in the light of electronic and chemical properties of the electrode materials.

CORROSION—ELECTRONICS

Abstract No. 77

Adsorption at Interfaces

J. H. de Boer, Wetenchappelijke Raad Voor de Kernenergie, Stadhoudersplantsoen 12, S-Gravenhage, Netherlands

Without adsorption life on earth would be impossible. Current problems of heat transfer affect the physisorption of inert gases. Chemisorption modifies the nature of surfaces seriously; it leads to "protecting" or to "promoting" effects if the result suits us, to "poisoning" if it does not. In many catalytic phenomena at solid-gas interfaces or in condensation-evaporation processes the movement of adsorbed species along the surface is as important as the move of gas molecules to or from the surface. If ions play a role, the forming and the conduct of ionic pairs may be of major importance. The same holds for phenomena at solid-electrolyte interfaces. The significance of the adsorption of solvent molecules is not always sufficiently appreciated. All adsorption phenomena lead to electrical double layers. However, these double layers at solid-gas interfaces and at solid-electrolyte interfaces differ in the magnitude of their effects. Molten electrolytes may contain ionic complexes, quite different from those in electrolyte solutions. The phenomena at solid-melt interfaces demand for their understanding a deeper knowledge of the liquid phase. The same holds true when the melt is a molten metal.

Abstract No. 78

Epitaxial Growth of Silicon by Vacuum Sublimation

E. Tannenbaum Handelman and **E. I. Povilonis,** Bell Telephone Labs., Inc., Murray Hill, N. J.

Silicon has been grown epitaxially on silicon substrates by a process of vacuum sublimation. The important new features of the system which have resulted in a high degree of control of process variables are that the reaction chamber contains only silicon and quartz and that the chamber is continuously pumped throughout the process to a pressure of 10^{-4}-10^{-5} torr. The physical support for the substrate acts as the source of silicon as well as the source of dopant. In this way a high degree of control of the thickness and resistivity uniformity and reproducibility have been obtained with both n- and p-type epitaxial films of several resistivities on both n- and p-type substrates. Details of the system and an analysis of the results are given. Preliminary results obtained on heterojunctions grown in a similar manner are reported also.

Abstract No. 79

Vapor Growth of Germanium-Silicon Alloy Films on Germanium Substrates

R. C. Newman and **J. Wakefield,** Associated Electrical Industries, Ltd., Aldermaston Court, Aldermaston, Berks., England

Silicon has been transported from a source at 1100°C onto germanium single crystal substrates at 700°-900°C in a sealed system by the disproportionation of the iodide. Deposits thus formed are found to be germanium-silicon alloys of variable composition. These structures have been examined by etching techniques, electron microbeam x-ray analysis, and electron diffraction. During deposition, plastic deformation of the germanium occurs resulting in dislocation densities of up to $5 \times 10^7/cm^2$, and appreciable cavity formation is found in monocrystalline deposits formed at high substrate temperatures.

Abstract No. 80

Masking of Epitaxial Germanium by Fluorocarbons

C. Z. LeMay and **J. C. Marinace,** IBM Corp., Thomas J. Watson Research Center, Yorktown Heights, N. Y.

Epitaxial growth of Ge and GaAs in an iodide disproportionation reaction can be masked by a thin (~10,000Å) film of a fluorocarbon such as Teflon applied by evaporation or by "writing-on." Temperature and ambient conditions affect the masking efficacy. Masking against common liquid etches and also against iodide vapor etch is effective. Infrared absorption spectra, surface properties, etching characteristics, and temperature effects suggest the masking mechanism is one of adsorption rather than chemisorption.

Abstract No. 81

The Evaporation Kinetics of Iron-Chromium Alloys

L. A. Morris and **W. W. Smeltzer,** Dept. of Metallurgy and Metallurgical Engineering, McMaster University, Hamilton, Ont., Canada

The evaporation kinetics of Fe-5% Cr and Fe-25% Cr polycrystalline alloys were investigated over the temperature range 900°-1100°C by weight loss measurements. Also, surface topographies were examined by hot-stage microscopy. Constant rates of evaporation were found for exposures to 40 hr. The heats of evaporation were 98 and 94 kcal/mole for the austenitic 5% and ferritic 25% chromium alloy, respectively. A comparison of these results with those from Knudsen cell measurements demonstrated that the evaporation coefficient did not exceed 0.5.

Abstract No. 82

Effects of Alloying Elements on the Oxidation of Tin

W. E. Boggs, R. H. Kachik, and **G. E. Pellissier,** Applied Research Lab., U. S. Steel Corp., Monroeville, Pa.

Small amounts of certain alloying elements change the oxidation behavior of tin. If the formation of SnO is thermodynamically favored, elements that enter the oxide with valence greater than tin increase the rate. When the formation of SnO is not favored, the alloying element is oxidized preferentially on the surface of the alloy in the form of a thin oxide film and discrete crystallites. The crystallites were found to be associated with dislocations.

Abstract No. 83

Imperfections at Interfaces

W. Dekeyser, University of Ghent, Ghent, Belgium

Some of the properties of the surface considered as a defect are discussed with special emphasis on work performed recently in the crystallography laboratory of the University of Ghent. In this way a treatment of the surface levels in III-V compounds will be considered as well as polarization currents due to trapped electrons in surface and subsurface levels in nearly stoichiometric rutile single crystals. As an example of the surface-gas interaction, new results on the mechanism of the reaction used for decorating dislocations are given (the high-temperature hydrogen treatment of silver and nitrate doped halide).

Abstract No. 84

Morphology Control of the Solid-Melt Interface

W. A. Tiller, Research Labs., Westinghouse Electric Corp., Beulah Rd., Churchill Boro., Pittsburgh 35, Pa.

The interface morphology to be discussed is that associated with the "macroscopically smooth-cellular or dendritic" interface transition. The theoretical evaluation of the physics involved in this transition is presented along with the quantitative relationship describing the onset of the transition in terms of the macroscopic variables of the system (thermal, hydrodynamic, constitutional, and crystallographic). Experimental support for these predictions is reviewed. The consequences, in terms of the degree of chemical segregation and physical imperfection density incorporated into a crystal, for crystals grown under conditions that fall in the stability domain of the cellular or dendritic interface morphology are also presented.

Abstract No. 85

Studies of the InSb Crystal-Melt Interface

N. Albon, Battelle Memorial Institute, 505 King Ave., Columbus 1, Ohio

The InSb interface was studied by microscopical examination of crystals after rapid removal from the melt. The crystals had been allowed to approach equilibrium at a curved melting point isotherm, and the magnitudes of the thermal gradients across the interface were measured. These observations revealed facets and characteristic features on the curved areas on all crystals examined. Some of these features can be related to crystal growth mechanisms. (Supported by the U.S.A.F.)

Abstract No. 86

Formation of Conical Hillocks on Crystals

S. E. Miller and **N. Albon,** Battelle Memorial Institute, 505 King Ave., Columbus 1, Ohio

Recent microscopic examinations of high-purity GaAs crystals, prepared by the horizontal gradient-freeze technique, have revealed a multitude of minute "conical hillocks" on the surface of the ingots. The hillocks are also quite prominent on InAs, InP, and GaP, and to a lesser degree on InSb and GaSb. A detailed description of the phenomena is presented illustrated with photomicrographs.

Abstract No. 87

The Travelling Solvent Method of Crystal Growth, Part II

A. I. Mlavsky and **Martin Weinstein,** Tyco Labs., Inc., Waltham, Mass.

A technique of crystal growth of compounds from solution has been developed in which a thin zone of solvent is moved through a material under the influence of a temperature gradient. The applications of this technique have been studied for the growth of GaAs from Ga, GaP from Ga and Sn, SiC from Cr, and $SrTiO_3$ from KF. In particular, single crystals of GaAs have been grown onto seeds by the movement of a thin zone of liquid Ga through GaAs at a temperature much below its congruent melting point. The conditions influencing zone movement for this system have been studied, including zone thickness, average temperature, temperature gradient, and seed orientation. The electrical properties of grown crystals have been measured, and it has been shown that the passage of the zone causes considerable purification. P-N junctions have been formed by doping the liquid zone with various impurities.

Abstract No. 88

Growth Processes of Three Twin Germanium Dendrites

R. G. Seidensticker and **D. R. Hamilton,** Research Labs., Westinghouse Electric Corp., Beulah Rd., Churchill Boro., Pittsburgh 35, Pa.

Growth velocity and tip morphology measurements have been made using three twin germanium dendrites. A comparison is made between two and three twin dendrites and between three twin dendrites grown in both the [2$\bar{1}$1] and the [$\bar{2}$11] directions. Each of these modes of growth has distinctive features which are examined in terms of the interface processes.

Abstract No. 89

Preferred Orientation in the Growth of Refractory Metals from the Melt

L. G. Tensmeyer, Speedway Labs., Linde Co., P. O. Box 8237, Indianapolis 24, Ind.

High-purity refractory metals (<100 ppm impurities) growing from a melt on polycrystalline seeds rapidly become essentially single crystals. The preferred ori-

entation, a <110> direction perpendicular to the solid-liquid interface, occurs by the extension of (110) planes along the S-L-I. The (110) planes are favored both kinetically and at near equilibrium conditions. Viewed in transverse section the S-L-I configuration during Verneuil-type heating has two maxima.

Abstract No. 90

Electrical and Optical Properties of Semiconductor Surfaces

E. Mollwo, Institute for Technical Physics, University of Erlangen, Erlangen, Germany

In spite of the fundamental and practical importance of semiconductor surfaces, our knowledge in this field is relatively poor. The reason for this fact is the difficulty in obtaining conditions of suitable purity for experimental and theoretical investigations. An attempt will be made to give a short survey of the theoretical concepts and models for pure surfaces as well as for coated surfaces. Some methods for the investigation of the electrical and optical properties of semiconductor surfaces are presented. The results are discussed for some particular examples.

Abstract No. 91

Surface Energy of Germanium and Silicon

R. J. Jaccodine, Bell Telephone Labs., Inc., Allentown, Pa.

Surface energy is one of the most fundamental parameters of a solid since it depends directly on the binding forces of the material. Indeed, it is a measure of the work necessary to separate a material into two parts along a plane. Very few measurements have been made of this quantity and these by indirect means because of difficulties of measurement and interpretation. This report deals with a direct measurement of surface energy of Ge and Si made by the cleavage technique. By measuring the force just necessary to move a crack "in reversible fashion" the surface energy can be obtained. The measured value for the {111} planes of Ge and Si are 1060 ergs/cm^2 and 1230 ergs/cm^2. From these measured values the energy of the other two planes of interest can be obtained. They are:

	{100}	{110}
Ge	1835 ergs/cm^2	1300 ergs/cm^2
Si	2130 ergs/cm^2	1510 ergs/cm^2

Using the measured value of surface energy, the bond strength of Si and Ge was obtained as Ge-Ge = 42.6 kcal/mole; Si-Si = 45.5 kcal/mole. Finally the temperature dependence of surface tension $d\gamma/dT$ was obtained as —0.46 ergs/cm^2 deg for Ge and —0.30 ergs/cm^2 deg for Si.

Abstract No. 92

The Surface-Barrier Photovoltaic Effect on Silicon, I

A. H. A. Pampanini, Maryjane MacLaren, and **A. I. Mlavsky,** Tyco Labs., Inc., Waltham, Mass.

The parameters affecting the behavior of photovoltaic cells utilizing the potential barrier at a metal-silicon surface have been isolated and studied in an effort to optimize the energy conversion efficiency. All of the relevant factors have been studied both experimentally and theoretically, and qualitative agreement between experiment and theory has been shown. The long-range objective of the study is the development of large-area solar cells based on the use of semiconductor films.

Abstract No. 93

The Surface-Barrier Photovoltaic Effect on Silicon, II

A. H. A. Pampanini and **Georg Rupprecht,** Tyco Labs., Inc., Waltham, Mass.

The photovoltaic effect which is observed when a metal film is deposited on an oxide-covered silicon surface has been used to yield direct information concerning the energy states at the semiconductor-oxide interface. The effect also provides a novel technique for studying the tunnelling of holes and electrons through the oxide film. The temperature dependence of the photovoltaic behavior has been measured and the results explained on the basis of energy states at the silicon surface.

Abstract No. 94

Effect of Light on the Electrochemical Behavior of the Zn-ZnO Electrode

W. R. Ware, R. A. Powers, and **G. K. Johnson,** Research Lab., Union Carbide Consumer Products Co., Parma 30, Ohio

A detailed experimental study has been made of the electrochemical behavior of the Zn-ZnO electrode under the influence of illumination. Quantitative determinations were made for: (*a*) the effect of light on the rate of zinc oxidation and oxygen formation at anodically polarized electrodes; (*b*) effect of illumination on anodic current-voltage relationships; (*c*) quantum yields as a function of film thickness, potential, and light intensity.

Abstract No. 95

The Oxide Films Formed on Copper Single Crystal Surfaces in Water, III. Effect of Light

Jerome Kruger and **J. P. Calvert,** National Bureau of Standards, Washington 25, D. C.

The effect of illumination by light in the visible region of the spectrum on the kinetics of oxide film growth on copper single crystals immersed in high-purity water containing oxygen at room temperature was studied using the ellipsometer. Depending on the wavelength and intensity of the illumination used and on the crystallographic orientation of the illuminated surface, the magnitude of the rate and type of rate law observed could be affected. (This work was supported in part by the Corrosion Research Council.)

Abstract No. 96

The Anodic Dissolution Reaction at Semiconductor Electrodes

W. W. Harvey, Lincoln Lab., Massachusetts Institute of Technology, Lexington 73, Mass.

The formation of a diffusion layer within the electrode and the participation of valence as well as conduction electrons distinguishes electrode reactions of semiconductors from those of metals. These factors modify the anodic dissolution rate anisotropy associated with bonding of surface atoms and can lead to different behavior for n- and p-type electrodes. Some results of a study of anodic etch patterns on germanium hemispheres using optical goniometry and electron microscopy are presented. (Operated with support from the U. S. Army, Navy, and Air Force.)

Abstract No. 97

On the Etching of III-V and II-VI Compounds

G. A. Wolff, J. J. Frawley, and **J. R. Hietanen,** Solid State Research & Electronics Div., Harshaw Chemical Co., Cleveland 15, Ohio.

Since most investigators pay a great deal of attention to the shape and orientation of etch pits (rather than to the crystallographically more informative light figures), crystallographic principles of preferential etching, polish etching, and dislocation etching are given which aid in their interpretation. Difficulties are pointed out which arise in the selection of crystal planes for dislocation etch pit investigations and also for the interpretation of etch pits for structures without a center of symmetry, *e.g.*, wurtzite and sphalerite. For various III-V and II-VI compounds of these structures, polarity, etching, and piezoelectric effect are correlated.

Abstract No. 98

Gallium Arsenide Etch Rate Characteristic

Allen Owen, J. F. Delord, and **W. C. Myers,** Tektronix, Inc., P. O. Box 500, Beaverton, Ore.

The difference in etch rates between A^{III} and B^{V} faces of gallium arsenide has been studied. Tests were per-

formed using several different etchants. Results show that the ratio of the etch rates is dependent on the etchant used. The electrode potential of the A and B faces in the same etchants was determined and correlated to the etch rates. The dissolution mechanism of GaAs in oxidizing media is discussed.

Abstract No. 99

The Movement of Ions during the Oxidation of Metals

R. C. Plumb, J. W. Swaine, Jr., and **J. E. Boggio,** Worcester Polytechnic Institute, Worcester, Mass.

Phase charging transients have been observed in experiments using the technique devised by Plumb for the study of the effect of oxide films on electrode potentials. The phase charging transient, when aluminum is brought into contact with an electrolyte, varies with the thickness of the oxide film. The transient is probably associated with transfer of metal ions from the metal to the solution. The experimentally observed dependence of the transport rate on the film thickness may be explained by a model in which the slow step is movement of ions through the oxide film.

Abstract No. 100

Becquerel Effect of Victoria Blue B on Platinum

S. A. Greenberg and **H. P. Silverman,** Lockheed Missiles & Space Co., Sunnyvale, Calif.

The Becquerel effect of thin films of Victoria Blue B on platinum foil electrodes in contact with aqueous solutions of oxidizing and reducing agents has been studied. The photopotential is a monotonic function of the incident light intensity, while the photocurrent is proportional to the intensity. Quantum yields of electron production were studied as functions of wavelength and film thickness. The results are interpreted in terms of barrier effects at the dye-metal and dye-electrolyte interfaces.

Abstract No. 101

Exchange of Silver Ions at Single Crystal-Solution Interfaces

I. I. Tingley, Mines Branch, Dept. of Mines and Technical Surveys, 555 Booth St., Ottawa, Canada

The exchange of silver ions between the (100), (110), and (111) surfaces of single crystal silver and silver nitrate solutions was studied, using Ag^{110} as tracer. The process involves adsorption, electron exchange, and diffusion in the solid, but the latter plays a much smaller role than in the case of polycrystalline silver, where grain-boundary diffusion is predominant. The penetration depth and diffusion coefficient in the metal were obtained by controlled electroetching of the surface.

Abstract No. 102

On the Formation of Electrochemical Etch Pits on the (111) Face of Copper

Ugo Bertocci, L. D. Hulett, L. H. Jenkins, and **F. W. Young, Jr.,** Solid State Div., Oak Ridge National Lab., Oak Ridge, Tenn. Operated for the U.S.A.E.C. by Union Carbide Corp.

In an effort to elucidate the role of defects on the anodic behavior of copper single crystals, information has been gathered about the etch pits formed at dislocations on the (111) face. The results of studies designed to determine the influence of such parameters as current density, solution composition, and orientation of the copper surface on the formation and characteristics of such pits are discussed.

ELECTRODEPOSITION—ELECTRONICS

Abstract No. 103

A Review of Semiconductor Device Cleaning Technology

H. M. Cleveland, Bell Telephone Labs., Inc., Murray Hill, N. J.

The electrical characteristics of many types of semiconductor devices may be greatly influenced by the surface conditions of the semiconductor. These conditions may be determined by processing in the early stages of fabrication, as well as by passivation or encapsulation treatments. Freedom from unwanted materials at critical stages of fabrication is important, therefore, in obtaining high yields of reliable devices. This paper reviews existing techniques for attaining, measuring, and handling surfaces with a high degree of freedom from contamination.

Abstract No. 104

Surface Research and Its Relation to Device Technology

S. S. Baird, Texas Instruments Inc., P. O. Box 1079, Dallas 22, Texas

The electrical characterization of some important failure modes of silicon transistors and diodes is presented briefly. A rationalization of real surface problems is given based on the electrical behavior of devices. The magnitudes of chemical contamination thus determined, the sources of this contamination are identified. A qualitative description of the chemical origin of fast and slow states is given.

Abstract No. 105

A New Chemical Polish for Gallium Arsenide

M. V. Sullivan and **G. A. Kolb,** Bell Telephone Labs., Inc., Murray Hill, N. J.

A new, nonaqueous chemical polishing composition has been developed for use on gallium arsenide. In conjunction with the intensive stirring reported by Sullivan and Finne at the Houston Meeting in 1960, this polish is able to produce surfaces with a roughness factor of ± 25Å and flatness of ± 2 μ/cm on both the {111} and the $\{\bar{1}\bar{1}\bar{1}\}$ faces as well as the other common faces of gallium arsenide.

Abstract No. 106

Plating of Metals on Semiconductors

G. L. Schnable and **W. J. Hillegas, Jr.,** Philco Corp., Lansdale Div., Lansdale, Pa.

The science and technology of plating of metals on semiconductors are reviewed. Reasons for plating on semiconductors and typical applications are summarized. Although plating on semiconductors is used principally to make electrical contact, it can also influence the nature of the semiconductor surface, or can provide information about the semiconductor substrate. The mechanisms by which plating can be obtained, and the aspects in which plating on semiconductors differs from conventional plating technology, are summarized.

Abstract No. 107

Jet Electrolytic Etching and Plating

W. M. Lilker and **G. L. Schnable,** Lansdale Div., Philco Corp., Lansdale, Pa.

An electrolytic processing technique using a small jet of solution has been employed to electropolish localized areas of germanium or silicon and to electrodeposit dots of various metals and alloys on metal or semiconductor substrates. Typical examples of solutions and conditions for jet electropolishing of Ge and Si and for jet plating of several metals are given. The differences between jet processing techniques and conventional bath electrolysis are discussed in detail.

Abstract No. 108

Method for Producing Diodes and Transistors by Electrodeposition

W. P. Alina, M. A. Blumenfeld, and **R. A. Straight,** Semiconductor and Materials Div., Radio Corp. of America, Somerville, N. J.

A technique has been developed for electrodepositing antimony and lead onto germanium wafers in a dot configuration for the purpose of obtaining alloy diffused n-p junctions. The advantage of the new system is that it eliminates the necessity for positioning dots onto

wafers by hand. The paper describes the necessary electrolytes, fixtures, cleaning cycles, and alloying temperatures employed in this process, along with a comparison of the electrical properties of standard diodes *vs.* diodes produced by electrodeposition.

Abstract No. 109

Electroless Palladium on Semiconductor Materials

R. N. Rhoda, Research Lab., International Nickel Co., Bayonne, N. J.

The development of the process for the deposition of palladium by chemical reduction is discussed briefly, and recent improvements are described. The technique can now be used for applying various thicknesses of sound and adherent palladium directly on silicon and germanium. Such coatings of palladium are envisioned as protective coatings with good electrical properties or as barrier layers between nickel and gold in order to minimize the ultimate interdiffusion of these metals.

Abstract No. 110

Immersion Gold Plating Semiconductor Materials

G. I. Edson, Western Electric Co., Inc., 555 Union Blvd., Allentown, Pa.

This paper presents a basic immersion gold formulation which will deposit adherent gold on the surface of silicon or germanium. By modification of the basic formula, adherent gold may also be deposited on nickel, kovar, copper, solder, and other base materials. This formulation operates in the acid range at temperatures from 150° to 200°F depending on the application. Applications on semiconductor materials include: (*a*) adherent base for overplating; (*b*) with overplating, provides good bondability or solderability; (c) provides a conductive surface for uniformly plating high resistance semiconductor materials; (*d*) controlled source of gold for diffusion. Similar and other applications are obviously obtainable on other base materials used in manufacture of semiconductor products.

ELECTRODEPOSITION

Abstract No. 111

Some Observations on Electrodeposited Dendrites

H. F. John and **J. W. Faust, Jr.,** Research Labs., Westinghouse Electric Corp., Beulah Rd., Churchill Boro., Pittsburgh 35, Pa.

Under certain conditions dendrites are obtained during the electrodeposition of metals. Twin planes are often found to occur parallel to the growth direction of dendrites of f.c.c. metals. This has led to the conclusion that nucleation of the reduced species is easier at a reentrant edge than elsewhere. It will be shown how the re-entrant edge at twin planes can modify the growing interface to provide a preferred growth direction. F.c.c. metals are compared with metals of other structures, and conditions for twin planes affecting the growth mechanism are discussed.

Abstract No. 112

Electrocrystallization, I. Electron Tunnelling and Crystal-Face Work Function in Electrocrystallization

Ram Mohan Mallya, Dept. of Chemistry, University of Pittsburgh, Pittsburgh, Pa.

The role of the electrical field at the metal-solution interface in electrocrystallization is examined phenomenologically for an ideal system. The electron tunnelling possibilities are scrutinized, and the situations under which the activation energies for dehydration, or for adion discharge are altered, or not, are illustrated using energy profiles. The application of the Fowler-Nordheim equation shows that the anisotropy of the crystal face work function can significantly alter the reaction rates on different faces under certain conditions.

Abstract No. 113

A Study of the Electroreduction of Chromic Ion at the Mercury Cathode

M. E. McLain, Jr., Atomic Energy Div., Phillips Petroleum Co., Idaho Falls, Idaho (present address: Atlantic Research Corp., Alexandria, Va.)

The reduction of chromium (III) to chromium (II) at the mercury cathode in 0.10*M* KNO_3 was investigated polarographically. A change in the electroreduction mechanism appears to occur near the half-wave potential. The thermodynamic parameters for the dual mechanisms were determined as a function of the concentration of surface-active material in the solution. Mechanisms are suggested which explain the electroreduction data.

Abstract No. 114

Radiochemical Studies of Thiourea in the Electroless Deposition Process

J. S. Sallo, J. Kivel, and **F. C. Albers,** Minneapolis-Honeywell Research Center, Hopkins, Minn.

Thiourea-C^{14} and thiourea-S^{35} have been used to study the inclusion of thiourea or its fragments in the electroless nickel deposit. The rate of inclusion in the deposit of S^{35} derived from thiourea was determined as a function of deposition rate, deposit thickness, and other parameters. Radiochemical techniques were utilized to determine the existence of breakdown products in the solution. A mechanism of addition agent action which is consistent with these and other data is suggested.

Abstract No. 115

Alloy Plating—Scientific Curiosity or Useful Technology?

M. E. Browning, Materials Branch, Advanced Research Dept., Alexandria Div., American Machine & Foundry Co., Alexandria, Va.

Pertinent factors in the history of alloy plating are examined. While development and industrial acceptance have been slow, progress in the field of alloy plating has been significant during the last 30 years. Current research and development indicate that alloy plating does have a promising future in both industrial and aerospace fields for coatings as well as the manufacture of structural components.

Abstract No. 116

Russian Research on Alloy Electrodeposition

George Dubpernell, Metal & Thermit Corp., Detroit 20, Mich.

Russian work on alloy deposition has been very extensive and in the past tended to parallel work in other countries. However, the recent drive for advancement in science is resulting in new developments. Several examples of such newer developments are described.

Abstract No. 117

Electrodeposition of Nickel-Molybdenum Alloys

N. W. Hovey, Albertine Krohn, and **G. M. Hanneken, Jr.,** University of Toledo, Toledo, Ohio

Previous studies showed that iron-molybdenum and cobalt-molybdenum alloys could be electrodeposited from pyrophosphate solutions. This investigation shows that a similar bath can be used to deposit nickel-molybdenum alloys. Hydrazine sulfate was added to prevent anodic oxidation of Ni(II) to Ni(IV). This greatly improved the cathode current efficiency, but lowered the molybdenum content of the deposits. Efficiency is further increased by wiping the cathode during plating.

Abstract No. 118

Electrodeposition of Zinc-Molybdenum Alloys

Albertine Krohn, N. W. Hovey, and **H. L. Lewis,** University of Toledo, Toledo, Ohio

Deposits of zinc-molybdenum alloys obtained from the pyrophosphate baths mentioned in previous studies

were of poor quality. The alloys were dark, nonadherent, low in molybdenum content, and plated with poor efficiency. A study of the variables was undertaken in an attempt to improve the physical properties of the alloy plates, since they had been reported as protecting iron and steel from atmospheric corrosion about 10 times as long as would an equivalent thickness of pure zinc plate.

Abstract No. 119

The Production of Thick Cobalt-Molybdenum Alloy Deposits

P. C. Rydel and **S. C. Barnes,** Joseph Lucas Group Research Centre, Marston Green, Birmingham 33, England

Thick cobalt-molybdenum alloy deposits have been obtained from a modified pyrophosphate bath using ultrasonic agitation. The current efficiency was low and decreased as the molybdenum content of the deposit increased. The best deposits contained about 35% molybdenum, were dull metallic gray in color, even, and showed little gross porosity. Adhesion to copper substrates was good. Other baths failed to produce satisfactory thick deposits. Anodes were prepared by powder metallurgical techniques.

Abstract No. 120

Deposition Mechanism of a Gold-Tungsten Codeposit

R. F. Walton, Electroplating Development Branch, Hermetic Seals Dept., Transistor Products Div., Texas Instruments Inc., Dallas, Texas

A mechanism for the codeposition of gold and tungsten from an electroplating solution is proposed. The plating solution used for gold-tungsten codeposition was composed of chloroauric acid, tungstic acid, sodium hydroxide, and tartaric acid. Methods were determined for controlling the concentration of tungsten codeposited with gold by the addition of Group 8 metal impurities such as iron, cobalt, and nickel. The effect of solution agitation in controlling the tungsten concentration is also described.

Abstract No. 121

On the Theory of Simultaneous Discharge of Metal Ions in Real Conjugated Systems

A. T. Vagramyan and **T. A. Fatueva,** Institute of Physical Chemistry, Academy of Sciences of the U.S.S.R., Leninsky Prospect 31, Moscow V71, U.S.S.R.

More satisfactory mathematical relationships are developed for the speed of discharge of individual metals in alloy deposition as related to electrode potential and the depolarizing effect of the deposit, or the lack of such an effect. The experimental results with nickel-cobalt and nickel-iron deposition are discussed and show that the theory of real conjugated systems which is presented takes into consideration the regularities of the codischarge of metal ions more correctly than previous theories.

Abstract No. 122

Magnetic Co-Ni Electrodeposition; Characterization of the Deposit as a Function of Process Parameters

J. D. Kresge, M. A. Sanborn, and **S. Simoliunas,** GPD Manufacturing Research Lab., IBM Corp., Endicott, N. Y.

On Co-Ni coatings intended for high density magnetic recording, the magnetic and crystallographic properties of thin deposits have been studied as a function of bath conditions. Typical process parameters are salt concentration, Co to Ni ratio, current density, temperature, pH, additives, etc. The results indicate that it is possible to cover the range between 150 and 500 oersteds by suitable choice of variables.

Abstract No. 123

Magnetic Co-Ni Electrodeposition; Study of Solutions with Stable and Unstable Additives

J. D. Kresge, M. A. Sanborn, and **S. Simoliunas,** GPD Manufacturing Research Lab., IBM Corp., Endicott, N. Y.

In this study, stable additives are defined as organic addition agents which produce leveling and/or brightening. Unstable additives are defined as hypophosphites or phosphites used as P source to produce Co-Ni-P electrodeposits. The relation between electrode potentials, total applied voltage, current, and resistance has been studied in these systems.

Abstract No. 124

Compositional Studies of Electrodeposited Fe-Ni Alloys

I. M. Croll, IBM Corp., Thomas J. Watson Research Center, P. O. Box 218, Yorktown Heights, N. Y.

Data are presented regarding the composition of electrodeposited Fe-Ni alloys as a function of cation ratio, anion species, current density, agitation, temperature, and addition agents. The effect of the addition agents on the Fe-Ni ratio and on cathodic polarization is discussed.

Abstract No. 125

Electrodeposition of Iron-Nickel-Phosphorus Thin Films for Computer Memory Use

W. O. Freitag, G. DiGuilio, and **J. Mathias,** Remington Rand Univac, Div. of Sperry Rand Corp., Blue Bell, Pa.

Thin films to ternary Fe-Ni-P alloy suitable for use in computer memories have been electrodeposited from a sulfate bath containing hypophosphite ion. Glass coated with conductive vacuum evaporated layers of chromium and gold was used as a substrate. The effect of bath composition and plating time on the magnetic properties and composition of the films are discussed. Essentially nonmagnetostrictive films 1200Å thick with coercivities of 2 oe and anisotropy fields of 3.5 oe were prepared reproducibly. Films are magnetically uniform over a 3 x 3 in. area.

Abstract No. 126

Tensile Strength and Ductility of Electrodeposited Brass

H. J. Read and **W. A. Nystrom,** Dept. of Metallurgy, College of Mineral Industries, Pennsylvania State University, University Park, Pa.

Brass with 10, 20, or 30% zinc was prepared from the customary cyanide solutions in several thicknesses. Hydraulic-bulge tests gave data for calculation of true stress and strain at fracture. Thickness variations only slightly affected either strength or ductility. Strength reached a maximum at 20% zinc instead of increasing steadily with increasing zinc content. X-ray diffraction data revealed considerable β phase in the 30%-zinc deposit, and this may account for the anomalous strength data.

Abstract No. 127

Thorium Fused Salt Electrodeposition into a Molten Zinc Cathode

R. E. Johnson, Atomics International, Div. of North American Aviation, Inc., P. O. Box 309, Canoga Park, Calif.

An improved technique has been developed for the electrodeposition of thorium into molten zinc at 600°C, using a fused salt bath of LiCl-KCl-$ThCl_4$. Stirring the zinc markedly improved the current efficiency. Approximately 100% current efficiency was obtained at the cathode between current densities of 0.02 and 0.53 amp/cm^2 and at the anode between 0.08 and 2.33 amp/cm^2 at a concentration of 15 w/o $ThCl_4$. The practical limit for the deposition of thorium in zinc at 600°C is about 15 w/o, at which concentration the alloy becomes paste-like and renders stirring difficult.

Abstract No. 128

Electrodeposition of Bright Aluminum Coatings from Fused Salt Baths

L. W. Austin, M. G. Vucich, and **E. J. Smith,** Research & Dev. Dept., National Steel Co., Weirton, W. Va.

Aluminum deposits from fused salt baths are characteristically white and nonlustrous in appearance. Deposits of an aluminum-manganese alloy containing at least 16% manganese have been discovered to be bright as produced. Means for controlling bath composition and optimum plating conditions are discussed. Evidence is presented that the corrosion resistance of the coating is improved as the percentage of manganese in the alloy deposit is increased.

ELECTRONICS—SEMICONDUCTORS

Abstract No. 129

Synthesis of Semiconducting Black Phosphorus

R. C. Ellis and **D. M. Warschauer,** Research Div., Raytheon Co., Waltham 54, Mass.

The Bridgman method of combined high pressure and temperature has been used to synthesize polycrystalline black phosphorus, a narrow gap semiconductor, and a new vitreous insulating polymorph to be described elsewhere. In addition, a catalytic method has been used to grow large ingots at pressures only slightly above atmospheric. The crystalline form can be obtained by slow conversion of the vitreous material under proper conditions.

Abstract No. 130

Properties of Semiconducting Black Phosphorus

D. M. Warschauer, Research Div., Raytheon Co., Waltham 54, Mass.

The earlier electrical work of Keyes has been extended to show that pressure-derived black phosphorus exhibits a Hall coefficient maximum near 27°K and an increase of optical transmission from the visible to beyond 20μ. Broad spectral photoconductivity is observed at helium temperature, but narrows by nitrogen temperature to a relatively sharp peak around 5μ which decreases at higher temperature. As-grown material from the catalytic method gives different results, probably due to mercury inclusion.

Abstract No. 131

Conversion and Resistivity Changes in Floating Zone Silicon

S. N. Levine and **H. Goldberg,** State University of New York, Long Island Center, Stony Brook, N. Y., and John Hopkins Applied Physics Lab., Baltimore, Md., respectively

High resistivity silicon prepared by the floating zone technique has been suggested for a variety of semiconductor devices such as the delay lines, filters, and memories. During the course of fabrication studies involving exposure of p-type silicon to high temperatures a number of effects were noted. Both conversion to n-type and resistivity changes were observed in high resistivity (1000-3000 ohm-cm) floating zone p-type silicon on heating this material to 800°C in the presence of graphite jigs. Less marked changes occurred on heating the silicon in the absence of graphite. The extent of conversion in the absence of graphite is not clear; however, no conversion or resistivity changes were noted on heating at 450°C or lower. Because of these effects, difficulty was experienced in forming ohmic or injecting contacts at a temperature of 800°C or higher, particularly when graphite jigs were employed. The effect of inert atmospheres was also studied. Evidence supporting a surface diffusion mechanism, possibly involving oxygen, is presented.

Abstract No. 132

Preparation and Electrical Properties of Bismuth Trisulfide

A. C. Glatz and **V. F. Meikleham,** Carrier Corp., Carrier Parkway, Syracuse 1, N. Y.

Bismuth trisulfide was synthesized directly from the elements in heavy-walled quartz ampoules with a minimum void volume. Differential thermal analysis studies were performed to determine the reaction temperature and melting point. Crystals of bismuth trisulfide were grown in a three-zone furnace to control the vapor pressure of sulfur. Seebeck coefficients, electrical and thermal conductivities, thermoelectric figure of merit, and carrier concentrations were measured at 300°K on both stoichiometric and doped specimens of bismuth trisulfide.

Abstract No. 133

A New Method of GaP Growth and Purification

G. A. Wolff and **J. D. Broder,** Solid State Research & Electronics Div., Harshaw Chemical Co., Cleveland 15, Ohio

GaP crystal rods are grown from GaP powder and/or purified by diffusion transport of P through a Ga solution. An r.f. heated solution of GaP in Ga, in a Stockbarger crucible, is made to dissolve its way upward through a packed and Ga-wetted GaP powder column, while depositing a solid rod at its lower end, at rates of 0.5 in./day, or less. This ensures an appropriate supersaturation at the crystal growth front, through controlled temperature and GaP concentration gradients. The usefulness of this method for the growth and purification of Ga(P,As) crystals is discussed.

Abstract No. 134

Electrical Properties of Some Peritectic Compounds from the CdTe-In_2Te_3 System

D. F. O'Kane and **D. R. Mason,** Dept. of Chemical and Metallurgical Engineering, University of Michigan, Ann Arbor, Mich.

Single phase, polycrystalline samples of three peritectic compounds from the pseudo-binary system of CeTe and In_2Te_3 were prepared by zone refining and zone leveling techniques. The compounds are 45 mole % CdTe = 55 mole % In_2Te_3 (β-phase), 20 mole % CdTe — 80 mole % In_2Te_3 ($CdIn_8Te_{13}$, γ-phase), and 9 mole % CdTe — 91 mole % In_2Te_3 (δ-phase). The following energy gap values were obtained from electrical conductivity and Hall effect measurements: 1.38 ev for the β-phase, 1.02 ev for the γ-phase, and 1.17 ev for the δ-phase. The compounds are structurally similar to the binary compound In_2Te_3, and they provide a measure of the variation in electrical properties with composition. (Contribution No. 12 from the Semiconductor Materials Research Lab. of the University. Work was supported by Texas Instruments Inc., Dallas, Texas.)

Abstract No. 135

X-Ray Studies of Twinned GaAs Blades Grown from the Vapor Phase

R. R. Monchamp, W. J. McAleer, and **P. I. Pollak,** Electronic Chemicals Research Dept., Merck Sharp & Dohme Research Labs., Rahway, N. J.

A method for demonstrating the existence of twinning in materials having the diamond structure by the use of x-rays is presented. The method has been used to demonstrate the existence of twins in GaAs blades grown from the vapor phase and Ge ribbons grown from the melt.

Abstract No. 136

High-Temperature Electrical Conduction in $CuInTe_2$

S. M. Zalar, Research Div., Raytheon Corp., Waltham, Mass.

The compound $CuInTe_2$ is a p-type semiconductor of the chalcopyrite structure. Depending on the concentration of extrinsic carriers, the intrinsic electrical conduction in $CuInTe_2$ starts between 200° and 400°C. By embedding specimens of $CuInTe_2$ into "cocoons" of liquid porcelain, the evaporation of tellurium above 500°C was prevented, and the electrical resistivity was measured up to the melting point (782°C) of the compound. Plots of $\ln \rho$ *vs.* $1/T$ are analyzed and the mechanism of intrinsic conduction in $CuInTe_2$ discussed.

Abstract No. 137

Hall Effect and Electrical Conductivity of Single Crystal Cuprous Oxide

M. R. Wright (present address: Physics Dept., Research Labs., General Motors Technical Center, Warren, Mich.), **R. S. Toth** (present address: Ford Scientific Lab., Dearborn, Mich.), and **Dan Trivich,** Dept. of Chemistry, Wayne State University, Detroit 2, Mich.

The electrical conductivity, σ, and Hall constant, R_H, were measured at $-100°C$ to $+100°C$ on single crystal cuprous oxide, previously equilibrated at 750° or 1020°C and at oxygen pressures of 10^{-7} to 10^{-2} torr. σ and R_H were reproducible below 40°C, but irreversible aging effects occurred above this temperature. R_H was always positive, indicating hole conduction. Plots of log σ and log R_H *vs.* $1/T$ were linear after aging ($E_a \approx 0.4$ ev) but not before. A multiple acceptor model is postulated.

Abstract No. 138

Mixed Conduction Measurements in $Zr_{0.85}Ca_{0.15}O_{1.85}$

R. W. Vest, Systems Research Labs., Inc., Dayton, Ohio and **N. M. Tallan,** Aeronautical Research Labs., Wright-Patterson AF Base, Ohio

Polarization and a-c conductivity measurements were made to determine the ionic diffusivity and transport numbers for $Zr_{0.85}Ca_{0.15}O_{1.85}$ over a range of temperature at a single oxygen pressure. Under these conditions it is found that $Zr_{0.85}Ca_{0.15}O_{1.85}$ is a pure oxygen ion conductor at high temperatures, but that it exhibits mixed ionic and electronic conductivity at temperatures below 600°C. The extent to which platinum electrodes can be considered to be blocking to oxygen ions for $Zr_{0.85}Ca_{0.15}O_{1.85}$ and the significance of the apparent decomposition potential measured are discussed. The relative merits of this and several other techniques for measuring mixed conduction are considered.

Abstract No. 139

Solubility of 3-5 Compound Semiconductors in Column 3 Liquids

R. N. Hall, Research Lab., General Electric Co., P. O. Box 1088, Schenectady, N. Y.

In the preparation and processing of 3-5 compound semiconductors it is often important to know the solubility of the semiconductor in the liquid phase of its column 3 constituent as a function of temperature. Phase diagrams of many of these systems have been published, but in general they do not extend to low temperatures which is the region of principal interest here. In this paper we report measurements of the solubility of InSb, InAs, and InP in In, and of GaSb, GaAs, and GaP in Ga, with particular attention being paid to the low-temperature region where the solubility becomes quite small.

Abstract No. 140

Magnesium Diffusion in Gallium Arsenide and Prevention of Surface Evaporation

D. C. Gupta and **S. R. Shortes,** Texas Instruments Inc., P. O. Box 1079, Dallas, Texas

The diffusion of magnesium in gallium arsenide is studied. It follows the complementary error function distribution, and its temperature dependence is of the customary form, $D = D_o \exp(-E/KT)$. Diffusion has also been carried through surface films which provide a selective mask during diffusion. A two-layer diffusion model is presented which determines the concentration at the interface of the film and bulk material theoretically.

Abstract No. 141

Segregation of Silicon in Gallium Phosphide

Martin Rubenstein, Research Labs., Westinghouse Electric Corp., Beulah Rd., Churchill Boro., Pittsburgh 35, Pa.

Gallium phosphide was prepared using a horizontal zone refining technique. The liquid zone was maintained close to the stoichiometric composition. An ingot was unintentionally doped with an appreciable amount of silicon. Electrical, optical transmission, and spectrochemical measurements were made on sections of this ingot indicating that silicon is a donor impurity and the segregation coefficient of silicon in gallium phosphide is less than unity (approximately 0.7).

Abstract No. 142

Electrical Properties of Mg_2Sn Crystals Grown from Nonstoichiometric Melts

B. D. Lichter, Metals and Ceramics Div., Oak Ridge National Lab., P. O. Box X, Oak Ridge, Tenn.

Resistivity and Hall measurements were carried out on Mg_2Sn crystals in the temperature range 300°-60°K. Single crystals were grown by a modified Bridgman technique from stoichiometric melts and from melts containing 1, 2, 10, and 18 at. % excess Sn and 3 at. % excess Mg. In the mixed conduction and extrinsic ranges, it was found possible to describe the calculated temperature dependence of the conduction mobility on the basis of a combination of lattice vibration (accoustic mode) and ionized impurity scattering. A stoichiometry effect is observed. The Mg_2Sn crystals appear to dissolve the excess constituent producing n-type crystals (excess Sn) and p-type crystals (excess Mg). The observed effect corresponds to a solubility of 10^{-15}-10^{-6} atom fraction excess constituent. This result is discussed in terms of bonding in Mg_2Sn. (Operated for the U.S.A.E.C. by the Union Carbide Corp.)

Abstract No. 143

Rare Earth Nitride and Hexaboride Semiconductors

Nathan Sclar, Nuclear Corp. of America, Danville, N. J.

Various rare earth nitrides and hexaborides have been synthesized and their optical and electrical properties surveyed. Optical transmission measurements have revealed intrinsic absorption edges from which energy gaps have been deduced. The energy gaps lie in the range of 2 ev for the nitrides and 3 ev for the hexaborides, respectively. The room temperature electrical measurements give metallic behavior with the resistivity increasing with increase in temperature. These results suggest these materials to be high energy gap semiconductors which are degenerate at room temperatures. (This work was supported by the U.S. Signal Corps under contract DA36-039 Sc 87392.)

Abstract No. 144

The Hall Effect in Semiconducting Glasses

W. F. Peck, Jr., and **J. F. Dewald,** Bell Telephone Labs., Inc., Murray Hill, N. J.

Hall effect measurements on semiconducting glasses from the arsenic-tellurium-iodine system are reported. The Hall field is linear in the drift field up to 1.7 v/cm and in the magnetic field up to 80 kilogauss. The sign of the effect is consistent with that of the thermoelectric power, in apparent contradiction with comparable measurements by Kolomiets and others on the As-Te-Se system. Hole mobilities are of the order of 0.05 cm^2/v-sec, with small temperature dependence. Conduction mechanisms are briefly discussed.

Abstract No. 145

Carrier Compensation in Germanium Telluride

M. S. Lubell and **R. Mazelsky,** Research Labs., Westinghouse Electric Corp., Beulah Rd., Churchill Boro., Pittsburgh 35, Pa.

It has been reported previously that germanium metal dissolves in the alloy $(1\text{-}x)GeTe_{1.025} + x\ Bi_2Te_3$. This solubility was attributed to the "neutral vacancies" introduced via Bi_2Te_3. The present work shows that tin, gallium, indium, and titanium are also soluble in germanium-bismuth telluride alloys. Using Hall, Seebeck, and resistivity measurements, the solubility is shown to vary with the number of neutral vacancies introduced into $GeTe_{1.025}$. The carrier compensation per atom dissolved is consistent with the normal valence state of the solute atom.

Abstract No. 146

Semiconducting Nature of Stannic Oxide

L. D. Loch, Research and Development Div., Carborundum Co., Niagara Falls, N. Y.

Measurements of electrical conductivity (σ) and Seebeck coefficient (S) of polycrystalline stannic oxide demonstrated that it is an n-type broad band semiconductor. By doping with antimony oxide, data on σ and S for a range of free electron concentrations were obtained at temperatures of 100°-1100°K. The observed values of σ correspond to a room temperature mobility of 10 cm^2-$volt^{-1}$-cm^{-1}. The data indicate that complete ionization of the donor atoms takes place below room temperature.

Abstract No. 147

Surface Damage Associated with Abraded Silicon Specimens

R. Stickler and **G. R. Booker,** Research and Development Center, Westinghouse Electric Corp., Beulah Rd., Churchill Boro., Pittsburgh 35, Pa.

Silicon specimens were abraded on one side, chemically thinned from the other side, and examined in transmission in an electron microscope. The examination showed that the damaged layer consisted mainly of dislocation networks. Further silicon specimens were abraded, known amounts were removed from the abraded surfaces, and the specimens were chemically thinned and examined as before. In this manner the depths of damage for various abrasive treatments were determined directly. The effect of annealing on the damaged layers was also investigated.

Abstract No. 148

Formation of Organo-Silicon Surfaces

J. A. Cunningham and **L. E. Sharif,** Corporate Research and Engineering, Texas Instruments Inc., P. O. Box 1079, Dallas, Texas

The formation of a silicon surface which terminates in organic groups, such as phenyl, should provide a semiconductor device surface which is less sensitive to wet ambients than is a "bare" surface. This paper presents a method of applying an organic film by means of a treatment with reactive substituted silanes, such as trichlorophenyl silane. Field effect measurements on treated silicon and tests made on a variety of devices are presented.

Abstract No. 149

Formation of Thermal Oxides of Silicon

H. W. Cooper, H. C. Evitts, and **S. S. Flaschen,** Semiconductor Products Div., Motorola Inc., 5005 E. McDowell Rd., Phoenix, Ariz.

Oxidation growth rates of SiO_2 have been studied using as variables Si conductivity types, crystal growing methods, and bulk resistivity. Rates were determined in closed systems of both dry O_2 and steam over a temperature range of 800°-1300°C. The conclusion is drawn that the only factors controlling oxide growth rate were time, temperature, and ambient. Results reported include a study of the optical properties of the oxide films. (This work was supported by the Electronic Research Directorate, Air Force Cambridge Research Center, Air Research and Development Command.)

Abstract No. 150

Electrical Evaluation of Passivating Coatings on Silicon

H. W. Cooper, R. W. Rader, and **S. S. Flaschen,** Semiconductor Products Div., Motorola Inc., 5005 E. McDowell Rd., Phoenix, Ariz.

Passivating glass coatings of various thicknesses were grown on silicon by (i) high-temperature dry oxygen, ((ii) high-temperature steam, and (iii) PbO accelerated low-temperature oxidation. The coatings were then evaluated with respect to: (*a*) dielectric strength; (*b*) dielectric constant; (*c*) bulk resistivity; (*d*) temperature coefficient of resistivity; (*e*) loss angle *vs.* frequency and temperature. A figure of merit for the dielectric properties of passivating coatings was developed and applied in this study. (This study was supported by the Electronic Research Directorate, Air Force Cambridge Research Center, Air Research and Development Command.)

Abstract No. 151

Etching Characteristics of Degenerately Doped P-N Junctions

L. Varettoni, E. T. Casterline, and **R. Glicksman,** Semiconductor and Materials Div., Radio Corp. of America, Somerville, N. J.

A study has been made of some of the factors affecting the series resistance of germanium tunnel diodes. Before etching, the series resistance through the diode is a spreading resistance and can be approximately calculated by the formula $R_s \cong \frac{\rho}{2\pi r_o}$. After electrochemical etching the unit exhibits a "necking" type of structure, and its resistance lies mainly in the stem. This resistance approximates the resistance of a cylinder, $R_S = \rho l/A$. For a fixed junction area, and a given set of etching conditions, the structure of the diode stem is dependent on the following factors: (*a*) the size of the alloy dot; (*b*) the resistivity of the base pellet; and (*c*) the type of base pellet doping. The contribution of each of these factors to the series resistance of tunnel diodes is discussed.

Abstract No. 152

Some Comments on Thermal Etching of Silicon Surfaces Treated in Sealed Quartz Tubes

A. N. Knopp, Westinghouse Electric Corp., Youngwood, Pa.

Thermal etching takes place at high temperatures depending on the amount of oxygen which is present in a given system. The process of a sealed tube heat treatment is described, and different surface patterns of silicon which had been in contact with each other, and with quartz, are shown. The influence of oxygen is discussed, and the similar nature of thermally etched and chemically etched silicon is demonstrated. An application to diffusion is pointed out.

Abstract No. 153

Gettering of Silicon Planar Diodes

S. W. Ing, Jr., R. E. Morrison, L. L. Alt, and **R. W. Aldrich,** Semiconductor Products Dept., General Electric Co., Syracuse, N. Y.

Experimental studies are presented in which reverse leakage current in diffused silicon planar diodes are reduced by orders of magnitude via an intermediate temperature (800°-1000°C) gettering of metallic impurities which presumably cause excess leakage. Life test data on gettered diodes are also presented. The effectiveness of such gettering processes is further demonstrated by experiments in which radioactive copper is utilized as the diffused contaminant.

Abstract No. 154

Effect of Adsorbed Molecules on Electrooptical Properties of Zinc Oxide

Eiichi Inoue, Graphic Engineering Lab., Tokyo Institute of Technology, Tokyo, Japan

The dark and photoconductivity of zinc oxide fine powders depend strongly on oxygen chemisorbed on its surface. When some electron acceptive molecules are adsorbed in place of oxygen the change of the electrooptical properties of zinc powders will be expected. By adsorption of benzoquinone, chloranyl, phthalic acid anhydride, maleic acid anhydride, iodine, it was found that the photoresponse increased remarkably with their concentration in both measurements of surface charge decay and conductivity.

Abstract No. 155

A Novel Technique for Preparing Low-Temperature Alloyed Gold Contacts to Silicon and Germanium

H. F. Gossenberger, E. Helpert, and **W. Mehl,** RCA Labs., Radio Corp. of America, Princeton, N. J.

A method has been developed which permits simultaneous reduction of the oxide film normally present

on silicon or germanium and deposition of a gold film on the clean surfaces. The gold films thus prepared will alloy with germanium and silicon at temperatures below 400°C. The properties of the contacts to very high resistivity silicon and very low resistivity (degenerate) germanium are discussed. (Sponsored by the Office of Ordnance Research, U. S. Army.)

Abstract No. 156

Operation of a Pilot Scale Vertical Epitaxial Silicon Reactor

J. M. Fairfield and **E. G. Grochowski,** Components Div., IBM Corp., P. O. Box 390, Poughkeepsie, N. Y.

The operation of a vertical system which produces epitaxial silicon films of constant thickness and resistivity for pilot scale operation is described. The particular configuration of the RF adapter as well as the gas flow over the substrates are related to the properties of the material obtained. Important conditions such as deposition rate, temperatures, and substrate surface preparation are reviewed.

Abstract No. 157

Disproportionation of Silicon Iodide in an Open-Tube Process

J. J. Oberly and **A. Adams, Jr.,** Research Div., Raytheon Co., Waltham, Mass.

The disproportionation of silicon iodide is being studied as a possible open-tube process for the deposition of silicon at substrate temperatures below 1000°C. It has been found that, at a silicon source temperature of 1200°C, about 25% of the silicon reacting with the passing iodine forms the di-iodide which subsequently disproportionates to deposit one-half of its silicon. The effect of various parameters on the reaction and the measures taken to reduce contamination are discussed.

Abstract No. 158

Measurement of Silicon Epitaxial Layer Resistivity with a Four-Point Probe

P. A. Schumann, Jr., and **J. F. Hallenback, Jr.,** Components Div., IBM Corp., Poughkeepsie, N. Y.

A nondestructive technique for the measurement of silicon epitaxial layer resistivity with a four-point probe is described. Conventional probe points are mounted so that the voltage drop is measured through the wafer. The relationship between the epitaxial layer resistivity and the physical parameters of the probe and wafer are discussed. Measurements evaluating the performance of the probe are described, and it is shown that epitaxial films on highly doped substrates can be readily characterized by this technique.

Abstract No. 159

The Epitaxial Growth of Silicon Carbide

V. J. Jennings, Armin Sommer, and **Hung-Chi Chang,** Research Lab., Westinghouse Electric Corp., Beulah Rd., Churchill Boro., Pittsburgh 35, Pa.

Silicon carbide has been grown epitaxially onto a heated substrate of single crystal hexagonal silicon carbide. The process consists of the high-temperature hydrogen reduction of gaseous silicon and carbon compounds at the substrate surface. Results are given of the study of the effect of various growth parameters on the grown layer properties. The problems of the stacking faults encountered in growing cubic on hexagonal silicon carbide are discussed. (This work was sponsored in part by the Electronics Research Directorate of the Air Force Cambridge Research Labs., Office of Aerospace Research, under Contract AF 19(604)-8499.)

Abstract No. 160

The Vapor Growth of Epitaxial Germanium Multijunction Structures

R. E. Gonzales, D. L. Malcuit, and **J. W. Sprague,** Defense Electronics Div., General Electric Co., Syracuse, N. Y.

The disproportionation and reduction reactions of germanium di-iodide and germanium tetrachloride, respectively, were investigated for the vapor growth of epitaxial multijunction structures. The process parameters of each reaction such as seed and source temperature, crystal orientation, gas flow, and gas saturation were studied, and the results are presented. In addition, masking techniques used during crystal growth were investigated and will be shown. Finally, a comparison of the results for the two reactions will be made.

Abstract No. 161

The Diffusivity of Arsenic in Silicon

W. J. Armstrong, Components Div., Developments Labs., IBM Corp., P. O. Box 390, Poughkeepsie, N. Y.

The diffusion coefficient of arsenic in silicon has been investigated over the temperature range of 1100°-1350°C using the p-n junction technique. Diffusion coefficients are in good agreement with previously published data, but the diffusion equation

$$D = 68.6 \exp \frac{-97{,}600}{RT}$$

has a higher D_0 and activation energy. Surface concentrations of arsenic were in the 10^{17} to 10^{19} range.

Abstract No. 162

Investigation of Effects of Process Variables in Gaseous P_2O_5 Diffusion

C. M. Lutfy, W. M. Gegg, J. E. Reynolds, and **S. S. Flaschen,** Semiconductor Products Div., Motorola Inc., 5005 E. McDowell Rd., Phoenix, Ariz.

A critical study of gaseous diffusion of phosphorus into p-type silicon has been made with the objective of correlating chemical process variables with electrical parameters. The chemical process variables studied were diffusion temperature, source temperature, carrier gas flow rate, and starting material. These were selected to give 7 or 10v avalanche breakdowns, and electrical evaluation included impedance, reverse current, and forward voltage. Variation in surface concentrations resulting from processing conditions gave statistically significant differences in the Zener properties. Of particular interest were results from 400°C P_2O_5 source temperature which have been related to an allotropic phase change in P_2O_5 at this temperature.

Abstract No. 163

Optical and Electrical Properties of Semiconducting Cadmium Oxide Films

T. K. Lakshmanan, Weston Instruments Div., Daystrom Inc., 614 Frelinghuysen Ave., Newark, N. J.

Indium-doped cadmium oxide films were prepared by sputtering from an alloy cathode. Electrical properties, spectral transmittance, and Hall effect were measured on doped and undoped specimens. Films showing a variety of properties ranging from high-resistivity transparent samples to degenerate, low-resistivity specimens were produced by varying the doping and sputtering conditions. The dependence of these properties on method of preparation is discussed. Doped and undoped films were found to form imperfect heterojunctions with selenium.

Abstract No. 164

Electrical Properties of Thin Organic Films

Arthur Bradley and **J. P. Hammes,** Radiation Research Corp., 1150 Shames Dr., Westbury, N. Y.

Thin organic polymer film specimens were prepared for electrical conductivity measurements by the glow discharge polymerization process. The experimental procedure for film preparation is described in detail. Data on film properties and deposition efficiencies (g/kwh) are presented for their possible bearing on the polymerization mechanisms. Dark conductivities (δ) were measured over the temperature range 75-275°C. Plots of log δ *vs.* $1/T_{abs}$ generally gave straight lines above about 125° with slopes characteristic of the chemical composition of the polymer film. Conductivities at 150°C ranged from 10^{-17} mho/cm (films

rich in halogen) to 10^{-11} mho/cm (N-nitrosopiperidine, triphenyl arsenic). A possible relationship between structure and conductivity is discussed.

ELECTROTHERMICS AND METALLURGY

Abstract No. 165

Variations in Hot-Pressing Techniques

W. W. Beaver and **R. S. Truesdale,** Brush Beryllium Co., Cleveland, Ohio

The consolidation of metal or ceramic powders through hot compaction has been used extensively as a method for making experimental metallic or nonmetallic laboratory specimens. In addition, special techniques for hot pressing have been applied industrially to a number of products in both the metallurgical and ceramic industries. Specific variations of hot compaction, particularly isopressing at elevated temperatures, wherein the pressure medium is a gas, liquid, or plastically flowing solid, have also indicated a good potential for utilization. Although many of these procedures are expensive, hot compaction generally provides an attainment of a combination of properties not easily reached by ceramic or powder metallurgy techniques, inasmuch as the process combines certain favorable elements of powder compaction under pressure, forging, and pressure welding. These factors are particularly desirable for materials difficult to fabricate, as well as for application to special configurations and composite structures. A discussion is presented describing certain technical and economic factors for utilization of hot-pressing techniques in relation to their influence on property design, as well as experimental hot-pressing methods used for obtaining unusual shapes or developing optimum properties in difficult to fabricate metals, ceramics, and mineral product mixtures. Types of equipment, pressure distribution methods, and die materials suitable for compacting various materials are presented.

Abstract No. 166

Relationship of the Yield Pressure to the Hot-Pressed Density of Metal Powders

G. W. Cunningham, Battelle Memorial Institute, 505 King Ave., Columbus 1, Ohio

The yield pressure of several metals has been determined as a function of time and temperature from hot hardness measurements and related to hot-pressed density. A detailed analysis of the results obtained with copper powder show that the hot-pressed density is directly related to the ratio of applied pressure to yield pressure for the particular time and temperature utilized. Densities on the order of 95% of theoretical are obtained at pressures equal to the yield pressure.

Abstract No. 167

The Continuous Hot Pressing of Refractory Materials

B. Best, (present address: IBM Corp., P. O. Box 390, Poughkeepsie, N. Y.) Carborundum Co., Niagara Falls, N. Y.

Refractory materials such as alumina and boron nitride have been hot pressed as rods ½-1½ in. diameter in a continuous manner. Active refractory powders are introduced intermittently into a heated mold and continuously hot pressed by a constant opposing pressure transmitted through the final product. The continuous hot pressing technique and equipment are discussed.

Abstract No. 168

The Effect of Hot-Pressing Variations on the Properties of Zirconium and Titanium Diboride

R. A. Alliegro and **A. R. Schultz,** Norton Co., Worcester 6, Mass.

The effect of hot-pressing conditions on the properties of titanium diboride and zirconium diboride were studied. Properties such as electrical resistivity, crytal size, modulus of elasticity, cross bending strength, and compressive strength were determined as a function of pressure applied, elapsed time at temperature, and degree of temperature attained. Photomicrographs are presented indicating the degree of crystal growth under the conditions of forming. The effect of purity on these properties is also discussed.

Abstract No. 169

Gas Evolution during Consolidation of Carbothermic TiB_2 Powders to High Density

R. D. Holliday, R. Mogstad, and **J. L. Henry,** Metals Div. Research, Kaiser Aluminum & Chemical Corp., Permanente, Calif.

TiB_2 powders prepared by carbothermic reduction, followed by milling to small particle size, contain TiO_2, B_2O_3, and carbonaceous reducing agents. During hot pressing CO evolution from such materials can cause explosion of compacts near 1600°C or can result in bodies structurally damaged by gas porosity. Procedures necessary to control CO evolution and yield high-density, high-strength compacts have been investigated in an apparatus in which high vacuum or controlled atmospheres can be maintained during hot pressing. The thermochemistry of the principal reactions yielding CO is discussed.

Abstract No. 170

Furnaces Used in Hot Pressing

D. T. Lapp and **G. R. Watson,** Research and Development Dept., Norton Co., Chippawa, Ont., Canada

The Ridgway electric resistance furnace (Patent No. 2,125,588) and a large high-frequency induction pressing facility are described. Electrical efficiency of each type is noted. Typical production operations are discussed with emphasis on the fabrication of boron carbide articles.

Abstract No. 171

Thermal-Pressing Analysis

B. Best (present address: Components Div., IBM Corp., P. O. Box 390, Poughkeepsie, N. Y.) Carborundum Co., Niagara Falls, N. Y.

This technique is used to evaluate the low-temperature thermal-pressing properties of a powder. A continual record of the sample densification and temperature is recorded as the powder, which is retained in a mold, is subjected to a constant pressure and temperature rise. The resulting information is presented as a curve showing the change in relative porosity as a function of temperature. The equipment and procedure are discussed, and curves for copper, nickel, bauxite, barium titanate, and raw petroleum coke are presented.

Abstract No. 172

The Influence of Gravity in Sintering

F. V. Lenel, H. H. Hausner, O. V. Roman, and **G. S. Ansell,** Dept. of Materials Engineering, Rensselaer Polytechnic Institute, Troy, N. Y.

The radial shrinkage of cylindrical copper powder compacts during sintering was measured and found to be nonuniform from the top to the bottom of the compacts. This nonuniformity is due to the effect of gravity forces during conventional sintering of compacts. No sharp dividing line can be drawn between it and hot-pressing under an externally applied stress.

Abstract No. 173

The Hot Pressing of Carbides, Metal-Ceramic Composites, and Oxides

W. B. Crandall and **J. R. Tinklepaugh,** State University of New York College of Ceramics, Alfred University, Alfred, N. Y.

Both induction and resistance heating techniques have been used to produce polycrystalline materials having a controlled microstructure. The effects of several additives have been studied, and samples were produced having a wide variance in microstructure and properties. Silicon carbide, metal fiber-ceramic composites, alumina, and magnesia are selected as examples of hot pressed materials with particular emphasis on the recent work with magnesia of R. K. Hanna at the College of Ceramics.

Abstract No. 174

Vaporization of Zinc Antimonide

Chikara Hirayama, Research and Development Center, Westinghouse Electric Corp., Beulah Rd., Churchill Boro., Pittsburgh 35, Pa.

The vapor pressure of ZnSb between 658° and 745°K may be expressed by $\log P_{atm} = -[8764 \pm 316]\ 1/T + 7.71 \pm 0.51$. The heat of reaction for $ZnSb(s) = Sb(s) + Zn(g)$ is $\Delta H_{298} = 40.81 \pm 1.5$ kcal/mole, and the heat of formation of ZnSb is $\Delta H_f^\circ = -9.62 \pm 1.5$ kcal/mole.

Abstract No. 175

Correlation between Ferromagnetic Tape Material Structure and the Magnetic Behavior of the Tape Material

P. Kuttner, Electronic Instruments Div., Burroughs Corp., 1209 Vine St., Philadelphia 7, Pa.

The magnetic properties of ferromagnetic tape materials are strongly influenced by lattice imperfections such as grain boundaries, inclusions, lamellar precipitates, and the crystalline surface. These factors were studied for a sample of 4-79 Molybdenum Permalloy tape cold-rolled to 1 mil and ⅛ mil thickness. The effects of different heat treatments on these tape samples were studied by photomicrography and the observation related to the magnetic behavior of the tape. These observations are discussed and related to previous work in this field.

Abstract No. 176

Thermodynamic Studies of Ternary Liquid Metallic Systems Containing Miscibility Gaps, I. The Aluminum-Bismuth-Lead System

T. C. Wilder and **J. F. Elliott,** P. R. Mallory and Co., Inc., Burlington, Mass., and Metallurgy Dept., Massachusetts Institute of Technology, Cambridge, Mass., respectively.

The thermodynamic properties of the liquid Al-Bi-Pb system have been determined by emf measurements of the reversible concentration cell

• Al (liq) | Al^{+++}($AlCl_3$ in KCl · NaCl) | Al (in Bi, Pb, or Bi-Pb) (liq) ⊕

in the range 700°-1000°C and distribution measurements of the two-phase alloys at 900°C. The measured properties of this system have been compared with estimates based on several theoretical treatments contained in the literature. It was found that the partial and integral molar free energies of mixing in this system have larger positive deviations from ideality than the theoretical treatments indicate. The miscibility gap in this system at 900°C is not as large as that reported in the literature.

Abstract No. 177

Thermodynamic Properties of the Manganese-Lead-Bismuth System

M. Weinstein and **J. F. Elliott,** Tyco Labs., Inc., Waltham, Mass., and Massachusetts Institute of Technology, Cambridge, Mass., respectively.

The thermodynamic properties in the liquid region of the Mn-Pb-Bi system from 700° to 1000°C are reported. They were obtained from the reversible potentials of the cell:

$$\mathrm{Mn(s)} \;\big|\; \begin{matrix} \mathrm{Mn^{++}} \\ \mathrm{KCl,\ NaCl} \end{matrix} \;\big|\; \begin{matrix} \mathrm{Mn} \\ \text{(In Pb-Mn-Bi sol'n)} \end{matrix}$$

The liquidus surface for the ternary system was also obtained for this temperature interval.

Abstract No. 178

EMF Response of Strained Nickel, Molybdenum, and Titanium Electrodes

S. M. Toy and **Ken Nobe,** Dept. of Engineering, University of California, Los Angeles 24, Calif.

EMF changes resulting from elastic strain of nickel, molybdenum, and titanium in aqueous solutions of $NiSO_4$, $MoCl_5$, and $TiCl_4$, respectively, have been measured. The potentials of the strained electrodes were positive with respect to the unstrained electrodes (Gibbs-Stockholm sign convention). The maximum emf response of each metal increased with strain. Theoretical interpretation is presented in terms of semiconductor or insulator properties of the film formed on the electrode and the electrical double layer.

Abstract No. 179

Electrodeposition of Dispersion-Hardened Ni-Al_2O_3 Alloys

F. K. Sautter, Advanced Research Lab., Research Branch, Watervliet Arsenal, Watervliet, N. Y.

Nickel-Al_2O_3 alloys were electrodeposited from a Watt's type Ni electrolyte which contained the second phase particles suspended in the solution. The effect of particle concentration, particle size, and plating conditions on microstructure and physical properties of the deposits were studied. Using submicroscopic Al_2O_3 articles, the room-temperature yield strength increased from 10,000 psi for pure nickel to 40,000 psi for an alloy containing 2 v/o Al_2O_3. It is believed that this increase was due to dispersion strengthening effects similar to those observed in sintered or internally oxidized metal-metal oxide systems.

Abstract No. 180

The Electrochemical Hall of Fame—The Story of the Men Who Built the Electrochemical Industry with Niagara Power

A special lecture will be given by F. L. Koethen at 4:15 P.M. on Tuesday, Sept. 18, in Parlor C, Mezzanine floor. While sponsored by the Electrothermics and Metallurgy Division, everyone registered at the Meeting is cordially invited to attend. Mr. Koethen, who has been associated with the electrochemical industry in the Niagara Falls area for over fifty years, is a well-known historian of the region and its industrial electrochemical development.

ELECTROTHERMICS AND METALLURGY—CORROSION

Abstract No. 181

There is no Abstract No. 181

Abstract No. 182

Solution and Diffusion of Corrosion Oxide Film in Zircaloy

R. M. Treco, Fuels Div., United Nuclear Corp., P. O. Box 1883, New Haven 4, Conn.

In Zircaloy-2 processing, an oxide surface film is formed during the water corrosion test. Removal by vacuum annealing, is an economical and rapid method. The effects of heating on the distribution of oxygen in the Zircaloy were reviewed and it is shown that subsequent pickling is desirable to remove the surface layer of diffused oxygen.

Abstract No. 183

Reaction of Lithium with Water Vapor

W. R. Irvine and **J. A. Lund,** Dept. of Metallurgy, University of British Columbia, Vancouver 8, B. C., Canada

This paper describes a thermal balance and x-ray diffraction study of the reaction of lithium with water vapor. Water was carried at partial pressures of up to 12.6 mm Hg in oxygen and argon gases, and runs were conducted between 20° and 45°C. The reaction was found to proceed in three distinct successive stages; (*a*) formation at constant rate of a lithium metal lattice, (*b*) localized nucleation and growth by spreading, of

lithium monohydrate ($LiOH \cdot H_2O$) at the outer surfaces of the hydroxide, and (c) simultaneous formation and hydration of the hydroxide, at constant rate, culminating in complete conversion of the metal to the monohydrate. Oxygen used dry or as a carrier for water vapor did not react with lithium at the temperatures investigated.

Abstract No. 184

High-Temperature Oxidation of Iron-Chromium Alloys in Water Vapor

C. T. Fujii and **R. A. Meussner,** U. S. Naval Research Lab., Washington 25, D. C.

Iron-chromium binary alloys containing 1, 5, 10, 15 and 20 w/o Cr were oxidized at 700°, 900°, and 1100°C in a 0.1 H_2O-0.9 Ar atm. Characteristics of the oxidation process were examined by continuous weight gain measurements and detailed analyses of the oxidized specimens. These studies include metallography, and x-ray and chemical analyses of the oxides. The weight gain measurements show a parabolic oxidation rate for specimens oxidized at 700°C, but a linear rate for specimens oxidized at 900° and 1100°C. The apparent activation energy for the over all oxidation process, determined from these measurements, is 21±1 kcal. All of the oxidized specimens had a characteristic two-layer oxide structure. The oxidation mechanism suggested by these data is one in which the rate-controlling process occurs at the wustite: gas interface.

Abstract No. 185

Corrosion of Al in Steam at 540°C and 60 psi

R. K. Hart, Argonne National Lab., Argonne, Ill.

(No abstract received)

Abstract No. 186

Reaction of Boron Carbide with Steam at Elevated Temperatures

L. M. Litz and R. A. Mercuri, Res. Lab., National Carbon Co., P. O. Box 6116, Cleveland 1, Ohio

The rate of oxidation of boron carbide by water vapor has been found to be appreciably greater than the rate of oxidation by air at temperatures below 650°C. Studies of the reaction with water at 240 millimeters water vapor pressure in both argon and air gave a temperature dependence of reaction rate corresponding to approximately 10 kilocalories per mole over the temperature range 250° to 750°C. The reaction rate of dry air with fresh B_4C surfaces gave an activation energy of approximately 45 kilocalories per mole. Equivalent rates of oxidation were obtained at about 670°C.

Abstract No. 187

Some Studies on the Oxidation of Graphite at Temperatures of 600°-1500°C and at Pressures of 2-76 Torr of Oxygen

E. A. Gulbransen, K. F. Andrew, and **F. A. Brassart,** Westinghouse Electric Corp., Beulah Rd., Churchill Boro., Pittsburgh 35, Pa.

Sensitive gravimetric, pressure change and mass spectrographic methods were used. Below 725°C the rate of oxidation showed a strong temperature dependence while above 725°C the rate of oxidation increased slowly with temperatures. Chemical processes limit the rate of oxidation below 725°C and transport of oxygen through a surface boundary layer of reaction products above 725°C. Carbon was found to react with oxygen at a much slower rate than either molybdenum or tungsten for the same conditions.

Abstract No. 188

Kinetics and Mechanism of the Oxidation of Uranium Dioxide Sintered Pellets

Tennyson Smith, Atomics International, P. O. Box 309, Canoga Park, Calif.

Oxidation of uranium dioxide sintered pellets with oxygen, in the pressure range 3-800 torr, 0°-450°C, and with a 0-5% concentration of fission product oxides (fissia), has been studied. The following mechanism is postulated: chemisorption of oxygen on the UO_2 surface, followed by adsorption of oxygen on this layer; diffusion through a thin layer (224 ± 74Å) of U_3O_7 or U_4O_9 (depending on the temperature); formation of U_3O_8 in grain boundaries which causes the surface layer to spall off and thereby pulverize the pellet.

Abstract No. 189

High-Pressure Oxidation of Metals; Nickel in Oxygen

J. P. Baur, Sperry Rand Corp., Salt Lake City, Utah; **R. W. Bartlett, J. N. Ong, Jr.,** and **W. M. Fassell, Jr.,** Aeronutronic, Ford Motor Co., Ford Rd., Newport Beach, Calif.

The oxidation of Mond nickel was studied from 1000° to 1200°C at oxygen pressures to 20.4 atm. The oxidation rate was controlled by cation vacancy exchange diffusion through the oxide and had a gross activation energy of 47.9 kcal/mole. The rate was proportional to $P_{O_2}^{1/4}$, indicating ionization of only one electron hole from the cation vacancy. The NiO oriented in a preferred manner with (100) planes parallel to the polycrystalline nickel base.

Abstract No. 190

A Method for the Determination of Composition of Microgram Quantities of Oxides of Platinum

G. C. Fryburg and **D. A. Otterson,** Lewis Research Center, NASA, Cleveland, Ohio

A method for determining the composition of microgram quantities of oxides of platinum is presented. The method involves reducing the oxide with hydrogen and determining the resultant water by a microtechnique recently developed. The method should be applicable to any oxide reducible by hydrogen; the only limitation is that the oxide is reducible at a temperature lower than that at which dissociation occurs.

Abstract No. 191

Oxidation of Molybdenum at High Temperatures and Low Pressures

J. Engelke, A. Buchler, and **J. B. Berkowitz-Mattuck,** A. D. Little, Inc., Acorn Park, Cambridge 40, Mass.

A Nuclide Analysis Associates 12 in. radius, 60°-sector, direction focusing mass spectrometer was used to study the interaction between oxygen gas and a molybdenum surface at temperatures between 1100° and 1700°C. The principal oxidation products were identified as $MoO_2(g)$ and $MoO_3(g)$. Gas pressures were sufficiently low so that there were essentially no collisions between product molecules in the gas phase prior to ionization and detection.

Abstract No. 192

Oxidation of Molten High-Purity Aluminum in Dry Oxygen

W. C. Sleppy, Research Labs., Aluminum Co. of America, New Kensington, Pa.

The rate of oxidation of high-purity aluminum, melted in vacuum at temperatures from 660° to 850°C and oxidized in dry oxygen, is strongly influenced by the initial surface conditions of the solid samples. The oxidation of initially "oxide free" molten aluminum is characterized by a logarithmic oxide growth at temperatures of 700°C, while at temperatures near 750°C, a modified parabolic oxidation law is obeyed. The disarray theory of Davies, Evans, and Agar is cited to account for the logarithmic oxide growth, while the parabolic controlled oxidation is attributed to the diffusion of aluminum ions through the eta-alumina oxide film to the oxide-gas interface. The activation energy for the diffusion controlled oxidation reaction is estimated to be 99 kcal/mole. A possible relationship between morphology and the kinetics of oxide growth on molten aluminum is presented in view of the correlation between data from the present work and that taken from a Russian publication concerning the morphology of oxide growth on molten aluminum.

Abstract No. 193

Liquid Bismuth Corrosion—A Review

A. L. Lowe, Jr., Atomic Energy Div., Babcock and Wilcox Co., Lynchburg, Va.

Present state-of-the-art is reviewed with emphasis on the fundamental mechanisms associated with liquid bismuth corrosion. The effects of system variables such as temperature, velocity, alloy composition, and corrosion inhibitors are discussed. Short and long duration corrosion data are reviewed as to their relative merits. A summary is made of the materials suitable for liquid bismuth service at various temperature ranges.

Abstract No. 194

Dissolution of Nuclear Fuel Additions in Molten Bismuth

A. F. Weinberg and **R. J. Van Thyne,** John Jay Hopkins Lab. for Pure and Applied Science, General Atomic Div., General Dynamics Corp., San Diego, Calif., and Metals and Ceramics Research, Armour Research Foundation, 10 West 35 St., Chicago, Ill., respectively.

Dissolution of uranium, zirconium, and magnesium in bismuth was studied in relation to preparation of initial fuel for the Liquid Metal Fuel Reactor Experiment and to adjust fuel concentration during operation. Dissolution of elemental uranium was controlled by the rate of formation of an intermetallic compound requiring solid-state diffusion. Master alloys of Bi-10 w/o U were required to provide sufficiently rapid dissolution rates. Elemental zirconium was adequate for initial additions, but Bi-Zr master alloys were required for "make-up" additions. (Sponsored by the Babcock and Wilcox Co., Atomic Energy Div., under AEC Subcontract No. AT (30-1)-1940-7.)

Abstract No. 195

Capsule Evaluation of Structural Materials for Liquid Bismuth Service

E. J. Rozic, Jr., Tubular Products Div., Babcock and Wilcox Co., Beaver Falls, Pa., and **A. L. Lowe, Jr.,** Atomic Energy Div., Babcock and Wilcox Co., Lynchburg, Va.

Tilting capsule tests were conducted to provide information on 10-1/4% Cr-1/2% Mo and 2-1/4% Cr-1% Mo steels in contact with an uranium-bismuth solution at elevated temperatures. Various levels of additives were explored and evaluated with respect to their effects on the mass transfer (corrosion) characteristics of the investigated materials. The need for a sufficient amount of zirconium in the fuel solution was confirmed. 1-1/4% Cr-1/2% Mo steel is markedly superior to 2-1/4% Cr-1% Mo steel with respect to resistance to mass transfer in liquid bismuth. (Work performed under A.E.C. Contract No. AT(30-1)-1940).

Abstract No. 196

Evaluation of Liquid Bismuth Corrosion in Dynamic Systems

O. H. Baker, Boiler Div., Babcock and Wilcox Co., Barberton, Ohio, **A. L. Lowe, Jr.,** Atomic Energy Div., Babcock and Wilcox Co., Lynchburg, Va., and

W. Markert, Jr., Research and Development Div., Babcock and Wilcox Co., Alliance, Ohio

Pumped loops were used to investigate the effects of temperatures, temperature differential, velocity, and additive concentration on the corrosive characteristics of liquid bismuth in the temperature range of 750°-1000°F. Two materials, 2-1/4 Cr-1 Mo and 1-1/4-Cr 1/2 Mo steels were studied as to the effect of heat treatment, welding, and surface preparation on corrosion resistance. Test results are discussed and compared with the findings from preliminary capsule and thermal loop tests. (Work performed under A.E.C. Contract No. AT(30-1)-1940.)

Abstract No. 197

The Investigation of Container Materials for Bi and Pb Alloys, I. Thermal Convection Loops

A. J. Romano, C. J. Klamut, and **D. H. Gurinsky,** Brookhaven National Lab., Upton, N. Y.

Materials for containing liquid Bi and Pb alloys have been studied with thermal convection loops operating at temperatures up to 650°C both with and without inhibitors. Zirconium was found to be the most effective inhibitor in retarding the corrosion of low alloy steels. Carbon steel loops were operated at a temperature differential of 150°C (550°-400°C) for over 10,000 hr with little corrosion detected. Pb and Pb-Bi eutectic were found less corrosive liquid metals than Bi and U-Bi. (This work was performed under the auspices of the U.S.A.E.C.)

Abstract No. 198

Possible Correlations between Thermoelectric Potentials and Liquid Metal Corrosion

J. R. Weeks and **S. G. Epstein,** Brookhaven National Lab., Upton, N. Y.

In liquid metal corrosion, selective attack on certain alloys and increased attack at high-temperature differentials may result from the thermoelectric potentials between the corroding surface and the liquid metal. Current flows in excess of 20 ma have been measured in a liquid Bi (500°C) cell between a 5% Cr steel anode and a carbon steel cathode. Electrolysis of Fe-Bi alloys shows Fe migrates against the electron flow, *i.e.*, toward the cathode. Thus attack of 5% Cr steel when it is coupled to carbon steel may be accelerated by the currents produced by the thermocouple cell.

Abstract No. 199

High-Temperature Hydrogen Attack of Steels

P. C. Rosenthal and **F. H. Vitovec,** Dept. of Minerals & Metals Engineering, University of Wisconsin, Madison, Wis.

The paper is concerned with the deterioration of steels in hydrogen environment at temperatures above those at which low strain-rate embrittlement occurs. In this temperature range two major effects of hydrogen can be distinguished. Hydrogen may cause a chemical attack which produces a visible change of the microstructure, and it introduces embrittlement by promoting the initiation and propagation of intercrystalline cracks under creep stress conditions. The effect of environmental condition, composition, and state of the material on these phenomena is discussed and analyzed.

Abstract No. 200

Corrosion of Carbon Steel by High-Temperature Mercury

A. H. Fleitman, A. J. Romano, and **C. J. Klamut,** Brookhaven National Lab., Upton, N. Y.

All liquid Hg thermal convection loop experiments have been carried out at a temperature differential of 400°F (1000°-600°F) for 8000 hr in carbon steel systems. The effect of Ti and Zr additions in inhibiting corrosion was evaluated. Results of these experiments show that no adherent deposits were formed on the loop walls, and the presence of Zr and Ti resulted in less over-all corrosion. A comparison of the amount of iron residue filtered from the loops indicates Zr is a more effective inhibitor than Ti. (This work was performed under the auspices of the U.S.A.E.C.)

Abstract No. 201

Corrosion and Inhibition of Titanium and Titanium Alloys in Mercury at Elevated Temperatures

J. Y. N. Wang, Argonne National Lab., 9700 South Cass Ave., Argonne, Ill.

It is shown that under static conditions the resistance of titanium alloys to attack by mercury at 371°C is generally higher than that of unalloyed titanium. Up to 538°C the attack on these materials is reduced either by the addition of a small amount of metallic additive, particularly zirconium, to mercury or by nitriding of the titanium surface. The practical significance of these results is discussed. (Work performed under auspices of U.S. A.E.C.)

Abstract No. 202

Accelerated High-Temperature Corrosion of Alloys Contaminated by Salt Deposits

J. J. Moran, J. R. Mihalisin, and **B. E. Hopkinson,** International Nickel Co., Inc., 67 Wall St., New York 5, N. Y.

It has long been known that the high-temperature corrosion behavior of metals and alloys is strongly influenced by contaminants either present in the atmosphere or deposited on the surface of the materials. In particular, concern has been expressed recently regarding the accelerating action of minute quantities of certain salts on the oxidation-sulfidation resistance of commercial "superalloys." In an effort to understand better the effect of this contamination a study was undertaken of a series of binary nickel-chromium alloys (0-50%Cr) exposed to mixtures of air plus sulfur dioxide at elevated temperatures. Salt contaminants were introduced by several methods. The results of these studies are presented and comparisons drawn between the performance of the simple binaries and the complex commercial alloys.

Abstract No. 203

Compatibility of Commercial Chromium-Nickel Alloys with Several Nitrogenous Atmospheres at 1750°F

J. S. Brunhouse and **G. W. Titus,** Aerojet-General Nucleonics, P. O. Box 77, San Ramon, Calif.

Commercial chromium-nickel alloys were tested for compatibility with selected nitrogenous reactor coolants at 1750°F. Corrosion and mechanical property changes were studied after exposure times up to 2500 hr. Exposure to nitrogen gas produced nitriding of Hastelloy-X, Inconel, and Inconel 702. An addition of 0.5 vol % oxygen to nitrogen was found to inhibit nitriding of Hastelloy-X and Inconel but not of Inconel 702. An addition of 0.1 vol % carbon monoxide to nitrogen resulted in carburization of Hastelloy-X and Inconel. Oxidation of all alloys was found to be minimal in air as well as the other oxidizing atmospheres.

Abstract No. 204

Prestressed Ceramic Linings

R. R. Pierce, Pennsalt Chemicals Corp., Natrona, Pa.

Ceramic, carbon, graphite, and other nonmetallic materials are formed into linings and prestressed inside metal vessels and towers to provide stress safe and impermeable linings which will withstand the influence of highly corrosive environments at high temperatures or high temperatures with high pressure. The concept, design mathematics, stress magnitudes, chemical, and temperature scopes of use are included. Examples of the linings and vessels and towers up to very large structures are given.

INDEX TO AUTHORS

(The number in the right-hand column is the abstract number used in the Technical Program and in the Abstracts.)

Candidates for Society Offices, 1963

Walter J. Hamer

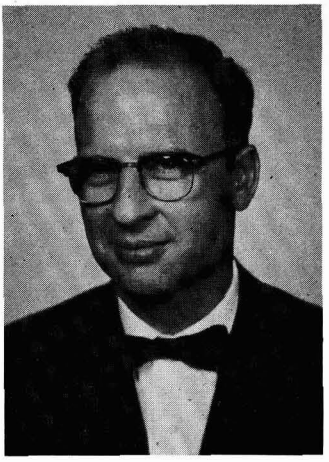

Richard F. Bechtold

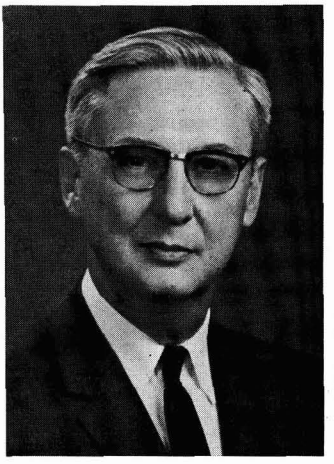

N. Corey Cahoon

The Board of Directors of The Electrochemical Society, in accordance with the provisions of our Constitution, has approved the following Report of the Nominating Committee.

Report of Nominating Committee

The Nominating Committee (Sherlock Swann, Jr., Chairman; M. L. Holt, E. B. Yeager, Morris Feinleib, R. R. Rogers) is offering the following nominees for the election to be held this fall:

For President (One-Year Term, 1963-1964)—
Walter J. Hamer
For Vice-President (Three-Year Term, 1963-1966)—
Richard F. Bechtold
N. Corey Cahoon
Harold J. Read

(Signed) Sherlock Swann, Jr., *Chairman*

All nominees have been contacted and have signified that they would accept the offices if elected.

The above slate will be voted on in the fall ballot-by-mail election, and the successful candidates will assume office in the spring of 1963 at the Pittsburgh Meeting of the Society.

The two other Vice-Presidents, Lyle I. Gilbertson and Ernest B. Yeager, since they were elected for three-year terms, will automatically become first and second Vice-Presidents, respectively.

Walter J. Hamer

Presidential Candidate

Walter J. Hamer has been at the National Bureau of Standards, Washington, D.C., since 1935, and chief of its Electrochemistry Section since 1950. A native of Altoona, Pa., he received his undergraduate training at Juniata College, Huntingdon, Pa., and his graduate training at Yale University, receiving the Ph.D. degree in physical chemistry in 1932. He returned to Yale as a Postdoctorate Fellow in 1932-1934 and then became research associate at M.I.T. in 1934-1935. At Yale, Dr. Hamer worked on electrolytes and the lead-acid accumulator. At M.I.T., he worked on isopiestic standards and the chemical potentials of solid-liquid and partially miscible solutions.

At the National Bureau of Standards, Dr. Hamer's main responsibility is the maintenance of the national standard of electromotive force. He also has worked on batteries, *p*H standards, fused salts, electrolysis, and the faraday. He has taught at Georgetown and Catholic Universities and at the Graduate Schools of the Department of Agriculture and N.B.S.

During the war, Dr. Hamer worked on the uranium problem for O.S.R.D. and the Manhattan Project. He was battery consultant to the Department of Defense in 1952-1954 and now is electrochemical consultant to the University of Pennsylvania and the A.I.E.E. Panel on Flight Vehicles. He is on the Commissions of Electrochemistry and Electrochemical Data of the International Union of Pure and Applied Chemistry, technical advisor on primary batteries to the U.S. National Committee of the International Electrotechnical Commission, and chairman of the dry cell committee and secretary of the electrochemical definitions committee of the American Standards Association. He is a member of the review committee of the International Standards Organization, of storage battery committees of the Society of Automotive Engineers, A.I.E.E. and A.S.A., and of a number of technical societies. He is a member of Alpha Chi Sigma, Sigma Xi, the Washington Academy of Sciences, and the Cosmos Club.

Dr. Hamer is a Vice-President of The Electrochemical Society, Chairman of the Ways and Means Committee, and a member of the Finance Committee. He has served on the Honors and Awards Committee (1958-1960), as Chairman of the Theoretical Division (1951-1953), on the Executive Board of the Battery Division (1954-1956), and as the Society's representative on A.S.A. Committees Y-10 and Y-32. He is Editor of the Society's monograph on "The Structure of Electrolytic Solutions," and is a member of the Advisory Board for a number of books on electrochemistry.

Richard F. Bechtold

Vice-Presidential Candidate

Richard F. Bechtold was born in Roslyn, Wash., in 1923. He was educated at the University of Washington in Seattle, graduating in 1945 with a degree of B.S. in chemical engineering.

Mr. Bechtold's present position is that of manager of inorganic chemicals products in the Chemicals Department of the Dow Chemical Co. In this capacity, he works with the production, research, development, and sales groups on all inorganic products, which include all of Dow's electrochemical products. He began his professional career, following graduation, at Dow's Pittsburg, Calif., plant in 1945. His initial position was that of technical assistant in the Electrochemical Production area. Subsequently, he became assistant superintendent in 1951 and superintendent in 1953. His work was concerned with all of the various areas of activity connected with the production of chlorine, caustic soda, caustic potash, and ammonia. He also was directly involved in the research and development activities concerning electrochemistry. In 1961, he transferred to Midland, Mich., to assume his present position.

Mr. Bechtold's activities in The Electrochemical Society began in 1948 at the time the San Francisco Section was formed. He served for several years as the original Secretary-Treasurer of the Section and, subsequently, became Vice-Chairman and Chairman and Representative to the Council of Local Sections. He is, at present, Representative of the Council of Local Sections for the Midland Section of the Society. He was General Chairman of the San Francisco Meeting of the Society held in 1956. Mr. Bechtold has served as Secretary-Treasurer and Vice-Chairman of the Industrial Electrolytic Division and at present is Chairman of that Division. On the Council of Local Sections, he has been Secretary and Vice-Chairman and currently is Chairman.

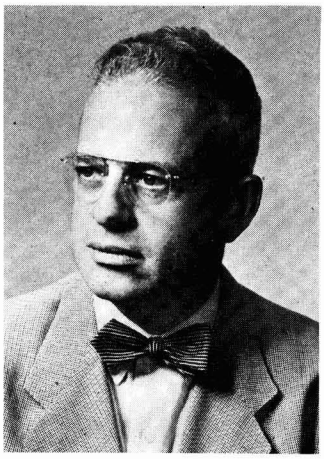

Harold J. Read

N. Corey Cahoon

Vice-Presidential Candidate

N. Corey Cahoon is technical assistant to the resident director of battery development at the Union Carbide Consumer Products Co. in Cleveland. He received his A.B. and M.A. degrees at the University of Toronto in 1925 and 1926, respectively, his research being done under Dr. W. Lash-Millar. He was born in Bloomfield, Ontario, in 1904.

His entire professional career has been spent in the field of batteries with the Union Carbide Corp. He joined the Canadian National Carbon Co., Toronto, in 1926, as a control chemist. In 1928, he was transferred to the Fremont, Ohio, organization of the National Carbon Co. as development engineer. In 1934, he moved to the Research Laboratories in Cleveland to join the newly organized research group for the study of the electrochemistry of primary batteries. He became group leader in the study of basic battery systems in 1953. He assumed his present responsibilities in the battery development organization in 1958.

The technical work to which Mr. Cahoon and a small group of associates were assigned has covered many areas of both theoretical and applied battery technology. Studies of the electrolyte equilibria, electrochemical methods of evaluating manganese dioxide types for battery use, the role of the surface area, and pore structure of oxide for optimum battery performance have provided important fundamental information. One result of these investigations was the selection of electrolytic manganese dioxide for premium quality batteries, a use for which it is still recognized as the optimum material after nearly 25 years. Another application of this technology to improvement in battery quality was a series of separator materials based primarily on synthetic plastics which have found use in high-quality dry cells. Mr. Cahoon's work on the elucidation of the cathode reaction mechanism has provided the industry with a theoretically sound approach to long-life high-capacity cells consistent with the practical demands of manufacture and operation. During World War II, he helped introduce the chlorine-depolarized cell as a high-capacity unit for specialized applications.

A series of 19 papers by Mr. Cahoon and his associates describing important phases of this work have been presented at ECS meetings and/or published in the JOURNAL. Ten U.S. Patents have been awarded to him as inventor or co-inventor.

In 1957, he received the Annual Award of the Chemical Profession in Cleveland. In 1962, he received the George W. Heise Medal from the Cleveland Section of The Electrochemical Society.

During his membership in The Electrochemical Society, which he joined in 1937, he has been active in the Cleveland Section, the Battery Division, and the National Society. He served the Cleveland Section as an officer, and has represented the Section on the Council of Local Sections. He was a member of the National Convention Committee in 1956.

Mr. Cahoon served the Battery Division as Divisional Editor from 1946 to 1952. As Vice-Chairman in 1952-1954, he helped introduce the first Enlarged Abstract booklets to the Division. He was Chairman of the Division in 1954-1956. He has served on many Division committees, including the Battery Award Committee of which he was Chairman in 1960. He was a member of the Board of Directors of the Society in 1954-1956 and in 1960-1962.

He is co-editor with Mr. G. W. Heise of a book on Primary Batteries sponsored by the Battery Division and the Society, now in preparation.

Other society memberships include the American Chemical Society, National Association of Corrosion Engineers, Sigma Xi, and the Faraday Society.

Harold J. Read

Vice-Presidential Candidate

Harold J. Read, 51, was born in Dubuque, Iowa, but grew up and received most of his education in Illinois. His first degree, with a major in chemistry, was received from the University of Illinois in 1934 and was followed by an M.S. degree from the same institution in 1935. Transferring to the University of Pennsylvania, he served as an assistant instructor while pursuing graduate work until 1937, when he was appointed as a du Pont Fellow. In February of 1939, he received a Ph.D. degree in physical chemistry, working under Martin Kilpatrick.

Dr. Read's professional career began before he had completed his education. In 1933-1934, he was a reporter and later editor with Commerce Clearing House in Chicago, Ill. From 1934 to 1935, he was a part-time chemist with the Engineering Experiment station at the University of Illinois. In 1937, he began a part-time association with A. K. Graham that has continued, with various interruptions, through the years and has contributed much to his interest in electrochemistry and metal finishing.

After receiving his doctorate, he continued at Penn as an instructor in electrochemistry and quantitative analysis until 1940, when he joined the Mellon Institute in Pittsburgh. There, his work until 1945 on projects for the H. H. Robertson Co. turned more and more toward metallurgy.

During World War II, Dr. Read turned his hobby of metal working into more serious channels and converted his private workshop to military work. This culminated in a part-time participation in the Manhattan Project with Dr. Maxwell Gensamer. When, in 1945, Dr. Gensamer became head of the Mineral Technology section of the College of Mineral Industries of the Pennsylvania State University, he invited Dr. Read to accompany him as associate professor of metallurgy. In this capacity, Dr. Read undertook the teaching of nonferrous metallography, the extractive metallurgy of the more unusual elements, as well as those recovered by electrolytic means, corrosion, and metal finishing.

In 1951, he was promoted to professor of physical metallurgy, his present position. In addition to regular course work at both undergraduate and graduate levels, he has directed the thesis investigations of many graduate students, most of whom have worked on some problem related to electrometallurgy.

Dr. Read joined the Electrochemical Society in 1934. While living in Philadelphia and Pittsburgh, he took an active part in Local Section affairs, having served as Secretary in both cities and as Chairman in Pittsburgh. He was General Chairman for the National Meeting in Pittsburgh in 1934. In Division affairs, he was Secretary-Treasurer of the Electrodeposition Division in 1940-1941 and Chairman in 1942. He has been active in the publication work of the Society and served on the Publication Committee from 1945 to 1950, being Chairman 1948-1950. He served also for a time as Technical Editor. Other committee work has involved eight appointments to the Membership Committee, service on the Roeber Research Fund Committee (Chairman 1949), the Acheson Award Committee, and numerous nominating committees.

He has contributed to all editions of "Modern Electroplating" and served on the Editorial Board of the first two versions of the book.

Dr. Read has been active in other societies wherein electroplating is a subject of interest and has served on many committees and task groups in them, particularly Committee B-8 of the American Society for Testing Materials.

He is the author or coauthor of numerous journal contributions, book reviews, and chapters in handbooks, textbooks, and encyclopedias. In 1961, he edited and contributed to a book entitled "Hydrogen Embrittlement in Metal Finishing," based on a symposium that he organized for the American Electroplaters' Society. Most of his contributions have concerned electrodeposition, but others have ranged from electroorganic reductions to Louisiana tax laws.

Dr. Read's other memberships include the American Society for Metals, British Institute of Metals, American Chemical Society, American Electroplaters' Society, National Association of Corrosion Engineers, and Sigma Xi. In 1961, he received the Proctor Memorial Leadership Award from the American Electroplaters' Society. He is licensed as a Professional Engineer in Pennsylvania.

Manuscripts and Abstracts for Spring 1963 Meeting

Papers are now being solicited for the Spring Meeting of the Society, to be held at the Penn Sheraton Hotel in Pittsburgh, Pa., April 14, 15, 16, 17, and 18, 1963. Technical sessions probably will be scheduled on: Electric Insulation, Electronics (including Luminescence and Semiconductors), Electrothermics and Metallurgy, Industrial Electrolytics, and Theoretical Electrochemistry.

To be considered for this meeting, **triplicate copies of the usual 75-word abstract, as well as of an extended abstract of 500-1000 words** (*see* notice on page 184C of this issue), must be received at Society Headquarters, 30 East 42 St., Rm. 1806, New York 17, N. Y., *not later than December 14, 1962. Please indicate on abstract for which Division's symposium the paper is to be scheduled, and underline the name of the author who will present the paper.* No paper will be placed on the program unless one of the authors, or a qualified person designated by the authors, has agreed to present it in person. An author who wishes his paper considered for publication in the JOURNAL or in ELECTROCHEMICAL TECHNOLOGY should send triplicate copies of the manuscript to the Managing Editor of the appropriate publication, 30 East 42 St., Rm. 1806, New York 17, N. Y.

Presentation of a paper at a technical meeting of the Society does not guarantee publication in the JOURNAL or in ELECTROCHEMICAL TECHNOLOGY. However, all papers so presented become the property of The Electrochemical Society, and may not be published elsewhere, either in whole or in part, unless permission for release is requested of and granted by the Editor. Papers already published elsewhere, or submitted for publication elsewhere, are not acceptable for oral presentation except on invitation by a Divisional program Chairman.

Committees of The Electrochemical Society, Inc., 1962-1963

Admissions Committee

	Term Expires
Martin F. Quaely, Chairman	Spring 1963
Gunnar D. Stendahl	Spring 1964
Joseph V. Petrocelli	Spring 1965

Finance Committee

	Term Expires
Ernest G. Enck, Chairman	Treas.'s Term
Ivor E. Campbell	Secy.'s Term
Walter J. Hamer	Spring 1963
Jerome Strauss	Spring 1963
Mars G. Fontana	Spring 1963

National Convention Committee

	Term Expires
Ernest G. Enck, Chairman	Treas.'s Term
Ivor E. Campbell	Secy.'s Term
Fielding Ogburn	Spring 1963
Oliver Osborn	Spring 1963
Ernest L. Koehler	Spring 1963

Honors and Awards Committee

	Term Expires
Hans Thurnauer, Chairman	Spring 1963
Lee O. Case	Spring 1963
E. F. Kiefer	Spring 1964
Alan U. Seybolt	Spring 1964
John Convey	Spring 1965
Stanley Wawzonek	Spring 1965
M. J. Pryor	Spring 1966
Charles W. Tobias	Spring 1966
Frank L. LaQue	Pres.'s Term

Investment Advisory Panel

	Term Expires
Ralph M. Hunter, Chairman	Spring 1966
George W. Heise	Spring 1963
Ralph A. Schaefer	Spring 1964
N. M. Winslow	Spring 1965
F. G. Breyer	Spring 1967

Membership Committee (Contributing)

Chairman to be announced later—Term Expires Spring 1963

Membership Committee (Personal)

Fred W. Koerker, Chairman—Term Expires Spring 1963

Nominating Committee

	Term Expires
Norman Hackerman, Chairman	Spring 1963
E. J. Ritchie	Spring 1963
Harold J. Read	Spring 1963
James P. Hoare	Spring 1963
H. A. Liebhafsky	Spring 1963

Palladium Medal Award Committee

	Term Expires
Robert B. Mears, Chairman	Spring 1964
Charles W. Tobias	Spring 1964
Allan T. Gwathmey	Spring 1964
Herbert H. Uhlig	Spring 1966
George A. Ellinger	Spring 1966

Perkin Medal Award Committee

	Term Expires
Frank L. LaQue, Chairman	Pres.'s Term
Henry B. Linford	Spring 1963
O. B. J. Fraser, Alternate	Spring 1963
Cecil V. King, Alternate	Spring 1963

Publication Committee

	Term Expires
Charles L. Faust, Chairman	Spring 1964
Norman Hackerman	Spring 1963
Cecil V. King	Spring 1964
Ivor E. Campbell	Secy.'s Term
A. C. Loonam	Spring 1964
R. B. MacMullin	Spring 1965
Martin F. Quaely	Spring 1965
H. A. Laitinen	Spring 1965

Committee on Protocol

	Term Expires
Henry B. Linford	Spring 1963
Norman Hackerman	Spring 1963
Sherlock Swann, Jr.	Spring 1963

Technical Committee

	Term Expires
Lyle I. Gilbertson, Chairman	Spring 1963
Ivor E. Campbell	Secy.'s Term
Division Chairmen	Elected Terms

Tellers of Election Committee

	Term Expires
Gerald A. Lux, Chairman	Spring 1963
Fred P. Peters	Spring 1963
Sam Tour	Spring 1963
Clarence H. Sample, Alternate	Spring 1963
R. Leigh Glover, Alternate	Spring 1963
Richard Glicksman, Alternate	Spring 1963

Ways and Means Committee

	Term Expires
Walter J. Hamer, Chairman	Spring 1963
Lyle I. Gilbertson	Spring 1963
Ernest B. Yeager	Spring 1963
Milton J. Allen	Spring 1963
Charles W. Tobias	Spring 1963
Frederick W. Fink	Spring 1963
Milton Stern	Spring 1963

Board Representative for Administration of the Corrosion Handbook Fund

Frank L. LaQue—Term Expires Spring 1963

(Continued on page 223C)

Looking Back at Los Angeles

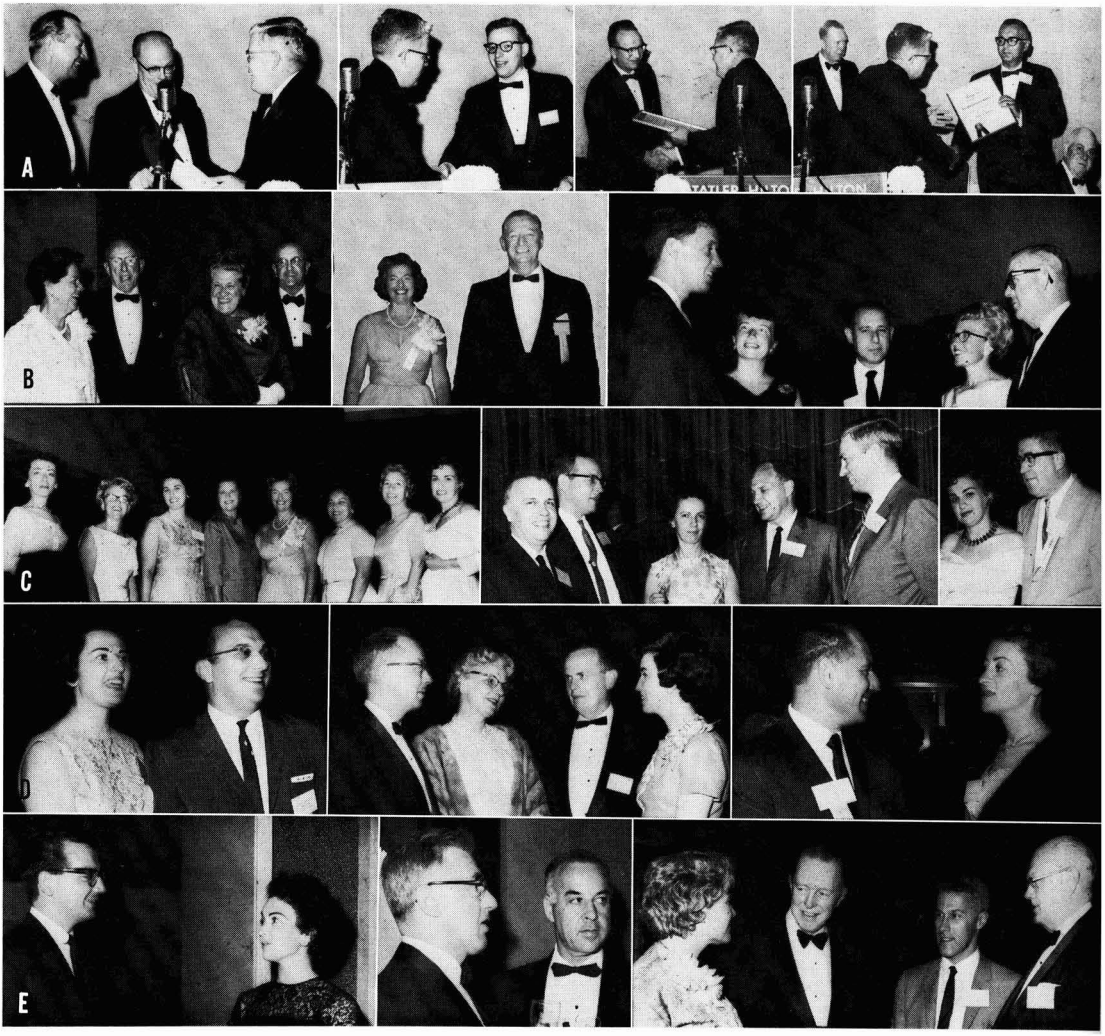

Row A—Joseph C. Schumacher (General Chairman Los Angeles Meeting), Lyle I. Gilbertson (ECS Vice-President), and Henry B. Linford (ECS President); President Linford presents Turner Memorial Award to Harlow Freitag; Alan U. Seybolt receives Certificate of Appreciation from President Linford; Robert K. Shannon (ECS Executive Secretary looks on while President Linford presents Certificate of Appreciation to Milton Stern, Frank L. LaQue (ECS President-Elect) is seated at lower right. **Row B**—Mrs. R. E. Vivian, Dr. and Mrs. Manning, and R. E. Vivian; Mrs. J. C. Schumacher (Chairman Ladies' Program) and J. C. Schumacher (General Chairman Los Angeles Meeting); Mr. and Mrs. Lee J. Droege, David R. Stern (Los Angeles Committee—Finance), Mrs. Hoffman, and Roger W. Hoffman (Los Angeles Committee—"After-the-Meeting" Trip). **Row C**—Mrs. David Stern, Mrs. Roger Hoffman, Mrs. George Larchian, Mrs. Birke Luckenbill, Mrs. Joseph Schumacher, Mrs. Bill Hetherington, Mrs. Tom Blair, and Mrs. George Sturtevant; Edwin M. Sherwood, Murray C. Udy, Rena Garlick, William E. Kuhn, and Jack H. Westbrook; Mrs. Sturtevant and George Sturtevant (Los Angeles Meeting Publicity). **Row D**—Mrs. Larchian and George Larchian (Los Angeles Committee—Registration); Charles L. Faust (ECS Publication Committee Chairman), Mrs. Faust, Ivor E. Campbell (ECS Secretary), and Mrs. Campbell; Dr. and Mrs. David R. Stern. **Row E**—Al Caprioglio and Janet Murphy; Walter J. Hamer (ECS Vice-President) and Hans Thurnauer; Mrs. Gilbertson, Robert K. Shannon, Morris Feinleib, and Lyle I. Gilbertson.

. . . May 1962

Row A—Richard F. Bechtold, Ruth G. Sterns, Hans R. Neumark, and Dr. and Mrs. Robert B. MacMullin; Oliver Osborn; Mr. and Mrs. George Larchian, Mrs. Schumacher, Mrs. Blair, Joseph C. Schumacher, and Thomas C. Blair (Los Angeles Committee—Entertainment). **Row B**—Mrs. Luckenbill, Mrs. Orsino, Sid Banks, Joseph A. Orsino, Mrs. Banks, and Birke Luckenbill (Los Angeles Committee—Plant Tours); William M. Hetherington (Los Angeles Committee—Arrangements), Mrs. Hetherington, and Mary Wiener; Boris D. Cahan, Ernest B. Yeager (ECS Vice President-Elect, back to camera), Vincent DeMarchi, and Henry B. Linford. **Row C**—Two group shots taken on Tuesday evening; group shot taken at Tuesday evening banquet.

Committees of the ECS (*Continued from page 221C*)

Representatives of The ECS to Other Societies

American Association for the Advancement of Science

Frederick A. Lowenheim—Term Expires Spring 1963
Sherlock Swann, Jr.—Term Expires Spring 1964

American Standards Association Subcommittees

	Term Expires
Y-10—Lee O. Case	Spring 1963
Y-32—Lee O. Case	Spring 1963
C-67—Upton B. Thomas	Spring 1963
C-40—Eugene Willihnganz	Spring 1963
C-40—R. C. Shair, Alternate	Spring 1963

National Academy of Sciences—National Research Council—Advisory Board for Office of Critical Tables

Ernest B. Yeager—Term Expires Spring 1964

National Research Council—Division of Chemistry and Chemical Technology

Norman Hackerman—Term Expires Spring 1964

American Society for Testing Materials

C-25—A. Gunzenhauser—Term Expires Spring 1963

Instrument Society of America

C-96—Thermocouple Sectional Committee of American Standards Association organized by Instrument Society
E. M. Sherwood—Term Expires Spring 1963

American Electroplaters' Society

C. H. Sample—Representative of Electrodeposition Division—Term Expires Spring 1963

National Association of Corrosion Engineers

Subcommittee on Standard Definitions and Terminology (Our Representative to be Vice-Chairman of the Corrosion Division)
Harry C. Gatos—Term Expires Spring 1963

National Electrical Manufacturers Association

Fuel Cell and Battery Subcommittee—Static Energy Conversion Section
W. J. Subcasky—Term Expires Spring 1963

Electrochemical Society Awards

J. D. Newson

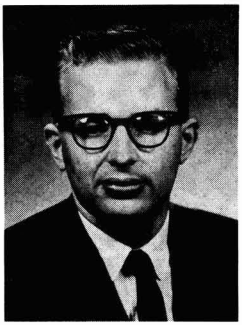

Harlow Freitag

Young Author's Prize for 1961

At the Annual Banquet held on Tuesday, May 8, during the Los Angeles Meeting of The Electrochemical Society, John D. Newson, of the Dept. of Chemistry, University of Southampton, Southampton, England, was announced as the winner of the 1961 Young Author's Prize of $100. His prize-winning paper, written in cooperation with A. C. Riddiford, entitled "The Kinetics of the Iodine Redox Process at Platinum Electrodes" appeared in the July 1961 issue of the JOURNAL.

Dr. Newson received his B.Sc. and Ph.D. degrees from the University of Southampton, England. On completing his period of study in 1957, he served for three years as a Lieutenant in the Royal Navy.

He now is teaching at King Edward VI School in Southampton. He is interested in the study and teaching of the history of science.

Turner Memorial Award for 1961

Harlow Freitag, International Business Machines Corp., Yorktown Heights, N. Y., is the winner of the Francis Mills Turner Memorial Award, Sponsored by the Reinhold Publishing Corp., in recognition of the paper by himself and Andrew Patterson, Jr., "The Wien Effect and Ionic Association," which was published in the June 1961 JOURNAL.

The award, consisting of $100 worth of scientific and technical publications was made to Dr. Freitag at the Society's Annual Banquet on May 8 in Los Angeles.

Dr. Freitag received his B.S. degree from New York University, receiving his M.S. degree in 1957 and his Ph.D. degree in 1959.

Since 1958, he has been employed by International Business Machines Corp. and currently is with the Research Division. His work has dealt with the kinetics of electrode processes, particularly those involving anodization.

Dr. Freitag is a member of The Electrochemical Society, the American Physical Society, the Faraday Society, and Sigma Xi.

Summer Fellowship Awards Announced for 1962

On recommendation of the Honors and Awards Committee, the Board of Directors of the Society voted in May to approve the issuance of three Summer Fellowship Awards for the year 1962, in the amount of $800 each, to cover the period June-September, one of which shall be designated as the Edward Weston Fellowship, one as the Colin Garfield Fink Fellowship, and one as the ECS Summer Fellowship Award. The funds for these awards are derived from income from investments in the Consolidated Fellowship Fund and the Edward Weston Fellowship Fund.

The Summer Fellowship Award is made "without regard to sex, citizenship, race, location, or financial need to a fellow or teaching assistant pursuing work between the degree of B.S. and Ph.D. on a subject in the field of interest to The Electrochemical Society. The recipient must be the possessor of a nine-month grant in this field of interest for the academic year 1962-1963 and must have been the holder of a similar grant for the academic year 1961-1962."

The following are the recipients of the Fellowship Awards for 1962.

Daniel C. Yohe, a graduate student at the Dept. of Chemistry, Western Reserve University, Cleveland, Ohio, has been designated as the recipient of the Edward Weston Fellowship.

Paul Brown, a graduate student at the Dept. of Chemistry, DePauw University, Greencastle, Ind., has been awarded the Colin Garfield Fink Fellowship.

Arlin Postma, a graduate student at the Chemical Engineering Dept., Oregon State University, Corvallis, Ore., will receive the Electrochemical Society Summer Fellowship Award.

Mr. Yohe is working toward his Ph.D. degree in chemistry, his main interest involving the study of the relationship of the kinetics of electrode reactions to the solid state properties of the electrodes on which these reactions are occurring.

Mr. Brown's interest centers in electrochemistry. He won second place in The Electrochemical Society's Essay Contest on Polarography conducted among Midwest liberal arts colleges of the MACTLAC association in 1961. His research will be in this field and involves, initially, the measurements of electrode potentials in nonaqueous systems, in particular Grignard systems.

Mr. Postma holds a B.S. degree in chemical engineering from Oregon

Notice to Members and Subscribers

(Re Changes of Address)

To insure receipt of each issue of the JOURNAL, please be sure to give us your old address, as well as your new one, when you move. Our records are filed by states and cities, not by individual names. The Post Office does not forward magazines.

We should have this information *by the 16th of the month* to avoid delays in receipt of the next issue.

State University and has spent two years with the General Electric Co. in Richland, Wash. He, at present, is pursuing the Ph.D. program in chemical engineering under the direction of Dr. R. E. Meredith.

The reports on these awards will appear in a later issue of the JOURNAL.

Storey, Skowronski, Seybolt, Stern, and Foley Honored at Los Angeles

Honorary Members

At the Annual Banquet on May 8, 1962, during the Los Angeles Meeting of the Society, President Henry B. Linford announced that, by action of the Board of Directors, Oliver W. Storey, of Santa Barbara, Calif., and Stanislaus Skowronski, of Metuchen, N. J., have been elected Honorary Members of the Society, "in recognition of distinguished service and significant contributions to the science of electrochemistry," and that appropriate Certificates would be presented to Dr. Storey and Dr. Skowronski at a later date since neither was present in Los Angeles.

Certificates of Appreciation

Certificates of Appreciation were presented by President Linford to:

Alan U. Seybolt—"In Appreciation for Meritorious Contribution to The Electrochemical Society, Inc., as Electrothermics and Metallurgy Division Editor of the Journal of the Society 1954-1960."

Milton Stern—"In Appreciation for Meritorious Contribution to The Electrochemical Society, Inc., as Corrosion Division Editor of the Journal of the Society 1958-1961."

To be presented at a later time, since he was not at Los Angeles, was a certificate of Appreciation to:

Robert T. Foley—"In Appreciation for Meritorious Contribution to The Electrochemical Society, Inc., as Corrosion Division Editor of the Journal 1957-1962."

Section News

Midland Section

The Midland Section held the following meetings during the 1961-1962 season:

November—Ladies' Night.
January 23—Dr. H. B. Linford—"The Effect of Soils on the Electrodeposition Process."
March 5—Dr. D. R. Turner—"The Electrochemistry of Semiconductors."
April 3—Mr. G. T. Sermon—"High-Purity Graphite."
May 28—Golf and business meeting.

During the spring outing of the Section held on May 28, Dr. Ralph M. Hunter shot the first hole-in-one of his long and distinguished golfing career.

Officers of the Section for the 1962-1963 season are:

Chairman—C. K. Bon, Dow Chemical Co., Bldg. 1705, Midland, Mich.
Vice-Chairman—J. L. Robinson, Dow Chemical Co., Bldg. 241, Midland, Mich.
Secretary-Treasurer—J. L. Kroon, Dow Chemical Co., Midland, Mich.
Local Section Councilors—R. F. Bechtold, 2108 Belaire, Midland, Mich., and D. Chapin, 3400 Bay City Rd., Midland, Mich.

J. L. Robinson,
Secretary-Treasurer

Pittsburgh Section

On April 11, the Pittsburgh Section jointly with the Electroplaters' Society heard Professor Harold J. Read of the Pennsylvania State University discuss "Hydrogen Embrittlement." Dr. Read presented metallurgical information of assistance to those who must face embrittlement problems. Stress-strain relationships in flow and fracture were discussed and the manner in which occluded hydrogen can affect the normal relationship was given particular attention. Before the meeting, Dr. Read was the Section's guest at a dinner.

The Pittsburgh Section annually sponsors an award at the Pittsburgh Regional School Science Fair. This year's award of $25 went to Edward M. Petrie of Brentwood, Pa., for his exhibit of an Ion-Exchange Fuel Cell.

The Buhl Planetarium School-Science Fair is a cooperative undertaking which annually mobilizes the educational, scientific, and industrial resources of the Greater Pittsburgh region to insure a continuing stream of able youths who will provide its technicians, scientists, and engineers in the years ahead.

The objectives of the regional Fair—and of its radio-television program, "School Science Experts"—are to discover and encourage the science potential in all students at the junior and senior high school level, and to help the exceptionally able to achieve outstanding careers in science and engineering. These ends it has accomplished, on a significantly increasing scale, for 23 years.

The Fair is under the general guidance of a Science Teachers' Committee, an Advisory Committee, and a Committee of Judges. Leading industrial and university research scientists, as well as hundreds of high school science teachers, give generously of their time, effort, and inspirational leadership.

This year, over 1200 students are competing in the Planetarium Science Fair. In addition, more than 15,500 other students competed in preliminary fairs, held as elimination contests in many district schools. The best exhibits in these local fairs are entered in the regional Planetarium Fair. The establishment and continued growth of local fairs are most desirable in terms of the number of students who are thus provided with the opportunity to explore the world of science through research and construction of a science exhibit.

Further enlarging the scope of the Fair's influence, more than 30,000 students and adults annually come to discover the drama—and the challenge—of science.

R. P. Frankenthal,
Secretary-Treasurer

New Members

In June 1962, the following were elected to membership in The Electrochemical Society by the Admissions Committee:

Active Members

R. W. Atteberry, Olin Mathieson Chemical Corp., Research Center, New Haven, Conn. (Theoretical Electrochemistry)
W. J. Babkes, Autonetics, Div. of North American Aviation; Mail add: 9354 Greenwell St., Bellflower, Calif. (Electrodeposition, Electronics—Semiconductors, Electrothermics & Metallurgy)

By action of the Board of Directors of the Society, all prospective members must include first year's dues with their applications for membership.

Also, please note that, if sponsors sign the application form itself, processing can be expedited considerably.

Maurice Back, Texas Instruments, Inc.; Mail add: 8739 Graywood Dr., Dallas 31, Texas (Electronics—Semiconductors)

E. V. Ballon, Lockheed Missiles & Space Co.; Mail add: 3449 Rambow Dr., Palo Alto, Calif. (Electrothermics & Metallurgy, Theoretical Electrochemistry)

P. R. Basford, Aeroneutronic Div., Ford Motor Co.; Mail add: 1111 S.E. Skyline Dr., Santa Ana, Calif. (Battery, Theoretical Electrochemistry)

Harry Bender, Autonetics, Div. of North American Aviation; Mail add: 12061 Cole St., Anaheim, Calif. (Electronics—Semiconductors)

D. F. Bowman, Autonetics, Div. of North American Aviation; Mail add: 3807 Andy, Long Beach 5, Calif. (Electric Insulation, Electronics—Semiconductors & Luminescence)

Giovanni Caprioglio, General Dynamics, General Atomic Div., P. O. Box 608, San Diego 12, Calif. (Theoretical Electrochemistry)

R. C. Carlston, Aerojet General Corp., Research Div.; Mail add: 823 E. Northridge, Glendora, Calif. (Electronics—Semiconductors)

J. Z. Cerych, Mallory Capacitor Co.; Mail add: 7032 E. 10 St., Indianapolis 19, Ind. (Electric Insulation, Electronics)

R. F. Cline, Consulting Engineer; Mail add: P. O. Box 931, Arcadia, Calif. (Electric Insulation, Electronics—Semiconductors & Luminescence)

G. R. Crabbs, Pacific Semiconductors, Inc.; Mail add: 826 N. Normandie Ave., Los Angeles 29, Calif. (Electronics—Semiconductors)

D. C. Cronemeyer, Bendix Research Labs.; Mail add: 30775 Rosemond Dr., Franklin, Mich. (Electronics—Luminescence)

J. C. Day, American Micro Devices, Inc.; Mail add: 3602 W. Sierra Vista, Phoenix, Ariz. (Electronics—Semiconductors)

A. F. Fairbanks, Westinghouse Astro Electronics Labs.; Mail add: 460 Skyline Dr., Thousand Oaks, Calif. (Electronics—Luminescence)

P. C. Fletcher, Electro-Optical Sys-

ECS Membership Statistics

The following three tables give breakdown of membership as of July 1, 1962. The Secretary's Office feels that a regular accounting of membership will be very stimulating to membership committee activities. In Table I it should be noted that the totals appearing in the right-hand column are *not* the sums of the figures in that line since members belong to more than one Division and, also, because Sustaining Members are not assigned to Divisions. But the totals listed are the total membership in each Section. In Table I, Sustaining Members have been credited to the various Sections.

Table I. *ECS Membership by Sections and Divisions*

Section	Division: Battery	Corrosion	Electric Insulation	Electro-deposition	Electronics	Electro-Organic	Electrothermics & Met.	Industrial Electrolytic	Theoretical Electrochem.	No Division	Total as of 1/1/62	Total as of 7/1/62	Net Change
Boston	19	43	16	39	88	6	30	8	40	5	197	200	+3
Chicago	30	35	13	38	36	17	15	16	44	6	163	166	+3
Cleveland	51	27	1	38	41	6	26	22	32	6	191	170	−21
Columbus, Ohio	4	14	2	20	18	2	26	4	9	2	67	59	−8
Detroit	31	23	3	48	23	8	10	9	37	6	121	113	−8
India	1	5	—	11	5	3	3	4	5	2	37	20	−17
Indianapolis	31	10	12	13	28	6	12	7	14	3	81	79	−2
Midland	10	16	2	5	7	3	10	17	10	—	47	50	+3
Mohawk-Hudson	18	26	19	9	24	3	13	4	26	4	89	88	−1
New York	132	104	35	176	206	38	114	73	135	33	669	666	−3
Niagara Falls	10	18	2	26	27	4	59	54	9	8	168	149	−19
Ontario-Quebec	5	16	2	10	8	1	31	25	10	4	87	79	−8
Pacific Northwest	5	10	—	11	5	1	7	8	16	3	37	39	+2
Philadelphia	41	23	8	39	75	7	22	23	47	16	221	209	−12
Pittsburgh	6	44	7	30	53	5	33	20	37	1	144	144	—
San Francisco	22	14	1	29	48	6	15	21	30	2	111	117	+6
S. Calif.-Nevada	31	30	11	51	108	14	38	20	61	6	173	214	+41
Texas	8	26	2	11	62	5	9	23	30	1	124	145	+21
Washington-Baltimore	42	35	8	35	33	3	14	6	26	3	145	122	−23
U. S. Non-Section	59	61	13	76	76	31	56	45	81	26	357	342	−15
Foreign-Non-Section	69	67	17	74	46	34	54	69	94	78	319	315	−4
Total as of Jan. 1, 1962	632	671	168	811	988	213	626	502	804	233	3548		
Total as of July 1, 1962	625	647	174	789	1017	203	597	478	793	215		3486	
Net Change	−7	−24	+6	−22	+29	−10	−29	−24	−11	−18			−62

Table II. *ECS Membership by Grade*

	Total as of 1/1/62	Total as of 7/1/62	Net Change
Active	2983	2949	−34
Faraday (Active)	37	31	− 6
Deutsche Bunsen Gesellschaft (Active)	21	21	0
Delinquent	174	153	−21
Active Representative Patron Members	10	10	0
Active Representative Sustaining Members	105	102	− 3
Total Active Members	3307	3251	−56
Life	16	16	0
Emeritus	93	94	+ 1
Associate	56	70	+14
Student	46	31	−15
Honorary	7	9	+ 2
Total	3548	3486	−62

The figures pertaining to Patron and Sustaining Member Representatives, and Faraday and Deutsche Bunsen Gesellschaft members subscribing to the JOURNAL, have been added to reflect reclassifications and changes in membership status.

Table III. *ECS Patron and Sustaining Membership*

	Total as of 1/1/62	Total as of 7/1/62	Net Change
Patron Member Companies	5	5	0
Sustaining Member Companies	149	149	0

tems, Inc., 125 N. Vinedo, Altadena, Calif. (Electronics—Luminescence)

J. B. Fredrickson, National Research Corp.; Mail add: 74 Robbins Rd., Sudbury, Mass. (Electric Insulation)

Myer Geller, Electro-Optical Systems, Inc.; Mail add: 355 Anna Marie Dr., Altadena, Calif. (Electronics—Semiconductors & Luminescence)

R. F. Gregori, Cornell-Dubilier Electronic Corp.; Mail add: 781 Neponset St., Norwood, Mass. (Electric Insulation)

J. J. Grossman, Hughes Research Labs., Malibu, Calif. (Electronics—Semiconductors, Electrothermics & Metallurgy, Theoretical Electrochemistry)

A. M. Holladay, IEI-SPS Electronic Labs.; Mail add: 2810 White Oak Dr., Nashville, Tenn. (Electronics)

C. E. Hyman, USAERDL, Fort Belvoir; Mail add: 1531 52nd Ave., N.E., Washington 27, D. C. (Electronics—Luminescence)

H. F. Jones, Autonetics, Div. of North American Aviation; Mail add: 1328 Circle Dr., Whittier, Calif. (Electronics—Semiconductors & Luminescence, Electrothermics & Metallurgy, Theoretical Electrochemistry)

F. R. Kalhammer, Stanford Research Institute; Mail add: 411 Magnolia St., South Pasadena, Calif. (Theoretical Electrochemistry)

Rudolf Keller, Stanford Research Institute, 820 Mission St., South Pasadena, Calif. (Theoretical Electrochemistry)

Bernard Kriegsman, General Instrument Corp., 600 W. John St., Hicksville, N. Y. (Electronics—Semiconductors)

Theodore Kuwana, Dept. of Chemistry, University of California, Riverside, Calif.

P. J. McDonough, General Electric Co. (TEMPO); Mail add: 1010 San Roque Rd., Santa Barbara, Calif. (Electronics)

J. E. Mann, Pacific Semiconductors, Inc.; Mail add: 1106 N. Pasadena Ave., Azusa, Calif. (Electronics—Semiconductors)

H. C. Mattraw, Sperry Rand Research Center; Mail add: 46 Hancock St., Lexington, Mass. (Electronics)

J. F. Miller, Battelle Memorial Institute, 505 King Ave., Columbus 1, Ohio (Electronics—Semiconductors & Luminescence)

S. C. Moore, Westinghouse Electric Corp.; Mail add: 649 Ruth Dr., Newbury Park, Calif. (Electronics—Semiconductors)

W. M. Nelson, Research Div., Kollsman Instrument Corp.; Mail add: 185-07 69th Ave., Flushing 65, N. Y. (Electronics—Semiconductors & Luminescence)

W. S. Netter, Atomics International; Mail add: 353½ S. Reeves Dr., Beverly Hills, Calif. (Electric Insulation)

A. M. Odok, General Electric Co.; Mail add: 349 Woodley Court, Santa Barbara, Calif. (Electronics)

A. G. Osborne, Autonetics, Div. of North American Aviation; Mail add: 1653 Palau Place, Costa Mesa, Calif. (Electric Insulation, Electrodeposition, Electronics—Semiconductors, Electro-Organic)

Gerhard Otto, Pacific Semiconductor Corp.; Mail add: 20801 Felker Dr., Torrance, Calif. (Electronics—Semiconductors)

Suresh Parkhani, Hughes Aircraft Corp.; Mail add: 310 Avocado St., Costa Mesa, Calif. (Electrodeposition, Electronics)

W. L. Paterson, Hoffman Electronics Corp., Semiconductor Div.; Mail add: 11102 E. Wildflower Rd., Temple City, Calif. (Electronics—Semiconductors)

L. J. Quintana, Autonetics, Div. of North American Aviation; Mail add: 1946 Cerritos Ave., Anaheim, Calif. (Electrodeposition)

K. V. Ramanathan, Hughes Aircraft Corp., Semiconductor Div.; Mail add: 1800 Wallace Ave., Costa Mesa, Calif. (Electrodeposition, Electronics)

Melvin Restivo, U. S. Semiconductor Products Inc.; Mail add: 2835 E. Voltair, Phoenix 22, Ariz. (Electric Insulation)

A. H. Rice, Hoffman Electronics Corp.; Semiconductor Div.; Mail add: 8462 Sunset Blvd., Hollywood 69, Calif. (Electronics—Semiconductors)

A. G. Richards, Bell & Howell Research Center; Mail add: 939 Arcadia Ave., Arcadia, Calif. (Electronics—Semiconductors)

J. H. Scott, Jr., R.C.A.; Mail add: 73 Shanley Ave., Newark, N. J. (Electronics—Semiconductors)

P. R. Segatto, Corning Glass Works; Mail add: 1060 West Water St., Elmira, N. Y. (Electric Insulation)

E. J. Sherman, R.C.A.; Mail add: 4 Everet Dr., Somerville, N. J. (Electric Insulation)

R. M. Shoho, Autonetics, Div. of North American Aviation; Mail add: 4732 Avocado Ave., Yorba Linda, Calif. (Electrodeposition)

Henry Shucker, Hoffman Electronic Corp.; Mail add: 445 N. Calmgrove Ave., Covina, Calif. (Electronics—Semiconductors)

H. E. Sivik, Bendix Semiconductor Div.; Mail add: 26 Harbor Greens Circle, Red Bank, N. J. (Electronics—Semiconductors)

Symposium on Stress Corrosion of Metals Rescheduled for March 1963

The Corrosion Division Symposium on Stress Corrosion of Metals originally planned for the 1963 Fall Meeting of The Electrochemical Society, as announced in the April, May, and June JOURNALS, has been rescheduled and will be held in conjunction with the Second International Congress on Metallic Corrosion in New York City, March 11-15, 1963.

Subjects suggested for this symposium are: classical stress corrosion; hydrogen embrittlement as a factor in stress-corrosion cracking; brittle fracture as affected by environmental conditions; and the application of modern concepts of solid-state physics to stress corrosion.

Papers giving data to support or disprove one of the current theories of the mechanism of stress-corrosion cracking would be considered under the classification of classical stress corrosion. Papers merely summarizing data on a particular alloy or group of alloys are not considered to have a place in the symposium.

Inasmuch as results of center or edge notch tests on very high-strength alloys are reported to be highly sensitive to the test environment, the Chairmen feel that papers giving results and particularly suggested mechanisms for these phenomena should be included.

Metal physics is an increasingly important field and papers in which the modern concepts of solid-state physics are applied to the theory would be desirable.

Titles of proposed papers should be submitted as soon as possible to one of the Co-Chairmen: E. H. Phelps, Applied Research Lab., U. S. Steel Corp., Monroeville, Pa., and Hugh L. Logan, National Bureau of Standards, Washington, D. C. Abstracts of about 1000 words and containing up to four figures are due October 31 and the completed papers at the time of the Conference.

R. A. Smith, General Electric Co.; Mail add: 2130 Alisos Dr., Santa Barbara, Calif. (Battery, Electronics—Luminescence, Theoretical Electrochemistry)

G. C. Spencer, Westinghouse Astroelectronics Lab.; Mail add: 3070 Camino Graciosa, Thousand Oaks, Calif. (Electronics—Semiconductors)

R. S. Steffanson, Dow Chemical Co., Pittsburg, Calif. (Industrial Electrolytic)

F. J. Steinebrey, Jr., Pacific Semiconductors, Inc.; Mail add: 625 W. Doran St., Glendale 3, Calif. (Electronics—Semiconductors)

Melvin Tecotzky, Lockheed Missiles & Space Co.; Mail add: 151 Calderon Ave., Mountain View, Calif. (Electronics—Semiconductors)

G. F. Wheeler, General Electric Co.; Mail add: 39 Proctor St., Salem, Mass. (Theoretical Electrochemistry)

W. B. Whitney, Phillips Petroleum Co.; Mail add: 6018 Whitney Lane, Bartlesville, Okla. (Electro-Organic)

Harvey Winston, Quantum Technology Labs., Inc.; Mail add: 238 Tustin Ave., Newport Beach, Calif. Electronics—Semiconductors & Luminescence)

L. M. Wood, General Dynamics; Mail add: 1477 Tulane Rd., Claremont, Calif. (Electronics—Semiconductors)

R. J. Yinger, Nuclide Analysis Associates, Box 752, State College, Pa. (Electrothermics & Metallurgy)

G. J. Young, Surface Processes R&D Corp.; Mail add: Country Club Rd., Dallas, Pa. (Industrial Electrolytic)

L. L. Young, Nortronics; Mail add: 1100 B Gash St., Fullerton, Calif. (Electronics—Semiconductors & Luminescence)

R. S. Zucker, Hoffman Electronics Corp.; Mail add: 940 S. Hollenbeck St., West Covina, Calif. (Electronics—Semiconductors)

Rainer Zuleeg, Hughes Aircraft Co., Semiconductor Div.; Mail add: 2300 Redlands Dr., Costa Mesa, Calif. (Electronics)

Associate Member

W. M. Sartain, III, Texas Instruments, Inc.; Mail add: 9190 Forest Lane, Dallas 30, Texas (Electronics—Semiconductors)

Reinstatement to Active Membership

H. F. Quinn, IBM (FSD) Space Guidance Center, Owego, N. Y., Attn. Dept. 509 (Electrodeposition, Electronics—Semiconductors, Electrothermics & Metallurgy)

Personals

Robert Bakish has joined Electronics and Alloys Inc. in Ridgefield, N. J., as executive vice-president. His duties will include the direction of the over-all research and development effort of the company. He was formerly with Alloyd Electronics Corp. of Cambridge, Mass.

Norbert D. Greene has been appointed associate professor of materials engineering at Rensselaer Polytechnic Institute, Troy, N. Y. Dr. Greene joined the Rensselaer faculty in 1959; he was previously associated with the Metals Research Labs., Union Carbide Corp., Niagara Falls, N. Y. Currently he is director of the Corrosion Research Lab. which is engaged in studies of metallic corrosion, electrode kinetics, and fuel cells.

Dr. Greene received the 1959 Young Author's Award from the National Association of Corrosion Engineers and is now serving as vice-chairman of the Editorial Review Committee of the Association. This spring, Dr. Greene was awarded the 1962 Alfred H. Geisler Award of the American Society for Metals by the Northeast New York Section for his work on metallic corrosion and passivity.

Philip M. Jaffe, senior research chemist at the Lamp Div. of the Westinghouse Electric Corp., Bloomfield, N. J., was awarded a Ph.D. degree in chemistry from the Polytechnic Institute of Brooklyn.

Book Review

The Electrochemistry of Semiconductors. Edited by P. J. Holmes. Published by Academic Press, London and New York, 1962. 396 pages; $12.00.

This book contains a well-integrated set of papers which should serve either as an excellent introduction or as a handy reference book to the field of the electrochemistry of semiconductors. The book contains articles ranging from the semiconductor gas interface and the electrochemical reactions at germanium and silicon surfaces to the practical applications of electrolytic and chemical etching treatments to semiconductors. The first paper by H. F. Gohr defines the electrochemical and thermodynamic terms and their relation to semiconductor parameters. The second paper by A. R. Plummer covers the semiconductor-gas and semiconductor-metal systems. It represents the most up-to-date and complete review paper on the subject of the electrical properties of clean and etched germanium and silicon surfaces. The next four papers deal with the chemical and electrochemical processes at the surface of a semiconductor. These articles serve to delineate the problems which investigators face in this area of research and also the way they are attempting to resolve them. One of the major problems to be overcome is the lack of knowledge of the structure and purity of the first few monolayers at the solid liquid interface.

For those whose main problems are related to the preparation of surfaces, the last two articles, on practical electrolytic treatments for semiconductors by J. I. Pankove and practical application of chemical etching by P. J. Holmes, should be most welcome. The lists of various chemical etches which may be used for each semiconductor, together with their major purpose, should also prove to be very useful.

Paul Handler
University of Illinois

News Items

1962 ECS Membership Directory

The 1962 Membership Directory of The Electrochemical Society, including an alphabetical listing of Members and Patron and Sustaining Members, Officers of the Society, and Division and Section Officers, will be off the press shortly.

The Directory will be available only to members of the Society (not including subscribers) at the price of $1.00 per copy. Members, who have not already done so, who wish to purchase the Directory should send in their orders (accompanied by check) to Society Headquarters, 30 East 42 St., Rm. 1806, New York 17, N. Y.

Third International Symposium on Quantum Electronics

The Third International Symposium on Quantum Electronics will be held at the UNESCO Palace in Paris on February 11-15, 1963. It is being sponsored by the Office of Naval Research, the Institute of Radio Engineers, and the Société Francaise des Electroniciens et des Radioélectriciens. It is also receiving support from the Fédération Nationale

des Industries Electroniques, which will hold an exposition of apparatus pertaining to quantum electronics during the same week. Professor P. Grivet, of the University of Paris, is chairman of the Organizing Committee. Professor N. Bloembergen, of Harvard University, is chairman of the Program Committee. Professor Louis de Broglie, Nobel Laureate and Secretary of the French Academy, is the Honorary President of the Symposium.

The First two Symposia on Quantum Electronics were sponsored by the Office of Naval Research and were held at High View, N. Y., in 1959 and at Berkeley, Calif., in 1961. As in the previous case, this Symposium will deal with such topics in quantum electronics as masers, lasers, coherence, optical pumping, atomic clocks, and applications to spectroscopy, magnetism, and relativity. Emphasis will be on basic physical principles rather than on engineering.

Scientists desiring to present papers should submit abstracts in triplicate before October 1, 1962 to: The Third International Symposium on Quantum Electronics, 7 Rue de Madrid, Paris 8, France.

Papers may be presented either in French or English. There will be simultaneous translation of each paper into the other language for the benefit of the audience. A registration fee of $12.00 will be required of all participants. Further information can be obtained from the above address.

First Australian Conference on Electrochemistry

The First Australian Conference on Electrochemistry will be held in February 1963 in Sydney and Hobart, under the joint sponsorship of the Royal Australian Chemical Institute, the University of Tasmania, and the University of New South Wales.

A number of distinguished chemists have signified that they will attend, including overseas and Australian experts who will act as Chairmen of the individual sessions.

Excursions will be arranged, and a Ladies' Program will be organized.

Following are the topics to be discussed in the Sydney sessions (February 13-15) and the Session Chairmen:

A. Solid State Chemistry—Dr. L. G. Rees, CSIRO Chemical Research Labs., Fishermens Bend, Victoria.
B. Thermodynamics of Electrolytes —Prof. R. H. Stokes, Univ. of New England, Armidale, N.S.W.
C. Electroanalytical Methods—Prof. P. Delahay, Louisiana State Univ., Baton Rouge, La.
D. Applications (Plating, Anodizing)—not yet finalized.
E. Corrosion—Assoc. Prof. J. J. Jenkins, Univ. of New South Wales.
F. Theory of Boundary Layers—Dr. James R. McDonald, Central Research Lab., Texas Instruments, Inc., Dallas, Texas.

The following are the topics in the Hobart sessions (February 18-20), and the Session Chairmen:

A. Electrowinning and Electrorefining—Dr. N. E. Richards, Reynolds Metals Corp., Sheffield, Ala.
B. Electrode Processes—Prof. J. O'M. Bockris, Univ. of Pennsylvania, Philadelphia, Pa.
C. Fused Salts—Dr. M. A. Bredig, Chemistry Div., Oak Ridge National Lab., Oak Ridge, Tenn.
D. Fuel Cells—Dr. Eric Blomgren, Stanford Research Institute, South Pasadena, Calif.
E. Nonaqueous Electrochemistry—Prof. N. H. Parton, Univ. of Otago, Christchurch, New Zealand.

Each session will consist of a review paper presented by the session

Chairman, followed by contributed papers giving results of original research.

Anyone who expects to be able to present a paper at the Conference is asked to supply the preliminary title as soon as possible. An abstract (200 words) will be required by September 1, 1962, and the final text of the paper (not more than 3000 words) by October 15, 1962, for publication in the Conference Proceedings. All communications should be directed to Dr. F. Gutmann, Honorary Secretary Sydney Committee, Dept. of Physical Chemistry, The University of New South Wales, P.O. Box 1, Kensington, N.S.W.

Metallurgical Society Fall Meeting

The Fall Meeting of The Metallurgical Society of AIME, to be held October 27-November 1, 1962 in the Statler Hotel, New York City, will include papers on materials, science and engineering, aerospace, powder metallurgy, and many other fields.

The Materials Science and Engineering Committee of the Society's Institute of Metals Division has announced a special program comprising an afternoon session and an evening panel on October 29.

Another important phase of the meeting will be joint sponsorship, October 27-28, with the American Society for Metals, of a seminar on "Surface Phenomena." The Institute of Metals Division has announced there will be 12 speakers, covering various facets of the nature of a solid surface.

A Nuclear Panel will be held the evening of October 31, following a daytime nuclear metallurgy session.

Conference of Metallurgists

A three-day Conference of Metallurgists will be held at McMaster University, Hamilton, Ont., Canada, September 5-7, 1962.

There will be five sessions on extraction metallurgy, including ore dressing, four on physical metallurgy, plus the two-session symposium on "Advances in the Metallurgy of Iron and Steel." Visits to the iron and steel facilities in the Hamilton area will take place on Tuesday, September 4.

Dr. John Convey, director of the Mines Branch, Dept. of Mines and Technical Surveys, is the general chairman of the Conference. R. D. Hindson, a Canadian Institute of Mines and Metallurgy vice-president, is coordinating the Conference as assistant general chairman.

1963 National Electronics Conference

James H. Kogen, National Electronics Conference President, has announced that the 1963 National Electronics Conference dates will be October 28, 29, and 30. This represents a change in the previously announced 1963 NEC dates of October 21, 22, and 23.

12th Annual Instrument Symposium

The 12th Annual Instrument Symposium and Research Equipment Exhibit will be held by the National Institutes of Health, Bethesda, Md., October 8-12, 1962.

Primary discussion topics for the Symposium on Recent Developments in Research Methods and Instrumentation include: 1—Thin Film and Gas Chromatography; 2—Ion Exchange Techniques; 3—Nuclear Magnetic Resonance; 4—Optical Masers; 5—Vacuum Ultraviolet; 6—X-Ray Microscopy; 7—Automation in Chemical and Biochemical Research; 8—Physiological Monitoring; 9—X-Ray Diffraction Studies of Proteins.

Chairman of the Symposium is Dr. Ellis R. Lippincott, Dept. of Chemistry, University of Maryland, College Park, Md.

Pacific Energy Conversion Conference

Technological advances in the rapidly developing field of direct conversion and expanding areas of potential application will be emphasized at the Pacific Energy Conversion Conference, August 13-16, at the Fairmont Hotel in San Francisco, Calif.

Topics to be covered are thermionic, photovoltaic, thermoelectric and magnetohydrodynamic generators, fuel cells, and energy storage.

Registration information can be obtained from Wendell B. Freeman, Registration Chairman, c/o General Electric Co., 235 Montgomery St., San Francisco 4, Calif.

Tantalum-Sputtered Resistors Improved by Adding Nitrogen

By sputtering tantalum films in a partial nitrogen atmosphere, Bell Telephone Laboratories has obtained improved thin-film resistors. The tantalum-nitride technique provides resistors with a stability and reliability formerly available only in the larger and more expensive hermetically sealed devices. The technique was described recently in a paper by Dieter Gerstenberg and Edward H. Mayer presented before the Electronics Components Conference in Washington, D. C.

Heretofore, tantalum devices have been sputtered in an atmosphere of inert gas such as argon. Traces of certain impurities, like oxygen and water vapor, usually appear in these tantalum films, resulting in resistors with relatively wide variances in resistivity and temperature coefficient.

Small amounts of nitrogen (1-10% by pressure) added to the argon tend to override the accidental impurities, resulting in resistors with much narrower spreads in resistivity and temperature coefficient.

Like ordinary sputtered-tantalum resistors, the tantalum-nitride devices can be protected with an oxide film and, indeed, it is the "anodizing" of a layer of tantalum-oxide that permits the close tolerances to which sputtered devices can be "trimmed." The anodizing technique produces resistors within 1/10 of 1% of their nominal resistance.

Silicon Solar Cells are Versatile Radiation Detectors

A study of silicon solar cells under various kinds of radiation has shown that the cells are the simplest and among the most useful devices available for measuring high-intensity radiation. These results are reported by Dr. Walter Rosenzweig of Bell

December 1962 Discussion Section

A Discussion Section, covering papers published in the January-June 1962 JOURNALS, is scheduled for publication in the December 1962 issue. Any discussion which did not reach the Editor in time for inclusion in the June 1962 Discussion Section will be included in the December 1962 issue.

Those who plan to contribute remarks for this Discussion Section should submit their comments or questions in triplicate to the Managing Editor of the JOURNAL, 30 East 42 St., New York 17, N. Y. *not later than September 3, 1962.* All discussion will be forwarded to the author(s) for reply before being printed in the JOURNAL.

Telephone Laboratories in the *Review of Scientific Instruments*, a publication of the American Institute of Physics. The cells are not useful for measuring very low levels of radiation such as that resulting from fallout.

The cells are made by forming a thick layer of n-type semiconductor on a base of p-type semiconductor. In this form, they are 10-15 times less subject to damage from radiation than are solar cells which follow the original Bell Labs. form of the device and have a p-type surface layer on an n-type base. The decrease in sensitivity to radiation damage makes the newer solar cell attractive for many radiation monitoring applications. N-on-p solar cells were first studied by J. Mandelkorn and W. R. Cherry of the U.S. Army Signal Corps Lab.

The major advantages of the solar cell over other types of radiation detectors are simplicity and economy. For most applications, all that is necessary is to solder wires to a solar cell and connect them to a relatively inexpensive, commercially available ammeter.

Dr. Rosenzweig has pointed out that the cells were not appreciably damaged by x-rays or electrons produced by generators rated at up to about 300,000v. The cells also can be used to measure heavy-particle radiation such as alpha particles and protons, but with these the cell is damaged more quickly. The damaging effect can be useful in measuring cumulative exposure and in obtaining permanent beam-intensity profiles. In the latter application, large area cells are exposed, and the intensity of the beam at various locations on the cell can be measured by measuring the degradation of the cell at these locations.

Federal System of Regional Technical Report Centers

Twelve universities and libraries have been selected as Regional Technical Report Centers, to make available more widely the unclassified results of Federally sponsored research and development, the National Science Foundation and the U. S. Department of Commerce announced recently.

The Office of Technical Services of the Dept. of Commerce, in accordance with its statutory mission, has accepted the responsibility for directing and coordinating the planning and operation of the system. Funding and other assistance for beginning the system will be provided by NSF through its Office of Science Information Service.

Three agencies that produce an estimated 90% of the Government's unclassified technical reports—the Dept. of Defense, National Aeronautics and Space Administration, and Atomic Energy Commission—have agreed to provide copies of their reports for deposit in each of the 12 centers.

Each center will: Receive from OTS or other Federal agencies, and their contractors and grantees, copies of unclassified technical reports and other appropriate bibliographic and reference publications; Organize and maintain a cumulative library collection of all material received; Furnish to the general public in the respective geographical region such services as personal reference, interlibrary loans, photocopy service, and assistance to users in obtaining retention copies where appropriate.

The centers are as follows: Georgia Institute of Technology, Atlanta, Ga.; Massachusetts Institute of Technology, Cambridge, Mass.; John Crerar Library, Chicago, Ill.; Southern Methodist University, Dallas, Texas; University of Colorado, Boulder, Colo.; Linda Hall Library, Kansas City, Mo.; University of California, Los Angeles, Calif.; Columbia University, New York, N. Y.; Carnegie Library of Pittsburgh, Pittsburgh, Pa.; University of California (Berkeley Campus), San Francisco, Calif.; University of Washington, Seattle, Wash.; Library of Congress, Washington, D. C.

Corning Science Prize

Little, Brown and Co., in cooperation with Corning Glass Works, has announced the establishment of the $10,000 Corning Science Prize to be awarded for the best book manuscript in the field of the natural or physical sciences for the general reader. The purpose of the award is to stimulate science writing and to encourage writers to undertake books on science.

To qualify for the prize, a manuscript must be of book length and written originally in the English language. Manuscripts must be on a scientific subject and intended for the intelligent layman. Scientific in this case is meant to include the natural and physical sciences.

The first prize-winning manuscript will be selected from entries received up to March 31, 1963. Manuscripts should be addressed to "Corning Science Prize Editor" and submitted to Little, Brown and Co., 34 Beacon St., Boston 6, Mass.

Of the $10,000 awarded the author of the Corning Science Prize book, $7,500 will be an outright grant and $2,500 will be an advance against royalties.

WPI Materials Engineering Lab.

Worcester Polytechnic Institute, Worcester, Mass., has announced plans for Materials Engineering Laboratories in renovated facilities on the campus. Worcester Tech plans next fall to initiate a new graduate curriculum in metallurgy. Simultaneously, the undergraduate program will be strengthened by additional courses.

The laboratories also will be able better to serve the Central New England area, heart of a great metalworking and ceramics industry, in research and development problems.

The specialized items will include 10 furnaces. They vary from general combustion furnaces for student use to an intricate vacuum melting fur-

ECS Boston Local Committee

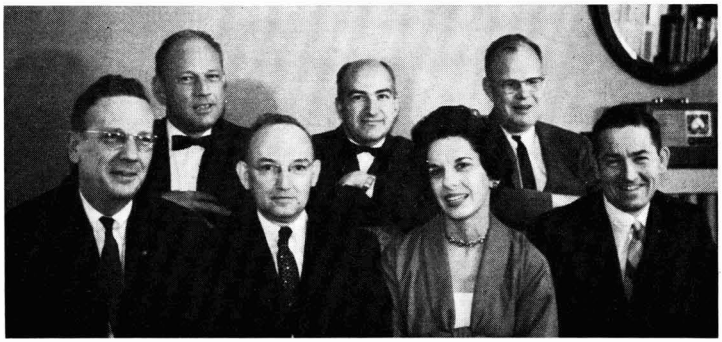

This is your Boston Local Committee, who are looking forward to greeting you at the Society's Boston Meeting this September. Left to right—top row: Paul T. Woodberry, Charles Levy, Charles W. Jerome; bottom row: Horace H. Homer, Emerson H. Newton, Mrs. Harry C. Gatos, Richard A. Peak.

nace to produce high-purity metals and alloys for research.

It is expected that the work will be completed for the opening of the next college term and that most of the new equipment will be in place.

Trace Metal Analysis Service

The electroplating industry's first free analysis service for measuring and controlling trace metals in a plating bath was made available recently by Technic, Inc., Providence, R. I.

The new service will give fast quantitative and qualitative analyses for the major metal and all normal trace metals at concentrations as low as 0.01 g/l. Heart of the new service is a direct-reading spectrometer.

The service is offered free of charge to companies in the electronics, defense, and decorative industries which electroplate with precious metals.

R. K. Smith, Technic president, has explained, "As little as 35 mg of silver per gallon of rhodium solution can result in decreased corrosion and tarnish resistance.

"Trace amounts of lead in a gold or rhodium bath can lead to a porous plate and poor corrosion resistance before anything can be detected visually.

"A controlled trace amount of antimony in a gold bath is beneficial to one type of transistor but will poison another type.

"Trace metals in some cases are desirable; in others they are detrimental. In fact, it is difficult to conceive of a plating solution where trace metals are of anything less than major importance."

The spectrometer will provide detailed, fast information to help platers in four areas: 1—It will analyze for the primary metal; 2—It will analyze alloys, with the analysis leading to better control of color, hardness, and/or electrical properties of the plate; 3—It will analyze impurities to predict approaching electrical, physical, plate corrosion, or color problems; 4—It will analyze impurities to catch poor rinsing, drag-in of prior solutions, and, in general, poor plating practices before they ruin an expensive bath or costly production parts.

Plating baths can be analyzed with samples as small as 3 or 4 cm^3. Concentrations as low as 11 ppm can be checked at this level, with accuracy within 5%.

As in the past, samples are sent to the company, and reports are issued by return mail or by teletype or phone if required.

Announcements from Publishers

"The Compatibility of Materials with Chlorine Trifluoride, Perchloryl Fluoride, and Mixtures of These," J. C. Grigger and H. C. Miller, Pennsalt Chemicals Corp., for Air Force Systems Command, U. S. Air Force, April 1961. Report AD 266 391,*102 pages; $2.50.

"Electrolytic Oxidation of Zirconium in Nitrate Solutions," Dec. 1961. AEC Report IDO-14571,* 13 pages; 50 cents.

"Electrolytic Dissolution of Nuclear Fuels, Part II. Nichrome in Nitrate Solutions," Dec. 1961. AEC Report IDO-14575,* 13 pages; 50 cents.

"Thorium Fused Salt Electrodeposition into a Molten Zinc Cathode," Jan. 1962. AEC Report NAA-SR-6802,* 17 pages; 50 cents.

"Semiconducting Polymers," Report PB 154 775*; $3.30.

"Organic Semiconductor Study," Report PB 171 177*; $1.75.

"Investigation of Organic Semiconductors," Report PB 171 340*; $2.25.

* Order from Office of Technical Services, Business and Defense Services Administration, U. S. Dept. of Commerce, Washington 25, D. C.

Literature from Industry

Tantalum. Brochure. This four-page illustrated folder contains information on applications, characteristics, grades, and types of tantalum powder, ingots, and mill products available. Also, it lists sales offices and warehouse facilities. Tantalum products listed include: capacitor grade powder and wire, melting grade powder, ingots, forging billets, plate, sheet, strip, foil, rod, wire, tubing, and alloy ingots and mill products.

Free copies of the brochure can be obtained from Mr. William V. King, National Research Corp., Metals Div., 45 Industrial Place, Newton 64, Mass.

Metex 157, a liquid phosphoric acid treatment to prepare metal and remove rust and corrosion before plating, painting, or similar surface treatment, is described in Product Data Sheet No. 31, available from MacDermid Inc., Waterbury, Conn.

Metex 157 is effective on ferrous basis metals, aluminum, zinc-base diecastings, and cadmium or zinc electrodeposits. It not only removes rust but also forms a light, integral phosphate coating on the metal surface to prevent further corrosion.

"Plating With Precious Metals," a new, four-page paper, gives latest techniques, methods, equipment required, and comparative costs of plating with such precious metals as gold, silver, rhodium, and platinum. Essentially a technical treatise for metalworking manufacturers, this paper has been reprinted by Sel-Rex Corp., Nutley, N. J., as a service to all persons considering the value of precious metals electroplate.

"Gallium and Gallium Compounds." New 10-page brochure provides a comprehensive outline of basic information concerning gallium. It describes properties, uses, potential applications, technical service, and available types.

Copies of the publication are available from Alcoa sales offices or on request to Alcoa Chemicals Div., 645 Alcoa Bldg., Pittsburgh 19, Pa.

Metex Blackzinc No. 1, a dry acid salt used to produce a black, inorganic coating on zinc base diecastings and zinc plate is fully described in Product Data Sheet No. 89. The coating gives a mild corrosion resistance against atmosphere and indoor exposure. The coating may be used effectively for decorative, engineering, or identification applications.

The data sheet is available from, Macdermid Inc., Waterbury 20, Conn.

Advertiser's Index

The Electrochemical Society

Patron Members

Aluminum Co. of Canada, Ltd.,
Montreal, Que., Canada

International Nickel Co., Inc.,
New York, N. Y.

Olin Mathieson Chemical Corp.,
Chemicals Div., Industrial Chemicals
Development Dept., Niagara Falls, N. Y.

Union Carbide Corp.
Divisions:
National Carbon Co., New York, N. Y.
Union Carbide Consumer Products Co.,
New York, N. Y
Union Carbide Metals Co.,
New York, N. Y.

Westinghouse Electric Corp., Pittsburgh, Pa.

Sustaining Members

Air Reduction Co., Inc., New York, N. Y.

Ajax Electro Metallurgical Corp.,
Philadelphia, Pa.

Allen-Bradley Co., Milwaukee, Wis.

Allied Chemical Corp.
Solvay Process Div., Syracuse, N. Y.
General Chemical Div., Morristown, N. J.

Alloy Steel Products Co., Inc., Linden, N. J.

Aluminum Co. of America,
New Kensington, Pa.

American Metal Climax, Inc.,
New York, N. Y.

American Potash & Chemical Corp.,
Los Angeles, Calif. (2 memberships)

American Smelting and Refining Co.,
South Plainfield, N. J.

American Zinc Co. of Illinois,
East St. Louis, Ill.

American Zinc, Lead & Smelting Co.,
St. Louis, Mo. (2 memberships)

American Zinc Oxide Co., Columbus, Ohio

M. Ames Chemical Works, Inc.,
Glens Falls, N. Y.

Armco Steel Corp., Middletown, Ohio

Basic Inc., Maple Grove, Ohio

Bell Telephone Laboratories, Inc.,
New York, N. Y. (2 memberships)

Bethlehem Steel Co., Bethlehem, Pa.
(2 memberships)

Boeing Airplane Co., Seattle, Wash.

Burgess Battery Co., Freeport, Ill.
(4 memberships)

Canadian Industries Ltd., Montreal,
Que., Canada

Carborundum Co., Niagara Falls. N. Y.

Catalyst Research Corp., Baltimore, Md.

Consolidated Mining & Smelting Co. of
Canada, Ltd., Trail, B. C., Canada
(2 memberships)

Continental Can Co., Inc., Chicago, Ill.

Cooper Metallurgical Associates, Cleveland,
Ohio

Corning Glass Works, Corning, N. Y.

Diamond Alkali Co., Painesville, Ohio

Dow Chemical Co., Midland, Mich.

Wilbur B. Driver Co., Newark, N. J.
(2 memberships)

E. I. du Pont de Nemours & Co., Inc.,
Wilmington, Del.

Eagle-Picher Co., Chemical and Metals Div.,
Joplin, Mo.

Eastman Kodak Co., Rochester, N. Y.

Thomas A. Edison Research Laboratory, Div.
of McGraw-Edison Co., West Orange, N. J.

Electric Auto-Lite Co., Toledo, Ohio
C & D Div., Conshohocken, Pa.

Electric Storage Battery Co., Yardley, Pa.

Engelhard Industries, Inc., Newark, N. J.
(2 memberships)

The Eppley Laboratory, Inc., Newport, R. I.
(2 memberships)

Exmet Corp., Tuckahoe, N. Y.

Fairchild Semiconductor Corp., Palo Alto,
Calif.

Food Machinery & Chemical Corp.
Becco Chemical Div., Buffalo, N. Y.
Westvaco Chlor-Alkali Div., South
Charleston, W. Va.

Foote Mineral Co., Exton, Pa.

Ford Motor Co., Dearborn, Mich.

General Electric Co., Schenectady, N. Y.
Chemistry & Chemical Engineering
Component, General Engineering
Laboratory
Chemistry Research Dept.
General Physics Research Dept.
Metallurgy & Ceramics Research Dept.
Aircraft Accessory Turbine Dept.,
West Lynn, Mass.

General Instrument Corp., Newark, N. J.

General Motors Corp.
Allison Div., Indianapolis, Ind.
Delco-Remy Div., Anderson, Ind.
Guide Lamp Div., Anderson, Ind.
Research Laboratories Div., Warren, Mich.

General Telephone & Electronics
Laboratories Inc., Bayside, N. Y.
(2 memberships)

Gillette Safety Razor Co., Boston, Mass.

Globe-Union, Inc., Milwaukee, Wis.

B. F. Goodrich Chemical Co.,
Cleveland, Ohio

(Sustaining Members cont'd)

Gould-National Batteries, Inc., Minneapolis, Minn.
Great Lakes Carbon Corp., New York, N. Y.
Hanson-Van Winkle-Munning Co., Matawan, N. J. (2 memberships)
Harshaw Chemical Co., Cleveland, Ohio (2 memberships)
Hercules Powder Co., Wilmington, Del.
Hill Cross Co., Inc., West New York, N. J.
Hoffman Electronics Corp., Semiconductor Div., El Monte, Calif. (2 memberships)
Hooker Chemical Corp., Niagara Falls, N. Y. (3 memberships)
HP Associates, Palo Alto, Calif.
Hughes Research Laboratories, Div. of Hughes Aircraft Co., Malibu, Calif.
International Business Machines Corp., New York, N. Y.
International Minerals & Chemical Corp., Skokie, Ill.
ITT Federal Laboratories, Div. of International Telephone & Telegraph Corp., Nutley, N. J.
Jones & Laughlin Steel Corp., Pittsburgh, Pa.
K. W. Battery Co., Skokie, Ill.
Kaiser Aluminum & Chemical Corp.
Div. of Chemical Research, Permanente, Calif.
Div. of Metallurgical Research, Spokane, Wash.
Kawecki Chemical Co., Boyertown, Pa.
Kennecott Copper Corp., New York, N. Y.
Leesona Moos Laboratories, Div. of Leesona Corp., Jamaica, N. Y.
Libbey-Owens-Ford Glass Co., Toledo, Ohio
Lockheed Aircraft Corp., Missiles & Space Div., Sunnyvale, Calif.
Mallinckrodt Chemical Works, St. Louis, Mo.
P. R. Mallory & Co., Indianapolis, Ind.
Merck & Co., Inc., Rahway, N. J.
Metal & Thermit Corp., Detroit, Mich.
Miles Chemical Co., Div. of Miles Laboratories, Inc., Elkhart, Ind.
Minneapolis-Honeywell Regulator Co., Minneapolis, Minn.
Minnesota Mining & Manufacturing Co., St. Paul, Minn.
Monsanto Chemical Co., St. Louis, Mo.
Motorola, Inc., Chicago, Ill.
National Cash Register Co., Dayton, Ohio
National Lead Co., New York, N. Y.
National Research Corp., Cambridge, Mass.
National Steel Corp., Weirton, W. Va.
North American Aviation, Inc., Rocketdyne Div., Canoga Park, Calif.
Northern Electric Co., Montreal, Que., Canada
Norton Co., Worcester, Mass.
Ovitron Corp., Long Island City, N. Y.
Owens-Illinois Glass Co., Toledo, Ohio
Peerless Roll Leaf Co., Inc., Union City, N. J.
Pennsalt Chemicals Corp., Philadelphia, Pa.
Phelps Dodge Refining Corp., Maspeth, N. Y.
Philco Corp., Research Div., Blue Bell, Pa.
Philips Laboratories, Inc., Irvington-on-Hudson, N. Y.
Pittsburgh Plate Glass Co., Chemical Div., Pittsburgh, Pa.
Potash Co. of America, Carlsbad, N. Mex.
The Pure Oil Co., Research Center, Crystal Lake, Ill.
Radio Corp. of America
Tube Div., Harrison, N. J.
RCA Victor Record Div., Indianapolis, Ind.
Ray-O-Vac Co., Madison, Wis.
Raytheon Co., Waltham, Mass.
Remington Rand, Div. of Sperry Rand Corp., New York, N. Y.
Reynolds Metals Co., Richmond, Va.
Rheem Semiconductor Corp., Mountain View, Calif.
Schering Corp., Bloomfield, N. J.
Shawinigan Chemicals Ltd., Montreal, Que., Canada
Socony Mobil Oil Co., Inc., Dallas, Texas
Speer Carbon Co.
International Graphite & Electrode Div., St. Marys, Pa.
Sprague Electric Co., North Adams, Mass.
Stackpole Carbon Co., St. Marys, Pa.
Stauffer Chemical Co., New York, N. Y.
Tennessee Products & Chemical Corp., Nashville, Tenn.
Texas Instruments, Inc., Dallas, Texas
Metals and Controls Corp., Attleboro, Mass.
Three Point One Four Corp., Yonkers, N. Y.
Titanium Metals Corp. of America, Henderson, Nev.
Tung-Sol Electric Inc., Newark, N. J.
Udylite Corp., Detroit, Mich. (4 memberships)
United States Borax & Chemical Corp., Los Angeles, Calif.
Universal-Cyclops Steel Corp., Bridgeville, Pa.
Upjohn Co., Kalamazoo, Mich.
U. S. Steel Corp., Pittsburgh, Pa.
Victor Chemical Works, Chicago, Ill.
Western Electric Co., Inc., Chicago, Ill.
Wyandotte Chemicals Corp., Wyandotte, Mich.
Yardney Electric Corp., New York, N. Y.